PHYSICAL REVIEW C **92**, 021602(R) (2015)

Universal damping mechanism of quantum vibrations in deep sub-barrier fusion reactions

Takatoshi Ichikawa[1] and Kenichi Matsuyanagi[1,2]
[1]*Yukawa Institute for Theoretical Physics, Kyoto University, Kyoto 606-8502, Japan*
[2]*RIKEN Nishina Center, Wako 351-0198, Japan*

(Received 26 June 2015; revised manuscript received 30 July 2015; published 24 August 2015)

We demonstrate the damping of quantum octupole vibrations near the touching point when two colliding nuclei approach each other in the mass-asymmetric $^{16}O + ^{208}Pb$ system, for which the strong fusion hindrance was clearly observed. We, for the first time, apply the random-phase approximation method to the heavy-mass asymmetric dinuclear system to calculate the transition strength $B(E3)$ as a function of the center-of-mass distance. The obtained $B(E3)$ strengths are substantially damped near the touching point, because the single-particle wave functions of the two nuclei strongly mix with each other and a neck is formed. The energy-weighted sums of $B(E3)$ are also strongly correlated with the damping factor, which is phenomenologically introduced in the standard coupled-channel calculations to reproduce the fusion hindrance. This strongly indicates that the damping of the quantum vibrations universally occurs in the deep sub-barrier fusion reactions.

DOI: 10.1103/PhysRevC.92.021602 PACS number(s): 21.60.Ev, 24.10.Eq, 25.70.Jj

Heavy-ion fusion reactions are an excellent probe to investigate the fundamental features of the dynamics for many-body quantum systems. When a projectile approaches a target, the Coulomb barrier is formed, because of the strong cancellation between the Coulomb repulsion and the nuclear attractive force. Nuclear fusion takes place when the projectile penetrates through this Coulomb barrier. At incident energies in the vicinity of the Coulomb barrier height, called the sub-barrier fusion, the strong enhancements of fusion cross sections, compared to the estimations of a simple one-dimensional potential model, have been observed in many systems. These enhancements are well accounted for in terms of the couplings between the relative motion of the colliding nuclei and the intrinsic degrees of freedom such as collective vibrations of the target and the projectile [1]. The coupled-channel (CC) model, which takes into account this mechanism, has been successful in describing such enhancements [2,3].

Recent experiments at extremely low incident energies, called the deep sub-barrier energies, revealed, however, that steep falloffs of the fusion cross sections, compared to the estimations of the standard CC model, emerge in a wide range of mass systems [4,5] (see Ref. [6] for details). These steep falloff phenomena are often called the fusion hindrance. An important quantity for understanding this fusion hindrance is the potential energy at the touching point of the colliding nuclei, which is strongly correlated with the threshold incident energy for the emergence of the fusion hindrance. That is, the fusion hindrance would be associated with the dynamics in the overlap region of the two colliding nuclei (see Fig. 1 in Ref. [7]).

A theoretical challenge is how to extend the standard CC model to describe these fusion hindrance phenomena in the overlap region. Two different models based on assumptions opposite to each other have been proposed [6]. One is the sudden approach proposed by Mişicu and Esbensen [8,9]. They constructed a heavy ion-ion potential with a shallow potential pocket considering the Pauli principle effect that acts when two colliding nuclei overlap with each other. The other is the adiabatic approach proposed by Ichikawa *et al.* [10]. In this approach, neck formations between the colliding nuclei are taken into account in the overlap region. Based on this picture, the sudden and adiabatic processes were smoothly jointed by phenomenologically introducing the damping factor in the coupling form factor [11]. Later, we showed that the physical origin of the damping factor is the damping of quantum vibrations of the target and the projectile near the touching point using the random-phase approximation (RPA) method for the light-mass symmetric $^{16}O + ^{16}O$ and $^{40}Ca + ^{40}Ca$ systems [12].

In recent years, another useful approach, different from the CC model, has been developed to describe heavy-ion fusion reactions on the basis of the self-consistent mean-field theory [6]: In particular, Umar and Oberacker proposed the density-constrained time-dependent Hartree-Fock method to calculate the energy-dependent ion-ion interaction potential [13]. By using this method, systematic investigations on deep sub-barrier fusions have been performed [14–16].

In this Rapid Communication, we show that the damping of the quantum vibrations near the touching point is a universal mechanism in the deep sub-barrier fusions and is responsible for the fusion hindrance. A typical example optimally suited for this purpose is the recent precise data for the $^{16}O + ^{208}Pb$ fusion [5]. The performances of both the sudden and adiabatic models have been well tested in this system [9,11]. The adiabatic model can reproduce well the experimental data rather than the sudden model for the fusion hindrance. To discriminate which model is a better description, we here show the physical origin of the damping factor introduced in Ref. [11] in the heavy-mass asymmetric $^{16}O + ^{208}Pb$ system.

In the standard CC model (and the sudden model), the vibrational modes of the individual colliding nuclei are assumed not to change, even when the two nuclei strongly overlap with each other. However, as shown in Ref. [12], the single-particle wave functions are drastically changed by level repulsions, which are associated with the neck formations. We apply the RPA method to the heavy-mass asymmetric system, $^{16}O + ^{208}Pb$, and show that these mechanisms lead to damping of quantum vibrations in the colliding nuclei near the touching point. This is exhibited by a drastic decreases

of the $B(E3)$ strengths carried by low-energy RPA excitation modes.

To illustrate our main idea, we first discuss the Nilsson diagram for protons as a function of the center-of-mass distance, R, in the $^{16}\mathrm{O} + {}^{208}\mathrm{Pb}$ system. We calculate the mean-field potential for the $^{16}\mathrm{O} + {}^{208}\mathrm{Pb}$ system using the folding procedure with the single Yukawa function [17]. Before the touching point, we assume the spherical shape for both nuclei. After the touching point, we describe the nuclear shapes with the reflection-asymmetric lemniscatoids parametrization [18]. (The parametrization dependence is negligible, because in this Rapid Communication we do not discuss the strongly overlapping region.) Based on these densities, we also calculate the Coulomb potential. We use the radius for the proton and neutron potentials, R_0, with $R_0 = 1.27A^{1/3}$ fm, where A is the total nucleon number. The depths of the neutron and proton potentials for individual $^{16}\mathrm{O}$ and $^{208}\mathrm{Pb}$ nuclei, V_T and V_P, are taken from Ref. [19]. In the folding procedure, we smoothly joint the two different depth parameters of the mean-field potentials for $^{16}\mathrm{O}$ and $^{208}\mathrm{Pb}$ by the function $V_0(z) = \frac{1}{2}[(V_T - V_P)\mathrm{erf}\{(z - z_c)/\mu\} + (V_T + V_P)]$, where z_c denotes the center position between the two surfaces of the colliding nuclei and μ denotes the smoothing parameter. We take $\mu = 0.8$ fm, which is the same as the diffuseness parameter of the single-particle potential. In the calculations, the origin is located at the center-of-mass position of the two nuclei.

Using the obtained mean-field potentials, we solve the axially symmetric Schrödinger equation with the spin-orbit force. The details of the model and the parameters are similar to Refs. [17,19]. Then, the z component of the total angular momentum, Ω, is the good quantum number. Note that the parity is not a good quantum number because the mean-field potential for the whole system breaks the space-reflection symmetry. We expand the single-particle wave functions in terms of the deformed harmonic-oscillator bases in the cylindrical coordinate representation. The deformation parameter of the basis functions is determined so as to cover the target and the projectile. The basis functions with energies lower than 26 $\hbar\omega$ are taken into account.

Figure 1 shows the Nilsson diagram as a function of the center-of-mass distance R. In the figure, we can see extremely strong Coulomb effect of $^{208}\mathrm{Pb}$ on $^{16}\mathrm{O}$. The single-particle $p_{1/2}$ and $p_{3/2}$ states in $^{16}\mathrm{O}$ are shown by the (red) thick solid lines. Even at the large separation distance $R = 20$ fm, the energies of these two states are higher than the Fermi energy of the $s_{1/2}$ state in $^{208}\mathrm{Pb}$. The mismatch of the two Fermi levels between $^{16}\mathrm{O}$ and $^{208}\mathrm{Pb}$ occurs due to the strong Coulomb effect. At an infinite separation distance, the energies of the $p_{1/2}$ and $p_{3/2}$ states for $^{16}\mathrm{O}$ are -5.88 and -10.7 MeV, respectively. Thus, at $R = 20$ fm, the depth of the mean-field potential for $^{16}\mathrm{O}$ becomes shallow by about 5 MeV due to the Coulomb effect from $^{208}\mathrm{Pb}$.

The single-particle energies of the $p_{1/2}$ and $p_{3/2}$ states in $^{16}\mathrm{O}$ remarkably increase with decreasing R due to the increasing Coulomb effect from $^{208}\mathrm{Pb}$. Then, many level crossings and repulsions between the energy levels of $^{16}\mathrm{O}$ and $^{208}\mathrm{Pb}$ occur. With decreasing R, the energy of the $p_{1/2}$ state becomes positive around $R = 18$ fm, that is, it changes into a *resonance* state, but there is still a sufficiently high Coulomb barrier. After that, it goes across the $f_{5/2}$ and $p_{3/2}$ states of $^{208}\mathrm{Pb}$ around $R = 16$ fm and the $p_{1/2}$ state of $^{208}\mathrm{Pb}$ around $R = 13$ fm. Below $R = 13$ fm, the Coulomb barrier becomes lower due to the attractive nuclear mean-field potential. Then, the strong mixture of the single-particle states between $^{16}\mathrm{O}$ and $^{208}\mathrm{Pb}$ starts in many levels, which causes many level splittings seen in the Nilsson diagram.

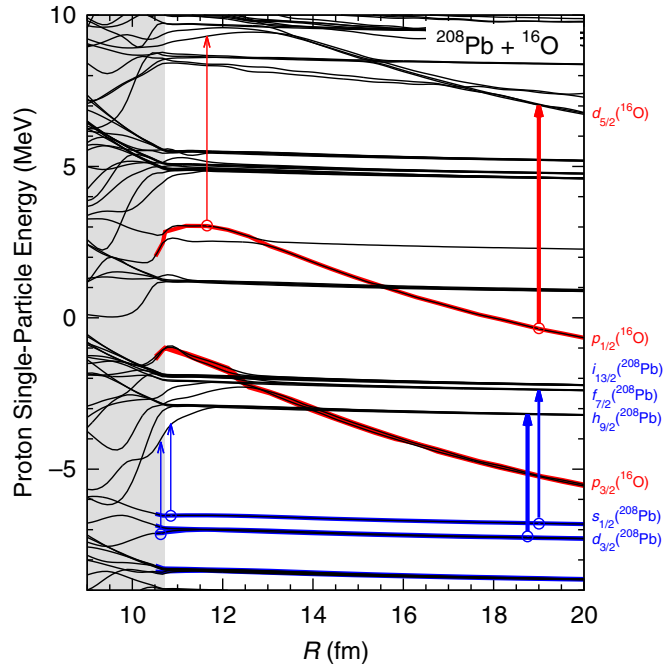

FIG. 1. (Color online) Nilsson diagram for the $^{16}\mathrm{O} + {}^{208}\mathrm{Pb}$ system as a function of R. The light gray (red) thick lines represent the occupied $p_{1/2}$ and $p_{3/2}$ states in $^{16}\mathrm{O}$. The dark gray (blue) thick solid lines show the occupied states in $^{208}\mathrm{Pb}$. The gray area indicates the overlap region of the colliding nuclei. The arrows represent the main particle-hole excitations constituting the RPA modes.

We now solve the RPA equation at each R for the mass-asymmetric $^{16}\mathrm{O} + {}^{208}\mathrm{Pb}$ system. We calculate the first excited 3^- (octupole vibrational) states of $^{16}\mathrm{O}$ and $^{208}\mathrm{Pb}$, which give the main contributions in the standard CC calculations. We can easily apply the RPA method to the di-nuclear system, because its wave function is described with a one-center Slater determinant. We take the single-particle levels for each neutron and proton up to the 200th and the coherent superposition of all one-particle–one-hole states with excitation energies below 30 MeV. We follow the diabatic single-particle configuration corresponding to the ground state of $^{16}\mathrm{O}$. The occupied $p_{1/2}$ and $p_{3/2}$ states in $^{16}\mathrm{O}$ are represented by the light gray (red) thick curves in Fig. 1. We carry out the RPA calculation, avoiding immediate vicinities of the level-crossing points. We use the density-dependent residual interaction taken from Ref. [20] and tune it so that the energy of the spurious center-of-mass motion becomes zero. We calculate $B(E3)$ values for the RPA solutions with $\Omega = 0$ in individual nuclei using the shifted octupole operator, $\widehat{Q}_{30}(R - R'_0)$, where R'_0 is the center-of-mass position of the projectile or target nucleus.

At the large separation distance $R = 20$ fm, we obtain the first 3^- excited states of individual nuclei. The obtained

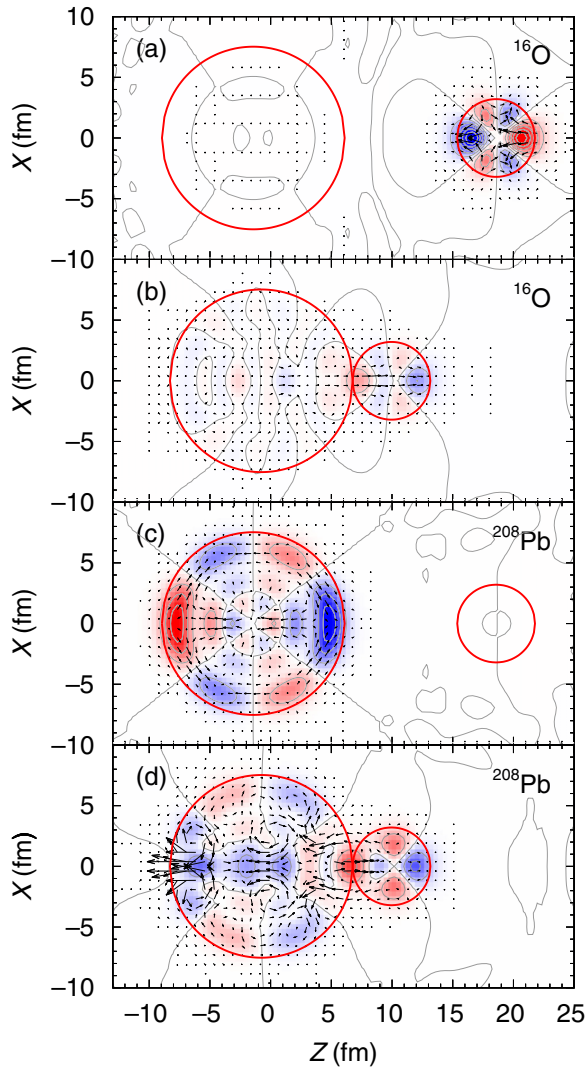

FIG. 2. (Color online) Contour maps of the proton transition densities and current distributions for the first excited 3^- states of ^{16}O and ^{208}Pb at $R = 20$ and 10.73 fm. The contour lines correspond to multiples of 0.01 and 0.005 fm^{-2} for ^{16}O and ^{208}Pb, respectively. The arrows represent the current density. The currents and colors are normalized at $R = 20$ fm in individual nuclei. The (red) thick solid circles indicate the half depth of the mean-field potential.

energies and $B(E3,\ 3^-_1 \rightarrow 0^+_1)$ values are 2.86 MeV and $7.13 \times 10^4 e^2$ fm^6 for ^{208}Pb and 4.64 MeV and 124 e^2 fm^6 for ^{16}O. The obtained transition densities and currents for the first 3^- states of ^{16}O and ^{208}Pb are depicted in Figs. 2(a) and 2(c). At $R = 20$ fm, these modes are isolated. When the two nuclei approach each other, however, these modes start to fragment into several states. To evaluate the octupole collective strengths carried by low-energy excitations, we then calculate the energy-weighted sum of $B(E3)$ strengths. By checking the spectrum of all obtained RPA modes as a function of R, we determined to take the sum for octupole excitations with $E \leqslant 4$ MeV and $E \leqslant 6$ MeV for ^{208}Pb and ^{16}O, respectively.

Figure 3 shows the $B(E3)$ strengths for (a) ^{16}O and (b) ^{208}Pb as functions of R. The calculated values (the solid circles)

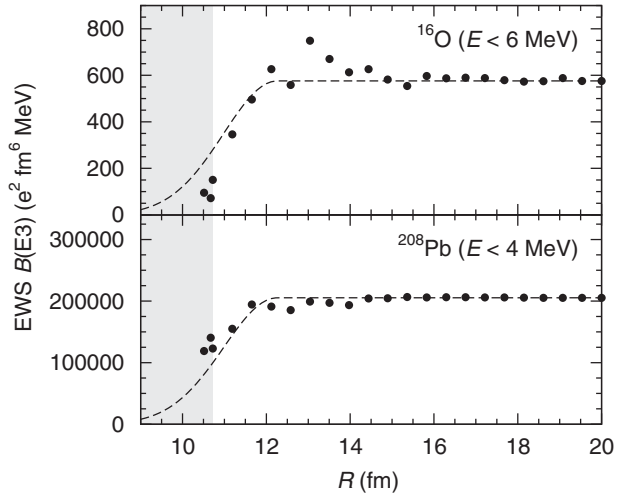

FIG. 3. Energy-weighted sums of $B(E3)$ for (a) ^{16}O and (b) ^{208}Pb as functions of R. The solid circles show the results of the RPA calculations. The dashed curves represent the damping factor, which well reproduces the experimental data of the fusion cross section for ^{16}O + ^{208}Pb taken from Ref. [11]. The gray area indicates the overlap region of the colliding nuclei.

drastically decrease near the touching point (the boundary between the white and gray areas) in both nuclei. The transition densities and currents for the RPA modes with the maximum $B(E3)$ at the touching point are depicted in Figs. 2(b) and 2(d). These figures indicate that the octupole collectivities of both ^{16}O and ^{208}Pb are considerably diminished by each colliding partner.

The microscopic origin of the damping of these vibrations is easily seen as follows. At $R = 20$ fm, the main proton components of the 3^- modes are the excitations $p_{1/2} \rightarrow d_{5/2}$ and $p_{3/2} \rightarrow d_{5/2}$ for ^{16}O, and the excitations $d_{3/2} \rightarrow h_{9/2}$ and $s_{1/2} \rightarrow f_{7/2}$ for ^{208}Pb [see the (red and blue) arrows around $R = 19$ fm in Fig. 1]. The density distributions of the $p_{1/2}$ and $d_{5/2}$ states in ^{16}O are displayed in Figs. 4(a) and 4(b). Their wave functions suffer major modifications near the touching point at $R = 11.65$ fm, as depicted in Figs. 4(c) and 4(d) [see also the (red) arrow at $R = 11.65$ fm in Fig. 1]. We can clearly see the neck formations in Fig. 4(d). Also for ^{208}Pb, similar drastic changes of single-particle wave functions occur for both protons and neutrons near the Fermi surface, causing the damping of the collectivity of the 3^- vibration [see the (blue) arrows around 10.6 fm in Fig. 1].

Finally, to see the correlation with the damping factor phenomenologically introduced in the CC calculation, we compare the calculated results with the damping factor that well reproduced the experimental data of the fusion cross section for ^{16}O + ^{208}Pb [11]. The damping factor is given by $\Phi(r,\lambda_\alpha) = e^{-(r-R_d-\lambda_\alpha)^2/2a_d^2}$ for $r < R_d + \lambda_\alpha$ (otherwise $\Phi = 1$), where a_d and λ_a denote the damping width and the eigenvalues of the coupling matrix elements, respectively. The parameter R_d is given by $R_d = r_d(A_T^{1/3} + A_P^{1/3})$, where r_d denotes the damping radius parameter, and A_T and A_P are the mass numbers of the target and the projectile, respectively. In the calculation of Ref. [11], $r_d = 1.298$ fm and $a_d = 1.05$ fm

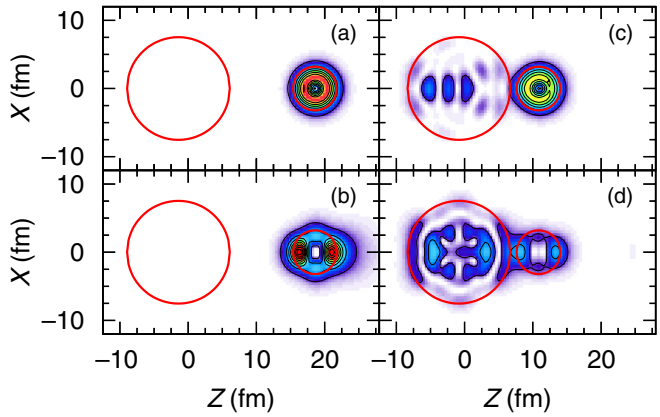

FIG. 4. (Color online) Density distributions of the $p_{1/2}$ and $d_{5/2}$ states originally belonging to ^{16}O at $R = 20$ fm and their evolutions at $R = 11.65$ fm. The (red) thick solid circles indicate the half depth of the mean-field potential. The contour lines correspond to multiples of 0.0015 fm^{-3}. The colors are normalized at 0.01 fm^{-3}.

are used. Then, the largest eigenvalue of λ_α is 1.46 fm. In Figs. 3(a) and 3(b), the dashed curves represent the damping factor with these parameters normalized at $R = 20$ fm. We can see that the damping factor strongly correlates with the calculated energy-weighted sums of $B(E3)$ in the low-energy region, which clearly indicates that the damping of the quantum vibrations indeed occurs when the colliding nuclei approach each other.

In summary, we have demonstrated the damping of the quantum octupole vibrations of both ^{16}O and ^{208}Pb, when they approach each other. To show this, we, for the first time, applied the RPA method to the heavy-mass asymmetric ^{16}O + ^{208}Pb system. We have discussed the Nilsson diagram as a function of the center-of-mass distance R and have shown that the single-particle energies in ^{16}O are largely shifted to the positive-energy direction by the strong Coulomb effects from the heavy-mass ^{208}Pb in a colliding process. We calculated the $B(E3)$ strengths for ^{16}O and ^{208}Pb as a function of R. The obtained $B(E3)$ strengths are substantially damped near the touching point of the colliding nuclei. The obtained energy-weighted sum of $B(E3)$ in the low-energy region exhibits a strong correlation with the damping factor that reproduces well the experimental data of the fusion cross section for ^{16}O + ^{208}Pb. This is a clear evidence that the damping of the quantum octupole vibrations indeed occur near the touching point in the deep sub-barrier fusion reactions. The drastic change of single-particle wave functions constituting the low-energy collective excitations discussed in this paper would commonly occur in all deep sub-barrier reactions. Therefore, the damping of quantum vibrations in both the target and the projectile near the touching point seems to be a universal mechanism causing the fusion hindrance, which should be taken into account in the standard CC model.

Part of this research was funded by the MEXT HPCI Strategic Program. This work was supported by JPSJ KAKENHI Grant No. 15K05078.

[1] M. Dasgupta *et al.*, Annu. Rev. Nucl. Part. Sci. **48**, 401 (1998).
[2] A. B. Balantekin and N. Takigawa, Rev. Mod. Phys. **70**, 77 (1998).
[3] K. Hagino and N. Takigawa, Prog. Theor. Phys. **128**, 1061 (2012).
[4] C. L. Jiang *et al.*, Phys. Rev. Lett. **89**, 052701 (2002); **93**, 012701 (2004); Phys. Rev. C **73**, 014613 (2006); **75**, 057604 (2007); Phys. Rev. Lett. **113**, 022701 (2014).
[5] M. Dasgupta *et al.*, Phys. Rev. Lett. **99**, 192701 (2007).
[6] B. B. Back *et al.*, Rev. Mod. Phys. **86**, 317 (2014).
[7] T. Ichikawa, K. Hagino, and A. Iwamoto, Phys. Rev. C **75**, 064612 (2007).
[8] Ş. Mişicu and H. Esbensen, Phys. Rev. Lett. **96**, 112701 (2006); Phys. Rev. C **75**, 034606 (2007).
[9] H. Esbensen and Ş. Mişicu, Phys. Rev. C **76**, 054609 (2007).
[10] T. Ichikawa, K. Hagino, and A. Iwamoto, Phys. Rev. C **75**, 057603 (2007).
[11] T. Ichikawa, K. Hagino, and A. Iwamoto, Phys. Rev. Lett. **103**, 202701 (2009); EPJ Web Conf. **17**, 07001 (2011).
[12] T. Ichikawa and K. Matsuyanagi, Phys. Rev. C **88**, 011602(R) (2013).
[13] A. S. Umar and V. E. Oberacker, Phys. Rev. C **74**, 021601(R) (2006).
[14] A. S. Umar and V. E. Oberacker, Eur. Phys. J. A **39**, 243 (2009).
[15] A. S. Umar, C. Simenel, and V. E. Oberacker, Phys. Rev. C **89**, 034611 (2014).
[16] R. Keser, A. S. Umar, and V. E. Oberacker, Phys. Rev. C **85**, 044606 (2012).
[17] M. Bolsterli *et al.*, Phys. Rev. C **5**, 1050 (1972).
[18] G. Royer and B. Remaud, Nucl. Phys. A **444**, 477 (1985).
[19] P. Möller *et al.*, At. Data Nucl. Data Tables **59**, 185 (1995).
[20] S. Shlomo and G. Bertsch, Nucl. Phys. A **243**, 507 (1975).

Microscopic derivation of the quadrupole collective Hamiltonian for shape coexistence/mixing dynamics

2016 J. Phys. G: Nucl. Part. Phys. 43 024006

(http://iopscience.iop.org/0954-3899/43/2/024006)

IOP Publishing Journal of Physics G: Nuclear and Particle Physics
J. Phys. G: Nucl. Part. Phys. **43** (2016) 024006 (20pp) doi:10.1088/0954-3899/43/2/024006

Microscopic derivation of the quadrupole collective Hamiltonian for shape coexistence/mixing dynamics

Kenichi Matsuyanagi[1,2], Masayuki Matsuo[3], Takashi Nakatsukasa[1,4], Kenichi Yoshida[5], Nobuo Hinohara[4,6] and Koichi Sato[1]

[1] RIKEN Nishina Center, Wako 351-0198, Japan
[2] Yukawa Institute for Theoretical Physics, Kyoto University, Kyoto 606-8502, Japan
[3] Department of Physics, Faculty of Science, Niigata University, Niigata 950-2181, Japan
[4] Center for Computational Sciences, University of Tsukuba, Tsukuba 305-8571, Japan
[5] Graduate School of Science and Technology, Niigata University, Niigata 950-2181, Japan
[6] National Superconducting Cyclotron Laboratory, Michigan State University, East Lansing, MI 48824-1321, USA

Received 4 July 2015, revised 20 August 2015
Accepted for publication 3 September 2015
Published 14 January 2016

Abstract

Assuming that the time-evolution of the self-consistent mean field is determined by five pairs of collective coordinate and collective momentum, we microscopically derive the collective Hamiltonian for low-frequency quadrupole modes of excitation. We show that the five-dimensional collective Schrödinger equation is capable of describing large-amplitude quadrupole shape dynamics seen as shape coexistence/mixing phenomena. We focus on basic ideas and recent advances of the approaches based on the time-dependent mean-field theory, but relations to other time-independent approaches are also briefly discussed.

Keywords: collective Hamiltonian, large-amplitude collective motion, shape coexistence, time-dependent self-consistent mean field

(Some figures may appear in colour only in the online journal)

1. Introduction

In this paper, we focus on low-frequency quadrupole motions which play the major role in low-energy excitation spectra. As is well known, various giant resonances appearing in highly

excited states are well described by the random-phase approximation (RPA), which is a small-amplitude approximation of the time-dependent Hartree–Fock (TDHF) theory. In contrast to the giant resonances, low-frequency quadrupole vibrations exhibit characteristic features associated with superfluidity of the finite quantum system (nucleus), that is, pairing correlations and varying shell structure of the self-consistent mean field play essential roles [1–4].

1.1. Quantum shape fluctuation, shape mixing and shape coexistence

The low-frequency quadrupole vibrations can be regarded as soft modes of the quantum phase transition towards equilibrium deformations of the mean field. As is well known, in nuclei situated in the transitional region from spherical to deformed, amplitudes of quantum shape fluctuation about the equilibrium remarkably increase. This is the case also for weakly deformed nuclei where the gain in binding energies due to the symmetry breaking is comparable in magnitude to the vibrational zero-point energies. The transitional region is wide and those nuclei exhibit quite rich excitation spectra. This is a characteristic feature of finite quantum systems and provides an invaluable opportunity to investigate the process of the quantum phase transition through analysis of quantum spectra. To describe such large-amplitude collective motions (LACM), we need to go beyond the small-amplitude approximation (quasiparticle RPA (QRPA)) of the time-dependent Hartree–Fock–Bogoliubov (TDHFB) theory for superfluid systems. It is required to develop a microscopic theory of LACM capable of describing the varying shell structure associated with the time-dependent mean field with superfluidity.

The spherical shell structure gradually changes with the growth of deformation and generates 'deformed shell structures' and 'deformed magic numbers,' that stabilize certain deformed shapes of the mean field. When a few local minima of the mean field with different shapes appear in the same energy region, LACM tunneling through potential barriers and extending between local minima may take place. These phenomena may be regarded as a kind of macroscopic quantum tunneling. Note that the barriers are not generated by external fields but self-consistently generated as a consequence of quantum dynamics of the many-body system under consideration. Quantum spectra of low-energy excitation that needs such concepts have been observed in almost all regions of the nuclear chart [5]. When different kinds of quantum eigenstates associated with different shapes coexist in the same energy region, we may call them '*shape coexistence phenomena.*' This is the case when shape mixing due to tunneling motion is weak and collective wave functions retain their localizations about different equilibrium shapes. On the other hand, if the shape mixing is strong, large-amplitude shape fluctuations (*delocalization* of the collective wave functions) extending to different local minima may occur.

1.2. Collective rotations restoring broken symmetries

As is well known, the central concept of the BCS theory of superconductivity is spontaneous breaking of the gauge symmetry and emergence of collective modes. The massless modes restoring the broken symmetry are called Anderson–Nambu–Goldstone (ANG) modes [6–8]. As emphasized by Bohr and Mottelson, nuclear rotation can be regarded as an ANG mode restoring the broken rotational symmetry in real space [1, 9].

In finite quantum systems such as nuclei, the rotational ANG modes may couple rather strongly with quantum shape-fluctuation modes. For instance, even when the self-consistent mean field acquires a deep local minimum at a finite value of β, the nucleus may exhibit a large-amplitude shape fluctuation in the γ degree of freedom, if the deformation potential is

flat in this direction. Here, as usual, β and γ represent the magnitudes of axially symmetric and asymmetric quadrupole deformations, respectively. Such a situation is widely observed in experiments and called γ-soft. Although the quantum-mechanical collective rotation is forbidden about the symmetry axis, the rotational degrees of freedoms about three principal axes are all activated once the axial symmetry is dynamically broken due to the quantum shape fluctuation. Rotational spectra in such γ-soft nuclei do not exhibit a simple $I(I+1)$ pattern. Such an interplay of the shape-fluctuation and rotational modes may be regarded as a characteristic feature of finite quantum systems and provides an invaluable opportunity to investigate the process of the quantum phase transition through analysis of quantum spectra.

Thus, we need to treat the two kinds of collective variables, i.e., those associated with the symmetry-restoring ANG modes and those for quantum shape fluctuations, in a unified manner to describe low-energy excitation spectra of nuclei.

1.3. Five-dimensional (5D) quadrupole collective Hamiltonian

Vibrational and rotational motions of the nucleus can be described as time-evolution of a self-consistent mean field. This is the basic idea underlying the unified model of Bohr and Mottelson [10, 11]. In this approach, the 5D collective Hamiltonian describing the quadrupole vibrational and rotational motions is given by [1, 12]

$$H_{\rm coll} = T_{\rm vib} + T_{\rm rot} + V(\beta, \gamma), \tag{1}$$

$$T_{\rm vib} = \frac{1}{2}D_{\beta\beta}(\beta, \gamma)\dot{\beta}^2 + D_{\beta\gamma}(\beta, \gamma)\dot{\beta}\dot{\gamma} + \frac{1}{2}D_{\gamma\gamma}(\beta, \gamma)\dot{\gamma}^2, \tag{2}$$

$$T_{\rm rot} = \sum_k \frac{I_k^2}{2\mathcal{J}_k(\beta, \gamma)}. \tag{3}$$

Here, β and γ are treated as dynamical variables, and $\dot{\beta}$ and $\dot{\gamma}$ represent their time-derivatives. They are related to expectation values of the quadruple operators (with respect to the time-dependent mean-field states) and their variations in time. The quantities ($D_{\beta\beta}$, $D_{\beta\gamma}$, and $D_{\gamma\gamma}$) appearing in the kinetic energies of vibrational motion, $T_{\rm vib}$, represent inertial masses of the vibrational motion. They are functions of β and γ. The quantities I_k and $\mathcal{J}_k(\beta, \gamma)$ in the rotational energy $T_{\rm rot}$ represent the three components of the angular momentum and the corresponding moments of inertia, respectively. Note that they are defined with respect to the principal axes of the body-fixed (intrinsic) frame that is attached to the instantaneous shape of the time-dependent mean-field.

In the case that the potential energy $V(\beta, \gamma)$ has a deep minimum at a finite value of β and $\gamma = 0^\circ$ (or $\gamma = 60^\circ$), a regular rotational spectrum with the $I(I+1)$ pattern may appear. In addition to the ground band, we can expect the β and γ bands to appear, where vibrational quanta with respect to the β and γ degrees of freedom are excited. Detailed investigations on the γ-vibrational bands over many nuclei have revealed, however, that they usually exhibit significant anharmonicities (non-linearlities) [13]. Also for the β-vibrational bands, it has been known [14–16] that they couple, sometimes very strongly, with pairing-vibrational modes (associated with fluctuations of the pairing gap). Recent experimental data indicate the need for a radical review of their characters [5].

1.4. Collective quantization of time-dependent mean fields

States vectors of time-dependent mean field are kinds of generalized coherent states, and we can rigorously formulate the TDHFB as a theory of classical Hamiltonian dynamical system

of large dimension [17–20]. Because time-evolution of the mean field is determined by the classical Hamilton equations, we cannot describe, within the framework of the TDHFB, quantum spectra of low-lying states and macroscopic quantum tunneling phenomena such as spontaneous fissions and subbarrier fusions. To describe these genuine quantum phenomena, we need to introduce a few collective variables determining the time-evolution of the mean field and quantize them. We refer this procedure '*collective quantization.*'

For small-amplitude vibrations about an HFB equilibrium, it is well known that we can introduce collective variables in a microscopic way by solving the QRPA equations. Single-particle spectra for a mean-field of a finite quantum system have rich shell structures, and thereby a variety of collective vibrational modes emerge. Even within the isoscalar quadrupole vibrations, two collective modes appear exhibiting quite different characteristics; the low- (usually first excited 2^+) and high-frequency (giant resonance) modes. One of the merits of the QRPA is that we can determine the microscopic structures of the collective coordinates and momenta starting from a huge number of microscopic (particle–hole, particle–particle, and hole–hole) degrees of freedom. We can thus learn how collective vibrations are generated as coherent superpositions of many two-quasiparticle excitations. Examining the microscopic structure of the low-frequency quadrupole vibrations, we see that the weights of two-quasiparticle excitations near the Fermi surface are much larger than those in the mass quadrupole operators (see, e.g., [21]). This clearly indicates the importance of describing collective modes in a microscopic way. Another merit of the QRPA is that it yields the ANG modes and their collective masses (inertial functions). In this way, we can restore the symmetries broken by the mean-field approximation [8, 22, 23].

It has been one of the longstanding fundamental subjects in nuclear structure physics to construct a microscopic theory of LACM by extending the QRPA concepts to non-equilibrium states [24–26]. Below we shall briefly review various ideas proposed up to now for this aim.

2. Basic ideas of large-amplitude collective motion

During the attempts to construct a microscopic theory of LACM since the latter half of the 1970s, significant progress has been achieved in the fundamental concepts of collective motion. Especially important is the recognition that microscopic derivation of the collective Hamiltonian is equivalent to extraction of a collective submanifold embedded in the TDHFB phase space, which is approximately decoupled from other non-collective degrees of freedom. From this point of view we can say that collective variables are nothing but local canonical variables which can be flexibly chosen on this submanifold. Below we review recent developments achieved on the basis of such concepts.

2.1. Extraction of collective submanifold

Attempts to formulate a LACM theory without assuming adiabaticity of large-amplitude collective motion were initiated by Rowe and Bassermann [27] and Marumori [28], and led to the formulation of the self-consistent collective coordinate (SCC) method [29]. In these approaches, collective coordinates and collective momenta are treated on the same footing. In the SCC method, basic equations determining the collective submanifold are derived by requiring maximal decoupling of the collective motion of interest and other non-collective degrees of freedom. The collective submanifold is a geometrical object that is invariant with respect to the choice of the coordinate system whereas the collective coordinates depend on it. The idea of coordinate-independent theory of collective motion was developed also by Rowe

[30] and Yamamura and Kuriyama [19]. This idea gave a deep impact on the fundamental question '*what are the collective variables.*' The SCC method was first formulated for TDHF, but later extended to TDHFB for describing nuclei with superfluidity [31].

In the SCC method, under the assumption that time evolution is governed by a few collective coordinates $q = (q_1, q_2, \ldots, q_f)$ and collective momenta $p = (p_1, p_2, \ldots, p_f)$, the TDHFB states vectors are written as

$$|\phi(t)\rangle = |\phi(q, p)\rangle = \mathrm{e}^{\mathrm{i}\hat{G}(q,p)} \left|\phi_0\right\rangle, \tag{4}$$

or equivalently,

$$|\phi(t)\rangle = \left|\phi\left(\eta, \eta^*\right)\right\rangle = \mathrm{e}^{\mathrm{i}\hat{G}(\eta,\eta^*)} \left|\phi_0\right\rangle, \tag{5}$$

where $\left|\phi_0\right\rangle$ denotes the HFB ground state and $\eta = (\eta_1, \eta_2, \ldots, \eta_f)$ with

$$\eta_i = \frac{1}{\sqrt{2}}\left(q_i + \mathrm{i}p_i\right), \qquad \eta_i^* = \frac{1}{\sqrt{2}}\left(q_i - \mathrm{i}p_i\right). \tag{6}$$

The TDHFB states $|\phi(t)\rangle$ are required to fulfill the canonical variable conditions

$$\left\langle\phi\left(\eta, \eta^*\right)\right| \frac{\partial}{\partial\eta_i} \left|\phi\left(\eta, \eta^*\right)\right\rangle = \frac{1}{2}\eta_i^*, \tag{7}$$

$$\left\langle\phi\left(\eta, \eta^*\right)\right| \frac{\partial}{\partial\eta_i^*} \left|\phi\left(\eta, \eta^*\right)\right\rangle = -\frac{1}{2}\eta_i, \tag{8}$$

which guarantee that (q, p) are canonical conjugate pairs. The one-body operator $\hat{G}(\eta, \eta^*)$ is determined by the time-dependent variational principle

$$\delta\left\langle\phi\left(\eta, \eta^*\right)\right| \mathrm{i}\frac{\partial}{\partial t} - H \left|\phi\left(\eta, \eta^*\right)\right\rangle = 0 \tag{9}$$

with

$$\frac{\partial}{\partial t} = \sum_i \left(\dot{\eta}_i \frac{\partial}{\partial\eta_i} + \dot{\eta}_i^* \frac{\partial}{\partial\eta_i^*} \right), \tag{10}$$

and the canonical variable conditions.

Making a power-series expansion of $\hat{G}$ with respect to (η, η^*),

$$\hat{G}\left(\eta, \eta^*\right) = \sum_i \left(\hat{G}_i^{(10)}\eta_i^* + \hat{G}_i^{(01)}\eta_i \right) + \sum_{ij} \left(\hat{G}_{ij}^{(20)}\eta_i^*\eta_j^* + \hat{G}_{ij}^{(11)}\eta_i^*\eta_i + \hat{G}_{ij}^{(02)}\eta_i\eta_j \right) + \ldots \tag{11}$$

and requiring that the time-dependent variational principle holds for every power of (η, η^*), we can successively determine the one-body operators $\hat{G}^{(m,n)}$ with $m+n = 1, 2, 3 \ldots$. This method of solution is called the (η, η^*) expansion method. The collective Hamiltonian is defined by the expectation value of the microscopic Hamiltonian with respect to $|\phi(\eta, \eta^*)\rangle$. Because (η, η^*) are canonical variables, they are replaced by boson operators after canonical quantization. The lowest linear order corresponds to the QRPA. Accordingly, the collective variables (η_i, η_i^*) correspond to specific QRPA modes in the small-amplitude limit. It is important to note, however, that the microscopic structure of $\hat{G}$ changes as a function of (η_i, η_i^*) due to the mode-mode coupling effects among different QRPA modes in the higher order. In this sense, the SCC method may be regarded as a dynamical extension of the boson expansion method [32]. Thus, the SCC is a powerful method of treating anharmonic effects to the QRPA vibrations originating from mode–mode couplings, as shown in its application to the two-phonon states of anharmonic γ vibration [13, 33]. The SCC method was also used for

derivation of the 5D quadrupole collective Hamiltonian and analysis of the quantum phase transition from spherical to deformed shapes [34], and for constructing diabatic representation in the rotating shell model [35].

2.2. Solution with adiabatic expansion

The (η, η^*) expansion about an HFB equilibrium point is not suitable for treating situations such as shape coexistence, where a few local minima energetically compete in the HFB potential energy surface. For describing adiabatic LACM extending over different HFB local minima, a new method has been proposed [36]. In this method, the basic equations of the SCC method are solved by an expansion with respect to the collective momenta. It is called 'adiabatic SCC (ASCC) method.' Similar methods have been developed also by Klein *et al* [37], and Almehed and Walet [38].

Let us assume that the TDHFB state vector can be written as

$$|\phi(q, p)\rangle = \mathrm{e}^{\mathrm{i}\sum_i p_i \hat{Q}^i(q)}\, |\phi(q)\rangle. \tag{12}$$

Here, $\hat{Q}^i(q)$ are one-body operators, called infinitesimal generators, and $|\phi(q)\rangle$ is an intrinsic state at the collective coordinate q, called a moving frame HFB state.

We determine the microscopic structures of $\hat{Q}^i(q)$ and $|\phi(q)\rangle$ by the time-dependent variational principle

$$\delta \langle \phi(q, p)|\, \mathrm{i}\frac{\partial}{\partial t} - \hat{H}\, |\phi(q, p)\rangle = 0. \tag{13}$$

Making power-series expansions with respect to the collective momenta p and retaining terms up to the second order in p, we obtain

moving-frame HFB equation

$$\delta \langle \phi(q)|\, \hat{H}_M(q)|\phi(q)\rangle = 0, \tag{14}$$

moving-frame QRPA equations (*local harmonic equations*)

$$\delta \langle \phi(q)|\left[\hat{H}_M(q),\, \hat{Q}^i(q)\right] - \frac{1}{\mathrm{i}}\sum_k B^{ik}(q)\hat{P}_k(q) + \frac{1}{2}\left[\sum_k \frac{\partial V}{\partial q^k}\hat{Q}^k(q),\, \hat{Q}^i(q)\right]|\phi(q)\rangle = 0, \tag{15}$$

$$\delta \langle \phi(q)|\left[\hat{H}_M(q),\, \frac{1}{\mathrm{i}}\hat{P}_i(q)\right] - \sum_j C_{ij}(q)\hat{Q}^j(q) - \frac{1}{2}\left[\left[\hat{H}_M(q),\, \sum_k \frac{\partial V}{\partial q^k}\hat{Q}^k(q)\right],\, \sum_j B_{ij}(q)\hat{Q}^j(q)\right]|\phi(q)\rangle = 0, \tag{16}$$

where $\hat{H}_M(q)$ represents the Hamiltonian in the frame attached to the moving mean field,

$$\hat{H}_M(q) = \hat{H} - \sum_i \frac{\partial V}{\partial q^i}\hat{Q}^i(q), \tag{17}$$

and is called 'moving-frame Hamiltonian.' The displacement operators $\hat{P}_i(q)$ and $C_{ij}(q)$ are defined by

$$\hat{P}_i(q)|\phi(q)\rangle = \mathrm{i}\frac{\partial}{\partial q^i}\, |\phi(q)\rangle \tag{18}$$

and

$$C_{ij}(q) = \frac{\partial^2 V}{\partial q^i \partial q^j} - \sum_k \Gamma^k_{ij} \frac{\partial V}{\partial q^k}, \tag{19}$$

respectively, with

$$\Gamma^k_{ij}(q) = \frac{1}{2} \sum_l B^{kl} \left(\frac{\partial B_{li}}{\partial q^j} + \frac{\partial B_{lj}}{\partial q^i} - \frac{\partial B_{ij}}{\partial q^l} \right). \tag{20}$$

The double-commutator term in equation (16) arises from the q-derivative of the infinitesimal generators $\hat{Q}^i(q)$ and represents the curvatures of the collective submanifold.

Solving these equations self-consistently, we can determine the microscopic expressions of the infinitesimal generators $\hat{Q}^i(q)$ and $\hat{P}_i(q)$ in bilinear forms of the quasiparticle creation and annihilation operators defined locally with respect to $|\phi(q)\rangle$. The collective Hamiltonian is given by

$$\begin{aligned} \mathcal{H}(q, p) &= \langle \phi(q, p)| \, \hat{H} \, |\phi(q, p)\rangle \\ &= V(q) + \frac{1}{2} \sum_{ij} B^{ij}(q) p_i p_j \end{aligned} \tag{21}$$

with

$$V(q) = \mathcal{H}(q, p)|_{p=0}, \qquad B^{ij}(q) = \frac{\partial^2 \mathcal{H}}{\partial p_i \partial p_j} \, |_{p=0}, \tag{22}$$

where $V(q)$ and $B^{ij}(q)$ represent the collective potential and the reciprocals of collective inertial mass, respectively. They are functions of the collective coordinate q. Note that equations (14)–(16) reduce to the HFB and QRPA equations at equilibrium points, where $\partial V/\partial q^i = 0$; namely, they are natural extensions of the HFB-QRPA equations to non-equilibrium states.

Let us note the following points.

- *Difference from the constrained HFB equations*. The moving-frame HFB equation (14) resembles the constrained HFB equation, but the infinitesimal generators $\hat{Q}^i(q)$ are here self-consistently determined together with $\hat{P}_i(q)$ as solutions of the moving-frame QRPA equations (15) and (16) at every point of the collective coordinate q. Thus, contrary to constrained operators in the constrained HFB theory, their microscopic structures change as functions of q. In other words, the optimal 'constraining' operators are locally determined at every point of q. The collective submanifold embedded in the TDHFB phase space is extracted in this way. The canonical quantization of the collective Hamiltonian described by a few collective variables (q, p) is similar to the quantization of constrained system [30], but the 'constraints' are here generated by the dynamics of the quantum many-body system under consideration.
- *Meaning of the term 'adiabatic'*. It is used here in the meaning that we can solve the time-dependent variational equation (13) in a good approximation by taking into account up to the second order in an expansion with respect to the collective momenta p. It is important to note that the effects of finite frequency of the LACM are taken into account through the moving-frame QRPA equations. No assumption is made like that the kinetic energy of LACM is much smaller than the lowest two-quasiparticle excitation energy at every point of q.
- *Physics of collective inertial mass*. The collective inertial mass represents the inertia of the many-body system against an infinitesimal change of the collective coordinate q

during the time evolution of the mean field. It is a local quantity and varies as a function of q. As the single-particle-energy spectrum in the mean field changes as a function of q, level crossing at the Fermi energy successively occurs during the LACM. In the presence of the pairing correlation, the many-body system can easily rearrange the lowest-energy configurations at every value of q, i.e., the system can easily change q. The easiness/hardness of the configuration rearrangements at the level crossings determines the adiabaticity/diabaticity of the system. Since the inertia represents a property of the system trying to keep a definite configuration, we expect that the stronger the pairing correlation becomes, the smaller the collective inertial mass becomes [39]. It remains as an interesting subject to investigate how the self-consistent determination of the optimal directions of collective motion and the finite frequency $\omega(q)$ of the moving-frame QRPA modes affect the level-crossing dynamics of the superfluid nuclear systems.

2.3. Consideration of gauge invariance

In the QRPA, the ANG modes such as the number-fluctuation (pairing rotational) modes are decoupled from other normal modes and thereby the QRPA restores the gauge invariance (number conservation) broken in the HFB mean field [8]. It is desirable to keep such a merits of the QRPA beyond the small-amplitude approximation. Otherwise, spurious number-fluctuation modes would unexpectedly mix in the LACM of interest. We can take into account the gauge invariance in the following way [40]. Introducing the number-fluctuation variables $n^{(\tau)}$ and the gauge angles $\varphi^{(\tau)}$ conjugate to them, we write the TDHFB state vector (12) in a more general form:

$$|\phi(q, p, \varphi, n)\rangle = \mathrm{e}^{-\mathrm{i}\sum_\tau \varphi^{(\tau)}\tilde{N}^{(\tau)}} \, |\phi(q, p, n)\rangle \tag{23}$$

with

$$|\phi(q, p, n)\rangle = \mathrm{e}^{\mathrm{i}\hat{G}(q,p,n)} \, |\phi(q)\rangle \tag{24}$$

and

$$\hat{G}(q, p, n) = \sum_i p_i \hat{Q}^i(q) + \sum_{\tau=n,p} n^{(\tau)} \hat{\Theta}^{(\tau)}(q). \tag{25}$$

Here $\tilde{N}^{(\tau)} \equiv \hat{N}^{(\tau)} - N_0^{(\tau)}$ are the number-fluctuation operators measured from $N_0^{(\tau)} \equiv \langle\phi(q)| \, \hat{N}^{(\tau)} \, |\phi(q)\rangle$, with the suffix τ distinguishing protons and neutrons, and $\hat{\Theta}^{(\tau)}(q)$ infinitesimal generators for the pairing-rotation degrees of freedom. The state vector $|\phi(q, p, n)\rangle$ may be regarded as an intrinsic state to the pairing rotation. Using $|\phi(q, p, \varphi, n)\rangle$ in place of $|\phi(q, p)\rangle$ in equation (13) and expanding it in $n^{(\tau)}$ as well as p up to the second order, we can determine $\hat{\Theta}^{(\tau)}(q)$ simultaneously with $\hat{Q}^i(q)$ and $\hat{P}^i(q)$ such that the moving-frame HFB + QRPA equations become invariant against the rotation of the gauge angle $\varphi^{(\tau)}$. The gauge invariance of the resulting equations implies that we need to fix a gauge in numerical applications. A convenient procedure of the gauge fixing is discussed in [40].

3. Microscopic derivation of the 5D quadrupole collective Hamiltonian

For collective submanifolds of two dimensions (2D) or more, large-scale numerical computation is needed to find fully self-consistent solutions of the ASCC equations. Then, a practical approximation scheme, called local QRPA (LQRPA) method, has been developed [41–43]. This scheme may be regarded as a first step of iterative solution of equations (14)–

(16). With use of it, we can easily derive the 5D collective Hamiltonian. We first derive the 2D collective Hamiltonian for vibrational motions corresponding to the (β, γ) deformations, and then consider the three-dimensional (3D) rotational motions.

First, we solve the constrained HFB equation

$$\delta \langle \phi(\beta, \gamma)| \hat{H}_{\rm CHFB}(\beta, \gamma)|\phi(\beta, \gamma)\rangle = 0 \tag{26}$$

with

$$\hat{H}_{\rm CHFB}(\beta, \gamma) = \hat{H} - \sum_{\tau} \lambda^{(\tau)}(\beta, \gamma)\tilde{N}^{(\tau)} - \sum_{m=0,2} \mu_m(\beta, \gamma)\hat{D}^{(+)}_{2m},$$

where $\lambda^{(\tau)}(\beta, \gamma)$, $\mu_m(\beta, \gamma)$ and $\hat{D}^{(+)}_{2m}$ are the chemical potentials, the Lagrange multipliers, and the quadrupole operators, respectively. The quadrupole deformation parameters (β, γ) are defined by

$$\beta \cos\gamma = \eta D^{(+)}_{20} = \eta \langle \phi(\beta, \gamma)| \hat{D}^{(+)}_{20} |\phi(\beta, \gamma)\rangle, \tag{27}$$

$$\frac{1}{\sqrt{2}}\beta \sin\gamma = \eta D^{(+)}_{22} = \eta \langle \phi(\beta, \gamma)| \hat{D}^{(+)}_{22} |\phi(\beta, \gamma)\rangle, \tag{28}$$

where η is a scaling factor [1, 44].

Next, we solve

$$\delta \langle \phi(\beta, \gamma)|\Big[\hat{H}_{\rm CHFB}(\beta, \gamma), \hat{Q}^i(\beta, \gamma)\Big] - \frac{1}{i}\hat{P}_i(\beta, \gamma)|\phi(\beta, \gamma)\rangle = 0, \quad (i = 1, 2) \tag{29}$$

$$\delta \langle \phi(\beta, \gamma)|\Big[\hat{H}_{\rm CHFB}(\beta, \gamma), \frac{1}{i}\hat{P}_i(\beta, \gamma)\Big] - C_i(\beta, \gamma)\hat{Q}^i(\beta, \gamma)|\phi(\beta, \gamma)\rangle = 0. \quad (i = 1, 2) \tag{30}$$

These are the moving-frame QRPA equations without the curvature terms and called local QRPA (LQRPA) equations. Making a similarity transformation such that the collective masses corresponding to the collective coordinates (q_1, q_2) become unity, we can write the kinetic energy of vibrational motions as

$$T_{\rm vib} = \frac{1}{2}\sum_{i=1,2}(p_i)^2 = \frac{1}{2}\sum_{i=1,2}\left(\dot{q}^i\right)^2 \tag{31}$$

without loss of generality. Changes of the quadrupole deformation due to variations with respect to (q_1, q_2) are given by

$$\mathrm{d}D^{(+)}_{2m} = \sum_{i=1,2}\frac{\partial D^{(+)}_{2m}}{\partial q^i}\mathrm{d}q^i. \qquad (m = 0, 2) \tag{32}$$

Thus, the kinetic energy of vibrational motions is given in terms of time derivatives of the quadrupole deformation,

$$T_{\rm vib} = \frac{1}{2}M_{00}\Big[\dot{D}^{(+)}_{20}\Big]^2 + M_{02}\dot{D}^{(+)}_{20}\dot{D}^{(+)}_{22} + \frac{1}{2}M_{22}\Big[\dot{D}^{(+)}_{22}\Big]^2, \tag{33}$$

where

$$M_{mm'}(\beta, \gamma) = \sum_{i=1,2}\frac{\partial q^i}{\partial D^{(+)}_{2m}}\frac{\partial q^i}{\partial D^{(+)}_{2m'}}. \tag{34}$$

It is straightforward to rewrite the above expression using the time derivatives of (β, γ). Subsequently we solve the LQRPA equations for 3D rotational motions at every point on the (β, γ) plane to obtain the inertial functions $D_k(\beta, \gamma)$ and the moments of inertia $\mathcal{J}_k(\beta, \gamma) = 4\beta^2 D_k(\beta, \gamma)\sin^2(\gamma - 2\pi k/3)$ determining the rotational energy $T_{\rm rot}$. This step is the same as in Thouless and Valatin [45], except that the procedure is applied for non-equilibrium points of (β, γ) as well as the equilibrium points in the potential energy surface $V(\beta, \gamma)$.

After quantizing in curvilinear coordinates (so-called Pauli prescription) [46], we obtain the quantized 5D quadrupole collective Hamiltonian,

$$\hat{H}_{\rm coll} = \hat{T}_{\rm vib} + \hat{T}_{\rm rot} + V(\beta, \gamma), \tag{35}$$

whose vibrational kinetic-energy term takes the following form:

$$\hat{T}_{\rm vib} = \frac{-\hbar^2}{2\sqrt{WR}}\left\{\frac{1}{\beta^3}\left[\frac{\partial}{\partial\beta}\left(\beta^3\sqrt{\frac{R}{W}}D_{\gamma\gamma}\frac{\partial}{\partial\beta}\right) - \frac{\partial}{\partial\beta}\left(\beta^3\sqrt{\frac{R}{W}}D_{\beta\gamma}\frac{\partial}{\partial\gamma}\right)\right]\right. \tag{36}$$

$$\left. + \frac{1}{\sin 3\gamma}\left[-\frac{\partial}{\partial\gamma}\left(\sqrt{\frac{R}{W}}\sin 3\gamma D_{\beta\gamma}\frac{\partial}{\partial\beta}\right) + \frac{\partial}{\partial\gamma}\left(\sqrt{\frac{R}{W}}\sin 3\gamma D_{\beta\beta}\frac{\partial}{\partial\gamma}\right)\right]\right\}, \tag{37}$$

where

$$W = D_{\beta\beta}(\beta, \gamma)D_{\gamma\gamma}(\beta, \gamma) - D^2_{\beta\gamma}(\beta, \gamma), \tag{38}$$

$$R = D_1(\beta, \gamma)D_2(\beta, \gamma)D_3(\beta, \gamma). \tag{39}$$

If the inertial functions $(D_{\beta\beta}, D_{\gamma\gamma}, D_1, D_2, D_3)$ are replaced by a common constant D and $D_{\beta\gamma}$ by 0, the above expression is reduced to

$$\hat{T}_{\rm vib} = -\frac{\hbar^2}{2D}\left(\frac{1}{\beta^4}\frac{\partial}{\partial\beta}\beta^4\frac{\partial}{\partial\beta} + \frac{1}{\beta^2\sin 3\gamma}\frac{\partial}{\partial\gamma}\sin 3\gamma\frac{\partial}{\partial\gamma}\right). \tag{40}$$

Such a drastic approximation may be valid only for small-amplitude vibrations about a spherical HFB equilibrium.

Writing the collective wave functions as

$$\Psi_{\alpha\, IM}(\beta, \gamma, \Omega) = \sum_{K={\rm even}} \Phi_{\alpha IK}(\beta, \gamma)\langle\Omega|IMK\rangle, \tag{41}$$

$$\langle\Omega|IMK\rangle = \sqrt{\frac{2I+1}{16\pi^2(1+\delta_{K0})}}\left[\mathcal{D}^I_{MK}(\Omega) + (-)^I\mathcal{D}^I_{M-K}(\Omega)\right] \tag{42}$$

and solving the eigenvalue equation for vibrational wave functions

$$\left[\hat{T}_{\rm vib} + V(\beta, \gamma)\right]\Phi_{\alpha IK}(\beta, \gamma) + \sum_{K'={\rm even}}\langle IMK|\,\hat{T}_{\rm rot}\,|IMK'\rangle\Phi_{\alpha IK'}(\beta, \gamma) = E_{\alpha I}\Phi_{\alpha IK}(\beta, \gamma), \tag{43}$$

we obtain quantum spectra of quadrupole collective motion. The symmetries and boundary conditions of the vibrational wave functions are discussed in [47].

4. Illustrative examples

We here present some applications of the LQRPA method for deriving the 5D collective Hamiltonian. In the numerical examples below, the pairing-plus-quadrupole (P + Q) model Hamiltonian [48] (including the quadrupole-pairing interaction) is employed in solving the CHFB + LQRPA equations. The single-particle energies and the P + Q interaction strengths are determined such that the results of the Skyrme-HFB calculation for the ground states are best reproduced within the P + Q model (see [42, 49] for details). The LQRPA method is quite general and it can be used in conjunction with various Skyrme interactions or modern density functionals. A large-scale calculation is required, however, and such an application of the LQRPA method with realistic interactions/functionals is a challenging future subject. A step toward this goal has recently been carried out for axially symmetric cases [50]. More examples can be found in [41, 51] for $^{68-72}$Se, [42] for ^{72,74,76}Kr, [52] for the ^{26}Mg region, [49] for $^{30-34}$Mg, [50] for $^{58-68}$Cr, [43] for $^{58-66}$Cr, and [53] for $^{128-132}$Xe and $^{130-134}$Ba.

4.1. Oblate–prolate shape coexistence and fluctuations in ^{72}Kr

The collective potential $V(\beta, \gamma)$ depicted in figure 1 exhibits two local minima. The oblate minimum is lower than the prolate minimum. This is expected from the deformed shell structure which gives rise to an oblate magic number at $Z = N = 36$. This figure also shows that the valley runs in the triaxially deformed region and the barrier connecting the oblate and prolate minima is low. Accordingly, one may expect large-amplitude quantum shape fluctuations to occur along the triaxial valley. In fact, the vibrational wave function of the ground 0_1^+ state peaks around the oblate potential minimum, but its tail extends to the prolate region. The vibrational wave function of the excited 0_2^+ state consists of two components: one is a sharp peak on the oblate side and the other is a component spreading around the prolate region somewhat broadly. It is interesting to notice that, as the angular momentum increases, the localization of the vibrational wave functions in the (β, γ) deformation plane develops; namely, the rotational effect plays an important role for the emergence of the shape-coexistence character.

We note that not only the vibrational inertial masses shown in figure 1 but also the rotational inertial functions (D_1, D_2, and D_3) and the pairing gaps significantly change as functions of (β, γ). Due to the time-odd contributions of the moving HFB self-consistent field, the collective inertial masses calculated with the LQRPA method are 20%–50% larger than those evaluated with the Inglis–Belyaev cranking formula. Their ratios also change as functions of (β, γ) [42]. As a consequence, as shown in figure 2, the excitation spectrum calculated with the LQRPA masses is in much better agreement with experimental data than that with the Inglis–Belyaev cranking masses.

4.2. Quantum shape transitions and fluctuations in ^{30,32,34}Mg

This is a new region of quantum shape transition currently under live discussions toward understanding the nature of the quadrupole deformation in these neutron-rich isotopes as well as the mechanism of its emergence.

Figure 3 shows the collective potentials $V(\beta, \gamma)$ and the vibrational wave functions squared, $\sum_K |\Phi_{\alpha IK}(\beta, \gamma)|^2$, of the 0_1^+, 2_1^+, and 0_2^+ states in ^{30,32,34}Mg. It is clearly seen that prolate deformation grows with the neutron number. The deformed magic numbers, $Z = 12$ of protons and $N = 20$, 22, 24 at different values of β of neutrons [56] act cooperatively for the appearance of the prolate minima. Interestingly, the vibrational wave functions of the 2_1^+ state

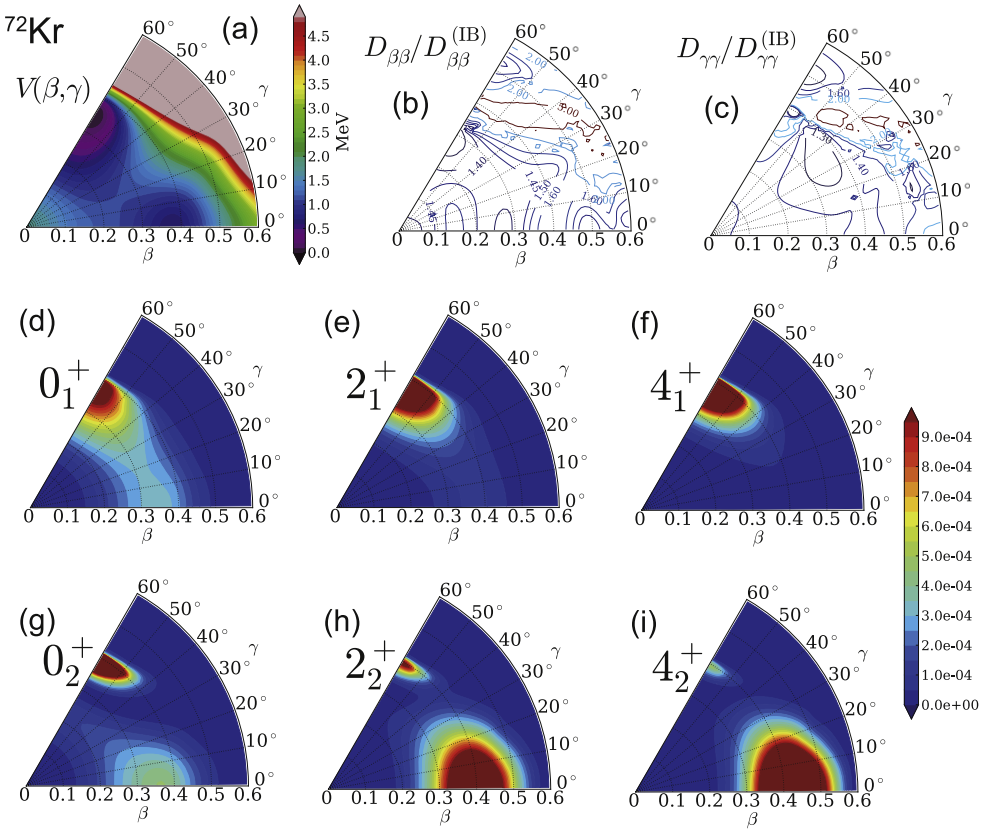

Figure 1. Application of the LQRPA method to the oblate–prolate shape coexistence/fluctuation phenomenon in ^{72}Kr (from [42]). (a) Collective potential $V(\beta, \gamma)$, (b) ratios of the collective inertial masses $D_{\beta\beta}(\beta, \gamma)$ to the Inglis–Belyaev cranking masses. (c) Same as (b) but for $D_{\gamma\gamma}(\beta, \gamma)$. Vibrational wave functions squared, $\sum_K \beta^4 |\Phi_{\alpha IK}(\beta, \gamma)|^2$, for (d) the 0^+_1 state, (e) the 2^+_1 state, (f) the 4^+_1 state, (g) the 0^+_2 state, (h) the 2^+_2 state, and (i) the 4^+_2 state. For the β^4 factor, see the text.

are noticeably different from those of the 0^+_1 state in ^{30}Mg and ^{32}Mg, while they are similar in ^{34}Mg.

In figure 4, we display the probability density of finding a shape with a specific value of β.

$$P(\beta) = \int \mathrm{d}\gamma |\Phi_{\alpha I=0,K=0}(\beta, \gamma)|^2 |G(\beta, \gamma)|^{1/2}. \tag{44}$$

Note that the volume element with $|G(\beta, \gamma)| = 4\beta^8 W(\beta, \gamma) R(\beta, \gamma) \sin^2 3\gamma$ is taken into account here. Let us first look at the ground 0^+_1 states. The peak position moves toward a larger value of β in going from ^{30}Mg to ^{34}Mg. The distribution for ^{32}Mg is much broader than those for ^{30}Mg and ^{34}Mg. Next, let us look at the excited 0^+_2 states. In ^{30}Mg, the bump at $\beta \simeq 0.1$ is much smaller than the major bump at $\beta \simeq 0.3$. In this sense, we can regard the 0^+_2 state of ^{30}Mg as a prolately deformed state. In the case of ^{32}Mg, the probability density exhibits a

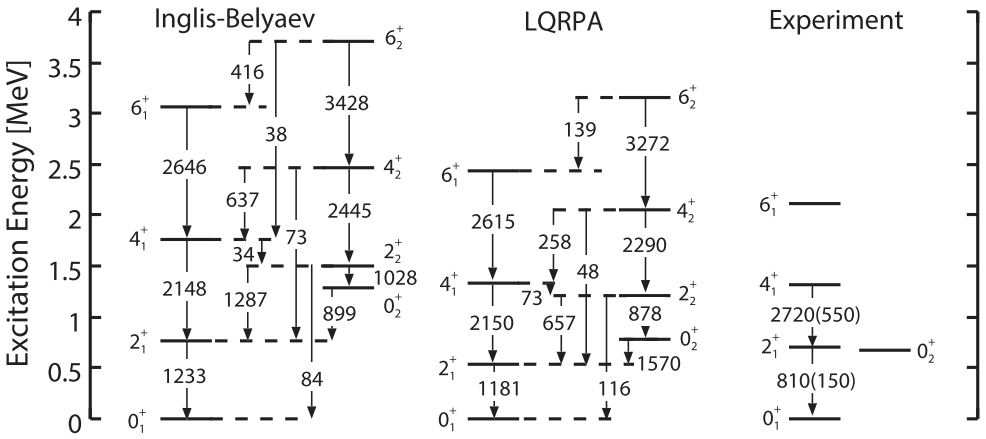

Figure 2. Excitation spectra and $B(E2)$ values calculated for ^{72}Kr by means of the CHB + LQRPA method (denoted by LQRPA) [42] and experimental data [54, 55]. For comparison, the results calculated using the Inglis–Belyaev cranking mass are also shown. Only $B(E2)$ larger than 1 Weisskopf unit are shown in units of e^2 fm^4.

very broad distribution extending from the spherical to deformed regions up to $\beta = 0.5$ with a prominent peak at $\beta \simeq 0.4$ and a node at $\beta \simeq 0.3$.

Thus, the shape coexistence picture that the deformed excited 0_2^+ state coexists with the spherical ground state approximately holds for ^{30}Mg. On the other hand, large-amplitude quadrupole-shape fluctuations dominate in both the ground and the excited 0^+ states in ^{32}Mg, in contrast to the interpretation of deformed ground and spherical excited 0^+ states [57] based on a naive picture of crossing between the spherical and deformed configurations. To test these theoretical predictions, an experimental search for the distorted rotational bands built on the excited 0_2^+ states in ^{30}Mg and ^{32}Mg is strongly desired.

5. Some remarks on other approaches

In section 2, we reviewed the basics of a microscopic theory of LACM focusing on new developments achieved after 2000. In this section, we give short remarks on other approaches to LACM. Typical approaches developed by 1980 are described in detail in the textbook of Ring and Schuck [22], and achievements during 1980–2000 are well summarized in the review by Do Dang, Klein, and Walet [58].

5.1. Constrained HFB + adiabatic perturbation

Historically, the Inglis–Belyaev cranking masses derived from the adiabatic perturbation theory [22] have been widely used in conjunction with phenomenological mean-field models, e.g. for the study of fission dynamics [59]. In recent years, it has become possible to carry out such studies using self-consistent mean fields obtained by solving the constrained HFB equations [60]. The Inglis–Belyaev cranking masses have also been used for low-frequency quadrupole collective dynamics [61–64]. At present, a systematic investigation on low-lying quadrupole spectra is underway using the 5D collective Hamiltonian with Inglis–Belyaev cranking masses and the relativistic (covariant) density functionals [65–71].

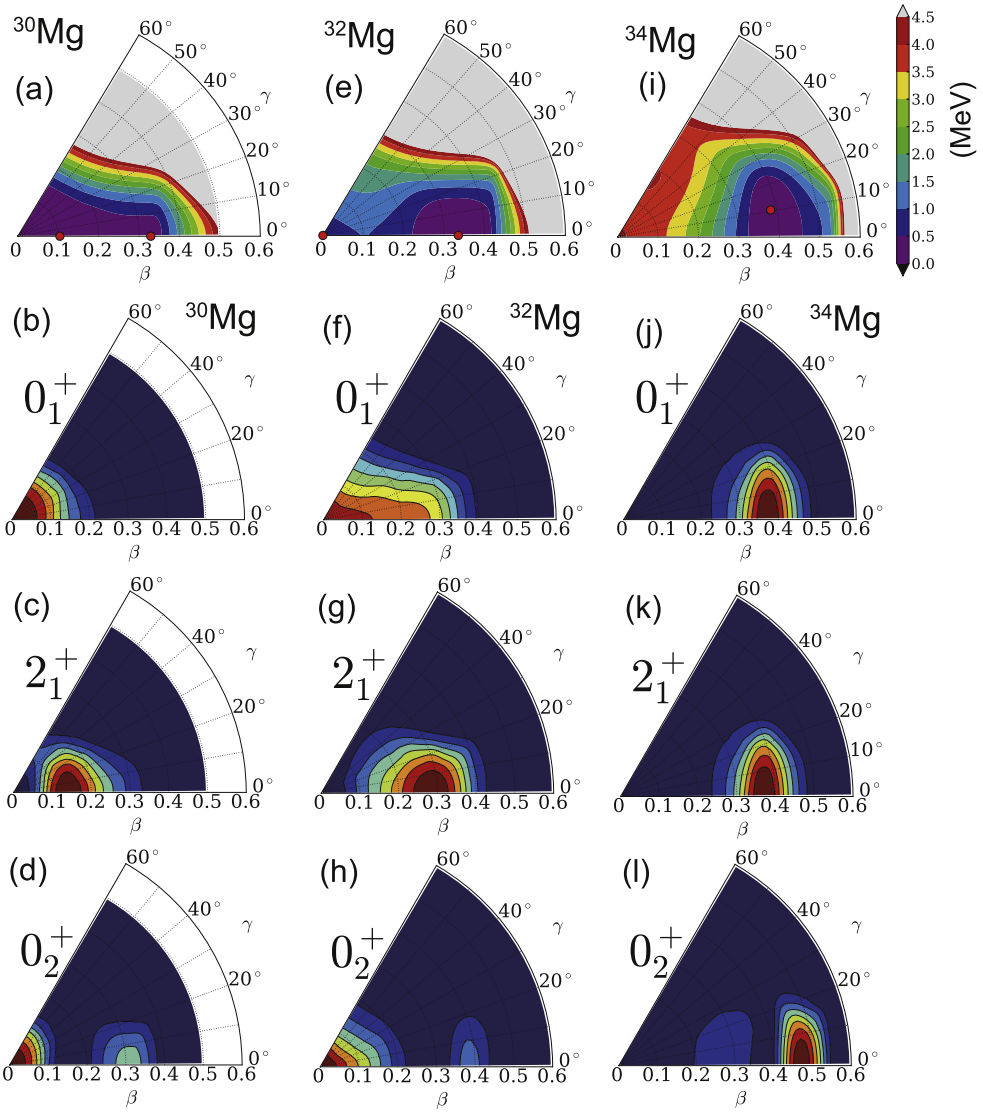

Figure 3. Application of the LQRPA method to the low-lying states in ^{30,32,34}Mg (from [49]). (a) Collective potential $V(\beta, \gamma)$ for ^{30}Mg. The HFB equilibrium points are indicated by red circles. (b)–(d) Vibrational wave functions squared, $\sum_K |\Phi_{\alpha IK}(\beta, \gamma)|^2$, of the 0_1^+, 2_1^+, and 0_2^+ states in ^{30}Mg. Contour lines are drawn at every tenth part of the maximum value. (e)–(h) and (i)–(l): same set of figures but for ^{32}Mg and ^{34}Mg, respectively.

A problem of the Inglis–Belyaev cranking formula is that time-odd mean-field effects are ignored and it underestimates the collective masses (inertial functions) [72]. Moving mean fields possess time-odd components that change sign under time reversal operation, but the cranking formula ignores their effects on the collective masses. By taking into account such time-odd corrections to the cranking masses, one can better reproduce low-lying spectra [53].

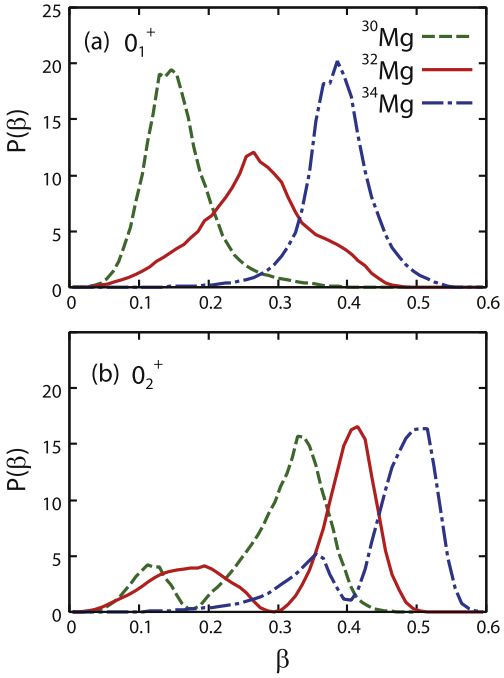

Figure 4. (a) Probability densities integrated over γ, $P(\beta) = \int d\gamma \left|\Phi_{\alpha I=0,K=0}(\beta, \gamma)\right|^2 |G(\beta, \gamma|^{1/2}$, for the ground 0_1^+ states in ^{30,32,34} Mg plotted as functions of β (from [49]). (b) Same as (a) but for the excited 0_2^+ states.

5.2. Adiabatic TDHF theory

Attempts to self-consistently derive the collective Hamiltonian using adiabatic approximation to time evolution of mean fields started in 1960s [44, 73]. In these pioneer works, the collective quadrupole coordinates (β, γ) were defined in terms of expectation values of the quadrupole operators and the 5D collective Hamiltonian was derived using the P + Q force model [48]. During 1970s this approach was generalized to be applicable to any effective interaction. This advanced approach is called adiabatic TDHF (ATDHF) [74–76].

In the ATDHF theory, the density matrix $\rho(t)$ is written in the following form and expanded as a power series with respect to $\chi(t)$.

$$\rho(t) = e^{i\chi(t)}\rho_0(t)e^{-i\chi(t)} \tag{45}$$

$$= \rho_0(t) + i\big[\chi(t), \rho_0(t)\big] - \frac{1}{2}\big[\chi(t), \big[\chi(t), \rho_0(t)\big]\big] + \cdots. \tag{46}$$

Baranger and Vénéroni [74] suggested a possibility to introduce collective coordinates as parameters describing the time evolution of the density matrix $\rho_0(t)$ and discussed an iterative procedures to solve the ATDHF equations. But this idea has not been realized until now. We note that the ATDHF does not reduce to the RPA in the small-amplitude limit if a few collective coordinates are introduced by hand. In fact it gives a collective mass different from the RPA [77].

The ATDHF theory developed by Villars [78] aims at self-consistent determination of the optimum collective coordinates on the basis of the time-dependent variational principle. This approach, however, encountered a difficulty that we could not get unique solutions of its basic equations determining the collective path. This problem was later solved by treating the second-order terms of the momentum expansion in a self-consistent manner [37, 79]. It was shown that, when the number of collective coordinate is only one, a collective path maximally decoupled from non-collective degrees of freedom runs along a valley in the multi-dimensional potential-energy surface associated with the TDHF states.

To describe low-frequency collective motions, it is necessary to take into account the pairing correlations. In other words, we need to develop the adiabatic TDHFB (ATDHFB) theory. This is one of the reasons why applications of the ATDHF have been restricted to collective phenomena where pairing correlations play minor roles such as low-energy collisions between spherical closed-shell nuclei [80] and giant resonances [77]. When large-amplitude shape fluctuations take place, single-particle level crossings often occur. To follow the adiabatic configuration across the level crossing points, the pairing correlation plays an essential role. Thus, an extension to ATDHFB is indispensable for the description of low-frequency collective excitations.

In the past, Dobaczewski and Skalski [81] tried to develop the ATDHFB theory assuming the axially symmetric quadrupole deformation parameter β as the collective coordinate. Quite recently, Li *et al* [82] tried to derive the 5D quadrupole collective Hamiltonian on the basis of the ATDHFB. The extension of ATDHF to ATDHFB is not straightforward, however. This is because, as discussed in section 2, we need to decouple the number-fluctuation degrees of freedom from the LACM of interest and respect the gauge invariance with respect the pairing rotational angles.

5.3. Boson expansion method

Boson expansion method is well known as a useful microscopic method of describing anharmonic (non-linear) vibrations going beyond the harmonic approximation of the QRPA. In this approach, we first construct a collective subspace spanned by many-phonon states of vibrational quanta (determined by the QRPA) in the huge-dimensional shell-model space, and then map these many-phonon states one-to-one to many-boson states in an ideal boson space. Anharmonic effects neglected in the QRPA are treated as higher-order terms in the power-series expansion with respect to the boson creation and annihilation operators. Starting from the QRPA about a spherical shape, one can thus derive the 5D quadrupole collective Hamiltonian in a fully quantum mechanical manner. The boson expansion method has been successfully applied to low-energy quadrupole excitation spectra in a wide range of nuclei including those lying in regions of quantum phase transitions from spherical to deformed [83, 84].

In the time-dependent mean-field picture, state vectors in the boson expansion method are written in terms of the creation and annihilation operators ($\Gamma_i^\dagger$, Γ_i) of the QRPA eigen-modes, or, equivalently, in terms of the collective coordinate and momentum operators ($\hat{Q}_i$, $\hat{P}_i$),

$$|\phi(t)\rangle = \exp\left[\sum_i \left(\eta_i(t)\Gamma_i^\dagger - \eta_i^*(t)\Gamma_i\right)\right]|\phi_0\rangle \tag{47}$$

$$= \exp\left[i\sum_i \left(p_i(t)\hat{Q}_i - q_i(t)\hat{P}_i\right)\right]|\phi_0\rangle. \tag{48}$$

With increasing amplitudes of the quadrupole shape vibration $|\eta_i(t)|$ (values of the collective coordinate $q_i(t)$), anharmonic (non-linear) effects become stronger. Strong non-linear effects may eventually change even the microscopic structure of the collective operators $(\hat{Q}_i, \hat{P}_i)$ determined by the QRPA. In such situations, it is desirable to construct a theory that allows variations of microscopic structure of collective operators as functions of $q_i(t)$. It may be said that the SCC method has accomplished this task.

5.4. Generator coordinate method (GCM)

The GCM has been used for a wide variety of nuclear collective phenomena [85–87]. Using the angular-momentum projector $\hat{P}_{IMK}$ and the neutron(proton)-number projector $\hat{P}_N$ $(\hat{P}_Z)$, we write the state vector as a superposition of the projected mean-field states with different deformation parameters (β, γ),

$$\left|\Psi^i_{NZIM}\right\rangle = \int \mathrm{d}\beta \mathrm{d}\gamma \sum_K f^i_{NZIK}(\beta, \gamma)\hat{P}_N\hat{P}_Z\hat{P}_{IMK}\,|\phi(\beta, \gamma)\rangle. \tag{49}$$

Because the projection operators contain integrations, it has been a difficult task to carry out such high-dimensional numerical integrations in solving the Hill–Wheeler equation for the states $|\phi(\beta, \gamma)\rangle$ obtained by the constrained HFB method. In recent years, however, remarkable progress has been taking place, which makes it possible to carry out such large-scale numerical computations [88–93]. The HFB calculations using the density dependent effective interactions are better founded by density functional theory (DFT). Accordingly, the modern GCM calculation is referred to as 'multi-reference DFT' [88].

It is well known that one can derive a collective Schrödinger equation by making a gaussian overlap approximation (GOA) to the Hill–Wheeler equation [94–96]. There is no guarantee, however, that dynamical effects associated with time-odd components of moving mean field are sufficiently taken into account in the collective masses (inertial functions) obtained through this procedure. In the case of center of mass motion, we need to use complex generator coordinates to obtain the correct mass, implying that collective momenta conjugate to collective coordinates should also be treated as generator coordinates [22, 97].

A fundamental question is how to choose the optimal generator coordinates. With the variational principle, Holzwarth and Yukawa [98] proved that the mean-field states parametrized by a single optimal generator coordinate run along a valley of the collective potential energy surface. This line of investigation was further developed [99] and greatly stimulated the challenge toward constructing a microscopic theory of LACM. In this connection, we note that conventional GCM calculations parametrized by a few real generator coordinates do not reduce to the QRPA in the small-amplitude limit, differently from the case that all two-quasiparticle (particle–hole) degrees of freedom are treated as complex generator coordinates [100].

It is very important to distinguish the 5D collective Hamiltonian obtained by making use of the GOA to the GCM from that derived in section 3 on the basis of the ASCC method. In the latter, the canonical conjugate pairs of collective coordinate and momentum are self-consistently derived on the basis of the time-dependent variational principle. The canonical formulation enables us to adopt the standard canonical quantization procedure. Furthermore, effects of the time-odd components of the moving mean field are automatically taken into account in the collective masses (inertial functions). In view of the above points, it is highly desirable to carry out a systematic comparison of collective inertial masses evaluated by different approximations including the ASCC, the ATDHFB, the GCM + GOA, and the adiabatic cranking methods for a better understanding of their physical implications. In this

connection, it is interesting to notice that the results of the recent GCM calculation for ^{76}Kr [92], using the particle-number and angular-momentum projected basis (49), are rather similar to those obtained by use of the 5D collective Hamiltonian with the Inglis–Belyaev cranking masses, except for an overall overestimation of the excitation energies by about 20%.

6. Challenges for future

As reviewed by Hyde and Wood [5], nature of low-lying excited 0^+ states, systematically found in recent experiments as well as those known from old days, is not well understood. It is thus quite challenging to apply, in a systematic ways, the 5D collective Hamiltonian approach to all of these data, from light to heavy and from stable to unstable nuclei, and explore the limit of its applicability. Recalling that the importance of the couplings between the quadrupole and pairing vibrations has been pointed out [14–16], one of the basic questions is 'under what situations we need to extend the 5D collective Hamiltonian to 7D by explicitly treating the proton and neutron pairing gaps as dynamical variables.'

Another interesting subject is to extend the collective Hamiltonian approach to a variety of collective phenomena, for example, those observed in rapidly rotating nuclei, heavy and super heavy nuclei, neutron-rich unstable nuclei, by taking into account the effects of rapid rotation and/or continuum, from the beginning in the single-particle (HFB) Hamiltonian. Macroscopic quantum tunnelings through self-consistently generated barriers, such as spontaneous fissions and deep sub-barrier fusions, are, needless to say, longstanding yet modern, fundamental subjects of nuclear structure physics.

It is a great challenge to develop the CHFB + LQRPA approach on the basis of the time-dependent DFT. To efficiently solve the large-dimensional LQRPA equations containing density-dependent terms, the finite-amplitude method recently developed in [101–104] may be utilized.

Acknowledgments

This work is supported by the JSPS KAKENHI Grant No. 25287065. One of the authors (KS) is supported by the Special Postdoctoral Researcher Program of RIKEN.

References

[1] Bohr A and Mottelson B R 1975 *Nuclear Structure* vol 2 (New York: Benjamin) (World Scientific, 1998)
[2] Åberg S, Flocard H and Nazarewicz W 1990 *Annu. Rev. Nucl. Part. Sci.* **40** 439
[3] Bender M, Heenen P-H and Reinhard P-G 2003 *Rev. Mod. Phys.* **75** 121
[4] Rowe D J and Wood J L 2010 Fundamentals of nuclear models *Foundational Models* (Singapore: World Scientific)
[5] Heyde K and Wood J L 2011 *Rev. Mod. Phys.* **83** 1467
[6] Anderson P W 1958 *Phys. Rev.* **112** 1900
Anderson P W 1963 *Phys. Rev.* **130** 439
[7] Nambu Y 1960 *Phys. Rev.* **117** 648
[8] Brink D M and Broglia R A 2005 *Nuclear Superfluidity, Pairing in Finite Systems* (Cambridge: Cambridge University Press)
[9] Frauendorf S 2001 *Rev. Mod. Phys.* **73** 463
[10] Bohr A 1976 *Rev. Mod. Phys.* **48** 365
[11] Mottelson B 1976 *Rev. Mod. Phys.* **48** 375
[12] Próchniak L and Rohoziński S G 2009 *J. Phys. G: Nucl. Part. Phys.* **36** 123101

[13] Matsuo M and Matsuyanagi K 1985 *Prog. Theor. Phys.* **74** 1227
Matsuo M and Matsuyanagi K 1986 *Prog. Theor. Phys.* **76** 93
Matsuo M and Matsuyanagi K 1987 *Prog. Theor. Phys.* **78** 591
[14] Iwasaki S, Marumori T, Sakata F and Takada K 1976 *Prog. Theor. Phys.* **56** 1140
[15] Weeks K J, Tamura T, Udagawa T and Hahne F J W 1981 *Phys. Rev.* C **24** 703
[16] Takada K and Tazaki S 1986 *Nucl. Phys.* A **448** 56
[17] Negele J W 1982 *Rev. Mod. Phys.* **54** 913
[18] Abe A and Suzuki T (ed) 1983 Microscopic theories of nuclear collective motions *Prog. Theor. Phys. Suppl.* **74 & 75** 1–416
[19] Yamamura M and Kuriyama A 1987 *Prog. Theor. Phys. Suppl.* **93** 1–175
[20] Kuriyama A, Matsuyanagi K, Sakata F, Takada K and Yamamura M (ed) 2001 Selected topics in the Boson mapping and time-dependent Hartree–Fock methods *Prog. Theor. Phys. Suppl.* **141** 1
[21] Nakatsukasa T, Walet N R and do Dang G 1999 *Phys. Rev.* C **61** 014302
[22] Ring P and Schuck P 1980 *The Nuclear Many-Body Problem* (Berlin: Springer)
[23] Blaizot J-P and Ripka G 1986 *Quantum Theory of Finite Systems* (Cambridge, MA: MIT Press)
[24] Matsuyanagi K, Matsuo M, Nakatsukasa T, Hinohara N and Sato K 2010 *J. Phys. G: Nucl. Part. Phys.* **37** 064018
[25] Nakatsukasa T 2012 *Prog. Theor. Exp. Phys.* **2012** 01A207
[26] Matsuyanagi K, Hinohara N and Sato K 2013 *Fifty Years of Nuclear BCS: Pairing in Finite Systems* (Singapore: World Scientific)
[27] Rowe D J and Bassermann R 1976 *Can. J. Phys.* **54** 1941
[28] Marumori T 1977 *Prog. Theor. Phys.* **57** 112
[29] Marumori T, Maskawa T, Sakata F and Kuriyama A 1980 *Prog. Theor. Phys.* **64** 1294
[30] Rowe D J 1982 *Nucl. Phys.* **391** 307
[31] Matsuo M 1986 *Prog. Theor. Phys.* **76** 372
[32] Matsuo M and Matsuyanagi K 1985 *Prog. Theor. Phys.* **74** 288
[33] Matsuo M, Shimizu Y R and Matsuyanagi K 1985 *Proc. Niels Bohr Centennial Conf. Nuclear Structure* (*North-Holland*) ed R Broglia *et al* p 161
[34] Yamada K 1993 *Prog. Theor. Phys.* **89** 995
[35] Shimizu Y R and Matsuyanagi K 2001 *Prog. Theor. Phys. Suppl.* **141** 285
[36] Matsuo M, Nakatsukasa T and Matsuyanagi K 2000 *Prog. Theor. Phys.* **103** 959
[37] Klein A, Walet N R and do Dang G 1991 *Ann. Phys.* **208** 90
[38] Almehed D and Walet N R 2004 *Phys. Rev.* C **69** 024302
[39] Barranco F, Bertsch G F, Broglia R A and Vigezzi E 1990 *Nucl. Phys.* A **512** 253
[40] Hinohara N, Nakatsukasa T, Matsuo M and Matsuyanagi K 2007 *Prog. Theor. Phys.* **117** 451
[41] Hinohara N, Sato K, Nakatsukasa T, Matsuo M and Matsuyanagi K 2010 *Phys. Rev.* C **82** 064313
[42] Sato K and Hinohara N 2011 *Nucl. Phys.* A **849** 53
[43] Sato K, Hinohara N, Yoshida K, Nakatsukasa T, Matsuo M and Matsuyanagi K 2012 *Phys. Rev.* C **86** 024316
[44] Baranger M and Kumar K 1965 *Nucl. Phys.* **62** 113
Baranger M and Kumar K 1968 *Nucl. Phys.* A **110** 529
Baranger M and Kumar K 1968 *Nucl. Phys.* A **122** 241
Baranger M and Kumar K 1968 *Nucl. Phys.* A **122** 273
[45] Thouless D J and Valatin J G 1962 *Nucl. Phys.* **31** 211
[46] Eisenberg J M and Greiner W 1987 *Nuclear Theory* vol 1 3rd edn (Amsterdam: North Holland)
[47] Kumar K and Baranger M 1967 *Nucl. Phys.* **92** 608
[48] Bes D R and Sorensen R A 1969 *Advances in Nuclear Physics* vol 2 (New York: Plenum) p 129
[49] Hinohara N, Sato K, Nakatsukasa T, Matsuo M and Matsuyanagi K 2011 *Phys. Rev.* C **84** 061302(R)
[50] Yoshida K and Hinohara N 2011 *Phys. Rev.* C **83** 061302(R)
[51] Hinohara N, Nakatsukasa T, Matsuo M and Matsuyanagi K 2009 *Phys. Rev.* C **80** 014305
[52] Hinohara N and Kanada-En'yo Y 2011 *Phys. Rev.* C **83** 014321
[53] Hinohara N, Li Z P, Nakatsukasa T, Nikšić T and Vretenar D 2012 *Phys. Rev.* C **85** 024323
[54] Fischer S M *et al* 2003 *Phys. Rev.* C **67** 064318
[55] Iwasaki H *et al* 2014 *Phys. Rev. Lett.* **112** 142502
[56] Hamamoto I 2012 *Phys. Rev.* C **85** 064329

[57] Wimmer K *et al* 2010 *Phys. Rev. Lett.* **105** 252501
[58] do Dang G, Klein A and Walet N R 2000 *Phys. Rep.* **335** 93
[59] Brack M, Damgaard J, Jensen A S, Pauli H C, Strutinsky V M and Wong C Y 1972 *Rev. Mod. Phys.* **44** 320
[60] Baran A, Sheikh J A, Dobaczewski J, Nazarewicz W and Staszczak A 2011 *Phys. Rev.* C **84** 054321
[61] Libert J, Girod M and Delaroche J-P 1999 *Phys. Rev.* C **60** 054301
[62] Yuldashbaeva E Kh, Libert J, Quentin P and Girod M 1999 *Phys. Lett.* B **461** 1
[63] Próchniak L, Quentin P, Samsoen D and Libert J 2004 *Nucl. Phys.* A **730** 59
[64] Delaroche J-P, Girod M, Libert J, Goutte H, Hilaire S, Péru S, Pillet N and Bertsch G F 2010 *Phys. Rev.* C **81** 014303
[65] Nikšić T, Li Z P, Vretenar D, Próchniak L, Meng J and Ring P 2009 *Phys. Rev.* C **79** 034303
[66] Li Z P, Nikšić T, Vretenar D, Meng J, Lalazissis G A and Ring P 2009 *Phys. Rev.* C **79** 054301
[67] Li Z P, Nikšić T, Vretenar D and Meng J 2010 *Phys. Rev.* C **81** 034316
[68] Li Z P, Nikšić T, Vretenar D, Ring P and Meng J 2010 *Phys. Rev.* C **81** 064321
[69] Li Z P, Yao J M, Vretenar D, Nikšić T, Chen H and Meng J 2011 *Phys. Rev.* C **84** 054304
[70] Nikšić T, Vretenar D and Ring P 2011 *Prog. Part. Nucl. Phys.* **66** 519
[71] Fu Y, Mei H, Xiang J, Li Z P, Yao J M and Meng J 2013 *Phys. Rev.* C **87** 054305
[72] Dobaczewski J and Dudek J 1995 *Phys. Rev.* C **52** 1827
[73] Belyaev S T 1965 *Nucl. Phys.* **64** 17
[74] Baranger M and Véneroni M 1978 *Ann. Phys.* **114** 123
[75] Brink D M, Giannoni M J and Veneroni M 1976 *Nucl. Phys.* A **258** 237
[76] Goeke K and Reinhard P-G 1978 *Ann. Phys.* **112** 328
[77] Giannoni M J and Quentin P 1980 *Phys. Rev.* C **21** 2060
Giannoni M J and Quentin P 1980 *Phys. Rev.* C **21** 2076
[78] Villars F 1977 *Nucl. Phys.* A **285** 269
[79] Mukherjee A K and Pal M K 1982 *Nucl. Phys.* A **373** 289
[80] Goeke K, Cusson R Y, Grummer F, Reinhard P-G and Reinhardt H 1983 *Prog. Theor. Phys. Suppl.* **74 & 75** 33
[81] Dobaczewski J and Skalski J 1981 *Nucl. Phys.* A **369** 123
[82] Li Z P, Nikšić T, Ring P, Vretenar D, Yao J M and Meng J 2012 *Phys. Rev.* C **86** 034334
[83] Sakamoto H and Kishimoto T 1988 *Nucl. Phys.* A **486** 1
Sakamoto H and Kishimoto T 1991 *Nucl. Phys.* A **528** 73
[84] Klein A and Marshalek E R 1991 *Rev. Mod. Phys.* **63** 375
[85] Reinhard P-G and Goeke K 1987 *Rep. Prog. Phys.* **50** 1
[86] Egido J L and Robledo L M 2004 *Extended Density Functionals in Nuclear Physics* (*Lecture Notes in Physics* vol 641) ed G A Lalazissis *et al* (Berlin: Springer) p 269
[87] Bender M 2008 *Eur. Phys. J. Spec. Top.* **156** 217
[88] Bender M and Heenen P-H 2008 *Phys. Rev.* C **78** 024309
[89] Rodríguez T R and Egido J L 2010 *Phys. Rev.* C **81** 064323
[90] Yao J M, Meng J, Ring P and Vretenar D 2010 *Phys. Rev.* C **81** 044311
[91] Yao J M, Mei H, Chen H, Meng J, Ring P and Vretenar D 2011 *Phys. Rev.* C **83** 014308
[92] Yao J M, Hagino K, Li Z P, Meng J and Ring P 2014 *Phys. Rev.* C **89** 054306
[93] Rodríguez T R 2014 *Phys. Rev.* C **90** 034306
[94] Griffin J J and Wheeler J A 1957 *Phys. Rev.* **108** 311
[95] Onishi N and Une T 1975 *Prog. Theor. Phys.* **53** 504
[96] Rohoziński S G 2012 *J. Phys. G: Nucl. Part. Phys.* **39** 095104
[97] Peierls R E and Thouless D J 1962 *Nucl. Phys.* **38** 154
[98] Holzwarth G and Yukawa T 1974 *Nucl. Phys.* A **219** 125
[99] Reinhard P-G and Goeke K 1979 *Phys. Rev.* C **20** 1546
[100] Jancovici B and Schiff D H 1964 *Nucl. Phys.* **58** 678
[101] Nakatsukasa T, Inakura T and Yabana K 2007 *Phys. Rev.* C **76** 024318
[102] Avogadro P and Nakatsukasa T 2011 *Phys. Rev.* C **84** 014314
[103] Avogadro P and Nakatsukasa T 2013 *Phys. Rev.* C **87** 014331
[104] Hinohara N, Kortelainen M and Nazarewicz W 2013 *Phys. Rev.* C **87** 064309

Microscopic derivation of the Bohr–Mottelson collective Hamiltonian and its application to quadrupole shape dynamics

2016 Phys. Scr. 91 063014

(http://iopscience.iop.org/1402-4896/91/6/063014)

IOP Publishing | Royal Swedish Academy of Sciences Physica Scripta

Phys. Scr. **91** (2016) 063014 (32pp) doi:10.1088/0031-8949/91/6/063014

Invited Comment

Microscopic derivation of the Bohr–Mottelson collective Hamiltonian and its application to quadrupole shape dynamics

Kenichi Matsuyanagi[1,2,8], Masayuki Matsuo[3], Takashi Nakatsukasa[1,4], Kenichi Yoshida[5], Nobuo Hinohara[4,6] and Koichi Sato[1,7]

[1] RIKEN Nishina Center, Wako 351-0198, Japan
[2] Yukawa Institute for Theoretical Physics, Kyoto University, Kyoto 606-8502, Japan
[3] Department of Physics, Faculty of Science, Niigata University, Niigata 950-2181, Japan
[4] Center for Computational Sciences, University of Tsukuba, Tsukuba 305-8571, Japan
[5] Graduate School of Science and Technology, Niigata University, Niigata 950-2181, Japan
[6] FRIB Laboratory, Michigan State University, East Lansing, Michigan 48824, USA

E-mail: matsuyanagi@riken.jp

Received 29 December 2015, revised 12 April 2016
Accepted for publication 22 April 2016
Published 26 May 2016

Abstract

We discuss the nature of the low-frequency quadrupole vibrations from small-amplitude to large-amplitude regimes. We consider full five-dimensional quadrupole dynamics including three-dimensional rotations restoring the broken symmetries as well as axially symmetric and asymmetric shape fluctuations. Assuming that the time evolution of the self-consistent mean field is determined by five pairs of collective coordinates and collective momenta, we microscopically derive the collective Hamiltonian of Bohr and Mottelson, which describes low-frequency quadrupole dynamics. We show that the five-dimensional collective Schrödinger equation is capable of describing large-amplitude quadrupole shape dynamics seen as shape coexistence/mixing phenomena. We summarize the modern concepts of microscopic theory of large-amplitude collective motion, which is underlying the microscopic derivation of the Bohr-Mottelson collective Hamiltonian.

Keywords: Bohr–Mottelson collective Hamiltonian, quadrupole shape dynamics, shape coexistence, time-dependent self-consistent mean field, TDHFB method, collective coordinates, microscopic theory of large-amplitude collective motion

(Some figures may appear in colour only in the online journal)

1. Introduction

The subject of this review has a long history of more than 50 years. Instead of describing the whole history, we mainly discuss the recent progress in the microscopic derivation of the Bohr–Mottelson collective Hamiltonian from a viewpoint of microscopic theory of large-amplitude collective motion. Special emphasis will be put on the development of fundamental concepts underlying the collective model. It is intended to motivate future studies by younger generations on the open problems suggested in this review.

Progress in fundamental concepts of the collective model

Vibrational and rotational motions of a nucleus can be described as time evolutions of a self-consistent mean field. This is the key idea of the collective model of Bohr and Mottelson, which opened up a new field of contemporary

[7] Present address: Department of Physics, Osaka City University, Osaka, 558-8585, Japan.
[8] Author to whom any correspondence should be addressed.

physics, *quantum many-body theory of nuclear collective dynamics*. The central theme in this field is to describe the single-particle and collective motions in finite quantum systems in a unified manner. After the first paper in 1952 [1], the basic concepts underlying the unified model of Bohr and Mottelson have been greatly developed. The progress achieved until 1975 is summarized in their textbook [2, 3] and Nobel lectures in 1975 [4, 5].

The unified description of complementary concepts such as the collective and single-particle motions in nuclei possess a great conceptual significance in theoretical physics in general. Needless to say, understanding the coexistence of complementary concepts (such as particle-wave duality) constitutes a central theme in theoretical physics. The physics underlying the Bohr-Mottelson unified model is deep and wide. Among the rich subjects pertinent to this model, we select and focus on the subject of microscopic derivation of the Bohr–Mottelson collective Hamiltonian: that is, we concentrate on the collective Hamiltonian $H_{\rm coll}$ in the unified model Hamiltonian

$$H_{\rm uni} = H_{\rm part} + H_{\rm coll} + H_{\rm coupl}, \tag{1}$$

where $H_{\rm part}$ describes the single-particle motions in a self-consistent mean field and $H_{\rm coupl}$ is the coupling Hamiltonian generating the interplay between the single-particle motions and collective motions. Specifically, we focus on the low-frequency quadrupole collective motions and call the quadrupole collective Hamiltonian *the Bohr–Mottelson collective Hamiltonian*. We discuss its generalized form as described in their textbook, where the mass parameters (collective inertial masses) appearing in the collective Hamiltonian are not constant but functions of deformation variables. In our point of view, it is desirable to adopt this general definition of the Bohr–Mottelson collective Hamiltonian in order to respect the conceptual progress achieved by collaborative efforts of many researchers worldwide during 1952 to 1975. In this connection, we would like to quote a sentence from their Nobel lectures: 'The viewpoints that I shall try to summarize gradually emerged in this prolonged period' [4].

Brief remarks about the history

Soon after the introduction of the collective model by Bohr and Mottelson in 1952–1953, attempts to formulate a microscopic theory of the collective model started. This became one of the major subjects of theoretical physics in the 1950's and greatly stimulated to open up a new fertile field, the nuclear many-body theory, to derive the collective phenomena starting from the nucleon degrees of freedom constituting the nucleus.

The major approach at that time was to introduce collective coordinates explicitly as functions of coordinates of individual nucleons and separate collective shape degrees of freedom from the rest. From among numerous papers, we refer Tomonaga theory [6, 7] and a similar work by Marumori *et al* [8] as representative examples. In spite of their conceptual significance, however, it turned out that these approaches fail for description of low-energy modes of shape fluctuations. The main reasons of this failure are 1) the assumption that the collective coordinates are given by local one-body operators (such as mass-quadrupole operators) leads to the inertial masses of irrotational fluids [3], in contradiction to experimental data which suggest that the inertial masses of the first excited quadrupole vibrational states are much larger than the irrotational masses, and, as we shall discuss in this review, 2) the quantum shell structure of the single-particle motion in the self-consistent mean field and the pairing correlations among nucleons near the Fermi surface play essential roles in the emergence of the low-frequency quadrupole modes of excitation in nuclei. Interestingly, it became clear much later that the Tomonaga theory is applicable to high-frequency giant resonances, rather than the originally intended low-frequency quadrupole vibrations [9–12]. One of the important lessons we learned from these early attempts is that, it is not trivial at all to define microscopic structure of collective coordinates appropriate to low-energy shape vibrations.

In 1960, the quasiparticle random-phase approximation (QRPA) based on the Bardeen–Cooper–Schrieffer (BCS) theory of superconductivity was introduced in nuclear structure theory [13, 14]. This was a starting point of the modern approach to determine, on the basis of the time-dependent mean-field picture, the microscopic structures of the collective coordinates and their conjugate momenta without postulating them by physical intuition.

After the initial success of the BCS+QRPA approach for small amplitude oscillations in the 1960's and its extensions by boson expansion methods [15] in succeeding years, attempts to construct a microscopic theory of large-amplitude collective motion (LACM) started in mid 1970's [16]. At that time, time-dependent Hartree-Fock (TDHF) calculations for heavy-ion collisions also started [17]. These attempts introduced collective coordinates as parameters specifying the time evolution of the self-consistent mean field, instead of explicitly defining them as functions of coordinates of individual nucleons. *This was a historical turning point in the basic concept of collective coordinate theory*: in these new approaches, it is unnecessary to define *global* collective operators as functions of coordinates of individual nucleons. In this paper, we shall discuss the basic ideas of such modern approaches and describe how to derive, in a microscopic way, the quadrupole collective Hamiltonian of Bohr and Mottelson on the basis of the moving self-consistent mean-field picture.

Contents of this review

Our major aim is to review the progress in the fundamental concept of '*collective motion, collective coordinates, and collective momenta*' which have been acquired during the long-term efforts of many researchers to give a *microscopic foundation* of the Bohr–Mottelson collective model. Special emphasis will be put on the developments during the 40 years after the Nobel Prize of 1975 to Bohr, Mottelson, and Rainwater [4, 5, 18]. Although we focus on the quadrupole collective motions, the techniques and underlying concepts are general and applicable to other collective motions at zero temperature as well, including octupole collective motions

[19] and various kinds of many-body tunneling phenomena of finite quantum systems, such as spontaneous fissions [20] and subbarrier fusion reactions [21].

In section 2, we summarize the basic properties of the low-frequency quadrupole collective excitations.

In section 3, the Bohr–Mottelson collective Hamiltonian is recapitulated.

In section 4, we discuss the basics of the microscopic theory of nuclear collective motion. We start from the QRPA as a small amplitude approximation of the time-dependent Hartree-Fock-Bogoliubov (TDHFB) theory, which is an extension of the TDHF to superfluid (superconducting) systems taking into account the pairing correlations. (We use the terms, superfluidity and superconductivity, in the same meaning.) We then discuss how to extend the basic ideas of the QRPA to treat LACM as seen in shape coexistence/mixing phenomena widely observed in nuclear chart.

In section 5, we introduce the *local* QRPA method and describe how to derive the Bohr–Mottelson collective Hamiltonian in a microscopic way on the basis of the TDHFB theory.

In section 6, we present an illustrative example of numerical calculation for a shape coexistence/mixing phenomenon.

In section 7, we briefly remark on other microscopic approaches to derive the Bohr–Mottelson collective Hamiltonian.

In section 8, we review fundamentals of the microscopic theory of LACM. The basic concepts underlying the adiabatic self-consistent coordinate (ASCC) method and the local QRPA method will be summarized.

In section 9, we discuss future outlook. Possible extensions to new regions of nuclear structure dynamics will be suggested.

In section 10, we conclude this review emphasizing future subjects awaiting applications and further extensions of the collective Hamiltonian approach.

This review is an extended version of the short article published quite recently [22][9] and provides more detailed discussions on the basic ideas and fundamental concepts in the microscopic derivation of the Bohr–Motteson collective Hamiltonian. As we develop the basic concepts of collective motion on the basis of the time-dependent self-consistent mean-field theory, we refer to the review by Próchniak and Rohoziński [23] for other microscopic approaches and a detailed account of the techniques of treating the Bohr–Motteson collective Hamiltonian. For the analysis of a wide variety of quadrupole collective phenomena in terms of various models related to the Bohr–Motteson collective Hamiltonian, we refer to the recent review by Frauendorf [24]. Because our major aim is the microscopic derivation of the collective inertial masses, we leave out discussions on phenomenological models reviewed by Cejnar, Jolie, and Casten [25], where the inertial masses are treated as parameters.

[9] Accordingly, there is some similarity between sections 2.3, 4.3, 7.1, 7.2 and 8.1, and reference [22].

2. Low-frequency quadrupole collective motions

In this section, we first summarize the basic properties of the low-frequency quadrupole collective excitations and then introduce the Bohr–Mottelson collective Hamiltonian.

2.1. Nature of the first excited 2^+ modes

Except for doubly magic nuclei in the spherical *j-j* coupling shell-model picture, the first excited states in almost all even-even nuclei (consisting of even numbers of neutrons and protons) have angular momentum two with positive parity ($I^\pi = 2^+$). Systematics of experimental data for these first 2^+ states shows that their excitation energies are very low in comparison to the energy gap 2Δ that characterizes nuclei with superfluidity (superconductivity), and that their electric quadrupole ($E2$) transition probabilities to the 0^+ ground states are very large compared to those associated with single-particle transitions. For nuclei whose mean fields are spherical, the first excited 2^+ states can be characterized as collective vibrations of finite quantum systems with superfluidity [26]. They are genuine quantum vibrations that are essentially different from surface oscillations of a classical liquid drop. In other words, the superfluidity and shell structure play indispensable roles in their emergence.

In axially deformed nuclei, whose mean fields break the rotational symmetry but conserve the axial symmetry, the first excited 2^+ state can be interpreted as quantum rotational states whose mean fields are uniformly rotating about an axis perpendicular to the symmetry axis. Regular rotational spectra appear when the amplitudes of quantum shape fluctuation are smaller than the magnitude of equilibrium deformation. Nuclei that have very small ratios, $E(2^+)/2\Delta$, of the 2^+ excitation energies to the energy gaps, (less than, as a rule of thumb, 0.1) belong to this category. The rotational moments of inertia evaluated from $E(2^+)$ are found to be about half of the rigid-body value. This deviation of the moment of inertia from the rigid-body value is one of the most clear evidences that the ground states of nuclei are in a superfluid phase. Large portion of nuclei exhibiting regular rotational spectra have the prolate (elongated spheroidal) shape. Origin of prolate shape dominance over oblate (flattened spheroidal) shape is an interesting fundamental problem (prolate-oblate asymmetry) [27, 28].

When the mean field of the ground state conserves the rotational symmetry, the first excited 2^+ state have been regarded as quadrupole vibrational excitation of a spherical shape with frequencies lower than the energy gap. They are more lowered as the numbers of neutrons and/or protons deviate from the spherical magic numbers. Eventually the vibrational 2^+ states turn into the rotational 2^+ states discussed above. Thus, one may regard low-lying quadrupole vibrations as soft modes of the quantum phase transition that breaks the spherical symmetry of the mean field. In finite quantum systems such as nuclei, however, this phase transition takes place rather gradually for a change of nucleon number, creating a wide transitional region in the nuclear chart. Low-energy excitation spectra of these nuclei exhibit

intermediate characters between the vibrational and rotational ones. Softer the mean field toward the quadrupole deformation, larger the amplitude and stronger the nonlinearity of the vibration.

2.2. Quantum shape transitions in nuclei

Why are nuclei deformed?

As is well known, the equilibrium shape of the classical liquid drop is spherical. When it rotates, it becomes oblate due to the effect of the centrifugal force. In contrast, most nuclei favor the prolate shape, except for nuclei situated near the closed shells of the *j-j* coupling shell model (whose proton number Z and/or neutron number N are near the spherical magic numbers). As we shall discuss later, even such nuclei whose ground state are spherical, deformed states appear in their excited states. The appearance of the deformed shapes in nuclei is due to quantum-mechanical shell effects associated with the single-particle motions in the mean field. Let us first start with what this means.

Deformable mean field and deformed shell structure

It is well known from the success of the *j-j* coupling shell model [29] that the concept of *single-particle motion in a mean field* holds in nuclear structure. Differently from electrons in an atom, the shell-model potential is collectively generated by all nucleons constituting the nucleus. In other words, the single-particle picture of the shell model emerges as a result of collective effects of all nucleons generating the self-consistent mean field. It implies that the single-particle potential of the nucleus is a deformable quantum object [4, 5, 18]. In fact, as we shall discuss below, the self-consistent mean field possesses *collective predisposition* to generate a variety of vibrational and rotational modes of excitation.

Because the nucleus is a finite quantum system, the single-particle states form a shell structure. The spherical shell structure in the *j-j* coupling shell model gradually changes with the growth of deformation in the mean field and generates *deformed shell structures* and *deformed magic numbers* at certain deformed shapes [30, 31]. The gain of binding energies associated with deformed magic numbers appearing at various deformed shapes for certain combinations of (Z, N) stabilizes the deformed shape. For instance, for a nucleus whose (Z, N) are far from the spherical magic numbers but near the deformed magic numbers associated with a certain prolate shape, it is energetically favorable for this nucleus to take the prolate shape. This is the major origin of the appearance of a rich variety of deformed shapes in nuclei. The deformed shell structure effects are clearly seen in the appearance of superdeformed nuclei having prolate shapes with the axis ratio about 2:1 [32, 33].

The shell structures can be defined, in a general concept, as regularly oscillating gross structures in the distribution of single-particle-energy eigenvalues [3, 20, 34]. It is very important to notice that those structures are quite sensitive to the shape of the mean-field potential. The oscillation pattern changes following the variation of the deformation parameter. Figure 1 illustrates this concept.

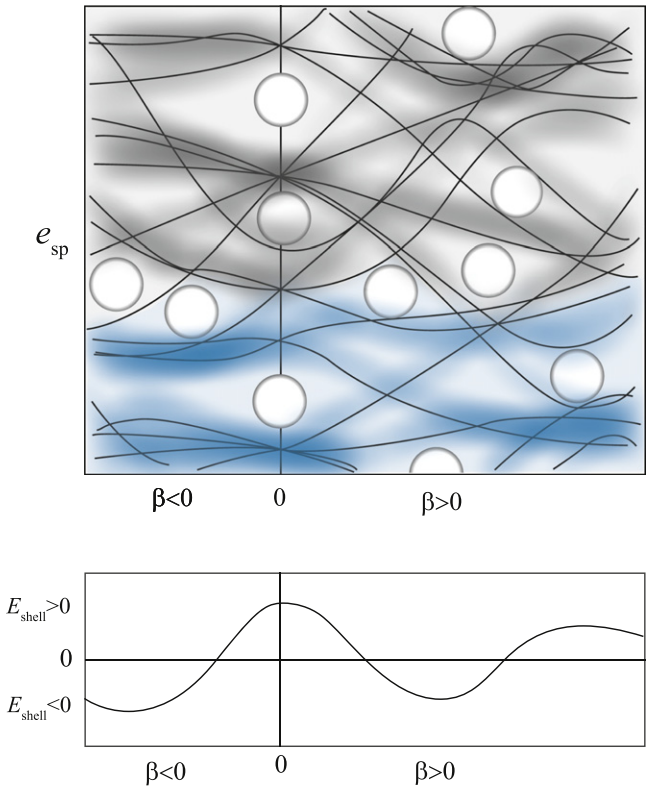

Figure 1. Illustration of shell structure and its change with increasing deformation. The level densities are drawn as functions of the single-particle energy e_{sp} and the deformation parameter β. Positive and negative β corresponds to the prolate and oblate shapes, respectively. Regions with high- and low-level densities are shown by shading (shade for high and light for low). Occupied and unoccupied regions are indicated by blue and gray shades, respectively. The circles indicate appearance of (spherical and deformed) magic numbers. The contribution of the shell structure to the binding energy (shell structure energy) for a fixed neutron (or proton) number changes as a function of β. Generally, it exhibits an oscillating pattern. This conceptual figure is drawn on the basis of the realistic calculation [35] by using the deformed Wood-Saxon potential for ^{80}Sr.

Although one can easily calculate single-particle-energy eigenvalues for a given shape of the mean field, such a quantum-mechanical calculation does not explain the origins of the appearance of such gross structures. For a deeper understanding of the origins, one can make use of the semi-classical theory of (deformed) shell structure. For further discussions on this subject, we refer to the textbook by Brack and Bhaduri [34] and the review by Arita [28].

Emergence of collective rotational motions restoring broken symmetries

The central concept of the BCS theory of superconductivity is spontaneous gauge-symmetry breaking and emergence of associated collective modes. The massless collective modes that restore the broken symmetry are called Anderson–

Nambu–Goldstone (ANG) modes [26, 36, 37]. Nuclear rotations are manifestations of this dynamics in finite quantum systems, as pointed out by Bohr and Mottelson [3, 4]; they are ANG modes restoring the spherical symmetry broken by the self-consistently generated mean field.

The spontaneous breaking of the spherical symmetry (deformation) in the self-consistent mean field enables us to define the orientation degrees of freedom that specify the orientation of the body-fixed (intrinsic) frame relative to the laboratory frame. The body-fixed frame can be defined as a principal-axis frame of the deformed self-consistent mean field generated by all nucleons constituting the nucleus. It is important to keep in mind that *the spontaneous breaking of symmetry can be hidden in finite quantum systems such as nuclei*; that is, the experimental measurements probe the states in the laboratory frame, which preserves the symmetries of the original Hamiltonian. Thus, nuclear rotations may be viewed as rotational motions of the self-consistent mean field relative to the laboratory frame.

'The spontaneous breaking of the rotational symmetry in the self-consistent mean field' is the key concept to a unified description of the single-particle motion and the collective rotational motion. With this concept we can generalize the notion of the single-particle motion in a spherical mean field to that in a deformed mean field. At the same time the deformed mean field is rotating to restore the broken symmetry. Thus, extension of the concept of single-particle excitation with spontaneous breaking of the symmetry and appearance of new collective excitation restoring the broken symmetry are *dual concepts* that underline the quantum many-body theory of nuclear structure. We shall discuss in section 8 how to generalize this concept of *particle-collective duality* to slowly vibrating mean fields where the time scales of the single-particle and vibrational motions are separated in a good approximation.

Excitation spectra in the transitional region

The low-frequency quadrupole vibrations can be regarded as soft modes of the quantum phase transition generating equilibrium deformations in the mean field. In nuclei situated in the transitional region from spherical to deformed, the amplitudes of quantum shape fluctuation about the equilibrium shape increase significantly. The large shape fluctuations occur also in weakly deformed nuclei where the binding-energy gains due to the symmetry breaking are comparable in magnitude to the vibrational zero-point energies. Such transitional situations are abundant in nuclear chart and those transitional nuclei show quite rich excitation spectra (see e.g., [38]). Existence of wide transitional regions is a characteristic feature of finite quantum systems and provides an invaluable opportunity to investigate the process of the quantum phase transition through the change of quantum spectra with nucleon number. A detailed account of instability phenomena and strong anharmonicity effects in the transitional region is given in chapter 6 of [3].

2.3. Quadrupole collective dynamics

Before introducing the Bohr–Mottelson collective Hamiltonian, we add some remarks on quadrupole collective phenomena that await its application.

Interplay of low-frequency shape fluctuations and rotational motions

In finite quantum systems such as nuclei, the rotational ANG modes may couple with quantum shape-fluctuation modes rather strongly. For example, even when the self-consistent mean field acquires a deep local minimum at a finite value of β in this direction, the deformation energy surface may be flat in the γ direction. In this case, the nucleus may exhibit a large-amplitude shape fluctuation in the γ degree of freedom. (Here, β and γ represent the magnitudes of axial and triaxial quadrupole deformations.) Actually, such a situation, called γ soft, is widely observed in experiments. In nuclei which preserve the axial symmetry, the quantum-mechanical collective rotation about the symmetry axis is forbidden. Once the axial symmetry is dynamically broken by quantum shape fluctuations, however, the rotational degrees of freedom about three principal axes are all activated. As a consequence, the rotational spectra in such γ-soft nuclei do not exhibit a simple $I(I+1)$ pattern of an axial rotor. Such an interplay of the shape-fluctuation and rotational modes may be regarded as a characteristic feature of finite quantum systems and provides an invaluable opportunity to investigate the process of the quantum phase transition through analysis of quantum spectra.

Thus, we need to treat the two kinds of collective modes (symmetry-restoring ANG modes and quantum shape fluctuation modes) in a unified manner to describe low-energy excitation spectra of nuclei.

Quantum shape fluctuations and shape coexistence

When different kinds of quantum eigenstates associated with different shapes coexist in the same energy region, we call them '*shape coexistence phenomena.*' This situation is realized when shape mixing due to tunneling motion is weak and collective wave functions retain their localizations about different equilibrium shapes. In contrast, when the shape mixing is strong, large-amplitude shape fluctuations (*delocalization* of the collective wave functions) extending to different local minima may occur.

When a few local minima of the mean field with different shapes appear in the same energy region, LACM tunneling through potential barriers and extending between local minima may take place. These phenomena may be regarded as a kind of macroscopic quantum tunneling. Note that the barriers are not given by external fields but are self-consistently generated as a consequence of quantum dynamics of the many-body system. Quantum spectra of low-energy excitation that needs such concepts have been observed in almost all regions of the nuclear chart [39–41].

3. Bohr–Mottelson collective Hamiltonian

Bohr and Mottelson introduced the five-dimensional (5D) quadrupole collective Hamiltonian describing the quadrupole vibrations and rotations in a unified manner [3]. It is written as

$$H_{\rm coll} = T_{\rm vib} + T_{\rm rot} + V(\beta, \gamma), \tag{2}$$

$$T_{\rm vib} = \frac{1}{2}D_{\beta\beta}(\beta, \gamma)\dot{\beta}^2 + D_{\beta\gamma}(\beta, \gamma)\dot{\beta}\dot{\gamma} + \frac{1}{2}D_{\gamma\gamma}(\beta, \gamma)\dot{\gamma}^2, \tag{3}$$

$$T_{\rm rot} = \frac{1}{2}\sum_{k=1}^{3}\mathcal{J}_k(\beta, \gamma)\dot{\varphi}_k^2. \tag{4}$$

Here, φ_k are components of the rotational angle on the three intrinsic axes. The quadrupole deformations (β, γ) and the rotational angles φ_k are treated as dynamical variables, and $(\dot{\beta}, \dot{\gamma})$ and $\dot{\varphi}_k$ represent their time derivatives. The $\dot{\varphi}_k$ are called angular velocities. We shall define in section 5 the (β, γ) deformations through the expectation values of the quadrupole operators with respect to the time-dependent mean-field states. The quantities $(D_{\beta\beta}, D_{\beta\gamma}, D_{\gamma\gamma})$ appearing in the kinetic energies of vibrational motion, $T_{\rm vib}$, represent inertial masses of the vibrational motion. They are functions of β and γ. The quantities $\mathcal{J}_k(\beta, \gamma)$ in the rotational energy $T_{\rm rot}$ represent the moments of inertia with respect to the intrinsic (body-fixed) axes. The intrinsic axes may be defined by the principal axes of the body-fixed frame that is attached to the instantaneous shape of the time-dependent mean field. The term, $V(\beta, \gamma)$, represents the potential energy as a function of β and γ.

The Bohr–Mottelson collective Hamiltonian (2) is often referred to in relation to the liquid drop model. It should be emphasized, however, that, the analogy with the *classical* liquid drop is irrelevant to low-frequency quadrupole collective motions. Already in the 1950's, it was recognized that the nucleus is 'an unusual idealized *quantum* fluid' and 'one is dealing with a most interesting new form of matter' [42]. Indeed, as discussed in section 2, most of nuclei may be regarded as a superfluid of extremely small size (with a radius of a few femtometer), and the nature of nuclear deformation is essentially different from that of surface shape oscillations of the classical liquid drop; that is, the nuclear deformation is associated with quantum shell structure and spontaneous breaking of the spherical symmetry in the self-consistent mean field.

The form of the collective Hamiltonian (2) is quite general and applicable to various finite many-body systems, but the specific dynamical properties of the system of interest are revealed by the values and the (β, γ)-dependence of the collective inertia masses $(D_{\beta\beta}, D_{\beta\gamma}, D_{\gamma\gamma}, \mathcal{J}_k)$ as well as the potential energy $V(\beta, \gamma)$. For understanding the dynamical properties of the nucleus, therefore, it is imperative to derive these quantities in a microscopic way and compare with what experimental data indicate. We shall show in this review that the collective Hamiltonian (2) with the collective inertial masses and the potential energy microscopically evaluated on the basis of the moving superfluid mean-field picture describes very well the low-frequency quadrupole collective dynamics of the nucleus. Furthermore, quantum correlations beyond the mean field are nicely described by quantizing the collective variables that govern the time evolution of the self-consistent mean field.

The classical Hamiltonian (2) is given in terms of the five curvilinear coordinates $(\beta, \gamma,$ and the three Euler angles which are connected with φ_k by a linear transformation) and their time derivatives. For quantization in curvilinear coordinates, we can adopt the so-called Pauli prescription [43]. (For convenience of readers, we recapitulate this prescription in appendix A.) We shall discuss on its foundation in section 5 describing the microscopic derivation of the Bohr–Mottelson collective Hamiltonian. The quantized 5D quadrupole collective Hamiltonian takes the following form:

$$\hat{H}_{\rm coll} = \hat{T}_{\rm vib} + \hat{T}_{\rm rot} + V(\beta, \gamma). \tag{5}$$

Here, the vibrational kinetic energy term $\hat{T}_{\rm vib}$ is given by

$$\begin{aligned}\hat{T}_{\rm vib} = -\frac{1}{2\sqrt{WR}}\Bigg\{&\frac{1}{\beta^4}\Bigg[\frac{\partial}{\partial\beta}\left(\beta^2\sqrt{\frac{R}{W}}D_{\gamma\gamma}\frac{\partial}{\partial\beta}\right)\\ &-\frac{\partial}{\partial\beta}\left(\beta^2\sqrt{\frac{R}{W}}D_{\beta\gamma}\frac{\partial}{\partial\gamma}\right)\Bigg]\\ &+\frac{1}{\beta^2\sin 3\gamma}\Bigg[-\frac{\partial}{\partial\gamma}\left(\sqrt{\frac{R}{W}}\sin 3\gamma D_{\beta\gamma}\frac{\partial}{\partial\beta}\right)\\ &+\frac{\partial}{\partial\gamma}\left(\sqrt{\frac{R}{W}}\sin 3\gamma D_{\beta\beta}\frac{\partial}{\partial\gamma}\right)\Bigg]\Bigg\},\end{aligned} \tag{6}$$

and the rotational energy term $\hat{T}_{\rm rot}$ is given by

$$\hat{T}_{\rm rot} = \sum_{k=1,2,3}\frac{\hat{I}_k^2}{2\mathcal{J}_k(\beta, \gamma)} \tag{7}$$

with $\hat{I}_k$ denoting three components of the angular momentum operator with respect to the intrinsic axes. In this paper, we use the unit with $\hbar = 1$. In the above equations,

$$\beta^2 W(\beta, \gamma) = D_{\beta\beta}(\beta, \gamma)D_{\gamma\gamma}(\beta, \gamma) - D_{\beta\gamma}^2(\beta, \gamma), \tag{8}$$

$$R(\beta, \gamma) = D_1(\beta, \gamma)D_2(\beta, \gamma)D_3(\beta, \gamma), \tag{9}$$

and $D_k(\beta, \gamma)\,(k = 1, 2, 3)$ are the rotational inertial functions related to the moments of inertia by

$$\mathcal{J}_k(\beta, \gamma) = 4\beta^2 D_k(\beta, \gamma)\sin^2(\gamma - 2\pi k/3). \tag{10}$$

If all inertial masses $(D_{\beta\beta}, D_{\gamma\gamma}\beta^{-2}, D_1, D_2, D_3)$ are replaced by a common constant D and $D_{\beta\gamma}$ is ignored, the above $\hat{T}_{\rm vib}$ is reduced to

$$\hat{T}_{\rm vib} = -\frac{1}{2D}\left(\frac{1}{\beta^4}\frac{\partial}{\partial\beta}\beta^4\frac{\partial}{\partial\beta} + \frac{1}{\beta^2\sin 3\gamma}\frac{\partial}{\partial\gamma}\sin 3\gamma\frac{\partial}{\partial\gamma}\right). \tag{11}$$

Such a drastic approximation may be valid only for small-amplitude vibrations about a spherical HFB equilibrium. The need to go beyond this simplest approximation for the inertia masses has been pointed out [3]. For recent experimental data

and phenomenological analyses of this problem, we refer [44, 45] and references therein.

The collective Schrödinger equation is

$$[\hat{T}_{\rm vib} + \hat{T}_{\rm rot} + V(\beta, \gamma)]\Psi_{\alpha IM}(\beta, \gamma, \Omega) = E_{\alpha I}\Psi_{\alpha IM}(\beta, \gamma, \Omega). \tag{12}$$

The collective wave function in the laboratory frame, $\Psi_{\alpha IM}(\beta, \gamma, \Omega)$, is a function of β, γ, and a set of three Euler angles Ω. It is specified by the total angular momentum I, its projection onto the z-axis in the laboratory frame M, and α that distinguishes the eigenstates possessing the same values of I and M. With the rotational wave function $\mathcal{D}^I_{MK}(\Omega)$, they are written as

$$\Psi_{\alpha IM}(\beta, \gamma, \Omega) = \sum_{K=\text{even}} \Phi_{\alpha IK}(\beta, \gamma)\langle\Omega|IMK\rangle, \tag{13}$$

where

$$\langle\Omega|IMK\rangle = \sqrt{\frac{2I+1}{16\pi^2(1+\delta_{K0})}}\,[\mathcal{D}^I_{MK}(\Omega) + (-)^I\mathcal{D}^I_{M,-K}(\Omega)]. \tag{14}$$

The vibrational wave functions in the body-fixed frame, $\Phi_{\alpha IK}(\beta, \gamma)$, are normalized as

$$\int \mathrm{d}\beta\mathrm{d}\gamma\sqrt{G(\beta, \gamma)}\,|\Phi_{\alpha I}(\beta, \gamma)|^2 = 1, \tag{15}$$

where

$$|\Phi_{\alpha I}(\beta, \gamma)|^2 \equiv \sum_{K=\text{even}} |\Phi_{\alpha IK}(\beta, \gamma)|^2, \tag{16}$$

and the volume element is given by $\sqrt{G(\beta, \gamma)}\,\mathrm{d}\beta\mathrm{d}\gamma$ with

$$G(\beta, \gamma) = 4\beta^8 W(\beta, \gamma)R(\beta, \gamma)\sin^2 3\gamma. \tag{17}$$

Thorough discussions of symmetries of the collective wave functions and the boundary conditions for solving the collective Schrödinger equation are given in [3, 23, 46, 47].

Inserting (13) into the collective Schrödinger equation (12), we obtain the eigenvalue equation for vibrational wave functions

$$[\hat{T}_{\rm vib} + V(\beta, \gamma)]\Phi_{\alpha IK}(\beta, \gamma) + \sum_{K'=\text{even}} \langle IMK|\,\hat{T}_{\rm rot}\,|IMK'\rangle\Phi_{\alpha IK'}(\beta, \gamma) = E_{\alpha I}\Phi_{\alpha IK}(\beta, \gamma). \tag{18}$$

Solving this equation, we obtain quantum spectra and collective wave functions. It is then straightforward to calculate electromagnetic transition probabilities among collective excited states. We recapitulate some basic formulae in appendix B.

Historical note

The simple expression (11) with a constant mass parameter D for the vibrational kinetic energy is valid for harmonic vibrations about a spherical equilibrium point of the mean field, as derived in the 1952 paper [1] by transforming the collective Hamiltonian for harmonic shape vibrations to the body-fixed frame defined as the instantaneous principal axis frame of the vibrating density distribution. Combined with the irrotational mass parameter $D_{\rm irrot}$ resulting from modeling the vibrational flow by that of the irrotational fluid, it is sometimes referred to the Bohr liquid drop Hamiltonian. It should be emphasized, however, that the inadequacy of the irrotational fluid model for the low-frequency quadrupole excitations was recognized from early on.

In the preface to the second edition (March 1, 1957) of the 1953 paper [48], Bohr and Mottelson wrote: 'As a first orientation, one attempted to employ for these parameters obtained from a liquid drop model, but already the early analysis of various nuclear properties showed the limitation of this comparison. The inadequacy of the liquid drop estimates was especially clearly brought out by the comparison of the nuclear moment of inertia with the deformations deduced from the rate of the electric quadrupole rotational transitions.' 'An improved understanding of the collective nuclear properties has come from the efforts to derive these directly from the motion of the nucleons; this analysis has revealed the important influence of the nuclear shell structure on the collective motion.' 'The inadequacy of the liquid drop model with irrotational flow implies that the collective coordinates considered as functions of the nucleonic variables are of more general form than (II.2) , ...' ((II.2) is the famous definition of the collective parameters $\alpha_{\lambda,\mu}$ in terms of the polar coordinates of individual particles).

Indeed, if we assume that a collective coordinate corresponds to a *local* one-body operator in the coordinate space (such as the mass-multipole operator), we obtain a collective mass parameter associated with an irrotational velocity field (see p. 510 of [3] and [49]).

Illustration of typical situations

Figure 2 illustrates typical patterns of the collective potential energy surface $V(\beta, \gamma)$; these are classified according to the location of the local minimum. In the case that the potential energy $V(\beta, \gamma)$ has a deep minimum at a finite value of β and $\gamma = 0°$ (or $\gamma = 60°$), a regular rotational spectrum with the $I(I+1)$ pattern may appear. In addition to the ground band, we can expect the β and γ bands to appear, where vibrational quanta with respect to the β and γ degrees of freedom are excited. Detailed investigations on the γ-vibrational bands over many nuclei have revealed, however, that they usually exhibit significant anharmonicities (non-linearlities) [50]. Situations for the β-vibrational bands are quite mysterious. Recent experimental data indicate the need for a radical review of their characters [41]. We shall discuss on this problem in section 9. The coexistence of two local minima at oblate and prolate shapes is a typical example of shape coexistence. Experimental data indicate that the potential barrier between the two minima is, in many cases, low and the collective wave functions extend over the oblate and prolate regions through quantum tunneling (shape mixing). Also, there are many nuclei exhibiting intermediate features between the large-amplitude collective vibrations associated with the oblate-prolate shape coexistence and the rotational motions associated with the triaxial shape. We present in appendix C a simple model that may be useful to understand several interesting limits of triaxial deformation dynamics in a

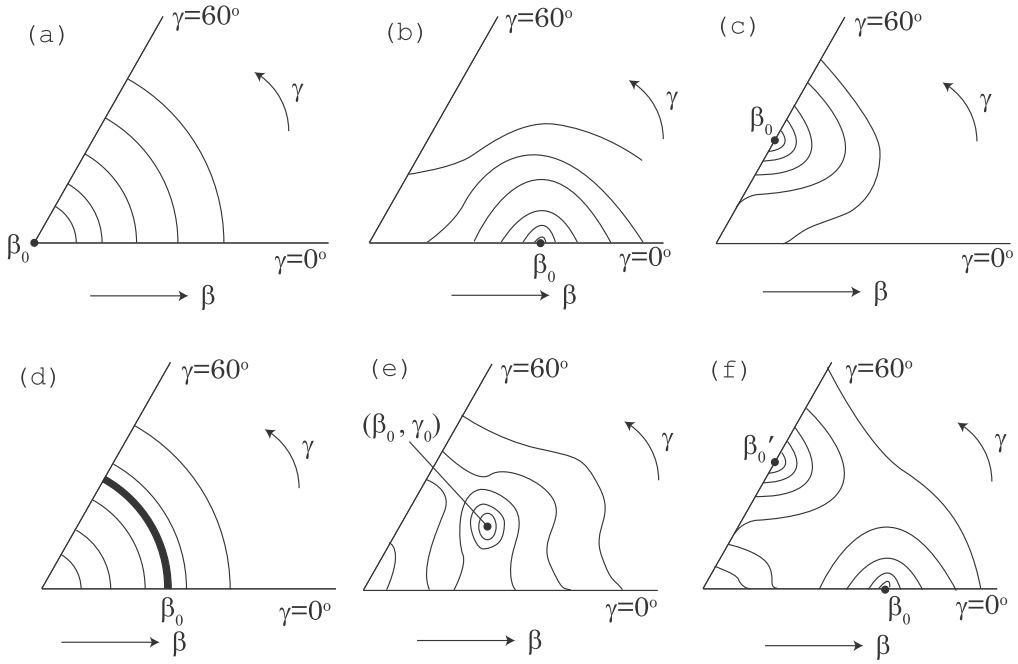

Figure 2. Illustration of typical patterns of the collective potential-energy surface $V(\beta, \gamma)$, classified according to the location of the local minimum point(s) (β_0, γ_0): (a) spherical, (b) prolate, (c) oblate, (d) $\beta_0 \neq 0$ in the β direction but the potential is flat with respect to γ (so-called γ-unstable situation [51]), (e) triaxial, and (f) coexistence of the oblate and prolate minima.

unified perspective, including the axially symmetric rotor model, the γ-unstable model [51], the triaxial rigid rotor model [52], and an ideal situation of the oblate-prolate shape coexistence.

4. QRPA and its extensions

In this section, we summarize the elementary concepts in microscopic theory of nuclear collective motion [53–57]. We adopt the time-dependent mean-field picture. The main reason is that it provides a basis for a clear understanding of the correspondence between the quantum and classical aspects of the nuclear collective motions. Furthermore, this approach enables us to microscopically derive the collective coordinates and momenta on the basis of the time-dependent variational principle.

We shall start from small-amplitude vibrations about the spherical equilibrium shape and then go to large-amplitude regime, where we need to consider full 5D quadrupole collective dynamics including three-dimensional (3D) rotations restoring the broken symmetries as well as axially symmetric and asymmetric shape fluctuations.

4.1. Collective motion as moving self-consistent mean field

Let us consider even-even nuclei whose ground states consist of correlated nucleon pairs occupying time-reversal conjugate single-particle states. The Hartree–Fock–Bogoliubov (HFB) method is a generalized mean-field theory treating the formation of the HF mean field and superfluidity (nucleon pair condensate) in a self-consistent manner [54, 55, 57, 58], and yields the concept of quasiparticles as single-particle excitation modes in the presence of the pair condensate. Bohr and Mottelson opened the way to a unified understanding of single-particle and collective modes of motion of nuclei by introducing the concept of moving self-consistent mean field [3–5]. The time-dependent extension of the HFB mean field, called the time-dependent HFB (TDHFB) theory, is suitable to formulate their ideas [47, 54, 55, 57].

It is well known that the time evolution of the TDHF state vectors can be written as time-dependent unitary transformations (see e.g., [59, 60]). It is called the generalized Thouless theorem. Adapting this theorem for nuclei with superfluidity, the TDHFB state vector $|\phi(t)\rangle$ may be written as [61]:

$$|\phi(t)\rangle = \mathrm{e}^{\mathrm{i}\hat{G}(t)}|\phi(t=0)\rangle = \mathrm{e}^{\mathrm{i}\hat{G}(t)}|\phi_0\rangle, \tag{19}$$

$$\mathrm{i}\hat{G}(t) = \sum_{(kl)}\{g_{kl}(t)a_k^\dagger a_l^\dagger - g_{kl}^*(t)a_l a_k\}, \tag{20}$$

where the HFB ground state $|\phi_0\rangle$ is a vacuum for quasiparticles $(a_k^\dagger, a_l)$,

$$a_k|\phi_0\rangle = 0, \tag{21}$$

with the suffix k distinguishing different quasiparticle states. (See appendix D for more details.) The functions $g_{kl}(t)$ in the one-body operator $\hat{G}(t)$ is determined by the time-dependent variational principle

$$\delta\langle\phi(t)|\left(\mathrm{i}\frac{\partial}{\partial t} - \hat{H}\right)|\phi(t)\rangle = 0. \tag{22}$$

The TDHFB states can be regarded as generalized coherent states, which are a kind of wave packets and cover the whole Hilbert space of a given Fermion many-body system [62, 63].

We call this space 'the TDHFB phase space.' It may also be called 'the TDHFB symplectic manifold' [63, 64]. This semiclassical concept is quite important because it provides a clear physical picture of collective dynamics. We shall see below that the unitary representation (19) is very convenient to develop a microscopic theory of nuclear collective motions.

4.2. Small-amplitude approximation (QRPA)

For small-amplitude vibrations around an HFB equilibrium point, one can make the linear approximation to the TDHFB equations and obtain the quasiparticle random phase approximation (QRPA). This is a starting point of microscopic theory of collective motion [13, 14]. Expanding equation (19) in a power series of $\hat{G}(t)$ and taking only the linear order, we obtain

$$\delta\langle\phi_0|[\hat{H}, \mathrm{i}\hat{G}] + \frac{\partial\hat{G}}{\partial t}|\phi_0\rangle = 0. \tag{23}$$

In place of the functions $g_{kl}(t)$ and $g^*_{kl}(t)$ in equation (20), let us introduce normal coordinates $q(t) = \{q^1(t), q^2(t), \cdots, q^f(t)\}$ and conjugate momenta $p(t) = \{p_1(t), p_2(t), \cdots, p_f(t)\}$, and represent $\hat{G}(t)$ in terms of the infinitesimal generators $(\hat{Q}^i, \hat{P}_i)$ of $(p_i(t), q^i(t))$ as

$$\hat{G}(t) = \sum_{i=1}^{f}(p_i(t)\hat{Q}^i - q^i(t)\hat{P}_i). \tag{24}$$

Here it is important to distinguish the *classical* dynamical variables $(q_i(t), p^i(t))$ from the *quantum* infinitesimal generators $(\hat{Q}^i, \hat{P}_i)$. This representation is equivalent to equation (20) if the number of normal coordinates, f, is equal to the number of independent two-quasiparticle configurations (kl). In reality, we shall be interested in only a few collective modes among the f normal modes. For small-amplitude vibrations under consideration, the harmonic approximation holds; that is, time dependence of $q^i(t)$ and $p_i(t)$ is given by

$$\dot{p}_i(t) = B_i\ddot{q}^i(t) = -C_iq^i(t), \tag{25}$$

where the $\dot{p}_i(t)$, C_i, and B_i denote time-derivative of $p_i(t)$, the stiffness (restoring force) parameter, and the inertial mass for the normal mode (specified by the suffix i), respectively. Inserting (24) into (23) and using (25), we obtain the QRPA equation

$$[\hat{H}, \hat{Q}^i] = -\mathrm{i}B^i\hat{P}_i, \tag{26}$$

$$[\hat{H}, \hat{P}_i] = \mathrm{i}C_i\hat{Q}^i. \tag{27}$$

where B^i denotes the reciprocal of B_i, i.e., $B^i = 1/B_i$. These equations determine the microscopic structure of $\hat{Q}^i$ and $\hat{P}_i$ as coherent superpositions of many two-quasiparticle excitations: expressing them as sums over independent two-quasiparticles states (kl),

$$\hat{Q}^i = \sum_{(kl)} q^i_{kl}(a^\dagger_k a^\dagger_l + a_l a_k), \tag{28}$$

$$\hat{P}_i = \mathrm{i}\sum_{(kl)} p^i_{kl}(a^\dagger_k a^\dagger_l - a_l a_k), \tag{29}$$

and inserting these into (26) and (27), we obtain linear eigenvalue equations determining the frequency squared, $\omega_i^2 = B^iC_i$, and the amplitudes (q^i_{kl}, p^i_{kl}). Actually, we have to choose appropriate solutions among large number of solutions (the number of independent two-quasiparticle configurations). It is not difficult to identify them, however, because the solutions corresponding to low-frequency quadrupole vibrations appear much lower than twice the pairing gap, 2Δ, (or the lowest two-quasiparticle excitation energy) and they are formed by coherent superpositions of many two-quasiparticle excitations. Because the time evolution of the TDHFB state $|\phi(t)\rangle$ is determined by the normal coordinates and momenta $(q^i(t), p_i(t))$, we can write it as $|\phi(q, p)\rangle$. Using equations (26), (27), and (35) below, we can easily calculate the expectation value of the microscopic Hamiltonian with respect to $|\phi(q, p)\rangle$:

$$\langle\phi(q,p)|\,\hat{H}\,|\phi(q,p)\rangle = \langle\phi_0|\,\hat{H}\,|\phi_0\rangle + \frac{1}{2}\sum_{i=1}^{f}(B^ip_i^2 + C_iq^{i2}). \tag{30}$$

The increase of the total energy due to the vibrational motion,

$$\mathcal{H}(q,p) \equiv \langle\phi(q,p)|\,\hat{H}\,|\phi(q,p)\rangle - \langle\phi_0|\,\hat{H}\,|\phi_0\rangle, \tag{31}$$

may be identified as the classical vibrational Hamiltonian. Below we shall not consider the ground-state energy (the second term in the r.h.s.), because it does not affect the equations of motion for $(q^i(t), p_i(t))$.

For vibrational modes whose frequencies, $\omega_i = \sqrt{B^iC_i}$, are positive, we can define the creation and annihilation operators $(\Gamma^\dagger_i, \Gamma_i)$ of the excitation mode as

$$\Gamma^\dagger_i = \frac{1}{\sqrt{2}}\left(\sqrt{\frac{\omega_i}{B^i}}\hat{Q}^i - \mathrm{i}\sqrt{\frac{B^i}{\omega_i}}\hat{P}_i\right) \tag{32}$$

and their Hermitian conjugates Γ_i. As is well known, they are written in terms of the quasiparticle operators as

$$\Gamma^\dagger_i = \sum_{(kl)}(x^i_{kl}a^\dagger_k a^\dagger_l - y^i_{kl}a_l a_k), \tag{33}$$

and obey the QRPA equation of motion,

$$[\hat{H}, \Gamma^\dagger_i] = \omega_i\Gamma^\dagger_i. \tag{34}$$

It is worth noting that the $(\hat{Q}^i, \hat{P}_i)$ representation possesses a wider applicability than the $(\Gamma^\dagger_i, \Gamma_i)$ representation. First, for the ANG modes with $\omega_i = 0$, the former is valid while the latter is undefined. Note that their inertial masses, B_i (inverse of B^i), are positive, whereas their frequencies ω_i become to zero because the restoring-force parameters C^i vanish. Second, the $(\hat{Q}^i, \hat{P}_i)$ representation is valid also for unstable HFB equilibria where C_i is negative and ω_i is imaginary. Obviously, we cannot define the creation and annihilation operators $(\Gamma^\dagger_i, \Gamma_i)$ for imaginary ω_i. We shall see that this is one of the key points when we try to extend the QRPA approach to non-equilibrium points far from the HFB local minima.

Merits of the QRPA

One of the beauties of the QRPA is that it is able to determine the microscopic structures of collective coordinates and momenta in terms of a large number of microscopic (particle-hole, particle-particle, hole-hole) degrees of freedom. We can thus learn how collective vibrations are generated as coherent superpositions of many two-quasiparticle excitations. It is well known that two kinds of isoscalar quadrupole vibration appear exhibiting quite different characteristics; the low- (usually first excited 2^+) and high-frequency (giant resonance) modes. Examining the microscopic structure of the low-frequency quadrupole vibrations, we see that the weights of two-quasiparticle excitations near the Fermi surface are much larger than those in the mass quadrupole operators (see, e.g., [65]). This example clearly shows the importance of describing collective modes in a microscopic way.

Another merit of the QRPA is that it yields the ANG modes as self-consistent solutions and determines their collective inertial masses. With use of the QRPA, we can restore the symmetries broken by the mean-field approximation. Furthermore, the QRPA fulfills the energy-weighted sum rules [66].

Quantization condition

In the QRPA, the following condition is customarily imposed to ortho-normalize the amplitudes (q^i_{kl}, p^i_{kl}) or (x^i_{kl}, y^i_{kl}).

$$\langle\phi_0|[\hat{Q}^i, \hat{P}_j]|\phi_0\rangle = \mathrm{i}\delta_{ij}, \tag{35}$$

or

$$\langle\phi_0|[\Gamma_i, \Gamma^\dagger_j]|\phi_0\rangle = \delta_{ij}. \tag{36}$$

We shall call this condition *canonical-variable condition*. It should be emphasized that, differently from the time-independent approaches, e.g. [13], these conditions cannot be derived within the standard framework of the TDHFB theory. For the derivation and justification of the canonical-variable conditions, we need to clarify the canonical structure of the TDHFB theory. We shall discuss on this point in section 8.

In this connection, we note that the inertial masses are not uniquely determined by (26) and (27), because the QRPA equations are invariant against the scale transformations $\hat{Q}^i \to s^i\hat{Q}^i$ and $\hat{P}_i \to \hat{P}_i/s^i$ with arbitrary values of s^i. It is therefore possible to adopt the values of s^i such that the collective inertial masses become unity. This arbitrariness is related to the freedom of scale transformations of the normal coordinates and momenta (q^i, p_i).

Because (q^i, p_i) are canonical variables, we can make canonical quantization and obtain the quantum collective Hamiltonian,

$$\hat{H}_{\mathrm{QRPA}} = \frac{1}{2}\sum_{i=1}^{f}(B^i(\hat{p}_i)^2 + C_i(\hat{q}^i)^2). \tag{37}$$

Here, the collective coordinates and momenta, $\hat{p}_i$ and $\hat{q}^i$, are quantum operators. It is important to note that the QRPA ground state after the quantization is different from the HFB ground state due to the quantum zero-point fluctuations.

The necessity of canonical quantization in order to derive QRPA from the TDHFB theory, discussed above, is not necessarily emphasized in standard textbooks on theoretical nuclear physics. We shall see in section 8, however, that the recognition of this point is essential to extend the basic ideas of the QRPA for small amplitude vibrations to LACM.

Effective interactions for QRPA calculations

In the investigation of low-energy excitation spectra, the pairing-plus-quadrupole (P + Q) model [67–69] and its extension [70] have been playing the major roles. This phenomenological effective interaction represents the competition between the pairing correlations favoring the spherical symmetry and the quadrupole (particle-hole) correlations leading to the quadrupole deformation of the mean field [3, 71].

In recent years, QRPA calculations using density-dependent effective interactions [72–76] have become possible. Density-dependent contact interactions such as the Skyrme interactions [72, 73, 76] may be founded on the density functional theory (DFT) [58]. From this point of view, the Skyrme interactions may be better called the Skyrme *energy density functionals* (EDFs). Accordingly, the self-consistent calculations that use the same density-dependent contact interactions in solving the HFB equations for the ground state and the QRPA for excited states may be regarded as small-amplitude approximations of the time-dependent DFT (TDDFT) [77]. A number of good textbooks on DFT and TDDFT are available, e.g., [78, 79]. Note, however, there are conceptual differences between those for condensed-matter and those for nuclei, since the nucleus is a self-bound system without an external potential [77].

For spherical mean fields, the QRPA matrix is block-diagonal with respect to the angular momentum (J) and the parity (π) of two-quasiparticle configurations. Usually, the $J^\pi = 2^+$ solution with lowest positive ω_i corresponds to the first excited quadrupole vibrational state. In this case, many calculations were performed [58, 80]. For axially symmetric deformed mean fields, the QRPA matrix is block-diagonal with respect to the K quantum number (projection of angular momentum on the symmetry axis) and the parity of two-quasiparticle configurations. The $K^\pi = 2^+$ (0^+) solution with lowest positive ω_i may correspond to the first excited γ (β)-vibrational state. It is well known, however, that the lowest $K^\pi = 0^+$ solution contains an appreciable mixture of the pairing vibrational modes of protons and/or neutrons (sensitively depending on the deformed shell structure around the Fermi surface) [3]. Moreover, as we shall discuss in section 9, recent experiments reveal mysterious characters of the lowest $K^\pi = 0^+$ excitations. Although the dimension of the QRPA matrix is much larger than that in the spherical case, large scale QRPA calculations with modern EDFs have been carried out also for deformed nuclei in recent years [81–89]. In this way, it becomes one of the modern subjects in nuclear structure physics to carry out fully self-consistent

QRPA calculations on the basis of DFT for superfluid (spherical and deformed) nuclei and treat low- and high-frequency vibrations (giant resonances) as well as the ground states in a unified way for all nuclei from the proton-drip line to the neutron-drip line.

For triaxial mean fields breaking the axial symmetry, the dimension of the QRPA matrix further increases and it becomes computationally too heavy to diagonalize it at the present time. To overcome this problem, a new method of solving the QRPA equations without recourse to diagonalization of the QRPA matrix has been developed in recent years [90–92]. It is called the *finite-amplitude method*, and applied mainly to calculate strength functions for giant resonances [93–97]. We shall suggest in section 5 that this method may be useful also for solving the *local* QRPA equations.

Relations to spherical shell-model calculations

The lowest 2^+ vibrational states are obtained in the spherical shell model as coherent superpositions of many configurations. The *coherence* is indirectly confirmed by, e.g. the enhancements of the electric-quadrupole (E2) transition probabilities $B(E2; 2_1^+ \rightarrow 0_1^+)$. In the QRPA, we can directly see the coherence in the QRPA amplitudes, x^i_{kl} and y^i_{kl} (or q^i_{kl} and p^i_{kl}). In the time-dependent mean-field picture, *this coherence represents the correlations generating the self-consistent deformed mean field.* In this way, the TDHFB theory provides a transparent physical interpretation on the microscopic mechanism of emergence of nuclear collective motions.

4.3. Beyond the QRPA

Boson expansion method

The boson expansion method is well known as a useful microscopic method for describing anharmonic (non-linear) vibrations going beyond the harmonic approximation of the QRPA. In this approach, we first construct a collective subspace spanned by many-phonon states of vibrational quanta (determined by the QRPA) in the huge-dimensional shell-model space, and then map these many-phonon states one-to-one to many-boson states in an ideal boson space. Anharmonic effects neglected in the QRPA are treated as higher-order terms in the power-series expansion with respect to the boson creation and annihilation operators. Starting from the QRPA about a spherical shape, one can thus derive the 5D quadrupole collective Hamiltonian in a fully quantum mechanical manner. The boson expansion method has been successfully applied to low-energy quadrupole excitation spectra in a wide range of nuclei including those lying in regions of quantum phase transitions from spherical to deformed [15, 98].

Non-perturbative approaches to LACM

The boson expansion about a single HFB local minimum is not suitable for treating a situation where a few local minima in the potential-energy surface $V(\beta, \gamma)$ compete in energy. In such situations the collective wave functions are not necessarily localized around a single minimum but tunnel through the potential barrier. We frequently encounter such situations, called 'shape coexistence/mixing phenomena' in low-energy excitation spectra. The need to develop non-perturbative approaches capable of treating quantum many-body barrier penetrations is high also for treating large-amplitude collective motions in low-energy regions, such as spontaneous fissions and sub-barrier fusion reactions. It has been one of the longstanding fundamental subjects in nuclear structure physics to construct a microscopic theory of LACM by extending the QRPA concepts to arbitrary points in the $V(\beta, \gamma)$ plane far from the HFB minima [77, 99, 100].

State vectors of time-dependent mean field are kinds of generalized coherent states, and we can rigorously formulate the TDHFB as a theory of classical Hamiltonian dynamical system of large dimension [63, 101]. Because time evolution of the mean field is determined by the classical Hamilton equations, we cannot describe, within the framework of the TDHFB, quantum spectra of low-lying states and macroscopic quantum tunneling phenomena such as spontaneous fissions and sub-barrier fusions. To describe these genuine quantum phenomena, we need to introduce a few collective variables determining the time evolution of the mean field and quantize them. Succeeding and developing the ideas in microscopic theories of LACM acquired during 1970's-1990's, we have developed a new method, called the ASCC method [102], and shown its usefulness by applying it to shape coexistence/mixing phenomena [103, 104].

Introduction to the ASCC method

Here we very briefly describe the basic ideas of the ASCC method [102]. It will be presented in section 8 in a more systematic way. In this approach, assuming that the time evolution of the TDHFB state is determined by a few collective coordinates $q = (q^1, q^2, \cdots, q^f)$ and collective momenta $p = (p_1, p_2, \cdots, p_f)$, we write the TDHFB state as $|\phi(t)\rangle = |\phi(q(t), p(t))\rangle$. The TDHFB states $|\phi(q, p)\rangle$ constitute the $2f$-dimensional submanifold in the TDHFB phase space, which is called *collective submanifold*. In the ASCC method, we further assume that $|\phi(q, p)\rangle$ can be written in a form

$$|\phi(q, p)\rangle = \exp\left\{\mathrm{i}\sum_{i=1}^{f} p_i \hat{Q}^i(q)\right\}|\phi(q)\rangle, \tag{38}$$

where $\hat{Q}^i(q)$ are one-body operators corresponding to infinitesimal generators of p_i locally defined at the state $|\phi(q)\rangle$ which represents a TDHFB state $|\phi(q, p)\rangle$ at $p \rightarrow 0$. This state $|\phi(q)\rangle$ is called a *moving-frame HFB state.* Inserting (38) into the time-dependent variational principle, equation (22), and considering that the time dependence is determined by the collective coordinates and momenta (q, p),

we obtain

$$\delta\langle\phi(q,p)|\left\{\mathrm{i}\sum_{i=1}^{f}\left(\dot{q}^i\frac{\partial}{\partial q^i}+\dot{p}_i\frac{\partial}{\partial p_i}\right)-\hat{H}\right\}|\phi(q,p)\rangle=0. \tag{39}$$

We shall give a rigorous formulation to determine the microscopic structures of the infinitesimal generator $\hat{Q}^i(q)$ of p_i on the basis of the time-dependent variational principle (39). We shall also introduce infinitesimal generators $\hat{P}_i(q)$ of q^i and determine their microscopic structures. Furthermore, we shall formulate the theory such that the collective variables (q, p) can be treated as canonical variables.

Quite recently, we have proposed a practical approximation scheme to the ASCC method. It is called the *local* QRPA (LQRPA) method [105–110]. Here, the adjective '*local*' means that it is locally defined around a point in the (β, γ) deformation space. More rigorously speaking, it is defined around a point on the collective submanifold embedded in the TDHFB phase space, and this point is mapped onto the (β, γ) space. The infinitesimal generators appearing in this method are nonlocal in the coordinate space. It may be regarded as an extension of the ordinary QRPA to non-equilibrium states, where the moving-frame HFB states $|\phi(q)\rangle$ play a role analogous to the static HFB ground state $|\phi_0\rangle$. Because of this analogy it may be easy to understand the LQRPA method. In the next section, we show how this method is used for a microscopic derivation of the Bohr-Mottelson collective Hamiltonian. Fundamentals and validity of the LQRPA method will be discussed later in section 8.

5. Microscopic derivation of the Bohr–Mottelson collective Hamiltonian

In this section, we derive the quadrupole collective Hamiltonian making use of the LQRPA method. We also discuss fundamental problems related to the microscopic derivation of the collective Hamiltonian.

5.1. Procedure for the microscopic derivation

Instead of treating the 5D collective coordinates simultaneously, we first calculate the collective inertial masses for two-dimensional (2D) vibrational motions corresponding to the (β, γ) deformation degree of freedom, and subsequently calculate the moments of inertia for 3D rotational motions at each point of (β, γ). We then derive the collective Hamiltonian for the 5D quadrupole collective dynamics and quantize it.

Microscopic calculation of the vibrational inertial masses

We first derive two canonical coordinates (q^1, q^2) that correspond to the (β, γ) vibrational degrees of freedom in the Bohr–Mottelson collective model. In this section we use the notation q to represent (q^1, q^2) and write the moving-frame HFB state as $|\phi(q)\rangle$.

First, we solve the moving-frame HFB equations,

$$\delta\langle\phi(q)|\,\hat{H}_{\mathrm{M}}(q)|\phi(q)\rangle=0, \tag{40}$$

$$\hat{H}_{\mathrm{M}}(q)=\hat{H}-\sum_{\tau}\lambda^{(\tau)}(q)\tilde{N}^{(\tau)}-\sum_{m=0,2}\mu_m(q)\hat{D}^{(+)}_{2m}, \tag{41}$$

where $\hat{D}^{(+)}_{2m}$ and $\tilde{N}^{(\tau)}\equiv\ \hat{N}^{(\tau)}-N_0^{(\tau)}$ are the mass quadrupole operators and the number operators (measured from the expectation values at the ground state) for protons and neutrons (τ = p, n), respectively. The quadrupole-deformation variables (β, γ) are defined through the expectation values of $\hat{D}^{(+)}_{2m}$ with respect to $|\phi(q)\rangle$:

$$\beta\cos\gamma=\eta D^{(+)}_{20}(q)=\eta\langle\phi(q)|\,\hat{D}^{(+)}_{20}\,|\phi(q)\rangle, \tag{42}$$

$$\frac{1}{\sqrt{2}}\beta\sin\gamma=\eta D^{(+)}_{22}(q)=\eta\langle\phi(q)|\,\hat{D}^{(+)}_{22}\,|\phi(q)\rangle, \tag{43}$$

where η is a scaling factor with the dimension of L^{-2}.

Through the above definitions of (β, γ) we can make a one-to-one correspondence between (q^1, q^2) and (β, γ). As illustrated in figure 3, this correspondence may be viewed as a mapping of the collective coordinates (q^1, q^2) onto the (β, γ) plane of the Bohr–Mottelson collective model. For our purpose, it is sufficient to assume that this correspondence is one-to-one in the neighborhood of an arbitrary point (q^1, q^2), because the collective inertial masses represent the inertia of the LACM for infinitesimal variation in time of the collective coordinates. Thus, the moving-frame HFB state $|\phi(q)\rangle$ may also be written as $|\phi(\beta, \gamma)\rangle$. The solutions of equation (40) for every point on the (q^1, q^2) plane provide the moving-frame HFB states $|\phi(\beta, \gamma)\rangle$ off the HFB ground state $|\phi(\beta_0, \gamma_0)\rangle$ at the local minimum (β_0, γ_0) on the potential energy surface $V(\beta, \gamma)$.

Next, we consider the TDHFB states of the form, equation (38), with $f = 2$. Assuming that the collective motion is slow, we expand it in powers of p and consider up to the second order in p. Then, under certain approximations explained in section 8, we obtain the following set of equations of motion for $\hat{Q}^i(q)$ and $\hat{P}_i(q)$,

$$\delta\langle\phi(q)|[\hat{H}_{\mathrm{M}}(q),\,\hat{Q}^i(q)]+\mathrm{i}B^i(q)\hat{P}_i(q)|\phi(q)\rangle=0, \tag{44}$$

$$\delta\langle\phi(q)|[\hat{H}_{\mathrm{M}}(q),\,\hat{P}_i(q)]-\mathrm{i}C_i(q)\hat{Q}^i(q)|\phi(q)\rangle=0, \tag{45}$$

with the 'weakly' canonical commutation relations,

$$\langle\phi(q)|[\hat{Q}^i(q),\,\hat{P}_j(q)]|\phi(q)\rangle=\mathrm{i}\delta_{ij}, \tag{46}$$

meaning that the canonical commutation relations hold only for their expectation values with respect to $|\phi(q)\rangle$. The equations (44) and (45) are called the LQRPA equations and may be regarded as generalizations of the QRPA equations (26) and (27) about the HFB ground state to those for a moving-frame HFB state $|\phi(q)\rangle$.

Analogously to the $(\hat{Q}^i, \hat{P}_i)$ operators in the ordinary QRPA, the one-body operators $\hat{Q}^i(q)$ and $\hat{P}_i(q)$, called infinitesimal generators of collective motion, can be written as linear combinations of bilinear products of the local quasiparticle operators $(a_k^\dagger, a_l)$ that are defined with respect to the

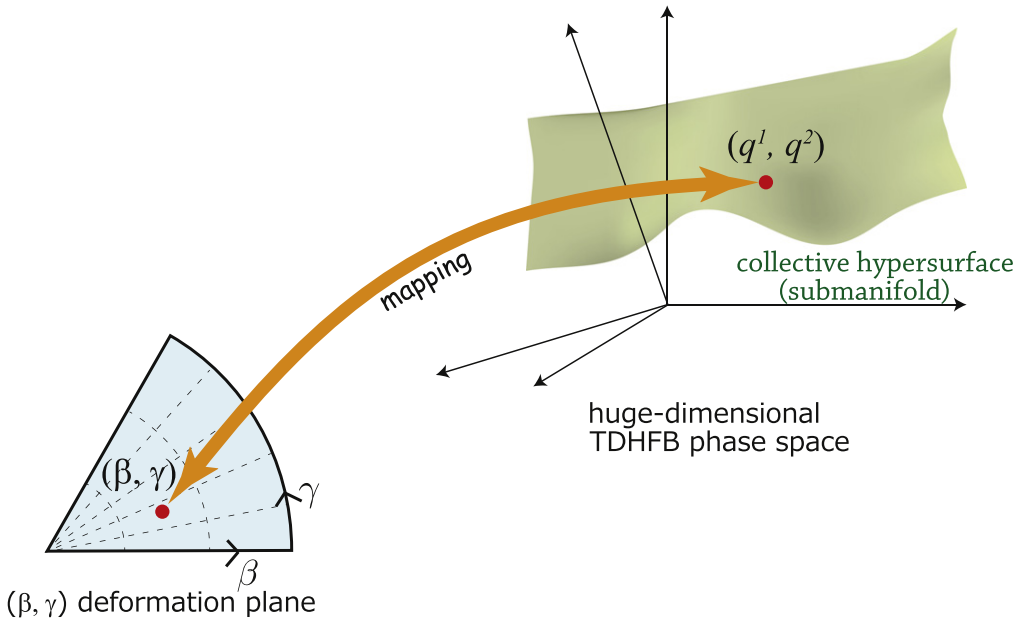

Figure 3. Illustration of the mapping of (q^1, q^2) defined on the collective submanifold onto the (β, γ) deformation plane of the Bohr-Mottelson collective model. The collective submanifold is illustrated as a hypersurface in the huge-dimensional TDHFB phase space.

moving-frame HFB state $|\phi(q)\rangle$ by $a_k\ |\phi(q)\rangle = 0$:

$$\hat{Q}^i(q) = \sum_{(kl)} q^i_{kl}(q)(a^\dagger_k a^\dagger_l + a_l a_k), \tag{47}$$

$$\hat{P}_i(q) = \mathrm{i}\sum_{(kl)} p^i_{kl}(q)(a^\dagger_k a^\dagger_l - a_l a_k). \tag{48}$$

Because the collective coordinates (q^1, q^2) corresponding to (β, γ) and their conjugate momenta (p_1, p_2) are canonical variables, it is possible to make a scale transformation such that the collective masses relating (p_1, p_2) to the time derivatives $(\dot{q}^1, \dot{q}^2)$ of (q^1, q^2) become unity. Thus, we can write the kinetic energy of vibrational motions as

$$T_{\mathrm{vib}} = \frac{1}{2}\sum_{i=1,2}(p_i)^2 = \frac{1}{2}\sum_{i=1,2}(\dot{q}^i)^2 \tag{49}$$

without loss of generality.

Microscopic calculation of the rotational moments of inertia

In a manner similar to the calculation of the vibrational inertial masses described above, we calculate, at every point on the (β, γ) plane, the rotational moments of inertia $\mathcal{J}_k$ for 3D rotational motions ($k = 1, 2, 3$). To treat the 3D rotational motions, we write rotating TDHFB states in the following form:

$$|\phi(q, \varphi, \dot{\varphi})\rangle = \exp\left[\mathrm{i}\sum_{k=1}^{3}\{\mathcal{J}_k(q)\dot{\varphi}_k\hat{\Psi}^k(q) - \varphi_k\hat{I}_k\}\right]|\phi(q)\rangle. \tag{50}$$

Here $\hat{\Psi}^k(q)$ are local angle operators conjugate to the angular-momentum operators $\hat{I}_k$ and satisfy the 'weak' canonical commutation relations,

$$\langle\phi(q)|[\hat{\Psi}^k(q), \hat{I}_l]|\phi(q)\rangle = \mathrm{i}\delta_{kl}. \tag{51}$$

The set $(\hat{\Psi}^k(q), \hat{I}_k)$ corresponds to the infinitesimal generators $(\hat{Q}^i(q), \hat{P}_i(q))$ for vibrational motions considered above. The variables φ_k and $\dot{\varphi}_k$ denote the rotational angles and their time derivatives. The set $(\varphi_k, \mathcal{J}_k(q)\dot{\varphi}_k)$ corresponds to the set of collective coordinates and momenta (q^i, p_i). The inverse of $B^i(q)$ corresponds to $\mathcal{J}_k(q)$. Needless to say, in contrast to $\hat{P}_i(q)$ for vibrational motions, the infinitesimal generators for rotational motions are the angular-momentum operators $\hat{I}_k$ *independent of* q, and the restoring-force parameters $C_k(q)$ are zero for rotational motions.

Inserting equation (50) for $|\phi(t)\rangle$ in the time-dependent variational principle equation (22) and considering only the linear-order terms with respect to $\hat{\Psi}^k(q)$ and $\hat{I}_k$, we obtain the LQRPA equations for 3D rotational motions:

$$\delta\langle\phi(q)|[\hat{H}_{\mathrm{M}}(q), \hat{\Psi}^k(q)] + \mathrm{i}\frac{\hat{I}_k}{\mathcal{J}_k(q)}|\phi(q)\rangle = 0. \tag{52}$$

These equations are the same as the Thouless–Valatin equations [111], except that we solve these equations not only at the equilibrium deformation (β_0, γ_0) but also at every points on the (β, γ) plane off the equilibrium.

Solving equations (52) at every point on the (q^1, q^2) plane and make a one-to-one mapping to the (β, γ) plane, we obtain the three moments of inertia $\mathcal{J}_k(\beta, \gamma)$, which determine the rotational masses $D_k(\beta, \gamma)$ through equation (10), and the rotational energy,

$$T_{\mathrm{rot}} = \frac{1}{2}\sum_{k=1,2,3}\mathcal{J}_k(\beta, \gamma)\dot{\varphi}^2_k, \tag{53}$$

in the collective Hamiltonian (2). If $D_k(\beta, \gamma)$ are replaced with a constant, $D_k(\beta, \gamma) = D$, then $\mathcal{J}_k(\beta, \gamma)$ reduce to the moments of inertia for irrotational fluid. As mentioned in section 2, this approximation may be valid only for harmonic vibrations about the spherical shape.

Derivation of the quadrupole collective Hamiltonian and its quantization

Displacements of (q^1, q^2) are related to variations of the expectation values $D^{(+)}_{2m}$ of the mass quadrupole operators by

$$\mathrm{d}D^{(+)}_{2m} = \sum_{i=1,2} \frac{\partial D^{(+)}_{2m}}{\partial q^i} \mathrm{d}q^i, \qquad m = 0, 2. \tag{54}$$

This relation leads to the kinetic energy of vibrational motions given in terms of time derivatives of the quadrupole deformation,

$$T_{\mathrm{vib}} = \frac{1}{2} \sum_{m,m'=0,2} M_{mm'} \dot{D}^{(+)}_{2m} \dot{D}^{(+)}_{2m'}, \tag{55}$$

where

$$M_{mm'}(\beta, \gamma) = \sum_{i=1,2} \frac{\partial q^i}{\partial D^{(+)}_{2m}} \frac{\partial q^i}{\partial D^{(+)}_{2m'}}. \tag{56}$$

Taking time derivatives of equations (42) and (43), we can straightforwardly transform the expression (55) to the form in terms of $(\dot{\beta}, \dot{\gamma})$. The vibrational masses $(D_{\beta\beta}, D_{\beta\gamma}, D_{\gamma\gamma})$ are then obtained from (M_{00}, M_{02}, M_{22}) through the following relations:

$$D_{\beta\beta} = \eta^{-2}\Big(M_{00}\cos^2\gamma + \sqrt{2}M_{02}\sin\gamma\cos\gamma + \frac{1}{2}M_{22}\sin^2\gamma\Big), \tag{57}$$

$$D_{\beta\gamma} = \beta\eta^{-2}\Big[-M_{00}\sin\gamma\cos\gamma + \frac{1}{\sqrt{2}}M_{02}(\cos^2\gamma - \sin^2\gamma) + \frac{1}{2}M_{22}\sin\gamma\cos\gamma\Big], \tag{58}$$

$$D_{\gamma\gamma} = \beta^2\eta^{-2}\Big(M_{00}\sin^2\gamma - \sqrt{2}M_{02}\sin\gamma\cos\gamma + \frac{1}{2}M_{22}\cos^2\gamma\Big). \tag{59}$$

In this way, we can calculate, in a microscopic way, all the collective inertial masses appearing in the Bohr–Mottelson collective Hamiltonian (2). For quantization, we can apply the quantization scheme for the 5D curvilinear coordinates (so-called Pauli prescription, see appendix A). After a somewhat lengthy but straightforward calculation, we obtain the quantized collective Hamiltonian (5).

5.2. Discussions

Let us discuss some fundamental problems related to the microscopic derivation of the quadrupole collective Hamiltonian.

Applicability of the Pauli prescription for quantization

In the pioneering work of Baranger and Kumar toward microscopic derivation of the Bohr–Motttelson collective Hamiltonian, they wrote [46]: 'The next problem is that of quantizing Hamiltonian H. There is no unique way of doing this. Bohr uses the Pauli prescription, which is designed to give the right answer when the variables can be transformed to Cartesian coordinates. But this is not the case here and therefore the Pauli prescription loses its only justification.'

In the 50 years since their work, we now have good prospects of justifying the use of the Pauli prescription. Because it is just the transformation of the Laplacian in Cartesian coordinates to that in the curvilinear coordinates, as Baranger and Kumar pointed out, the crucial question is whether or not we can derive the 5D collective coordinates which are Cartesian. As we have shown above, we have derived a local 5D canonical coordinate system on the collective submanifold embedded in the large-dimensional TDHFB phase space. (This concept will be further discussed in section 8.) In our view, to derive the kinetic energy term and the inertial masses, it is enough to define *a local coordinate system* at each point of the collective submanifold; that is, it is unnecessary to define a *global* canonical coordinate system. It remains, however, as an interesting subject to develop a firm theoretical formulation to clarify the validity and limitation of the use of the Pauli prescription for quantization of collective coordinates.

Treatment of 3D rotational motions

It should be emphasized that we can define the local angle operators $\hat{\Psi}^k(q)$, although the global angle operators canonically conjugate to $\hat{I}_k$ do not exist. For the microscopic calculation of the moments of inertia $\mathcal{J}_k$, it is sufficient to determine the microscopic structure of the local angle operators $\hat{\Psi}^k(q)$. This is because, similarly to the vibrational inertial masses, $\mathcal{J}_k(q)$ represents the inertia for an infinitesimal change of the rotational angles of the moving-frame HFB state $|\phi(q)\rangle$. It should be kept in mind that we use the expression (50) for rotating TDHFB states only for infinitesimal rotations, i.e., for very small rotational angles φ_k. For large φ_k, we have to consider higher-order effects associated with the non-Abelian nature of the angular momentum operators [112]. Fortunately, it is unnecessary to consider such higher-order effects for our aim of evaluating the inertial masses for rotational motions.

Effective interaction in the microscopic Hamiltonian

The LQRPA method is quite general and it can be used for any microscopic Hamiltonian $\hat{H}$. Inserting equations (47) and (48) into equations (44) and (45), we obtain linear eigenvalue equations for the amplitudes q^i_{kl} and p^i_{kl}. For effective interactions of separable type such as the P + Q force model, we can rewrite these equations into a form of dispersion equation determining the frequencies squared $\omega_i^2 = B^i C_i$ and the amplitudes, q^i_{kl} and p^i_{kl} (see e.g., [113]). It is then easy to find the solutions satisfying the dispersion equation. For effective interactions of the Skyrme type or modern density functionals, we have to diagonalize the QRPA matrix of very large dimension. This is the case for deformed HFB states,

especially for triaxial deformations, and the computation becomes heavy. Although a large-scale calculation is required, such an application of the LQRPA method with realistic interactions/functionals is a challenging future subject. A step toward this goal has recently been carried out for axially symmetric cases [108]. To overcome this computational problem, the finite-amplitude method [90–92] may be utilized. In particular, the recently developed technique [114–117] may be useful to find a few low-frequency solutions possessing strong collectivities. It is a great challenge to develop the LQRPA approach on the basis of the TDDFT and nuclear EDFs.

Physical meaning of the collective inertial masses

The pairing correlation plays a crucial role in determining the inertial masses of collective motion. The reason may be understood microscopically as follows.

The single-particle energies and wave functions are determined by the nuclear mean field. The time evolution of the mean field changes them and causes a number of single-particle level crossings. The level crossing near the Fermi surface induces the change of the lowest-energy configuration. Without the pairing, it is difficult for the system to rearrange to more energetically favorable configurations at the level crossing. In the presence of the pairing correlation, however, the nucleon pairs can make a hopping from up-sloping levels to down-sloping levels at the level crossing [118]. Such easiness/hardness of the configuration rearrangements at level crossings determines the adiabaticity/diabaticity of the collective motion. The collective inertia represents a property of the system trying to keep a definite configuration during the collective motion. Thus, the inertia becomes smaller for stronger pairing.

In spherical mean fields, the pairing correlation acts for monopole nucleon pairs that couples to an angular momentum $J = 0$. In deformed mean fields, the nucleon pair becomes a superposition of multiple angular momenta J because of the rotational symmetry breaking. In particular, the quadrupole $J = 2$ pairing correlation plays an important role. The reason is understood as follows. When a mean field develops toward a larger prolate deformation, single-particle levels favoring the prolate deformation are pushed down, while those that favor the oblate deformation are pushed up. At the level crossing, the easiness/hardness of the rearrangement depends on the magnitude of the pairing matrix elements between the crossing single-particle levels. The spacial overlaps between the single-particle wave functions of the up-sloping and down-sloping levels are smaller than those at the spherical limit. Such reductions of the pairing matrix elements between the prolate-favoring and the oblate favoring levels are well described by taking into account the quadrupole pairing (in addition to the monopole pairing) [26]. The Galilean invariance provides a link between the monopole and quadrupole pairing strengths [119]. It is shown with the use of the ASCC and LQRPA methods [105, 120] that the quadrupole pairing induces time-odd components (that change sign under time reversal) in the moving mean field and enhances the inertial masses. This indicates that the the collective dynamics associated with the pairing correlations is well described by these microscopic methods. More detailed investigation on the roles of the pairing in level crossing dynamics will prove fruitful for a deeper understanding of the microscopic mechanism determining the inertial masses.

5.3. Remarks on microscopic derivation of the particle-collective coupling Hamiltonian

In this review, we concentrate on the collective Hamiltonian $H_{\rm coll}$ in the unified model Hamiltonian (1) of Bohr and Mottelson. Needless to say, it is a great challenge to develop a microscopic theory capable of treating the single-particle and collective motions in a unified manner. The particle-collective coupling Hamiltonian $H_{\rm coupl}$ in the unified model Hamiltonian may be derived by using the same concept of time-dependent self-consistent mean field which has been used in the microscopic derivation of the collective Hamiltonian $H_{\rm coll}$. As is well known, properties of single-particle motions are determined by the mean fields which are collectively generated by all nucleons constituting the nucleus. This implies that the dynamical time evolution of the mean field affects the single-particle motion and generates the particle-collective couplings.

For small-amplitude vibrations about an equilibrium point of the HFB mean field, we can expand the single-particle Hamiltonian associated with mean field of the moving HFB state $|\phi(\beta, \gamma)\rangle$ in terms of the vibrational amplitudes. We then obtain the particle-vibration coupling Hamiltonian in the linear order [3, 121]. To overcome the problem of over-completeness and non-orthogonality that arises from the use of the basis states consisting of both the single-particle modes (defined at the HFB minimum point) and the elementary modes of vibrations, the 'Nuclear Field Theory (NFT)' has been developed since 1970's [122]. The NFT has been used for microscopic analyses of anharmonicities of vibrational motions as well as the 'dressing' of single-particle motions due to the particle-vibration couplings. For these applications and recent achievements of the NFT, we refer the contribution by Broglia *et al* to this Special Edition [123].

A promising approach to derive the particle-vibration coupling Hamiltonian beyond the linear order is to derive the single-particle Hamiltonian in the moving self-consistent mean field and expand it in powers of collective variables. An interesting attempt in this direction was done by Yamada [124] using the self-consistent collective coordinate (SCC) method with the (η, η^*) expansion (described in section 8.2). It is interesting to further develop this approach. Looking for future, it will certainly become an important fundamental subject in nuclear structure theory to derive the particle-vibration coupling Hamiltonian starting from the TDDFT.

We should also remark the longstanding problem of deriving the particle-rotation coupling Hamiltonian starting from a microscopic many-body theory. In [125], the single-particle motions in rapidly rotating mean field are described by means of the SCC method with a power-series expansion in the rotational frequency, and the alignments of single-

quasiparticle and the rotational angular momenta are studied. Developing this line of approach, the SCC method may be used also for deriving the particle-rotation coupling Hamiltonian, but this subject remains for future. In our view, construction of a microscopic theory capable of treating the single-particle and collective motions in a unified manner, initiated by Bohr and Mottelson, still remains as the most fundamental and principal subject in nuclear structure dynamics.

Historical note

The construction of a self-consistent microscopic theory of collective motion capable of deriving the unified-model Hamiltonian of Bohr and Mottelson is a longstanding and difficult subject which always inspires the development of fundamental new concepts. Let us quote some remarks by Villars, which may be worthwhile to keep in mind:

'Although such a synthesis of the collective and the particle aspect of nuclear dynamics is rather easily achieved in words, by simply combining results borrowed from various models, a decent mathematical formulation of the same programme is far from easy.' in 1967 [126].

'It always appeared to this author that the proper formulation of a microscopic theory of nuclear collective motion is a strangely difficult subject.' 'Much is to be learned yet in the problem of formulating a consistent quantum theory of collective motion.' in 1982 [127].

6. Illustrative examples

We here present some applications of the LQRPA method for deriving the 5D collective Hamiltonian. In the numerical examples below, the P + Q model Hamiltonian [69] (including the quadrupole-pairing interaction) is employed in solving the LQRPA equations. The single-particle energies and the P + Q interaction strengths are determined such that the results of the Skyrme-HFB calculation for the ground states are best reproduced within the P + Q model (see [106, 107] for details). More examples can be found for $^{68-72}$Se [104, 105], ^{72,74,76}Kr [106], the ^{26}Mg region [128], $^{30-34}$Mg [107], $^{58-68}$Cr [108], $^{58-66}$Cr [109], and $^{128-132}$Xe, $^{130-134}$Ba [129].

Oblate-prolate shape coexistence and fluctuations in ^{74}Kr

The collective potential $V(\beta, \gamma)$ depicted in figure 4 exhibits two local minima. The prolate minimum is lower than the oblate minimum, and the spherical shape is a local maximum. This figure also shows that the valley runs in the triaxially deformed region and the barrier connecting the oblate and prolate minima is low. Accordingly, one may expect large-amplitude quantum shape fluctuations to occur along the triaxial valley. In fact, the vibrational wave function of the ground 0_1^+ state has bumps around the two potential minima, but the wave function spreads over the entire γ region along the potential valley. It is interesting to notice that, as the angular momentum increases, the localization of the vibrational wave functions in the (β, γ) deformation plane develops; namely, the rotational effect plays an important role for the emergence of the shape coexistence character. This development of localization results from the $\beta - \gamma$ dependence of the rotational moments of inertia. One can clearly see the oblate-prolate asymmerty of the moment of inertia $\mathcal{J}_1$ shown in figure 4(c). Due to this asymmetry, the localization on the prolate side develops in the ground band. In the yrare band, although the vibrational wave functions have a two-peak structure, the localization on the oblate side develops due to the orthogonality to the yrast states.

We note that the rotational inertial functions (D_1, D_2, D_3) and the pairing gaps significantly change as functions of (β, γ), as well as the vibrational inertial masses $(D_{\beta\beta}, D_{\gamma\gamma}, D_{\beta\gamma})$. Due to the time-odd contributions of the moving HFB self-consistent field, the collective inertial masses calculated with the LQRPA method are 20%–50% larger than those evaluated with the Inglis-Belyaev cranking formula. Their ratios also change as functions of (β, γ) [106]. As a consequence, as shown in Figure 5(a), the excitation spectrum calculated with the LQRPA masses is in much better agreement with experimental data than that with the Inglis-Belyaev cranking masses. Figure 5(b) shows the spectroscopic quadrupole moments calculated with the LQRPA masses for ^{74}Kr. One sees that, aside from a minor deviation for the 2_3^+ state, the calculated spectroscopic quadrupole moments are in excellent agreement with the experimental data. In particular, the signs and the increasing tendency of the magnitudes with angular momentum in the ground band are well reproduced.

7. Some remarks on other approaches

In this section, we give short remarks on other methods widely used for microscopic calculation of collective inertial masses.

7.1. Constrained HFB + adiabatic perturbation

This method is convenient and widely used in the microscopic description of LACM [131–135]. It is based on the adiabatic assumption that the collective motion is much slower than the single-particle motion. In this approach, we first postulate a few one-body operators $\hat{F}_i$ corresponding to collective coordinates α^i, and solve the constrained HFB (or constrained HF + BCS) equation,

$$\delta \langle \phi_0(\alpha)| \hat{H} - \sum_i \mu^i(\alpha)\hat{F}_i \ |\phi_0(\alpha)\rangle = 0, \tag{60}$$

to find the constrained HFB states $|\phi_0(\alpha)\rangle$. Here, $\mu^i(\alpha)$ are the Lagrange multipliers whose values are determined to fulfill the constraining conditions,

$$\alpha^i = \langle \phi_0(\alpha)| \ \hat{F}_i \ |\phi_0(\alpha)\rangle. \tag{61}$$

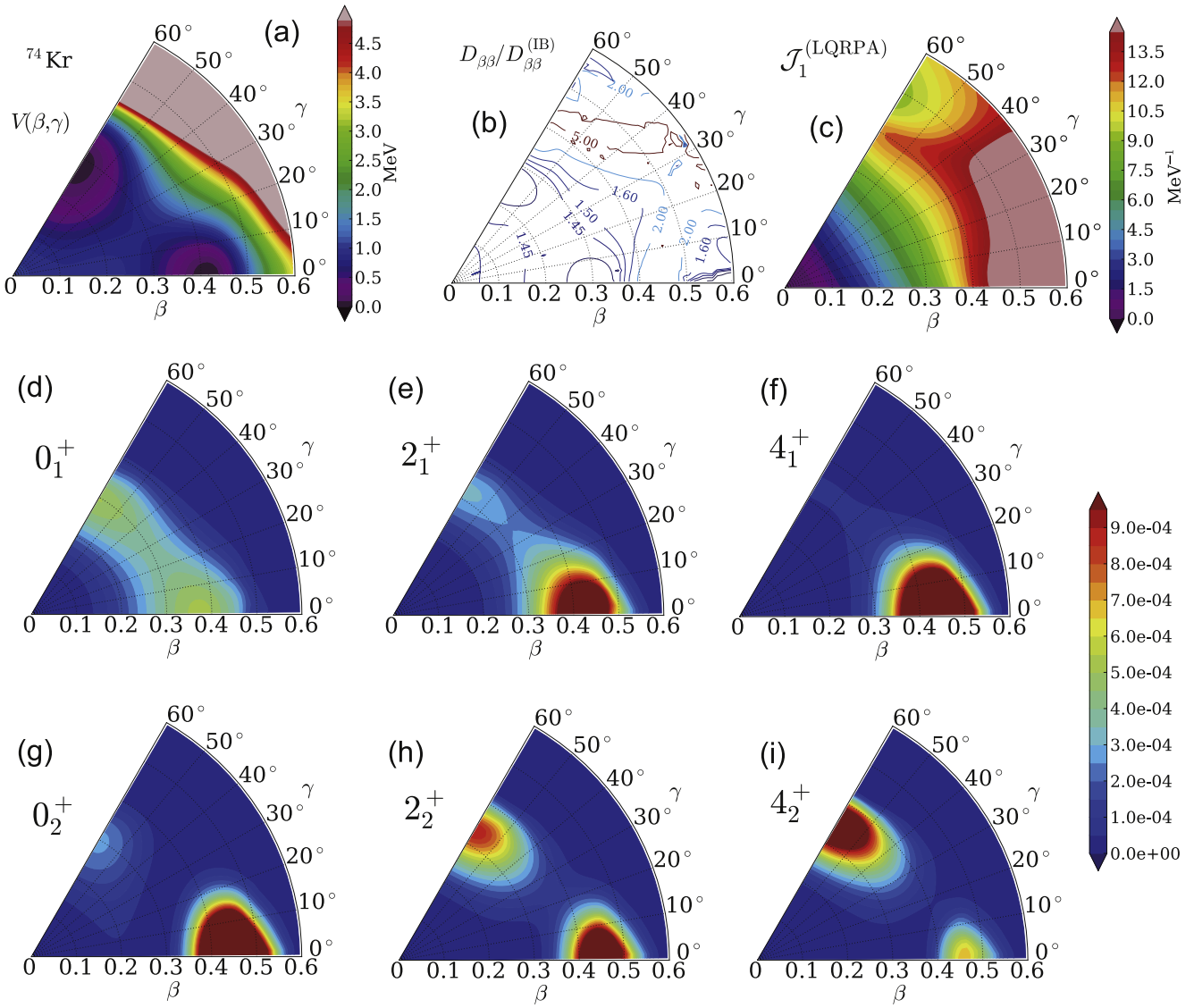

Figure 4. Application of the LQRPA method to the oblate-prolate shape coexistence/fluctuation phenomenon in ^{74}Kr (from [106]). Reproduced with permission. Copyright Elsevier 2011. (a) Collective potential $V(\beta, \gamma)$, (b) Ratio of the collective inertial mass $D_{\beta\beta}(\beta, \gamma)$ to the Inglis-Belyaev cranking mass. (c) The LQRPA moment of inertia $\mathcal{J}_1$ for rotation about the $x-$ axis. Vibrational wave functions squared, $\sum_K \beta^4 |\Phi_{\alpha IK}(\beta, \gamma)|^2$, for (d) the 0_1^+ state, (e) the 2_1^+ state, (f) the 4_1^+ state, (g) the 0_2^+ state, (h) the 2_2^+ state, and (i) the 4_2^+ state. For the β^4 factor, see the text.

Assuming that the frequencies of the collective motion are much smaller than those of non-collective two-quasiparticle excitation, we then calculate the collective kinetic energy T_{coll} using the adiabatic perturbation theory:

$$T_{\mathrm{coll}} = \frac{1}{2}\sum_{ij} D_{ij}(\alpha)\dot{\alpha}^{i*}\dot{\alpha}^{j}, \tag{62}$$

where

$$D_{ij}(\alpha) = 2\sum_n \frac{\langle\phi_0(\alpha)|\ \frac{\partial}{\partial\alpha^{i*}}\ |\phi_n(\alpha)\rangle\langle\phi_n(\alpha)|\ \frac{\partial}{\partial\alpha^{j}}\ |\phi_0(\alpha)\rangle}{E_n(\alpha) - E_0(\alpha)} \tag{63}$$

are called Inglis-Belyaev cranking masses [54]. Here $|\phi_0(\alpha)\rangle$ and $|\phi_n(\alpha)\rangle$ represent the ground and two-quasiparticle excited states for a given set of values $\alpha = \{\alpha^i\}$. In most of applications it is simplified furthermore by introducing an assumption that the derivatives of the constrained HFB Hamiltonian with respect to α^i is proportional to $\hat{F}_i$. Equation (63) then reduces to

$$D_{ij}(\alpha) = \frac{1}{2}[\mathcal{M}_1^{-1}(\alpha)\mathcal{M}_3(\alpha)\mathcal{M}_1^{-1}(\alpha)]_{ij} \tag{64}$$

with

$$\mathcal{M}_k(\alpha)_{ij} = \sum_n \frac{\langle\phi_0(\alpha)|\ \hat{F}_i^{\dagger}\ |\phi_n(\alpha)\rangle\langle\phi_n(\alpha)|\ \hat{F}_j\ |\phi_0(\alpha)\rangle}{(E_n(\alpha) - E_0(\alpha))^k}. \tag{65}$$

In recent years, a systematic investigation on low-lying quadrupole spectra has been carried out in terms of the quadrupole collective Hamiltonian by using the Inglis-

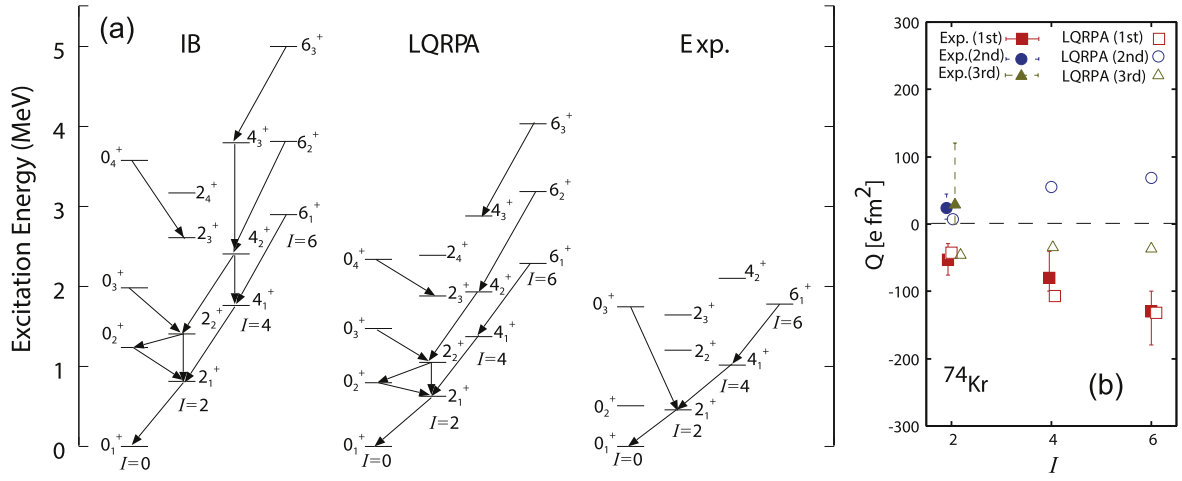

Figure 5. (a) Partial excitation spectrum calculated for ^{74}Kr by means of the LQRPA method [106] and experimental data [130]. For comparison, the results calculated using the Inglis-Belyaev cranking masses (denoted by IB) are also shown. Only the levels with even angular momentum are shown (see [106] for the whole spectrum.) The $E2$ transitions with $B(E2)$ larger than 50 Weisskopf units are indicated by arrows. (b) Spectroscopic quadrupole moments in unit of $e$fm^2 of the first (square), second (circle) and third (triangle) states for each angular momentum in ^{74}Kr (from [106]). Calculated values are shown by open symbols, while experimental data [130] are indicated by filled symbols.

Belyaev cranking formula and the collective potential energies derived from the relativistic (covariant) density functionals [136–142].

A problem of the Inglis–Belyaev cranking formula is that the collective inertial masses are underestimated [143]. Moving mean fields induce time-odd components that change sign under time reversal. However, the Inglis–Belyaev cranking formula ignores their effects on the collective inertial masses. By taking into account such time-odd corrections to the cranking masses, one can better reproduce low-lying spectra [129]. For rotational moments of inertia, we may estimate the time-odd corrections taking the limit of $\omega_{\rm rot} \to 0$ for the solution of the HFB equation in the rotating frame, that is defined by adding the cranking term $-\omega_{\rm rot}\hat{J}_x$ to the constrained HFB Hamiltonian. Since this provides about 20%–40% enhancement from the Inglis–Belyaev formula, the similar enhancement factors of 1.2–1.4 have been often utilized for vibrational inertial masses without solid justification.

7.2. Adiabatic TDHF theory

In the 1960's, Belyaev, Baranger, and Kumar began efforts to self-consistently derive the collective Hamiltonian using adiabatic approximation to time evolution of mean fields [47, 69]. In these pioneer works, they derived the quadrupole collective Hamiltonian using the P + Q force model [67]. During the 1970's, the time-dependent mean-field approach with the use of the P + Q force model was generalized to be applicable to any effective interaction. This advanced approach is called adiabatic TDHF (ATDHF) [144–146].

In the ATDHF theory of Baranger and Véneroni [144], the density matrix $\rho(t)$ is written in the following form and expanded as a power series with respect to $\chi(t)$.

$$\rho(t) = {\rm e}^{{\rm i}\chi(t)}\rho_0(t){\rm e}^{-{\rm i}\chi(t)} \tag{66}$$

$$= \rho_0(t) + {\rm i}[\chi(t), \rho_0(t)] - \frac{1}{2}[\chi(t), [\chi(t), \rho_0(t)]] + \cdots. \tag{67}$$

Here the matrix elements $\rho_{ij}(t)$ of $\rho(t)$ are defined by $\rho_{ij}(t) = \langle\phi_{\rm HF}(t)|\, c_j^\dagger c_i \,|\phi_{\rm HF}(t)\rangle$ with the time-dependent HF state $|\phi_{\rm HF}(t)\rangle$ and the nucleon creation and annihilation operators, $c_i^\dagger$ and c_j, in the single-particle states i and j. The above expansion is regarded as an adiabatic expansion with respect to $\chi(t)$ which plays the role of the collective momentum associated with the time-even density matrix $\rho_0(t)$. Baranger and Véneroni suggested a possibility of introducing collective coordinates as parameters that describe the time evolution of the density matrix $\rho_0(t)$. They discussed an iterative procedure to solve the ATDHF equations. This idea has not been realized until now, however. We note that the ATDHF does not reduce to the RPA in the small-amplitude limit if a few collective coordinates are introduced by hand. In fact it gives a collective mass different from the RPA [147].

Villars developed another ATDHF theory with the aim of self-consistently determining the optimum collective coordinates on the basis of the time-dependent variational principle [148]. In the same way as in the ASCC method described in section 8, the TDHFB states are written in the form of equation (38). Villars encountered a difficulty, however, that he could not get unique solutions of the basic equations determining the collective path. This problem was later solved by treating the second-order terms of the momentum expansion in a self-consistent manner (see Mukherjee and Pal [149], and Klein *et al* [150, 151]). It was shown that, when the number of collective coordinate is only one, a collective path maximally decoupled from non-collective degrees of freedom runs along a valley in the multi-dimensional potential-energy surface associated with the TDHF states.

To describe low-frequency collective motions, it is necessary to take into account the pairing correlations. In other words, we need to develop the adiabatic TDHFB (ATDHFB) theory. This is one of the reasons why applications of the ATDHF have been restricted to collective phenomena where pairing correlations play minor roles such as low-energy collisions between spherical closed-shell nuclei [152] and giant resonances [147]. As discussed in section 5.2, when large-amplitude shape fluctuations take place, single-particle level crossings often occur. To follow the adiabatic configuration across the level crossing points, the pairing correlation plays an essential role. Therefore, we need to develop the ATDHFB theory to describe low-frequency collective excitations.

In the past, Dobaczewski and Skalski [153] tried to develop the ATDHFB theory assuming the axially symmetric quadrupole deformation parameter β as the collective coordinate. Quite recently, Li *et al* [154] tried to derive the 5D quadrupole collective Hamiltonian on the basis of the ATDHFB. The extension of ATDHF to ATDHFB is not straightforward, however. This is because, as will be discussed in section 8, we need to decouple the number-fluctuation degrees of freedom from the LACM of interest, respecting the gauge invariance with respect the pairing rotational angles.

7.3. Generator coordinate method

The generator coordinate method (GCM) has been used for a wide variety of nuclear collective phenomena [155–157]. Using the angular-momentum projector $\hat{P}_{IMK}$ and the neutron (proton)-number projector $\hat{P}_N$ ($\hat{P}_Z$), we write the state vector as a superposition of the projected mean-field states with different deformation parameters (β, γ),

$$|\Psi^i_{NZIM}\rangle = \int \mathrm{d}\beta \mathrm{d}\gamma \sum_K f^i_{NZIK}(\beta, \gamma)\hat{P}_N\hat{P}_Z\hat{P}_{IMK}\,|\phi(\beta, \gamma)\rangle. \tag{68}$$

Because the projection operators contain integrations, it has been a difficult task to carry out such high-dimensional numerical integrations in solving the Hill–Wheeler equation for the states $|\phi(\beta, \gamma)\rangle$ obtained by the constrained HFB method. In recent years, however, remarkable progress has been taking place, which makes it possible to carry out such large-scale numerical computations [158–163]. The HFB calculations with use of density-dependent effective interactions are better founded on density functional theory (DFT). Accordingly, the modern GCM calculation is referred to as 'multi-reference DFT' [158].

We can derive a collective Schrödinger equation by making the gaussian overlap approximation (GOA) to the Hill–Wheeler equation [164–167]. There is no guarantee, however, that dynamical effects associated with time-odd components of moving mean field are sufficiently taken into account in the collective inertial masses obtained through this procedure. It is well known for the case of center of mass motion that we need to use complex generator coordinates to obtain the correct mass. This fact indicates that collective momenta conjugate to collective coordinates should also be treated as generator coordinates [54, 168].

A fundamental question is how to choose the optimal generator coordinates. With the variational principle, Holzwarth and Yukawa [169] proved that the mean-field states parametrized by a single optimal generator coordinate run along a valley of the collective potential energy surface. This line of investigation stimulated the challenge toward constructing a microscopic theory of LACM [170]. In this connection, we note that conventional GCM calculations parametrized by a few real generator coordinates do not reduce to the (Q)RPA in the small-amplitude limit. It should be distinguished from the case that all two-quasiparticle (particle-hole) degrees of freedom are treated as complex generator coordinates [171].

It is very important to distinguish the 5D collective Hamiltonian obtained by making use of the GOA to the GCM from that derived in the preceding section by using the LQRPA to the ASCC method. In the latter, the canonical conjugate pairs of collective coordinate and momentum are self-consistently derived on the basis of the time-dependent variational principle. The canonical formulation enables us to adopt the standard canonical quantization procedure. Furthermore, effects of the time-odd components of the moving mean field are automatically taken into account in the collective inertial masses. It is therefore misleading to say as if the 5D collective Hamiltonian approach is an approximation to the full 5D (three Euler angles, β, and γ) GCM calculation.

Additional remarks

In view of the above points, it is desirable to carry out a systematic comparison of collective inertial masses evaluated by different approximations including the LQRPA (based on the ASCC method summarized in the next section), the adiabatic cranking methods, the ATDHFB, and the GCM + GOA for a better understanding of their physical implications. In this connection, we notice that the results of the recent GCM calculation for ^{76}Kr [162], using the particle-number and angular-momentum projected basis, equation (68), are rather similar to those obtained by use of the Bohr–Mottelson collective Hamiltonian with the Inglis–Belyaev cranking masses, except for an overall overestimation of the excitation energies by about 20%. This work casts an interesting question as to why the two different approaches yield rather similar results.

8. Fundamentals of microscopic theory of LACM

In this section, we review the modern concept of LACM and the fundamental theory underling the LQRPA method used in section 5 to derive the Bohr–Mottelson collective Hamiltonian.

8.1. Extraction of collective submanifold

It is possible to formulate the TDHFB dynamics as the classical Hamilton equations for canonical variables in the TDHFB phase space [63, 75, 101]. The dimension of this phase space is very large; twice of the number of all the two-quasiparticle pairs. The TDHFB state vector $|\phi(t)\rangle$ can be regarded as a generalized coherent state moving on a trajectory in the large-dimensional TDHFB phase space. For low-frequency collective motions, however, we assume that the time evolution is governed by a few collective variables.

During the attempts to construct microscopic theory of LACM since the latter half of the 1970's, significant progress has been achieved in the fundamental concepts of collective motion. Especially important is the recognition that microscopic derivation of the collective Hamiltonian is equivalent to extraction of a collective submanifold embedded in the TDHFB phase space, which is approximately decoupled from other 'non-collective' degrees of freedom. From this point of view we can say that collective variables are nothing but *local canonical variables* which can be flexibly chosen on this submanifold. Here, we recapitulate recent developments achieved on the basis of such concepts.

Attempts to formulate a LACM theory without assuming adiabaticity of large-amplitude collective motion were initiated by Rowe and Bassermann [172] and Marumori [173] and led to the formulation of the SCC method by Marumori, Maskawa, Sakata, and Kuriyama [59]. In these approaches, collective coordinates and collective momenta are treated on the same footing. In the SCC method, basic equations determining the collective submanifold are derived by requiring *maximal decoupling* of the collective motion of interest from other non-collective degrees of freedom. The collective submanifold is invariant with respect to the choice of the coordinate system, whereas the collective coordinates depend on it. The idea of coordinate-independent theory of collective motion was developed also by Rowe [174], and Yamamura and Kuriyama [63]. This idea had a significant impact on the fundamental question, '*what are the collective variables?*'. The SCC method was first formulated on the basis of the TDHF theory without pairing. Later, it is extended to treat pairing correlations in superfluid nuclei on the basis of the TDHFB theory [61].

In the SCC method, the TDHFB state $|\phi(t)\rangle$ is written as $|\phi(q, p)\rangle$ under the assumption that the time evolution is governed by a few collective coordinates $q = (q^1, q^2, \cdots, q^f)$ and collective momenta $p = (p_1, p_2, \cdots, p_f)$. The parametrization of the TDHFB state with the $2f$-degrees of freedom (q, p) means that we define a submanifold inside the TDHFB phase space, which is called '*collective submanifold*.' Below, we summarize the basic equations that determine the collective submanifold on which the TDHFB state $|\phi(q, p)\rangle$ evolves in time. (For simplicity, we here omit the terms arising from the pairing-rotational degrees of freedom, which will be discussed in section 8.4.)

8.1.1. Invariance principle of the TDHFB equation We require that the TDHFB equation of motion is invariant in the collective submanifold. In a variational form, this requirement can be written as

$$\delta\langle\phi(q,p)|\left(\mathrm{i}\frac{\partial}{\partial t}-\hat{H}\right)|\phi(q,p)\rangle=0. \tag{69}$$

Here, the variation δ is given by $\delta\,|\phi(q,p)\rangle = a_i^\dagger a_j^\dagger\,|\phi(q,p)\rangle$ in terms of the quasiparticle operators $(a_i^\dagger, a_j)$, which satisfy the vacuum condition, $a_i\,|\phi(q,p)\rangle = 0$. Under the basic assumption, we can replace the time derivative with

$$\frac{\partial}{\partial t}=\sum_{i=1}^{f}\left(\dot{q}^i\frac{\partial}{\partial q^i}+\dot{p}_i\frac{\partial}{\partial p_i}\right)=\dot{q}^i\frac{\partial}{\partial q^i}+\dot{p}_i\frac{\partial}{\partial p_i}. \tag{70}$$

Hereafter, to simplify the notation, we adopt the Einstein summation convention and remove $\sum_{i=1}^{f}$. Accordingly, we can rewrite equation (69) as

$$\delta\langle\phi(q,p)|\{\dot{q}^i\mathring{P}_i(q,p)-\dot{p}_i\mathring{Q}^i(q,p)-\hat{H}\}|\phi(q,p)\rangle=0, \tag{71}$$

where the local infinitesimal generators are defined by

$$\mathring{P}_i(q,p)|\phi(q,p)\rangle=\mathrm{i}\frac{\partial}{\partial q^i}\,|\phi(q,p)\rangle, \tag{72}$$

$$\mathring{Q}^i(q,p)|\phi(q,p)\rangle=-\mathrm{i}\frac{\partial}{\partial p_i}\,|\phi(q,p)\rangle. \tag{73}$$

These are one-body operators which can be written as linear combinations of bilinear products $\{a_i^\dagger a_j^\dagger, a_j a_i\}$ of the quasiparticle operators defined with respect to $|\phi(q,p)\rangle$.

8.1.2. Canonicity conditions. We require q and p to be canonical variables. According to the Frobenius-Darboux theorem [175], pairs of canonical variables (q, p) exist for the TDHFB states $|\phi(q,p)\rangle$ satisfying the following *canonicity conditions*,

$$\langle\phi(q,p)|\,\mathring{P}_i(q,p)|\phi(q,p)\rangle=p_i+\frac{\partial S}{\partial q^i}, \tag{74}$$

$$\langle\phi(q,p)|\,\mathring{Q}^i(q,p)|\phi(q,p)\rangle=-\frac{\partial S}{\partial p_i}, \tag{75}$$

where S is an arbitrary differentiable function of q and p [59, 63, 64]. By specifying the functional form of $S(q, p)$ and $S'(q', p')$ and demanding that the form of these equations be preserved, we can fix the type of allowed canonical transformations, $(q, p) \to (q', p')$ among the collective variables. We shall discuss typical examples in sections 8.2 and 8.3, and call the canonicity conditions with a specified function $S(q, p)$ '*canonical-variable conditions.*' Taking derivatives of equations (74) and (75) with respect to p_i and q^i, respectively, we can easily confirm that the local infinitesimal generators satisfy the 'weakly' canonical commutation relations,

$$\langle\phi(q,p)|[\mathring{Q}^i(q,p),\mathring{P}_j(q,p)]|\phi(q,p)\rangle=\mathrm{i}\delta_{ij}. \tag{76}$$

Taking variations of equation (71) in the direction of the collective variables, q and p, generated by $\mathring{P}_i$ and $\mathring{Q}^i$, we

obtain the Hamilton equations of motion,

$$\frac{\mathrm{d}q^i}{\mathrm{d}t} = \frac{\partial \mathcal{H}}{\partial p_i}, \quad \frac{\mathrm{d}p_i}{\mathrm{d}t} = -\frac{\partial \mathcal{H}}{\partial q^i}. \tag{77}$$

Here, the total energy $\mathcal{H}(q, p) \equiv \langle \phi(q, p)| \hat{H} |\phi(q, p)\rangle$ plays the role of the classical collective Hamiltonian.

8.1.3. Equation of collective submanifold. The variational principle (71) and equation (77) lead to the equation of collective submanifold:

$$\delta \langle \phi(q, p)| \left\{ \hat{H} - \frac{\partial \mathcal{H}}{\partial p_i} \mathring{P}_i(q, p) - \frac{\partial \mathcal{H}}{\partial q^i} \mathring{Q}^i(q, p) \right\} |\phi(q, p)\rangle = 0. \tag{78}$$

Taking variations $\delta_\perp$ in the directions orthogonal to q and p, we see that

$$\delta_\perp \langle \phi(q, p)| \hat{H} |\phi(q, p)\rangle = 0. \tag{79}$$

This implies that the energy expectation value is stationary with respect to all variations except for those along directions tangent to the collective submanifold. In other words, the large-amplitude collective motion is decoupled from other modes of excitation.

8.2. Solution with (η, η^*) expansion

In the original paper of the SCC method [59], the TDHFB state $|\phi(q, p)\rangle$ is written as

$$|\phi(q, p)\rangle = U(q, p)|\phi_0\rangle = \mathrm{e}^{\mathrm{i}\hat{G}(q,p)}|\phi_0\rangle. \tag{80}$$

Here, $U(q, p)$ is a time-dependent unitary transformation written in terms of an Hermitian one-body operator $\hat{G}(q, p)$. The HFB ground state $|\phi_0\rangle$ is taken as an initial state; $U(q, p) = 1$ at $(q, p) = (0, 0)$.

Using complex variables $\eta = (\eta_1, \eta_2, \cdots, \eta_f)$ defined by

$$\eta_i = \frac{1}{\sqrt{2}}(q^i + \mathrm{i}p_i), \quad \eta_i^* = \frac{1}{\sqrt{2}}(q^i - \mathrm{i}p_i), \tag{81}$$

we can rewrite the TDHFB state as

$$|\phi(\eta, \eta^*)\rangle = U(\eta, \eta^*)|\phi_0\rangle = \mathrm{e}^{\mathrm{i}\hat{G}(\eta,\eta^*)}|\phi_0\rangle. \tag{82}$$

Correspondingly, we define local infinitesimal generators, $\mathring{O}_i^\dagger(\eta, \eta^*)$ and $\mathring{O}_i(\eta, \eta^*)$, by

$$\mathring{O}_i^\dagger(\eta, \eta^*)|\phi(\eta, \eta^*)\rangle = \frac{\partial}{\partial \eta_i} |\phi(\eta, \eta^*)\rangle, \tag{83}$$

$$\mathring{O}_i(\eta, \eta^*)|\phi(\eta, \eta^*)\rangle = -\frac{\partial}{\partial \eta_i^*} |\phi(\eta, \eta^*)\rangle. \tag{84}$$

Replacing (q, p) by (η, η^*), the equation of collective submanifold (78) is rewritten as

$$\delta \langle \phi_0| U^\dagger(\eta, \eta^*) \left\{ \hat{H} - \frac{\partial \mathcal{H}}{\partial \eta_i^*} \mathring{O}_i^\dagger(\eta, \eta^*) - \frac{\partial \mathcal{H}}{\partial \eta_i} \mathring{O}_i(\eta, \eta^*) \right\} U(\eta, \eta^*)|\phi_0\rangle = 0. \tag{85}$$

Here, the variation is to be performed only for the HFB ground state $|\phi_0\rangle$.

Let us consider the following canonical-variable conditions,

$$\langle \phi(\eta, \eta^*)| \mathring{O}_i^\dagger(\eta, \eta^*)|\phi(\eta, \eta^*)\rangle = \frac{1}{2}\eta_i^*, \tag{86}$$

$$\langle \phi(\eta, \eta^*)| \mathring{O}_i(\eta, \eta^*)|\phi(\eta, \eta^*)\rangle = \frac{1}{2}\eta_i, \tag{87}$$

which are obtained by a specific choice of $S = -\frac{1}{2}\sum_i q^i p_i$ in the canonicity conditions, (74) and (75). From equations (86) and (87), we can easily obtain the 'weak' boson commutation relations,

$$\langle \phi(\eta, \eta^*)|[\mathring{O}_i(\eta, \eta^*), \mathring{O}_j^\dagger(\eta, \eta^*)]|\phi(\eta, \eta^*)\rangle = \delta_{ij}. \tag{88}$$

We note that only linear canonical transformations among η and η^*, which do not change the power of (η, η^*), are allowed under the conditions, (86) and (87). Therefore, these canonical-variable conditions are suitable for solving the variational equation (85) by means of a power series expansion of $\hat{G}$ with respect to (η, η^*):

$$\hat{G}(\eta, \eta^*) = \hat{G}_i^{(10)}\eta_i^* + \hat{G}_i^{(01)}\eta_i + \hat{G}_{ij}^{(20)}\eta_i^*\eta_j^* + \hat{G}_{ij}^{(11)}\eta_i^*\eta_j + \hat{G}_{ij}^{(02)}\eta_i\eta_j + \cdots. \tag{89}$$

Requiring that the variational principle (85) holds for every power, we can successively determine the one-body operator $\hat{G}^{(m,n)}$ with $m + n = 1, 2, 3, \cdots$. This method of solution is called the '(η, η^*)-expansion method.' Because (η, η^*) are complex canonical variables, they are replaced by boson operators after the canonical quantization. The lowest linear order corresponds to the QRPA. Accordingly, the collective variables (η_i, η_i^*) correspond to a specific QRPA mode in the small-amplitude limit. In the higher orders, however, the microscopic structure of $\hat{G}$ changes as a function of (η, η^*) due to the mode-mode coupling effects among different QRPA modes. In this sense, the (η, η^*)-expansion method may be regarded as a dynamical extension of the boson expansion method [176]. Thus, it is a powerful method of treating anharmonic effects originating from mode-mode couplings, as shown in its application to the two-phonon states of anharmonic γ vibration [50, 177]. The SCC method was also used for derivation of the 5D collective Hamiltonian and analysis of the quantum phase transition from spherical to deformed shapes [178] and for constructing diabatic representation in the rotating shell model [125]. The validity of the canonical quantization procedure, including a treatment of the ordering ambiguity problem, was examined in [176]. Description of the 3D rotational motions by means of the

SCC method was discussed in [112] from a viewpoint of constrained dynamical system.

8.3. Solution with adiabatic expansion

The (η, η^*) expansion about a single HFB equilibrium point is not suitable for treating situations where a few local minima having different shapes energetically compete in the HFB potential-energy surface and large-amplitude shape-mixing vibrations occur. It is also difficult to apply the expansion method to a collective motion which goes far away from the equilibrium, such as nuclear fission. The time evolution of these low-energy LACM's in nuclei are usually slow (adiabatic) in comparison with the time scale of the single-particle motions. For describing adiabatic LACM extending over very far from the HFB equilibrium, a new method of solution has been proposed [102]. In this method, the basic equations of the SCC method are solved by an expansion with respect to the collective momenta, keeping full orders in the collective coordinates. It is called '*adiabatic SCC (ASCC) method*.' Similar methods have been proposed also by Klein, Walet, and Do Dang [150], and Almehed and Walet [179], but the gauge invariance in the TDHFB theory (discussed in section 8.4 below) were not considered in these papers.

A microscopic theory for adiabatic LACM is constructed by the ASCC method in the following way. We assume that the TDHFB state $|\phi(q, p)\rangle$ can be written in a form

$$|\phi(q, p)\rangle = \exp\{\mathrm{i}p_i\hat{Q}^i(q)\}|\phi(q)\rangle, \tag{90}$$

where $\hat{Q}^i(q)$ are infinitesimal generators of p_i locally defined at the state $|\phi(q)\rangle$ that represents a TDHFB state $|\phi(q, p)\rangle$ at $p \to 0$. This state $|\phi(q)\rangle$ is called a 'moving-frame HFB state.'

We use the following canonical-variable conditions different from (86) and (87),

$$\langle\phi(q, p)|\,\mathring{P}_i(q, p)|\phi(q, p)\rangle = p_i, \tag{91}$$

$$\langle\phi(q, p)|\,\mathring{Q}^i(q, p)|\phi(q, p)\rangle = 0, \tag{92}$$

which are obtained by putting $S =$ const. in the canonicity conditions (74) and (75). These canonical-variable conditions are suitable for the adiabatic expansion with respect to the collective momenta p, because only point transformations, $q \to q'(q)$ (more generally, similarity transformations) which do not mix p and q, are allowed under the conditions, (91) and (92). We insert the above form of the TDHFB state (90) into the equation of collective submanifold (85) and the canonical-variable conditions, (91) and (92), and make a power-series expansion in p. We can determine the microscopic structures of $\hat{Q}^i(q)$ and $|\phi(q)\rangle$ by requiring that these equations hold for every power of p. We take into account up to the second order. The canonical variable conditions, (91) and (92), then yield the 'weakly' canonical commutation relations,

$$\langle\phi(q)|[\hat{Q}^i(q), \hat{P}_j(q)]|\phi(q)\rangle = \mathrm{i}\delta_{ij}. \tag{93}$$

Here, $\hat{P}_i(q)$ are infinitesimal generators of q^i, locally defined at the state $|\phi(q)\rangle$ by

$$\hat{P}_i(q)|\phi(q)\rangle = \mathrm{i}\frac{\partial}{\partial q^i}\,|\phi(q)\rangle. \tag{94}$$

We also obtain $\langle\phi(q)|\,\hat{Q}^i(q)|\phi(q)\rangle = 0$ and $\langle\phi(q)|\,\hat{P}_i(q)|\phi(q)\rangle = 0$, which are trivially satisfied. Note that $\hat{Q}^i(q)$ and $\hat{P}_i(q)$ operate on $|\phi(q)\rangle$, while $\mathring{Q}^i(q, p)$ and $\mathring{P}_i(q, p)$ on $|\phi(q, p)\rangle$.

The time derivatives, $\dot{q}^i$ and $\dot{p}_i$, are determined by the Hamilton equations of motion (77) with the classical collective Hamiltonian $\mathcal{H}(q, p)$ expanded with respect to p up to the second order,

$$\mathcal{H}(q, p) = V(q) + \frac{1}{2}B^{ij}(q)p_ip_j, \tag{95}$$

where

$$V(q) = \mathcal{H}(q, p = 0), \quad B^{ij}(q) = \frac{\partial^2\mathcal{H}}{\partial p_i\partial p_j}\bigg|_{p=0}. \tag{96}$$

The collective inertial tensors $B_{ij}(q)$ are defined as the inverse matrix of $B^{ij}(q)$, $B^{ij}B_{jk} = \delta^i_k$. Under these preparations, the following equations, which constitute the core of the ASCC method, can be derived [102]. Here, to further simplify the expression, we show the case for normal systems with TDHF (see the next subsection about the extension to TDHFB).

1. *Moving-frame HF(B) equation*

$$\delta\langle\phi(q)|\,\hat{H}_{\mathrm{M}}(q)|\phi(q)\rangle = 0, \tag{97}$$

where $\hat{H}_{\mathrm{M}}(q)$ represents the Hamiltonian in the frame attached to the moving mean field,

$$\hat{H}_{\mathrm{M}}(q) = \hat{H} - \frac{\partial V}{\partial q^i}\hat{Q}^i(q), \tag{98}$$

and is called 'moving-frame Hamiltonian.'

2. *Moving-frame (Q)RPA equations (or 'Local harmonic equations')*

$$\delta\langle\phi(q)|[\hat{H}_{\mathrm{M}}(q), \hat{Q}^i(q)] - \frac{1}{\mathrm{i}}B^{ij}(q)\hat{P}_j(q) + \frac{1}{2}\left[\frac{\partial V}{\partial q^j}\hat{Q}^j(q), \hat{Q}^i(q)\right]|\phi(q)\rangle = 0, \tag{99}$$

$$\delta\langle\phi(q)|[\hat{H}_{\mathrm{M}}(q), \frac{1}{\mathrm{i}}\hat{P}_i(q)] - C_{ij}(q)\hat{Q}^j(q) - \frac{1}{2}\left[\left[\hat{H}_{\mathrm{M}}(q), \frac{\partial V}{\partial q^k}\hat{Q}^k(q)\right], B_{ij}(q)\hat{Q}^j(q)\right]|\phi(q)\rangle = 0, \tag{100}$$

where

$$C_{ij}(q) = \frac{\partial^2 V}{\partial q^i\partial q^j} - \Gamma^k_{ij}\frac{\partial V}{\partial q^k}, \tag{101}$$

$$\Gamma^k_{ij}(q) = \frac{1}{2}B^{kl}\left(\frac{\partial B_{li}}{\partial q^j} + \frac{\partial B_{lj}}{\partial q^i} - \frac{\partial B_{ij}}{\partial q^l}\right). \quad (102)$$

The double-commutator term in equation (100) arises from the q-derivative of the infinitesimal generators $\hat{Q}^i(q)$ and represents the curvatures of the collective submanifold. Diagonalizing the matrix, $B^{ik}C_{kj}$, at each point of q, we may identify the local normal modes and eigen-frequencies $\omega_i(q)$ of the moving-frame QRPA equations.

Extension from TDHF to TDHFB for superfluid nuclei can be achieved by introducing the number fluctuation $n \equiv N - N_0$ and their conjugate angle φ as additional collective variables [102] (see section 8.4).

Solving equations (97), (99), and (100) self-consistently, we can determine the microscopic expressions of the infinitesimal generators, $\hat{Q}^i(q)$ and $\hat{P}_i(q)$, in bilinear forms of the quasiparticle creation and annihilation operators defined locally with respect to $|\phi(q)\rangle$. These equations reduce to the HF(B) and (Q)RPA equations at the equilibrium point where $\partial V/\partial q^i = 0$. Therefore, they are regarded as natural extensions of the well-known HFB-QRPA equations to non-equilibrium states.

Some key points of the ASCC method are noted below:

i. *Meaning of adiabatic approximation.* The term 'adiabatic approximation' is frequently used for different meanings. In the present context, we use this term for the approximate solution of the variational equation (71) by taking into account up to the second order in an expansion with respect to the collective momenta p. It is important to note that the effects of finite frequency of the LACM are taken into account through the moving-frame QRPA equation. No assumption is made, such as that the kinetic energy of LACM is much smaller than the lowest two-quasiparticle excitation energy at every point of q.

ii. *Difference from the constrained HFB equations.* The moving-frame HFB equation (97) resembles the constrained HFB equation. An essential difference is that the infinitesimal generators $\hat{Q}^i(q)$ are here self-consistently determined together with $\hat{P}_i(q)$ as solutions of the moving-frame QRPA equations, (99) and (100), at every point of the collective coordinate q. Thus, contrary to constrained operators in the constrained HFB theory, their microscopic structure changes as functions of q. The optimal 'constraining' operators are locally determined at each q. The collective submanifold embedded in the TDHFB phase space is extracted in this way.

iii. *Canonical quantization.* The collective inertial tensors $B_{ij}(q)$ take a diagonal form when the classical collective Hamiltonian is represented in terms of the local normal modes of the moving-frame QRPA equations. We can then make a scale transformation of the collective coordinates q such that they become unity. The kinetic energy term in the resulting collective Hamiltonian depends only on p. Thus, there is no ordering ambiguity between q and p in the canonical quantization procedure.

iv. *Collective inertial mass.* Although the collective submanifold is invariant against coordinate transformations, $q \to q'(q)$, the collective inertial tensors $B_{ij}(q)$ depends on the adopted coordinate system. The scale of the coordinates can be arbitrarily chosen as far as the canonical-variable conditions are satisfied. To obtain physical insights and to examine the effects of time-odd components in the mean field, however, it is convenient to adopt a conventional coordinate system, such as the quadrupole (β, γ) variables.

8.4. Inclusion of the pairing rotation and gauge invariance

In the QRPA at the HFB equilibrium, the ANG modes such as the number fluctuation (pairing rotational) modes are decoupled from other normal modes. Thereby, the QRPA restores the gauge invariance (number conservation) broken in the HFB mean field [26]. It is desirable to retain this merit of the QRPA beyond the small-amplitude regime. Otherwise, spurious number-fluctuation modes would heavily mix in the LACM of interest. It is possible to achieve this aim by using the SCC method for superfluid nuclei [61].

Introducing the number fluctuation $n = N - N_0$ and the gauge angle φ (conjugate to n) as additional collective variables, we generalize the TDHFB state (90) to

$$|\phi(q, p, \varphi, n)\rangle = \mathrm{e}^{-\mathrm{i}\varphi\hat{N}}|\phi(q, p, n)\rangle, \quad (103)$$

$$|\phi(q, p, n)\rangle = \mathrm{e}^{\mathrm{i}[p_i\hat{Q}^i(q) + n\hat{\Theta}(q)]}|\phi(q)\rangle. \quad (104)$$

Here $\hat{N}$ and $\hat{\Theta}(q)$ denote the nucleon-number operator and the infinitesimal generator of n, respectively, and N_0 is a reference value of the nucleon number N. In the generalized TDHFB state, (103), the number operator $\hat{N}$ and the state vector $|\phi(q, p, n)\rangle$ may be regarded as an infinitesimal generator of the gauge angle φ and an intrinsic state with respect to the pairing rotational motion, respectively. It is straightforward to extend the equation for the collective submanifold (71) as

$$\delta\langle\phi(q, p, \varphi, n)|\left\{\mathrm{i}\dot{q}^i\frac{\partial}{\partial q^i} + \mathrm{i}\dot{p}_i\frac{\partial}{\partial p_i} + \mathrm{i}\dot{\varphi}\frac{\partial}{\partial\varphi} - \hat{H}\right\}|\phi(q, p, \varphi, n)\rangle = 0. \quad (105)$$

Note that $\dot{n} = 0$, because the Hamilton equations for the canonical conjugate pair (n, φ) are

$$\dot{\varphi} = \frac{\partial\mathcal{H}}{\partial n}, \quad \dot{n} = -\frac{\partial\mathcal{H}}{\partial\varphi}, \quad (106)$$

and the classical collective Hamiltonian $\mathcal{H}(q, p, \varphi, n) \equiv \langle\phi(q, p, \varphi, n)|\,\hat{H}\,|\phi(q, p, \varphi, n)\rangle$ does not depend on φ. Making a power-series expansion with respect to n as well as p and considering up to the second order, we can determine $\hat{\Theta}(q)$ simultaneously with $\hat{Q}^i(q)$ and $\hat{P}_i(q)$ such that the moving-frame equations become invariant against the rotation of the gauge angle φ. In fact, we introduce two sets of

$(\hat{N}, \hat{\Theta}(q))$ to describe the pairing rotations of neutrons and protons, separately.

Writing the time derivative $\dot{\varphi}$ of the gauge angle as λ, we can easily confirm that the term proportional to $\dot{\varphi}$ in (105) leads to an operator $\lambda\hat{N}$ on the intrinsic state $|\phi(q, p, n)\rangle$. In this form, $\dot{\varphi}$ corresponds to the chemical potential in the BCS theory of superconductivity. The term, $\lambda\hat{N}$, in the BCS theory is usually interpreted as a constraining term to impose the condition that $\langle\phi(q, p, n)|\ \hat{N}\ |\phi(q, p, n)\rangle = N$. It should be emphasized, however, that this term is naturally derived by introducing the concept that the moving-frame TDHFB state, $|\phi(q, p, n)\rangle$, is an intrinsic state with respect to the pairing-rotational motion of the gauge angle φ. In the microscopic approach under discussion, the 'chemical potential' λ plays a role analogous to the rotational velocities $\dot{\varphi}_k$ in equation (50) for the rotational motions in the 3D coordinate space; that is, they are not introduced as Lagrange multipliers but dynamical variables.

Hinohara *et al* investigated the gauge-invariance properties of the ASCC equations and extended the infinitesimal generators $\hat{Q}^i(q)$ to include quasiparticle creation-annihilation $(a_i^\dagger a_j)$ parts in addition to two-quasiparticle creation $(a_i^\dagger a_j^\dagger)$ and annihilation $(a_j a_i)$ parts [180]. This is the reason why equations (99) and (100) are written in a more general form than those originally given in [102]. The gauge invariance of the ASCC method implies that we need to fix the gauge in numerical applications. A convenient procedure for the gauge fixing is given in [180]. A more general consideration on the gauge symmetry of the ASCC method is given from a viewpoint of constrained dynamical systems in a recent paper [181].

8.5. Solution with the LQRPA method

The LQRPA method used in section 5 for the microscopic derivation of the Bohr-Mottelson collective Hamiltonian may be regarded as a non-iterative solution of (97)–(100) in the ASCC method, without the consistency in the generator $\hat{Q}^i(q)$ between the moving-frame HFB equation and the moving-frame QRPA equations. It may also be regarded as a first step of the iterative procedure for solving the self-consistent equations. Equation (40) corresponds to the moving-frame HFB equation (97) with $\hat{Q}^i(q)$ replaced by global one-body operators $\hat{D}^{(+)}_{2m}$. It is worth noting that the moving-frame HFB Hamiltonian $\hat{H}_{\rm M}$ contains terms, $-\lambda^{(\tau)}\hat{N}^{(\tau)} - \mu_m\hat{D}^{(+)}_{2m}$, which naturally appear from the ASCC equations with the approximation to replace $\hat{Q}^i(q)$ in $\hat{H}_{\rm M}(q)$ by $\hat{D}^{(+)}_{2m}$. In fact, the origin of these terms are not constraints, but the time-derivative terms in equation (105). The LQRPA equations, (44) and (45), are obtained by ignoring the curvature term in the moving-frame QRPA equations, (99) and (100).

The validity of the LQRPA method was examined for the cases where a well-defined valley (collective path) exists in the collective potential $V(\beta, \gamma)$ [105]. The rotational and vibrational inertial masses calculated by using the LQRPA method were compared with those obtained by the fully self-consistent ASCC calculations. It was confirmed that they agree very well, indicating that the LQRPA is a good approximation to the ASCC calculation along the collective path on the (β, γ) plane. The accuracy of the LQRPA method on the full (β, γ) plane may be checked by making an iterative calculation; that is, by solving equation (40) replacing $\hat{D}^{(+)}_{2m}$ with the solutions $\hat{Q}^i(q)$ of the LQRPA equations (44) and (45), and evaluate the deviations from the result of the lowest-order LQRPA calculation. This task remains for future, however.

9. Open problems in quadrupole collective dynamics

Nowadays, the domain of quadrupole collective phenomena awaiting applications of the Bohr–Mottelson collective model is increasing enormously covering wide regions from low to highly excited states, from small to large angular momenta, and from proton-drip line to neutron-drip line. Among many interesting subjects, we remark here on only a few.

9.1. Shape coexistence, pairing fluctuation and mysterious 0^+ states

As mentioned in section 2, when two different HFB equilibrium shapes coexist in the same energy region, large-amplitude shape mixings through the potential barriers take place. These phenomena may be regarded as a kind of macroscopic quantum tunneling where the potential barrier itself is generated as a consequence of the dynamics of the self-bound quantum system. For instance, two strongly distorted rotational bands built on the oblate and prolate shapes, which seem to coexist and interact with each other, have been found in ^{68}Se [41, 105]. Such phenomena are widely seen in low-energy spectra from light to heavy nuclei [41]. We have applied the Bohr–Mottelson collective Hamiltonian to some of these shape coexistence/mixing phenomena with the use of the collective inertial masses microscopically calculated by means of the LQRPA method. An illustrative example is presented for ^{74}Kr in section 6.

One of the issues related to the shape coexistence/fluctuation is to clarify the nature of deformation in neutron-rich nuclei around ^{32}Mg having the magic number $N = 20$ of the spherical shell model [41]. In the P + Q model, the major properties of low-lying states in open-shell nuclei are determined by the competition between the pairing (particle-particle, hole-hole) and quadrupole (particle-hole) correlations acting among nucleons in partially filled major shells. On the other hand, in situations where the pairing and quadrupole correlations *across* the spherical major shells play the major role, such as in neutron-rich Mg isotopes around ^{32}Mg, the two different correlations seem to act coherently and generate interesting collective phenomena where large-amplitude fluctuations in the monopole and quadrupole pairing gaps as well as the quadrupole shape take place simultaneously [107].

In some nuclei, the first excited 0^+ state appears below the first excited 2^+ state. An example is the first excited 0^+ state of ^{72}Ge which is known from old days but still poorly understood. This anomaly occurs in the vicinity of $N = 40$

where the $g_{9/2}$ shell starts to be partially filled (due to the pairing). It has been pointed out [182–185] that the mode-mode coupling between the 0^+ member of the two quadrupole-phonon triplet and the neutron pairing vibration becomes especially strong near $N = 40$ and generates such anomalous 0^+ states with extremely low-excitation energy.

As reviewed by Hyde and Wood [41] and by Garrett [186], the nature of the low-lying excited 0^+ states systematically found in recent experiments, in addition to those known from old days, is not well understood. It is thus quite challenging to apply, in a systematic ways, the Bohr–Mottelson collective Hamiltonian approach to all of these data, from light to heavy and from stable to unstable nuclei, and explore the limit of the applicability. Considering the suggestion [182–185] about the coupling effects with pairing vibrations, one of the basic questions is *'under what situations we need to extend the 5D collective Hamiltonian to 7D by explicitly treating the proton and neutron pairing gaps as dynamical variables.'*

We should mention about a few fundamental subjects that are closely related to the shape coexistence phenomena in low-lying states: in the decays of superdeformed rotational bands [187], macroscopic quantum tunnelings through self-consistently generated barriers are very clearly seen. Needless to say, microscopic description of spontaneous fissions is a longstanding yet modern fundamental subject of nuclear structure physics [20, 75]. Recent experimental progress in deep sub-barrier fusion reactions [188] provides another modern problem of macroscopic tunnelings in finite quantum systems.

9.2. Vibrational and rotational modes at high angular momentum

As a nucleus rotates rapidly, excitations of aligned quasiparticles take place [189, 190]. Rapid rotation changes the deformation and shell structure of the mean field. The pair field also disappears eventually at high-spin [191]. These structural changes in the high-spin yrast states significantly affect the properties of vibrational motions built on them (the yrast state is the 'ground' states for given angular momenta). Unfortunately experimental data for low-frequency shape vibrations in the vicinity of the high-spin yrast states have not been accumulated enough. Considering the role of the BCS pairing in forming the collective low-frequency quadrupole vibrations built on the ground state, existence of low-frequency collective vibrations built on the high-spin yrast states is actually not evident, since we expect that the role of the pairing is much less in high-spin states. On the other hand, we expect that the vibrations could compete with rotations in high-spin states because the rotational frequency increases with the angular momentum, and becomes comparable to the vibrational frequencies [192].

Discovery of superdeformed bands [32, 33] shed a new light on the above situation. In superdeformed states, a new shell structure called *superdeformed shell structure* emerges and it creates new low-frequency octupole vibrations on superdeformed states at high angular momentum [193, 194]. These vibrational modes simultaneously break the axial symmetry and the reflection symmetry. Moreover, some experimental data for γ vibrations (quadrupole shape vibration that breaks the axial symmetry) at high spin have been reported [195, 196]. It has been discussed for a long time that the triaxial deformation may be realized at high spin states due to the weakening of the pairing correlations. When the mean field breaks the axial symmetry, a new rotational mode called *wobbling motion* is expected to emerge. Observation of the wobbling rotational band is therefore a clear signature of the occurrence of the triaxial deformation in the mean field. About 15 years ago, the first experimental data on the wobbling band were obtained [197] (see also [198, 199]). Their properties have been theoretically analyzed from various points of view [200–203]. These investigations show that the aligned quasiparticle plays a crucial role in the emergence of the wobbling motion. There is another new phenomenon expected to emerge in the axial-symmetry-broken nuclei under certain conditions: *chiral rotation* and its experimental signature, chiral doublet bands [189]. Experimental search for chiral doublet bands and its precursor phenomena called *chiral vibrations* [204] is currently in progress.

The Bohr–Mottelson collective Hamiltonian as reviewed in this paper is not applicable to quadrupole collective phenomena at high angular momenta. This is because the collective inertial masses and the collective potential $V(\beta, \gamma)$ are calculated at low angular momenta. It seems, however, possible to extend it to describe such high-spin phenomena. We have learned through the success of the cranked shell model [189, 190] that the concept of single-particle motion in a rotating mean field holds very well. This means that major effects of rapid rotation (Coriolis- and centrifugal-force effects) can be captured in the self-consistent mean-field by defining the single-particle motion in a rotating frame of reference attached to the rapidly rotating nucleus. In the extension of the self-consistent mean field to a rotating frame, the time-reversal symmetry is broken, but it opens a new dimension in nuclear structure physics. *In the history of nuclear structure physics, we have been successfully extending the concept of the single-particle motion to a more general mean field. Such extensions have been achieved by breaking some symmetries of the self-consistent mean field.* Let us recall that extension of the concept of single-particle excitation (with spontaneous breaking of the symmetry) and appearance of new collective excitation (restoring the broken symmetry) are *dual concepts* that underline the quantum many-body theory of nuclear structure.

9.3. Low-frequency collective excitations in nuclei near the neutron drip line

The mean field in unstable nuclei near the neutron drip line possesses new features associated with the large neutron to proton ratio, the formation of neutron skin, the weak binding of single-particles states near the Fermi surface, the excitation of neutron pairs into the continuum, etc. The collectivity of surface vibrations may change reflecting the modification of shell structure [205] and the variation of pairing properties

[206]. Thus, the QRPA method has been extended to properly treat the excitations into the continuum [207]. The extended version is called *continuum QRPA*, and it has been applied to weakly bound unstable nuclei [208–210]. The particle-vibration coupling theory has also been extended to include the continuum effects by means of the continuum QRPA method [211].

In stable nuclei, overlaps of different single-particle wave functions become maximum at the surface and generate a strong coherence among many quasiparticle excitations [2]. In the weak binding situation, single-particle wave functions significantly extend from the surface (half-density radius) to the low-density region and acquire strong individualities. It is an open problem how the pairing correlation in such a situation acts to generate the collectivity of vibrational modes. Nowadays, it is one of the central subject in nuclear structure-reaction theory to carry out fully self-consistent HFB+QRPA calculations using the same energy density functional and simultaneously taking into account the deformation, pairing and excitations into the continuum [210]. From such microscopic calculations, for instance, it is suggested [82] that a strong coherence among the quadrupole shape fluctuation and the fluctuations of the monopole and quadrupole pairing gaps may generate a collective vibration unique to the weakly bound neutron-rich nuclei.

At the present time, the major efforts are devoted to clarifying the properties of the ground states and a few excited states of nuclei near the drip line. In the coming future, more experimental data on excitation spectra will be obtained with the progress of ambitious experimental projects now ongoing in the world. We shall then encounter a variety of phenomena that cannot be understood within the small-amplitude approximation for collective motions. It will become necessary to explore the nature of collective motions in nuclei near the drip line by an extension of the collective Hamiltonian approach reviewed in this paper.

10. Concluding remarks

We have reviewed recent approaches to microscopically derive the Bohr–Mottelson collective Hamiltonian on the basis of the time-dependent self-consistent mean field. The *moving* self-consistent mean field is the key concept to the unified understanding of the single-particle and collective motions in nuclei. We hope that this paper fits the aim of this special edition for the 40 year anniversary of Nobel Prize 1975.

Although the progress achieved during these 40 years with the Bohr–Mottelson collective Hamiltonian is spectacular, many interesting subjects of fundamental significance are awaiting our challenge in our road towards understanding quantum collective dynamics in nuclei. As we briefly remarked in the preceding section, it will be very interesting to explore the limits of applicability of the Bohr–Mottelson collective Hamiltonian by systematically applying it to shape coexistence/fluctuation/mixing phenomena. At the present time, the quadrupole collective Hamiltonian is used mainly for low-spin states. It seems possible, however, to extend the microscopic approach reviewed in this paper to collective phenomena at high-spin states by taking into account the effects of rapid rotation from the beginning in the self-consistent mean fields. In a similar manner, it will be interesting to extend the collective Hamiltonian approach to describe low-lying excited states in neutron-rich unstable nuclei, by taking into account the effects of weak binding and continuum coupling in constructing the self-consistent mean fields. These extensions will open new dimensions in quantum collective dynamics of nuclear structure. Finally, it should be emphasized that one of the great challenges is to calculate the collective inertial masses using the LQRPA method on the basis of the density functional theory.

Acknowledgments

It is a great pleasure for us to contribute this paper to the Special Physica Scripta Edition for the 40 year anniversary of Nobel Prize '75. In this occasion, two of the authors (K M and M M) wish to express their deep appreciations to Aage Bohr and Ben R Mottelson for giving us invaluable ideas and inspirations to explore nuclear structure dynamics during our stay (1976-1978 and 1990-1991, respectively) in the Niels Bohr Institute, Copenhagen. We thank T Ichikawa for carefully checking the manuscript. This work was supported in part by JSPS KAKENHI Grants No. 24105006, No. 25287065, and No. 26400268. The numerical calculations were carried out on RIKEN Cluster of Clusters (RICC) facility.

Appendix A. Quantization in curvilinear coordinates

For Cartesian coordinates $q = (q^1, q^2, \ldots, q^f)$ in a f-dimensional space, the kinetic energy in classical mechanics is given by $T = \frac{1}{2}\sum_{i=1}^{f}(\dot{q}^i)^2$ in a unit with mass $m = 1$, where $\dot{q}^i$ are time derivatives (velocities) of q^i. After the canonical quantization, we obtain the kinetic energy operator

$$\hat{T} = -\frac{1}{2}\sum_{i=1}^{f}\frac{\partial^2}{\partial q^{i2}} = -\frac{1}{2}\Delta \tag{107}$$

in the unit with $\hbar = 1$, where Δ is the Laplacian in the Cartesian coordinates.

For the curvilinear coordinates $x = (x^1, x^2, \ldots, x^f)$ in a f-dimensional curved space, the line element squared may be written as

$$\mathrm{d}s^2 = \sum_{i,j} g_{ij}(x)\mathrm{d}x^i\mathrm{d}x^j \tag{108}$$

with $g_{ij}(x) = g_{ji}(x)$, using the metric tensor $\{g_{ij}(x)\}$ characterizing the curved space. The kinetic energy in classical

mechanics is then given by

$$T = \frac{1}{2}\left(\frac{\mathrm{d}s}{\mathrm{d}t}\right)^2 = \frac{1}{2}\sum_{i,j} g_{ij}(x)\frac{\mathrm{d}x^i}{\mathrm{d}t}\frac{\mathrm{d}x^j}{\mathrm{d}t}. \quad (109)$$

Note that the metric tensor $\{g_{ij}(x)\}$ depends on the coordinate x.

According to the Pauli prescription for quantization in curvilinear coordinates, the corresponding kinetic energy operator in quantum mechanics is given by

$$\hat{T} = -\frac{1}{2}\Delta = -\frac{1}{2\sqrt{g(x)}}\sum_{i,j}\frac{\partial}{\partial x^i}\sqrt{g(x)}\,g^{ij}(x)\frac{\partial}{\partial x^j}, \quad (110)$$

where $g(x)$ denotes the determinant of the metric tensor, $g(x) = \det\{g_{ij}(x)\}$, and $g^{ij}(x)$ are the components of the inverse matrix $\{g_{ij}(x)\}^{-1}$. This expression is obtained in a straightforward way by rewriting the Laplacian Δ in the curvilinear coordinates. The Schrödinger equation is written as

$$\left(-\frac{1}{2\sqrt{g(x)}}\sum_{i,j}\frac{\partial}{\partial x^i}\sqrt{g(x)}\,g^{ij}(x)\frac{\partial}{\partial x^j} + V(x)\right) \times \psi(x) = E\psi(x). \quad (111)$$

The normarization of the wave function is

$$\int |\psi(x)|^2 \mathrm{d}\tau = 1 \quad (112)$$

with the volume element $\mathrm{d}\tau = \sqrt{g(x)}\,\mathrm{d}x \equiv \sqrt{g(x^1, x^2, \ldots, x^f)}\,\mathrm{d}x^1\mathrm{d}x^2 \cdots \mathrm{d}x^f$.

For the Bohr–Mottelson collective model, $f = 5$ and the five collective variables consist of the (β, γ) deformation variables and the three Euler angles ϑ_k; that is, $(x^1 = \beta, x^2 = \gamma, x^3 = \vartheta_1, x^4 = \vartheta_2, x^5 = \vartheta_3)$. The three components of the angular velocity (time-derivatives of the rotational angle) on the intrinsic axes, $\dot{\varphi}_k$ appearing in the classical expression of the rotational energy $T_{\mathrm{rot}} = \frac{1}{2}\sum_{k=1}^{3}\mathcal{J}_k(\beta, \gamma)\dot{\varphi}_k^2$, are related with the time derivatives of the Euler angles $\dot{\vartheta}_k$ by

$$\dot{\varphi}_k = \sum_{k'=1}^{3} V_{kk'}\dot{\vartheta}_{k'} \quad (113)$$

with

$$V_{kk'} = \begin{pmatrix} -\sin\vartheta_2\cos\vartheta_3 & \sin\vartheta_3 & 0 \\ \sin\vartheta_2\sin\vartheta_3 & \sin\vartheta_3 & 0 \\ \cos\vartheta_2 & 0 & 1 \end{pmatrix}. \quad (114)$$

After the quantization, the classical expression T_{rot} for the rotational energy becomes to $\hat{T}_{\mathrm{rot}} = \sum_k \frac{\hat{I}_k^2}{2\mathcal{J}_k(\beta,\gamma)}$, where the components of the angular-momentum operator on the intrinsic axes, $(\hat{I}_1, \hat{I}_2, \hat{I}_3)$, are represented in terms of the Euler angles $(\vartheta_1, \vartheta_2, \vartheta_3)$ and the derivatives with respect to them. In the same way, we obtain, after carrying out somewhat lengthy but straightforward calculations, the quantum operator $\hat{T}_{\mathrm{vib}}$ for the kinetic energy of the vibrational motion, given in equation (6), and the determinant of the metric tensor,

$$g(\beta, \gamma, \vartheta_1, \vartheta_2, \vartheta_3) = G(\beta, \gamma)\sin^2\vartheta_2, \quad (115)$$

with $G(\beta, \gamma)$ given by equation (17). Note that the determinant does not depend on ϑ_1 and ϑ_3. For the definitions of the Euler angles and more details of the calculation, see, e.g., chapter 6 in the textbook of Eisenberg and Greiner [43].

Appendix B. Calculation of *E*2 transitions and moments

The electric quadrupole ($E2$) operators in the body-fixed frame are given as a sum of neutron and proton contributions with effective charges $e_{\mathrm{eff}}^{(\tau)}$,

$$\hat{D}_m^{(E2)} = \sum_{\tau=n,p} e_{\mathrm{eff}}^{(\tau)}\hat{D}_{2m}^{(\tau)}, \quad (116)$$

where $\hat{D}_{2m}^{(\tau)}$ are the quadrupole operator of neutrons and protons, and $\sum_\tau \hat{D}_{2m}^{(\tau)} = \hat{D}_{2m}$. The $E2$ operator in the laboratory frame is related with that in the intrinsic frame as

$$\hat{D}_m'^{(E2)} = \sum_{m'}\mathcal{D}^2_{mm'}(\Omega)\hat{D}_{m'}^{(E2)}, \quad (117)$$

where $\mathcal{D}$ are Wigner's rotational matrices. The experimental observables such as the $B(E2)$ and the spectroscopic quadrupole moment Q are defined as

$$B(E2; \alpha I \to \alpha' I') = (2I+1)^{-1}|\langle \alpha I \| \hat{D}'^{(E2)} \| \alpha' I' \rangle|^2, \quad (118)$$

$$Q(\alpha I) = \sqrt{\frac{16\pi}{5}}\,\langle \alpha, I, M = I |\, \hat{D}_0'^{(E2)}\, | \alpha, I, M = I \rangle. \quad (119)$$

Here, the reduced matrix element in equation (118) is defined with the Wigner-Eckart theorem,

$$\langle \alpha, I, M = I |\, \hat{D}_0'^{(E2)}\, | \alpha', I', M' = I \rangle = \begin{pmatrix} I & 2 & I' \\ -I & 0 & I \end{pmatrix}\langle \alpha I \| \hat{D}'^{(E2)} \| \alpha' I' \rangle. \quad (120)$$

Substituting equation (13) into $|\alpha, I, M\rangle$, we obtain [46]

$$\begin{aligned}\langle \alpha I \| \hat{D}'^{(E2)} \| \alpha' I' \rangle = {} & \sqrt{(2I+1)(2I'+1)}\,(-)^I \\ & \times \sum_K \Bigg\{ \begin{pmatrix} I & 2 & I' \\ -K & 0 & K \end{pmatrix}\langle \Phi_{\alpha,I,K} |\, \hat{D}_{0+}^{(E2)}\, | \Phi_{\alpha',I',K} \rangle \\ & + \sqrt{(1+\delta_{K0})}\Bigg[\begin{pmatrix} I & 2 & I' \\ -K-2 & 2 & K \end{pmatrix} \\ & \times \langle \Phi_{\alpha,I,K+2} |\, \hat{D}_{2+}^{(E2)}\, | \Phi_{\alpha',I',K} \rangle \\ & + (-)^{I+I'}\begin{pmatrix} I & 2 & I' \\ K & 2 & -K-2 \end{pmatrix} \\ & \times \langle \Phi_{\alpha,I,K} |\, \hat{D}_{2+}^{(E2)}\, | \Phi_{\alpha',I',K+2} \rangle \Bigg] \Bigg\} \end{aligned} \quad (121)$$

with $\hat{D}_{m+}^{(E2)} = (\hat{D}_m^{(E2)} + \hat{D}_{-m}^{(E2)})/2$.

The quadrupole matrix elements between the intrinsic states are evaluated using the collective wave functions as

$$\langle \Phi_{\alpha,I,K}|\ \hat{D}^{(E2)}_{m+}\ |\Phi_{\alpha',I',K'}\rangle = \int \mathrm{d}\beta\mathrm{d}\gamma\sqrt{G(\beta,\gamma)}\,\Phi^{*}_{\alpha IK}(\beta,\gamma)D^{(E2)}_{m+}(\beta,\gamma)\Phi_{\alpha'I'K'}(\beta,\gamma), \tag{122}$$

where

$$D^{(E2)}_{m+}(\beta,\gamma) = \langle \phi(\beta,\gamma)|\ \hat{D}^{(E2)}_{m+}\ |\phi(\beta,\gamma)\rangle. \tag{123}$$

Appendix C. Illustration of triaxial deformation dynamics

We consider a simple model that may be useful to understand several interesting limits of triaxial deformation dynamics in a unified perspective. The model discussed below includes several situations, such as the axially symmetric rotor model, the γ-unstable model [51], the triaxial rigid rotor model [52], and oblate-prolate shape coexistence in an ideal situation. This model enables us to describe the smooth change between these extreme situations by changing a few parameters. Here we show only the simplest example, referring [212] for more general cases. To focus our attention on the γ degree of freedom, we fix the β degree of freedom at a constant value β_0 in the Bohr–Mottelson collective Hamiltonian (5) and parametrize the collective potential $V(\beta,\gamma)$ as $V(\beta_0,\gamma) = V_\beta(\beta_0) + V_\gamma(\beta_0,\gamma)$ with

$$V_\gamma(\beta_0,\gamma) = V_0(\beta_0)\sin^2 3\gamma + V_1(\beta_0)\cos 3\gamma. \tag{124}$$

This form is readily obtained by expanding $V(\beta,\gamma)$ in powers of the basic second- and third-order invariants, β^2 and $\beta^3\cos 3\gamma$, and keeping up to the second order in $\beta^3\cos 3\gamma$.

When $V_1 = 0$, the collective potential is symmetric with respect to the reflection about $\gamma = 30°$. For positive V_0, two minima appear at the oblate ($\gamma = 60°$) and prolate ($\gamma = 0°$) shapes. They are degenerated and separated by a barrier located at $\gamma = 30°$. For negative V_0, on the other hand, the barrier top at $\gamma = 30°$ turns out to be the single minimum, and it becomes deeper as $|V_0|$ increases. The term V_1 breaks the oblate-prolate symmetry, and controls the magnitude of the symmetry breaking. For positive (negative) V_1, the oblate (prolate) shape becomes the minimum (when V_0 is positive).

Let us discuss the simplest case where $V_1 = 0$, and the collective inertial masses ($D_{\beta\beta}$, $D_{\gamma\gamma}\beta_0^{-2}$, D_1, D_2, D_3) are replaced by a common constant D, and $D_{\beta\gamma}$ is ignored. In this case, both the collective potential and the moments of inertia $\mathcal{J}(\beta,\gamma)$ are symmetric with respect to the reflection about $\gamma = 30°$, so that the collective Hamiltonian possesses the oblate-prolate symmetry. Furthermore, D and β_0 appear only in the form $(2D\beta_0^2)^{-1}$ in the kinetic energy. Therefore the ratio $2D\beta_0^2 V_0$ is a single quantity that enters in the collective Schrödinger equation (12) and determines the dynamics. A particular case of $V_0 = 0$ is known to be the Wilets-Jean γ-unstable model [51]. In this case the excitation spectra just scale with the factor $(2D\beta_0^2)^{-1}$.

Figure 6 shows excitation spectra as functions of V_0. The excitation energies are normalized with the excitation energy of the second 0^+ state (first excited 0^+ state) $E(0_2^+)$ at $V_0 = 0$ (which is 1.8 MeV for $\beta_0^2 = 0.1$ and $D = 50$ MeV^{-1}). Because of the scaling property of the collective Schrödinger equation, this figure is valid for any value of $(2D\beta_0^2)^{-1}$. In the lower panels, the collective potentials $V(\beta_0,\gamma)$ are shown for three extreme situations, namely 1) a triaxially deformed case with a deep minimum at $\gamma = 30°$, 2) a γ-unstable case, and 3) an ideal case of oblate-prolate shape coexistence with two degenerated minima. Note that the collective potential $V(\beta,\gamma)$ is a periodic function of 60° in γ. The solid line in figure 6(d) shows the region $0° \leqslant \gamma \leqslant 60°$.

When V_0 is positive, a doublet structure appears with increasing the barrier-height parameter V_0. In other words, an approximately degenerated pair of eigenstates emerges for every angular momentum when $V_0/E(0_2^+) \gg 1$. This is a well-known doublet pattern in the double-well potential problem. We can associate this doublet structure with the oblate-prolate symmetry as seen in figure 6(d). Furthermore, we notice a very unique behavior of the 0_2^+ state; when V_0 decreases in the positive-V_0 side, its energy rises more rapidly than those of the yrare 2_2^+, 4_2^+, and 6_2^+ states. It crosses with $E(2_2^+)$ at $V_0/E(0_2^+) \simeq 3$, and finally at $V_0 = 0$, the 0_2^+ state is degenerated with 4_2^+ and 6_1^+ states, as expected in the Wilets-Jean model [51].

In the negative-V_0 side, the excitation energies of 3_1^+ and 5_1^+ states rapidly decrease with decreasing V_0, and when the potential minimum at $\gamma = 30°$ becomes very deep, the spectrum becomes similar with that of the Davydov-Filippov rigid triaxial rotor model [52].

Appendix D. Time-dependent unitary transformation of the HFB state vectors

Let us first consider the TDHF case. It is convenient to define the particle-hole concept with respect to the HF ground state $|\phi_{\mathrm{HF}}\rangle$ for doubly even nuclei by

$$\begin{aligned} c_i^\dagger &= (1-n_i)c_i^\dagger + n_i c_i^\dagger = a_i^\dagger + b_{\bar{\imath}}, \\ c_{\bar{\imath}} &= (1-n_i)c_{\bar{\imath}} + n_i c_{\bar{\imath}} = a_{\bar{\imath}} - b_i^\dagger. \end{aligned} \tag{125}$$

Here $c_i^\dagger$ and $c_{\bar{\imath}}$ are the nucleon creation and annihilation operators in the HF states i and its time-conjugate states $\bar{\imath}$, respectively, and n_i is 1 or 0 according to whether a pair of the HF states $(i,\bar{\imath})$ is occupied or unoccupied. The nucleon operators $(c_i^\dagger, c_{\bar{\imath}})$ correspond to the particle operators $(a_i^\dagger, a_{\bar{\imath}})$ for unoccupied space and the hole operators $(b_{\bar{\imath}}, b_i^\dagger)$ for the occupied space. Obviously, the HF ground state is a vacuum for the particles and holes:

$$a_i|\phi_{\mathrm{HF}}\rangle = b_j|\phi_{\mathrm{HF}}\rangle = 0. \tag{126}$$

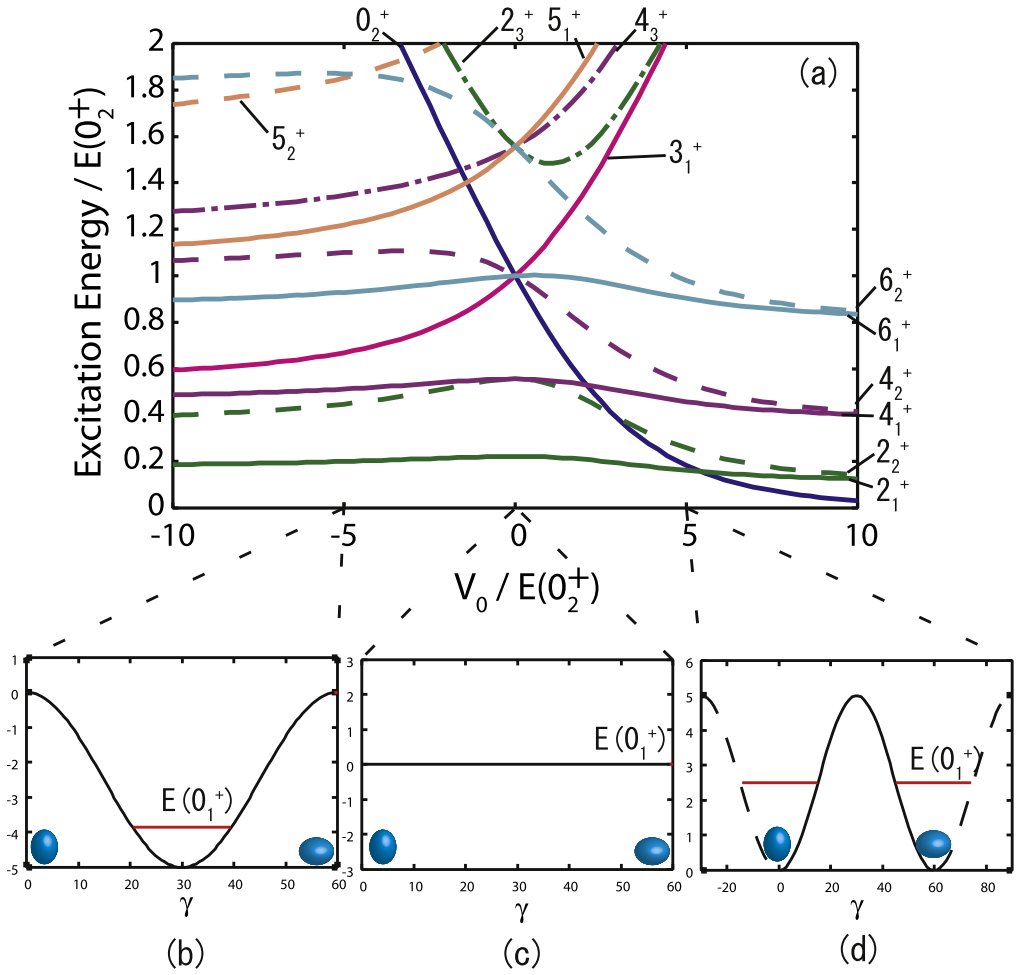

Figure 6. (a): excitation energies as functions of the parameter V_0. Both the excitation energies and the V_0 are normalized by the excitation energy of the second 0^+ state for $V_0 = 0$. (b), (c), (d): the collective potentials $V(\gamma)$ and the ground state energies $E(0_1^+)$ at $V_0/E(0_2^+) = -5.0$ (b), 0.0 (c), and 5.0 (d). Note that $E(0_1^+) = 0$ for $V_0 = 0$. The collective potential is a periodic function of 60° in γ, and only the region $0° \leqslant \gamma \leqslant 60°$ is drawn with a solid line in (d). This figure is taken from [212].

According to the Thouless theorem [213], another HF state $|\phi_{\rm HF}(t)\rangle$ non-orthogonal to $|\phi_{\rm HF}\rangle$ can be written as

$$|\phi_{\rm HF}(t)\rangle = N(t)\exp\left(\sum_{ij} z_{ij}(t) a_i^\dagger b_j^\dagger\right)|\phi_{\rm HF}\rangle \tag{127}$$

with the normalization constant $N(t)$. It may be more convenient to describe the same HF state as a unitary transformation of $|\phi_{\rm HF}\rangle$ [59, 214]:

$$|\phi_{\rm HF}(t)\rangle = {\rm e}^{{\rm i}\hat{G}_{\rm HF}(t)}|\phi_{\rm HF}(t=0)\rangle \tag{128}$$

with

$${\rm i}\hat{G}_{\rm HF}(t) = \sum_{ij}(f_{ij}(t) a_i^\dagger b_j^\dagger - f_{ij}^*(t) b_j a_i). \tag{129}$$

Here, $|\phi_{\rm HF}\rangle$ is denoted $|\phi_{\rm HF}(t=0)\rangle$ to emphasize that equation (128) can be regarded as a time-dependent unitary transformation describing the time evolution of the TDHF state vectors. In this generalized form, in contrast to the original Thouless theorem, even the HF states orthogonal to $|\phi_{\rm HF}(t=0)\rangle$ can be described.

It is straightforward to generalize the above formulation to the TDHFB case including the pairing correlations. The particle-hole concept in the HF theory is replaced by the quasiparticle concept, which is introduced through the generalized Bogoliubov transformations [54],

$$\begin{aligned} c_i^\dagger &= \sum_j (u_{ij}^* a_j^\dagger + v_{ij} a_j), \\ c_i &= \sum_j (u_{ij} a_j + v_{ij}^* a_j^\dagger), \end{aligned} \tag{130}$$

(separately for protons and neutrons) in the HFB theory. (The use of the same notation ($a_i^\dagger$, $a_{\bar{i}}$) for the quasipartcles in the HFB theory and the particles in the HF theory may not cause any confusion.) The particle-hole pair creation and annihilation operators ($a_i^\dagger b_j^\dagger$, $b_j a_i$) are then replaced by the two-quasipartcle creation and annihilation operators ($a_i^\dagger a_j^\dagger$, $a_j a_i$). Similarly to equation (128) in the TDHF case, the time evolution of the TDHFB state $|\phi(t)\rangle$ can be described as a time-dependent unitary transformation [62, 215]:

$$|\phi(t)\rangle = {\rm e}^{{\rm i}\hat{G}(t)}|\phi(t=0)\rangle, \tag{131}$$

where $\mathrm{i}\hat{G}(t)$ is a one-body anti-Hermitian operator given by

$$\mathrm{i}\hat{G}(t) = \sum_{(ij)} (g_{ij}(t) a_i^\dagger a_j^\dagger - g_{ij}^*(t) a_j a_i). \tag{132}$$

Here, the sum is taken over independent two-quasiparticle configurations (ij). For the HFB state at $t = 0$, one may choose the HFB ground state $|\phi_0\rangle$ which satisfies the vacuum condition for the quasiparticles:

$$a_i \; |\phi_0\rangle = 0. \tag{133}$$

It is important to note that equation (131) is valid for any choice of the initial HFB state $|\phi(t=0)\rangle$, if the quasiparticle operators in $\mathrm{i}\hat{G}(t)$ are defined with respect to $|\phi(t=0)\rangle$.

Because $\hat{G}(t)$ is a one-body operator, it is possible to define quasiparticle creation and annihilation operators $\{a_i^\dagger(t), a_j(t)\}$ with respect to $|\phi(t)\rangle$ as follows:

$$\begin{aligned} a_i(t) &= \mathrm{e}^{\mathrm{i}\hat{G}(t)} a_i \mathrm{e}^{-\mathrm{i}\hat{G}(t)} \\ &= a_i + [\mathrm{i}\hat{G}, a_i] + \frac{1}{2}[\mathrm{i}\hat{G}, [\mathrm{i}\hat{G}, a_i]] \\ &\quad + \frac{1}{6}[\mathrm{i}\hat{G}, [\mathrm{i}\hat{G}, [\mathrm{i}\hat{G}, a_i]]] + \cdots \\ &= \sum_j (U_{ji} a_j + V_{ji} a_j^\dagger). \end{aligned} \tag{134}$$

The matrices, $U(t)$ and $V(t)$, composed of the amplitudes $U_{ij}(t)$ and $V_{ij}(t)$, are given by [60, 215]

$$U^T(t) = \cos\sqrt{G^\dagger G}, \tag{135}$$

$$V^T(t) = G^\dagger \frac{\sin\sqrt{GG^\dagger}}{\sqrt{GG^\dagger}}, \tag{136}$$

where G is a matrix composed of the components g_{ij}. Obviously, the quasiparticle operators $\{a_i^\dagger(t), a_j(t)\}$ satisfy the vacuum condition for $|\phi(t)\rangle$:

$$\begin{aligned} a_i(t)|\phi(t)\rangle &= \mathrm{e}^{\mathrm{i}\hat{G}(t)} a_i \mathrm{e}^{-\mathrm{i}\hat{G}(t)} \mathrm{e}^{\mathrm{i}\hat{G}(t)} |\phi(t=0)\rangle \\ &= \mathrm{e}^{\mathrm{i}\hat{G}(t)} a_i |\phi(t=0)\rangle \\ &= 0. \end{aligned} \tag{137}$$

References

[1] Bohr A 1952 *Mat. Fys. Medd. Dan. Vid. Selsk.* **26** 14, 1–40
[2] Bohr A and Mottelson B R 1969 *Nuclear Structure* vol 1 (New York: Benjamin)
[3] Bohr A and Mottelson B R 1975 *Nuclear Structure* vol 2 (New York: Benjamin)
[4] Bohr A 1976 *Rev. Mod. Phys.* **48** 365
[5] Mottelson B 1976 *Rev. Mod. Phys.* **48** 375
[6] Tomonaga S-I 1955 *Prog. Theor. Phys.* **13** 467
[7] Miyazima T and Tamura T 1956 *Prog. Theor. Phys.* **15** 255
[8] Marumori T, Yukawa J and Tanaka R 1955 *Prog. Theor. Phys.* **13** 442
[9] Rowe D J 1985 *Rep. Prog. Phys.* **48** 1419
[10] Rowe D J, McCoy A E and Caprio M A 2016 *Phys. Scr.* **91** 033003
[11] Suzuki T 1980 *Prog. Theor. Phys.* **64** 1627
[12] Kurasawa H and Suzuki T 1996 *Nucl. Phys.* A **597** 374
[13] Baranger M 1960 *Phys. Rev.* **120** 957
[14] Marumori T 1960 *Prog. Theor. Phys.* **24** 331
[15] Klein A and Marshalek E R 1991 *Rev. Mod. Phys.* **63** 375
[16] *Microscopic Theories of Nuclear Collective Motions* Abe A and Suzuki T (ed) 1983 (*Prog. Theor. Phys. Suppl.* 74 & 75) pp 1–416
[17] Davies K T R, Devi K R S, Koonin S E and Strayer M R 1985 (*Treatise on Heavy-Ion Physics* vol 3) ed D A Bromley (New York: Plenum) 3
[18] Rainwater J 1976 *Rev. Mod. Phys.* **48** 385
[19] Butler P A and Nazarewicz W 1996 *Rev. Mod. Phys.* **68** 349
[20] Brack M, Damgaard J, Jensen A S, Pauli H C, Strutinsky V M and Wong C Y 1972 *Rev. Mod. Phys.* **44** 320
[21] Hagino K and Takigawa N 2012 *Prog. Theor. Phys.* **128** 1061
[22] Matsuyanagi K, Matsuo M, Nakatsukasa T, Yoshida K, Hinohara N and Sato K 2016 *J. Phys. G.: Nucl. Part. Phys.* **43** 024006
[23] Próchniak L and Rohoziński S G 2009 *J. Phys. G. Nucl. Part. Phys.* **36** 123101
[24] Frauendorf S 2015 *J. Int. Mod. Phys.* E **24** 1541001
[25] Cejnar P, Jolie J and Casten R F 2010 *Rev. Mod. Phys.* **82** 2155
[26] Brink D M and Broglia R A 2005 *Nuclear Superfluidity Pairing in Finite Systems* (Cambridge: Cambridge University Press)
[27] Arita K 2012 *Phys. Rev.* C **86** 034317
[28] Arita K 2016 *Phys. Scr.* **91** 063002
[29] Mayer M G and Jensen J H D 1955 *Elementary Theory of Nuclear Shell Structure* (New York: Wiley)
[30] Ragnarsson I, Nilsson S G and Sheline R K 1978 *Phys. Rep.* **45** 1
[31] Nilsson S G and Ragnarsson I 1995 *Shapes and Shells in Nuclear Structure* (Cambridge: Cambridge University Press)
[32] Nolan P J and Twin P J 1988 *Annu. Rev. Nucl. Part. Sci.* **38** 533
[33] Janssens R V F and Khoo T L 1991 *Annu. Rev. Nucl. Part. Sci.* **41** 321
[34] Brack M and Bhaduri R K 1997 *Semiclassical Physics* (Reading, MA: Addison-Wesley)
[35] Nazarewicz W, Dudek J, Bengtsson R, Bengtsson T and Ragnarsson I 1985 *Nucl. Phys.* A **435** 397
[36] Anderson P W 1958 *Phys. Rev.* **112** 1900
Anderson P W 1963 *Phys. Rev.* **130** 439
[37] Nambu Y 1960 *Phys. Rev.* **117** 648
[38] Sakamoto H and Kishimoto T 1991 *Nucl. Phys.* A **528** 73
[39] Åberg S, Flocard H and Nazarewicz W 1990 *Annu. Rev. Nucl. Part. Sci.* **40** 439
[40] Wood J L, Heyde K, Nazarewicz W, Huyse M and van Duppen P 1992 *Phys. Rep.* **215** 101
[41] Heyde K and Wood J L 2011 *Rev. Mod. Phys.* **83** 1467
[42] Hill D L and Wheeler J A 1953 *Phys. Rev.* **89** 1102
[43] Eisenberg J M and Greiner W 1987 *Nuclear Theory* vol 1 3rd edn (Amsterdam: North Holland)
[44] Jolos R V and von Brentano P 2009 *Phys. Rev.* C **79** 044310
[45] Bonatsos D, Minkov N and Petrellis D 2015 *J. Phys. G.: Nucl. Part. Phys.* **42** 095104
[46] Kumar K and Baranger M 1967 *Nucl. Phys.* A **92** 608
[47] Belyaev S T 1965 *Nucl. Phys.* **64** 17
[48] Bohr A and Mottelson B R 1953 *Mat. Fys. Medd. Dan. Vid. Selsk.* **27** 16, 1–174 (ed 2. 1957)
[49] Reinhard P-G, Brack M and Genzken O 1990 *Phys. Rev.* A **41** 5568
[50] Matsuo M and Matsuyanagi K 1985 *Prog. Theor. Phys.* **74** 1227
Matsuo M and Matsuyanagi K 1986 *Prog. Theor. Phys.* **76** 93
Matsuo M and Matsuyanagi K 1987 *Prog. Theor. Phys.* **78** 591
[51] Wilets L and Jean M 1956 *Phys. Rev.* **102** 788
[52] Davydov A S and Filippov G F 1958 *Nucl. Phys.* **8** 237

[53] Rowe D J 1970 *Nuclear Collective Motion: Models and Theory* (London: Methuen)
[54] Ring P and Schuck P 1980 *The Nuclear Many-Body Problem* (New York: Springer-Verlag)
[55] Blaizot J-P and Ripka G 1986 *Quantum Theory of Finite Systems* (Cambridge, MA: The MIT Press)
[56] Bertsch G F and Broglia R A 1994 *Oscillations in Finite Quantum Systems* (Cambridge: Cambridge University Press)
[57] Rowe D J and Wood J L 2010 *Fundamentals of Nuclear Models, Foundational Models* (Singapore: World Scientific)
[58] Bender M, Heenen P-H and Reinhard P-G 2003 *Rev. Mod. Phys.* **75** 121
[59] Marumori T, Maskawa T, Sakata F and Kuriyama A 1980 *Prog. Theor. Phys.* **64** 1294
[60] Sakata F, Marumori T, Hashimoto Y and Une T 1983 *Prog. Theor. Phys.* **70** 424
[61] Matsuo M 1986 *Prog. Theor. Phys.* **76** 372
[62] Suzuki T 1983 *Nucl. Phys.* A **398** 557
[63] Yamamura M and Kuriyama A 1987 *Prog. Theor. Phys. Suppl.* **93** 1
[64] Kuriyama A and Yamamura M 1984 *Prog. Theor. Phys.* **71** 973
[65] Nakatsukasa T, Walet N R and Dang G Do 1999 *Phys. Rev.* C **61** 014302
[66] Bohigas O, Lane A M and Martorell J 1979 *Phys. Rep.* **51** 267
[67] Bes D R and Sorensen R A 1969 *Advances in Nuclear Physics* vol 2 (New York: Plenum Press) 129
[68] Kisslinger L S and Sorensen R A 1963 *Rev. Mod. Phys.* **35** 853
[69] Baranger M and Kumar K 1965 *Nucl. Phys.* **62** 113
Kumar K and Baranger M 1968 *Nucl. Phys.* A **110** 529
Baranger M and Kumar K 1968 *Nucl. Phys.* A **122** 241
Kumar K and Baranger M 1968 *Nucl. Phys.* A **122** 273
[70] Sakamoto H and Kishimoto T 1989 *Nucl. Phys.* A **501** 205
Sakamoto H and Kishimoto T 1989 *Nucl. Phys.* A **501** 242
[71] Mottelson B 1998 *Trends in Nuclear Physics, 100 year later Les Houches, Session LXVI* ed H Nifenecker, J-P Blaizot, G F Bertsch, W Weise and F David (Amsterdam: North Holland) p 25
[72] Vautherin D and Brink D M 1972 *Phys. Rev.* C **5** 626
[73] Vautherin D 1973 *Phys. Rev.* C **7** 296
[74] Dechargé J and Gogny D 1980 *Phys. Rev.* C **21** 1568
[75] Negele J W 1982 *Rev. Mod. Phys.* **54** 913
[76] Stone J R and Reinhard P-G 2007 *Prog. Part. Nucl. Phys.* **58** 587
[77] Nakatsukasa T 2012 *Prog. Theor. Exp. Phys.* **2012** 01A207
[78] Fiolhais C, Nogueira F and Marques M (ed) 2003 *A Primer in Density Functional Theory* (Berlin: Springer)
[79] Marques M A L, Ullrich C A, Nogueira F, Rubio A, Burke K and Gross E K U (ed) 2006 *Time-Dependent Density Functional Theory* (Berlin: Springer)
[80] Vretenar D, Afanasjev A V, Lalazissis G A and Ring P 2005 *Phys. Rep.* **409** 101
[81] Terasaki J, Engel J and Bertsch G F 2008 *Phys. Rev.* C **78** 044311
[82] Yoshida K and Yamagami M 2008 *Phys. Rev.* C **77** 044312
[83] Péru S and Goutte H 2008 *Phys. Rev.* C **77** 044313
[84] Arteaga D P, Khan E and Ring P 2009 *Phys. Rev.* C **79** 034311
[85] Losa C, Pastore A, Døssing T, Vigezzi E and Broglia R A 2010 *Phys. Rev.* C **81** 064307
[86] Terasaki J and Engel J 2010 *Phys. Rev.* C **82** 034326
[87] Terasaki J and Engel J 2011 *Phys. Rev.* C **84** 014332
[88] Yoshida K and Nakatsukasa T 2011 *Phys. Rev.* C **83** 021304(R)
[89] Yoshida K and Nakatsukasa T 2013 *Phys. Rev.* C **88** 034309
[90] Nakatsukasa T, Inakura T and Yabana K 2007 *Phys. Rev.* C **76** 024318
[91] Avogadro P and Nakatsukasa T 2011 *Phys. Rev.* C **84** 014314
[92] Avogadro P and Nakatsukasa T 2013 *Phys. Rev.* C **87** 014331
[93] Stoitsov M, Kortelainen M, Nakatsukasa T, Losa C and Nazarewicz W 2011 *Phys. Rev.* C **84** 041305(R)
[94] Inakura T, Nakatsukasa T and Yabana K 2013 *Phys. Rev.* C **88** 051305(R)
[95] Mustonen M T, Shafer T, Zenginerler Z and Engel J 2014 *Phys. Rev.* C **90** 024308
[96] Liang H, Nakatsukasa T, Niu Z and Meng J 2013 *Phys. Rev.* C **87** 054310
[97] Nikšić T, Kralj N, Tutiš T, Vretenar D and Ring P 2013 *Phys. Rev.* C **88** 044327
[98] Sakamoto H and Kishimoto T 1988 *Nucl. Phys.* A **486** 1
Sakamoto H and Kishimoto T 1991 *Nucl. Phys.* A **528** 73
[99] Matsuyanagi K, Matsuo M, Nakatsukasa T, Hinohara N and Sato K 2010 *J. Phys. G.: Nucl. Part. Phys.* **37** 064018
[100] Matsuyanagi K, Hinohara N and Sato K 2013 *Fifty Years of Nuclear BCS: Pairing in Finite Systems* ed R A Broglia and V Zelevinsky (Singapore: World Scientific) 111
[101] *Selected Topics in the Boson Mapping and Time-Dependent Hartree-Fock Methods* Kuriyama A, Matsuyanagi K, Sakata F, Takada K and Yamamura M (ed) 2001 (*Prog. Theor. Phys. Suppl.* 141) 1
[102] Matsuo M, Nakatsukasa T and Matsuyanagi K 2000 *Prog. Theor. Phys.* **103** 959
[103] Hinohara N, Nakatsukasa T, Matsuo M and Matsuyanagi K 2008 *Prog. Theor. Phys.* **119** 59
[104] Hinohara N, Nakatsukasa T, Matsuo M and Matsuyanagi K 2009 *Phys. Rev.* C **80** 014305
[105] Hinohara N, Sato K, Nakatsukasa T, Matsuo M and Matsuyanagi K 2010 *Phys. Rev.* C **82** 064313
[106] Sato K and Hinohara N 2011 *Nucl. Phys.* A **849** 53
[107] Hinohara N, Sato K, Nakatsukasa T, Matsuo M and Matsuyanagi K 2011 *Phys. Rev.* C **84** 061302(R)
[108] Yoshida K and Hinohara N 2011 *Phys. Rev.* C **83** 061302(R)
[109] Sato K, Hinohara N, Yoshida K, Nakatsukasa T, Matsuo M and Matsuyanagi K 2012 *Phys. Rev.* C **86** 024316
[110] Matsuo M, Hinohara N, Sato K, Matsuyanagi K, Nakatsukasa T and Yoshida K 2014 *Phys. Scr.* **89** 054020
[111] Thouless D J and Valatin J G 1962 *Nucl. Phys.* **31** 211
[112] Kaneko K 1994 *Phys. Rev.* C **49** 3014
[113] Sakamoto H 1997 *Int. J. Mod. Phys.* E **6** 251
[114] Hinohara N, Kortelainen M and Nazarewicz W 2013 *Phys. Rev.* C **87** 064309
[115] Hinohara N, Kortelainen M, Nazarewicz W and Olsen E 2015 *Phys. Rev.* C **91** 044323
[116] Hinohara N 2015 *Phys. Rev.* C **92** 034321
[117] Kortelainen M, Hinohara N and Nazarewicz W 2015 *Phys. Rev.* C **92** 051302(R)
[118] Barranco F, Bertsch G F, Broglia R A and Vigezzi E 1990 *Nucl. Phys.* A **512** 253
[119] Sakamoto H and Kishimoto T 1990 *Phys. Lett.* B **245** 321
[120] Hinohara N, Nakatsukasa T, Matsuo M and Matsuyanagi K 2006 *Prog. Theor. Phys.* **115** 567
[121] Mottelson B R 1977 *Elementary Modes of Excitation in Nuclei* (*Proceedings of the international school of physics (Enrico Fermi), 1976*) ed A Bohr and R A Broglia (Amsterdam: Elsevier) 31
[122] Bortignon P F, Broglia R A, Bes D R and Liotta R 1977 *Phys. Rep.* **30** 305
[123] Broglia R A, Bortignon P F, Barranco F, Vigezzi E, Idini A and Potel G *Contribution to this Special Physica Scripta Edition*
[124] Yamada K 1991 *Prog. Theor. Phys.* **85** 805
[125] Shimizu Y R and Matsuyanagi K 2001 *Prog. Theor. Phys. Suppl.* **141** 285
[126] Villars F 1957 *Ann. Rev. Nucl. Sci.* **7** 185
[127] Villars F M H 1983 *Prog. Theor. Phys. Suppl.* **74 & 75** 184

[128] Hinohara N and Kanada-En'yo Y 2011 *Phys. Rev.* C **83** 014321
[129] Hinohara N, Li Z P, Nakatsukasa T, Nikšić T and Vretenar D 2012 *Phys. Rev.* C **85** 024323
[130] Clément E *et al* 2007 *Phys. Rev.* C **75** 054313
[131] Libert J, Girod M and Delaroche J-P 1999 *Phys. Rev.* C **60** 054301
[132] Yuldashbaeva E Kh, Libert J, Quentin P and Girod M 1999 *Phys. Lett.* B **461** 1
[133] Próchniak L, Quentin P, Samsoen D and Libert J 2004 *Nucl. Phys.* A **730** 59
[134] Delaroche J-P, Girod M, Libert J, Goutte H, Hilaire S, Péru S, Pillet N and Bertsch G F 2010 *Phys. Rev.* C **81** 014303
[135] Baran A, Sheikh J A, Dobaczewski J, Nazarewicz W and Staszczak A 2011 *Phys. Rev.* C **84** 054321
[136] Nikšić T, Li Z P, Vretenar D, Próchniak L, Meng J and Ring P 2009 *Phys. Rev.* C **79** 034303
[137] Li Z P, Nikšić T, Vretenar D, Meng J, Lalazissis G A and Ring P 2009 *Phys. Rev.* C **79** 054301
[138] Li Z P, Nikšić T, Vretenar D and Meng J 2010 *Phys. Rev.* C **81** 034316
[139] Li Z P, Nikšić T, Vretenar D, Ring P and Meng J 2010 *Phys. Rev.* C **81** 064321
[140] Li Z P, Yao J M, Vretenar D, Nikšić T, Chen H and Meng J 2011 *Phys. Rev.* C **84** 054304
[141] Nikšić T, Vretenar D and Ring P 2011 *Prog. Part. Nucl. Phys.* **66** 519
[142] Fu Y, Mei H, Xiang J, Li Z P, Yao J M and Meng J 2013 *Phys. Rev.* C **87** 054305
[143] Dobaczewski J and Dudek J 1995 *Phys. Rev.* C **52** 1827
[144] Baranger M and Véneroni M 1978 *Ann. of Phys.* **114** 123
[145] Brink D M, Giannoni M J and Veneroni M 1976 *Nucl. Phys.* A **258** 237
[146] Goeke K and Reinhard P-G 1978 *Ann. of Phys.* **112** 328
[147] Giannoni M J and Quentin P 1980 *Phys. Rev.* C **21** 2060
Giannoni M J and Quentin P 1980 *Phys. Rev.* C **21** 2076
[148] Villars F 1977 *Nucl. Phys.* A **285** 269
[149] Mukherjee A K and Pal M K 1982 *Nucl. Phys.* A **373** 289
[150] Klein A, Walet N R and Dang G Do 1991 *Ann. of Phys.* **208** 90
[151] Dang G Do, Klein A and Walet N R 2000 *Phys. Rep.* **335** 93
[152] Goeke K, Cusson R Y, Grümmer F, Reinhard P-G and Reinhardt H 1983 *Prog. Theor. Phys. Suppl.* **74 & 75** 33
[153] Dobaczewski J and Skalski J 1981 *Nucl. Phys.* A **369** 123
[154] Li Z P, Nikšić T, Ring P, Vretenar D, Yao J M and Meng J 2012 *Phys. Rev.* C **86** 034334
[155] Reinhard P-G and Goeke K 1987 *Rep. Prog. Phys.* **50** 1
[156] Egido J L and Robledo L M 2004 *Extended Density Functionals in Nuclear Structure Physics* (*Lecture Notes in Physics* vol 641) ed G A Lalazissis, P Ring and D Vretenar (Berlin: Springer) 269
[157] Bender M 2008 *Eur. Phys. J. Spec. Top.* **156** 217
[158] Bender M and Heenen P-H 2008 *Phys. Rev.* C **78** 024309
[159] Rodríguez T R and Egido J L 2010 *Phys. Rev.* C **81** 064323
[160] Yao J M, Meng J, Ring P and Vretenar D 2010 *Phys. Rev.* C **81** 044311
[161] Yao J M, Mei H, Chen H, Meng J, Ring P and Vretenar D 2011 *Phys. Rev.* C **83** 014308
[162] Yao J M, Hagino K, Li Z P, Meng J and Ring P 2014 *Phys. Rev.* C **89** 054306
[163] Rodríguez T R 2014 *Phys. Rev.* C **90** 034306
[164] Griffin J J and Wheeler J A 1957 *Phys. Rev.* **108** 311
[165] Onishi N and Une T 1975 *Prog. Theor. Phys.* **53** 504
[166] Rohoziński S G 2012 *J. Phys. G. Nucl. Part. Phys.* **39** 095104
[167] Rohoziński S G 2013 *Phys. Scr.* T **154** 014016
[168] Peierls R E and Thouless D J 1962 *Nucl. Phys.* **38** 154
[169] Holzwarth G and Yukawa T 1974 *Nucl. Phys.* A **219** 125
[170] Reinhard P-G and Goeke K 1979 *Phys. Rev.* C **20** 1546
[171] Jancovici B and Schiff D H 1964 *Nucl. Phys.* **58** 678
[172] Rowe D J and Bassermann R 1976 *Canad. J. Phys.* **54** 1941
[173] Marumori T 1977 *Prog. Theor. Phys.* **57** 112
[174] Rowe D J 1982 *Nucl. Phys. A* **391** 307
[175] Arnold V I 1989 *Mathematical Methods of Classical Mechanics* (Berlin: Springer)
[176] Matsuo M and Matsuyanagi K 1985 *Prog. Theor. Phys.* **74** 288
[177] Matsuo M, Shimizu Y R and Matsuyanagi K 1985 *Proceedings of The Niels Bohr Centennial Conf. on Nuclear Structure* ed R Broglia, G Hagemann and B Herskind (Amsterdam: North-Holland) 161
[178] Yamada K 1993 *Prog. Theor. Phys.* **89** 995
[179] Almehed D and Walet N R 2004 *Phys. Rev.* C **69** 024302
[180] Hinohara N, Nakatsukasa T, Matsuo M and Matsuyanagi K 2007 *Prog. Theor. Phys.* **117** 451
[181] Sato K 2015 *Prog. Theor. Exp. Phys.* **2015** 123D01
[182] Iwasaki S, Marumori T, Sakata F and Takada K 1976 *Prog. Theor. Phys.* **56** 1140
[183] Weeks K J, Tamura T, Udagawa T and Hahne F J W 1981 *Phys. Rev.* C **24** 703
[184] Tazaki S, Takada K, Kaneko K and Sakata F 1981 *Prog. Theor. Phys. Suppl.* **71** 123
[185] Takada K and Tazaki S 1986 *Nucl. Phys.* A **448** 56
[186] Garrett P E 2001 *J. Phys. G.: Nucl. Part. Phys.* **27** R1
[187] Yoshida K, Matsuo M and Shimizu Y R 2001 *Nucl. Phys.* A **696** 85
[188] Back B B, Esbensen H, Jiang C L and Rehm K E 2014 *Rev. Mod. Phys.* **86** 317
[189] Frauendorf S 2001 *Rev. Mod. Phys.* **73** 463
[190] Satuła W and Wyss R A 2005 *Rep. Prog. Phys.* **68** 131
[191] Shimizu Y R, Garrett J D, Broglia R A, Gallardo M and Vigezzi E 1989 *Rev. Mod. Phys.* **61** 131
[192] Bohr A and Mottelson B R 1981 *Nucl. Phys.* A **354** 303c
[193] Nakatsukasa T, Matsuyanagi K, Mizutori S and Shimizu Y R 1996 *Phys. Rev.* C **53** 2213
[194] Roßbach D *et al* 2001 *Phys. Lett.* B **513** 9
[195] Pattison L K *et al* 2003 *Phys. Rev. Lett.* **91** 182501
[196] Ollier J *et al* 2011 *Phys. Rev.* C **83** 044309
[197] Ødegård S W *et al* 2001 *Phys. Rev. Lett.* **86** 5866
[198] Jensen D R *et al* 2002 *Phys. Rev. Lett.* **89** 142503
[199] Görgen A *et al* 2004 *Phys. Rev.* C **69** 031301(R)
[200] Hamamoto I and Hagemann G B 2003 *Phys. Rev.* C **67** 014319
[201] Matsuzaki M, Shimizu Y R and Matsuyanagi K 2004 *Phys. Rev.* C **69** 034325
[202] Shoji T and Shimizu Y R 2009 *Prog. Theor. Phys.* **121** 319
[203] Frauendorf S and Dönau F 2014 *Phys. Rev.* C **89** 014322
[204] Almehed D, Dönau F and Frauendorf S 2011 *Phys. Rev.* C **83** 054308
[205] Hamamoto I 2012 *Phys. Rev.* C **85** 064329
[206] Matsuo M 2013 *Fifty Years of Nuclear BCS: Pairing in Finite Systems* ed R Broglia and V Zelevinsky (Singapore: World Scientific) 61
[207] Matsuo M 2001 *Nucl. Phys.* A **696** 371
[208] Mizuyama K, Matsuo M and Serizawa Y 2009 *Phys. Rev.* C **79** 024313
[209] Serizawa Y and Matsuo M 2009 *Prog. Theor. Phys.* **121** 97
[210] Matsuo M and Nakatsukasa T 2010 *J. Phys. G.: Nucl. Part. Phys.* **37** 064017
[211] Mizuyama K, Colò G and Vigezzi E 2012 *Phys. Rev.* C **86** 034318
[212] Sato K, Hinohara N, Nakatsukasa T, Matsuo M and Matsuyanagi K 2010 *Prog. Theor. Phys.* **123** 129
[213] Thouless D J 1960 *Nucl. Phys.* **21** 225
[214] Rowe D J, Ryman A and Rosensteel G 1980 *Phys. Rev.* A **22** 2362
[215] Ring P and Schuck P 1977 *Nucl. Phys.* A **292** 20

IOP Publishing | Royal Swedish Academy of Sciences Physica Scripta

Phys. Scr. **91** (2016) 073008 (21pp) doi:10.1088/0031-8949/91/7/073008

Invited Comment

Quantal rotation and its coupling to intrinsic motion in nuclei

Takashi Nakatsukasa[1,2,3,7], **Kenichi Matsuyanagi**[3,4], **Masayuki Matsuzaki**[5] **and Yoshifumi R Shimizu**[6]

[1] Center for Computational Sciences, University of Tsukuba, Tsukuba 305-8577, Japan
[2] Faculty of Pure and Applied Sciences, University of Tsukuba, Tsukuba 305-8571, Japan
[3] RIKEN Nishina Center, Wako 351-0198, Japan
[4] Yukawa Institute for Theoretical Physics, Kyoto University, Kyoto 606-8502, Japan
[5] Department of Physics, Fukuoka University of Education, Munakata, Fukuoka 811-4192, Japan
[6] Department of Physics, Graduate School of Science, Kyushu University, Fukuoka 819-0395, Japan

E-mail: nakatsukasa@nucl.ph.tsukuba.ac.jp

Received 26 January 2016, revised 25 April 2016
Accepted for publication 3 May 2016
Published 27 June 2016

Abstract

Symmetry breaking is an important concept in nuclear physics and other fields of physics. Self-consistent coupling between the mean-field potential and the single-particle motion is a key ingredient in the unified model of Bohr and Mottelson, which could lead to a deformed nucleus as a consequence of spontaneous breaking of the rotational symmetry. Some remarks on the finite-size quantum effects are given. In finite nuclei, the deformation inevitably introduces the rotation as a symmetry-restoring collective motion (Anderson–Nambu–Goldstone mode), and the rotation affects the intrinsic motion. In order to investigate the interplay between the rotational and intrinsic motions in a variety of collective phenomena, we use the cranking prescription together with the quasiparticle random phase approximation (QRPA). At low spin, the coupling effect can be seen in the generalized intensity relation. A feasible quantization of the cranking model is presented, which provides a microscopic approach to the higher-order intensity relation. At high spin, the semiclassical cranking prescription works well. We discuss properties of collective vibrational motions under rapid rotation and/or large deformation. The superdeformed shell structure plays a key role in emergence of a new soft mode which could lead to instability toward the $K^{\pi} = 1^{-}$ octupole shape. A wobbling mode of excitation, which is a clear signature of the triaxiality, is discussed in terms of a microscopic point of view. A crucial role played by the quasiparticle alignment is presented.

Keywords: unified model, symmetry breaking, high-spin nuclear structure, superdeformation, QRPA

(Some figures may appear in colour only in the online journal)

1. Introduction

There are a variety of rotating objects in the Universe. We are living on the rotating Earth which is revolving around the Sun. The Sun is a part of our rotating Galaxy. The neutron star is often observed as a 'pulsar' whose rotational period can be as small as 10^{-3} s. However, if we look into a microscopic world, we find much faster rotating objects, such as nuclei. The nuclear rotational period in heavy nuclei is typically $\tau_{\rm rot} = 10^{-19} \sim 10^{-20}$ s. This time scale is $100 - 1,000$ times larger than the period of the single-particle Fermi motion inside the nucleus, $\tau_{\rm F} \sim 10^{-22}$ s. Thus, the rotational motion

[7] Author to whom any correspondence should be addressed.

can be treated as 'slow' motion at low-spin states. However, in high-spin states produced by the fusion reaction, it could reach $\tau = 10^{-21} \sim 10^{-22}$ s which is comparable to τ_F. Therefore, the nuclei provide a unique laboratory to study rapidly rotating quantum systems under strong Coriolis and centrifugal fields.

The nucleus is a finite quantum many-body system. Since the Hamiltonian is rotationally invariant, its energy eigenstate has a definite total angular momentum I. In order to realize the nuclear rotation, the nucleus needs to define its orientation. Since it is impossible to do it for spherical systems, a deformed *intrinsic* state, which is produced by breaking the rotational symmetry, is necessary. The word 'intrinsic' means the degrees of freedom approximately independent of the rotational motion. The spontaneous breaking of symmetry (SBS) is an important concept to constitute the unified model of Bohr and Mottelson [1]. Hereafter, we denote the textbook [1] by 'BM2'.

The SBS is strictly defined only in infinite systems. Therefore, in the beginning of this article (sections 2, 3, and 4), we address the following basic questions.

(i) What is the origin of nuclear deformation?
(ii) What is the meaning of the SBS in finite systems?
(iii) What kind of collective motion will emerge due to the SBS?

These are important issues to understand the essence of the nuclear structure physics. We hope that these sections are useful, especially for students and non-practitioners.

The rotational motion is a collective motion emerged from the SBS, corresponding to the massless Anderson–Nambu–Goldstone (ANG) mode [2–7] in the infinite system. It is approximately decoupled from the intrinsic motions, however, the decoupling is never exact. Moreover, as we mentioned in the beginning, we may generate a nucleus spinning extremely fast in experiments. Coupling between the rotational and intrinsic motions produces a variety of phenomena. We will discuss several related topics in sections 5–7.

The coupling introduces the Coriolis mixing among different bands. The angular momentum dependence (I-dependence) of the transition matrix elements is very sensitive to this, even at low spin. The unified model predicts a form of the I-dependent intensity relation, however, a systematic way of calculating intrinsic moments entering in the intensity relation was missing. We present a feasible microscopic method for the calculation of the intrinsic moments using the cranking model at an infinitesimal rotational frequency (section 5).

Low-lying vibrational modes of excitation strongly reflect the underlying shell structure. Therefore, the new shell structure produced by rapid rotation and large deformation may significantly change their properties, and could lead to new soft modes and instability. Octupole vibrations at large angular momenta and in superdeformed (SD) bands are discussed. We present a possible banana-shaped superdeformation as a consequence of the SD shell structure (section 6).

Nuclear wobbling motion, predicted by Bohr and Mottelson (section 4-5e in BM2), has been observed in ^{163}Lu and neighboring nuclei. This mode corresponds to a non-uniform three-dimensional rotation and provides a clear signature of nuclear deformation without the axial symmetry. Microscopic analysis reveals an important role played by the quasiparticle alignment. In fact, without the alignment, the wobbling motion cannot exist in ^{163}Lu. These issues and precession motion of the high-K isomers are discussed in section 7.

For most of these studies, we use the quasiparticle-random-phase approximation (QRPA) in the rotating shell model, which we have developed for studies of rapidly rotating nuclei [8–11]. Further inclusion of the quasiparticle-vibration coupling has been carried out for odd nuclei [12–14]. The method is still very useful and illuminating to obtain insights into nuclear structure in extreme conditions. In the present article, we do not present details of the theoretical models. Instead, we would like to concentrate our discussion on basic concepts and emergent phenomena.

2. Unified model and SBS

The atom is a finite-size quantum system, composed of electrons bound by the Coulombic attraction of the central nucleus. The nucleus is also a quantum finite-size fermionic system composed of nucleons. In both systems, the independent-particle (single-particle) motion is a prominent feature which leads to the 'shell model'. In the first order approximation, the constituent particles (electrons in the atom and nucleons in the nucleus) freely move in the confining potential. However, there is an obvious but important difference between the atom and the nucleus. Namely, the nuclear potential binding the nucleons is generated by the nucleons themselves.

The electrons in the atom are bound by the attractive Coulomb potential generated by the nucleus. This potential is spherical, $-Ze^2/r$, in the atomic scale ($r \sim$ Å). Although the repulsive interaction creates correlations among the electrons, the strong attractive potential always produces a restoring force which favors the spherical shape. In contrast, the shape of the nuclear potential is determined by the shape of the nucleus itself. It is often referred to as '*nuclear self-consistency*'. Therefore, we expect that the nucleus may change its shape, much easier than the atomic case. In other words, the nucleus is rather 'soft' and produces low-energy 'slow' shape vibrations.

2.1. Unified model Hamiltonian

Bohr and Mottelson treated these shape degrees of freedom as collective variables α in addition to the single-particle degrees of freedom ξ. In general, the shape dynamics described by α is considerably slower than the single-particle motion. Thus, we could adopt a picture that the nucleons move in a one-body potential $V(\xi, \alpha)$ which is specified by the nuclear shape α. The idea ends up with the unified-model

Hamiltonian

$$H = H_{\rm coll}(\alpha) + H_{\rm sp}(\xi) + H_{\rm int}(\xi, \alpha), \tag{1}$$

where $H_{\rm coll}$ is the *collective* Hamiltonian to describe the low-energy shape vibrations. $H_{\rm sp}$ corresponds to the *single-particle* (shell model) Hamiltonian at the spherical shape, $H_{\rm sp}(\xi) = T_{\rm kin}(\xi) + V(\xi, \alpha = 0)$. $T_{\rm kin}$ is the kinetic energy term and the nuclear self-consistency requires the potential $V(\xi, \alpha)$ to vary with respect to the shape α. The *interaction* between the collective and single-particle motions, given by the third term $H_{\rm int}(\xi, \alpha)$, is indispensable to take into account this important property of nuclear potential.

2.2. Symmetry breaking mechanism

The coupling term in equation (1) could lead the nucleus to deformation. This is associated with the SBS mechanism. To elucidate the idea, let us adopt a simple adiabatic (Born–Oppenheimer) approximation. First, we solve the eigenvalue problem for the Schrödinger equation for the variables ξ with a fixed value of α

$$H_{\rm def}(\alpha)|\phi_n(\alpha)\rangle = \epsilon_n(\alpha)|\phi_n(\alpha)\rangle, \tag{2}$$

where $H_{\rm def}(\alpha) \equiv H_{\rm sp} + H_{\rm int}(\alpha)$. This gives the adiabatic collective Hamiltonian, $H^{(n)}_{\rm ad}(\alpha) = H_{\rm coll}(\alpha) + \epsilon_n(\alpha)$, for each intrinsic eigenstate $\phi_n(\xi; \alpha) \equiv \langle\xi|\phi_n(\alpha)\rangle$. $H^{(n)}_{\rm ad}$ is an effective Hamiltonian for the collective variables α. The total wave function is given by a product of the intrinsic and the collective parts [15], $\Psi_n(\alpha, \xi) = \psi^{(n)}(\alpha)\phi_n(\xi; \alpha)$.

There are two possible mechanisms of the SBS in the unified model to realize the deformed ground state with $\alpha \neq 0$. When $\epsilon_0(\alpha)$ strongly favors the deformation, even if $H_{\rm coll}(\alpha)$ has the potential minimum at $\alpha = 0$, the adiabatic potential in $H^{(0)}_{\rm ad}(\alpha)$ may have a deformed minimum. Apparently, this mechanism requires the deformation-driving nature of $H_{\rm int}(\xi, \alpha)$, which we call '*coupling-driven mechanism*'. On the other hand, there is another mechanism which can deform the nucleus even if the spherical shape ($\alpha = 0$) is favored by the adiabatic ground state $\epsilon_0(\alpha)$. This is due to the additional coupling caused by the kinetic term of $H_{\rm coll}$; $T_{\rm kin}(\alpha) = -(1/2)B\partial^2_\alpha$. We adopt units of $\hbar = 1$ throughout the present article. Roughly speaking, the SBS takes place when the level spacing in $\epsilon_n(\alpha)$ is smaller than the additional coupling. It is analogous to the Jahn-Teller effect in the molecular physics [16], which we call '*degeneracy-driven mechanism*'.

2.3. Degeneracy-driven SBS; diagonal approximation

In order to understand the degeneracy-driven mechanism, we make the argument simpler, neglecting the off-diagonal elements, $\langle\phi_n(\alpha)|T_{\rm kin}(\alpha)|\phi_0(\alpha)\rangle$ ($n \neq 0$). Integrating the intrinsic (single-particle) degrees ξ, the effective Hamiltonian for the collective variable α is obtained as

$$H^{(0)}_{\rm eff}(\alpha) = \langle\phi_0(\alpha)|H|\phi_0(\alpha)\rangle = H^{(0)}_{\rm coll}(\alpha) + \epsilon_0(\alpha) + \Phi_0(\alpha), \tag{3}$$

where $H^{(0)}_{\rm coll}$ is identical to $H_{\rm coll}$ except that its kinetic energy is modified into $T^{(0)}_{\rm kin}(\alpha) = -(1/2)B(\partial_\alpha + \langle\phi_0|\partial_\alpha\phi_0\rangle)^2$. This is equivalent to introduction of a 'vector' potential [17], $A(\alpha) \equiv {\rm i}\langle\phi_0|\partial_\alpha\phi_0\rangle$. If the coordinate α is one-dimensional, the 'vector' potential $A(\alpha)$ can be eliminated by a gauge transformation, $\exp\left({\rm i}\int A(\alpha){\rm d}\alpha\right)$. However, the following 'scalar' potential remains

$$\begin{aligned}\Phi_0(\alpha) &= \frac{1}{2}B\langle\partial_\alpha\phi_0|(1 - |\phi_0\rangle\langle\phi_0|)|\partial_\alpha\phi_0\rangle \\ &= \frac{1}{2}B\sum_{n\neq 0}\langle\partial_\alpha\phi_0|\phi_n\rangle\langle\phi_n|\partial_\alpha\phi_0\rangle \\ &= \frac{1}{2}B\sum_{n\neq 0}\left|\frac{\langle\phi_n(\alpha)|(\partial_\alpha H_{\rm def}(\alpha))|\phi_0(\alpha)\rangle}{\epsilon_0(\alpha) - \epsilon_n(\alpha)}\right|^2.\end{aligned} \tag{4}$$

From equation (4), it is apparent that $\Phi_0(\alpha)$ is positive and becomes large where the adiabatic ground state is approximately degenerate in energy, $\epsilon_0 \approx \epsilon_n$ ($n \neq 0$). When the spherical ground state ($\alpha = 0$) shows degeneracy, it could be significantly unfavored by $\Phi_0(\alpha)$. The system tends to avoid the degenerate ground state, which leads to the SBS with nuclear deformation.

We would like to emphasize again that the coupling between the collective (shape) degrees of freedom α and the intrinsic (single-particle) motion ξ is essential to produce the nuclear deformation. This is apparent for the coupling-driven mechanism, and is also true for the degeneracy-driven case. If the coupling term $H_{\rm int}(\xi, \alpha)$ is absent, the adiabatic states $\phi_n(\xi)$ are independent of α, thus, produce no gauge potentials, $A(\alpha) = \Phi_0(\alpha) = 0$. We also note here that the present argument on the degeneracy-driven (Jahn-Teller) mechanism explains why the instability of a spherical state occurs, but not what kind of deformation takes place. This will be discussed in sections 3.3 and 6.2.

2.4. Field coupling

The oscillation of the variable α correspond to the shape vibration. Thus, it can be quantized to a boson operator. In order to describe the vibrational motion associated with α, we introduce a boson space with the n-phonon state $|n\rangle$. When α is small, we may linearize the coupling term in equation (1) with respect to α as

$$H_{\rm int}(\xi, \alpha) = -\kappa\alpha F(\xi), \tag{5}$$

where κ is a coupling constant which depends on the normalization of α and F. If the operator F is given, the normalization of α is usually chosen as follows. The action of the one-body operator F on the ground state (a Slater determinant) produces many one-particle-one-hole states; $F|\Phi_0\rangle = \sum_{ph}|\Phi_{ph}\rangle\langle\Phi_{ph}|F|\Phi_0\rangle$. This is identified with the operation of α in the collective (boson) space:

$$\sum_{ph}|\langle\Phi_{ph}|F|\Phi_0\rangle|^2 = |\langle n = 1|\alpha|n = 0\rangle|^2. \tag{6}$$

The coupling constant κ can be also determined by this self-consistency. See chapter 6 of BM2 for details of the field coupling techniques.

If the matrix elements of F are identical to those of α as in equation (6), the field coupling (5) can be interpreted as an

residual two-body interaction

$$H_{\rm res}(\xi) = -\frac{1}{2}\kappa F^2. \quad (7)$$

This kind of separable effective interactions have been extensively adopted in nuclear structure studies. Among them, the most famous one is the pairing-plus-quadrupole model [18–20], which was originally proposed by Bohr, Mottelson, and their colleague. It represents two kinds of important low-energy correlations in nuclei; one is the quadrupole correlations, $F \sim r^2 Y_{2\mu}$, which are inspired by existence of low-lying 2^+ vibrational excitations in even-even nuclei. Another correlation is the pairing, $F \sim P + P^\dagger$ and $F \sim P - P^\dagger$ where P is the pair annihilation operator. This is important in heavy nuclei in which the nuclear superfluidity associated with the pair condensation is well established [21]. We also adopt this separable form as a residual interaction for the QRPA calculations in sections 5–7.

3. Finite-size effect

Nuclei on Earth are of finite size ($R < 10$ fm) with finite number of nucleons ($A < 300$). Strictly speaking, the SBS in the ground state is realized in the infinite system. For finite systems, the quantum fluctuation associated with the zero-point motion restores the broken symmetry. Thus, the symmetry-broken state is not stable for finite systems, in a rigorous sense. However, the SBS is ubiquitous in macroscopic objects in nature, which are made of big but *finite* number of particles. Thus, everybody agrees that the zero-point motion to restore the symmetry can be safely neglected in the macroscopic number, say $A \sim 10^{23}$. Then, how about the case of $A \sim 200$?

3.1. Finite correlation time

Let us consider a deformed nucleus and the single-particle states ϕ_i^0 in the deformed Nilsson potential. The deformed ground state is simply assumed to be a Slater determinant, $|\Phi_0\rangle \equiv \det\{\phi_1^0 \phi_2^0 \cdots \phi_A^0\}$. If we rotate the nucleus by angle θ, we have a state $|\Phi_\theta\rangle = \det\{\phi_1^\theta \phi_2^\theta \cdots \phi_A^\theta\}$. where $\phi_i^\theta = \hat{R}(\theta)\phi_i^0$ with the rotation operator $\hat{R}(\theta)$. Each single-particle state ϕ_i^θ in the tilted Nilsson potential can be expanded in terms of the untilted state ϕ_i^0, as $\phi_i^\theta = \sum_j^\infty c_{ij}^\theta \phi_j^0$. When the angle θ is small, we can estimate the diagonal coefficients as $|c_{ii}| \sim 1 - c|\theta|$ with $c > 0$, and the off-diagonal ones ($i \neq j$) as $|c_{ij}| \sim O(\theta)$. As far as the nucleon number A is finite, the tilted ground state $|\Phi_\theta\rangle$ can be written in terms of the untilted Nilsson basis, $\{\phi_i^0\}$. This is due to the fact that $|\Phi_0\rangle$ and $|\Phi_\theta\rangle$ belong to the same Hilbert space.

However, in the limit of $A \to \infty$, this is no longer true. The tilted ground state is expanded in terms of the untilted Slater determinants as

$$|\Phi_\theta\rangle = \det\{\phi_1^\theta \cdots \phi_A^\theta\} = \sum_{j_1,\cdots,j_A} C_{j_1\cdots j_A} \det\{\phi_{j_1}^0 \cdots \phi_{j_A}^0\}, \quad (8)$$

where $C_{j_1 j_2 \cdots j_A} = c_{1j_1} c_{2j_2} \cdots c_{Aj_A}$. For a small value of θ, the largest coefficient among $\{|C_{j_1\cdots j_A}|\}$ is apparently $|C_{1\cdots A}|$ whose absolute magnitude is $|C_{1\cdots A}| \sim (1 - c|\theta|)^A$. Therefore, all the coefficients $C_{j_1\cdots j_A}$ vanish exponentially as functions of A. This means that $|\Phi_0\rangle$ and $|\Phi_\theta\rangle$ belong to different Hilbert spaces at $A \to \infty$, thus, $|\Phi_\theta\rangle$ is no longer expandable in terms of the untilted Slater determinants. In other words, the deformed *infinite* nucleus never rotates.

The same issue can be examined in terms of the excitation spectra. The rotational spectra of deformed nuclei show $E_I = I(I+1)/2\mathcal{J}$, in which the moment of inertia $\mathcal{J}$ is approximately of order of $A^{5/3}$. The rotational motion is *quantized* due to the finiteness of $\mathcal{J}$. In the limit of $A \to \infty$, the excitation spectra becomes *gapless* and the ground state ($I = 0$) is degenerate with other states ($I \neq 0$). Therefore, an infinitesimally weak external field can fix its orientation by superposing states with different I.

Now, let us come back to the question, 'How about heavy deformed nuclei?'. As far as A is finite, the 'tilted' and 'untilted' Hilbert spaces are equivalent. The zero-point fluctuation may connect $|\Phi_0\rangle$ and $|\Phi_\theta\rangle$, thus, the wave packet $|\Phi_0\rangle$ loses its direction in finite correlation time. If this time scale is significantly larger than that of the single-particle motion $\tau_{\rm F} \sim 10^{-22}$ s, we can claim that the SBS takes place and the nucleus is deformed. In fact, this condition is well satisfied for heavy nuclei. Let us limit the orientation of the deformed nucleus to an angle range of unity ($\Delta\theta \sim 1$), then, the quantum fluctuation produces the angular momentum with the magnitude of $\Delta I \sim (\Delta\theta)^{-1} \sim 1$. This leads to the correlation time, $\tau_{\rm cor} \sim \mathcal{J}/\Delta I \sim \mathcal{J}$, that amounts to 10^{-19} s for typical deformed actinide nuclei. This argument is consistent with the vanishing behavior of the coefficients $C_{j_1\cdots j_A}$. Suppose the overlaps $|\langle\phi_i^0|\phi_i^\theta\rangle| \sim 0.9$ for $i = 1, \cdots, A$, then, we have $C_{12\cdots A} \sim (0.9)^A \sim 7 \times 10^{-10}$ for $A = 200$. Therefore, the rotational fluctuation is significantly hindered for heavy deformed nuclei. These simple exercises also tell us that, the concept of SBS has a greater significance for nuclei with larger A and larger deformation.

From a similar argument replacing the single-particle states ϕ_i^0 in the Slater determinant $\det\{\phi_{j_1}^0 \cdots \phi_{j_A}^0\}$ by those in a spherical potential, we may understand why the description based on the 'symmetry-broken' deformed basis is important. It is apparent that, if we adopt a spherical shell model basis for such heavy well-deformed nuclei, we need to treat very small coefficients, $C_{j_1\cdots j_A}$, with enormous number of basis states. In the limit of $A \to \infty$, this treatment becomes impossible. The impossibility here is in a strict sense, not in a practical sense due to computational limitation. Thus, instead of superposing the 'symmetry-preserving' (spherical) Slater determinants, the theories of restoring broken symmetry, such as the projection method, have been extensively developed in nuclear physics, to take into account effects of the zero-point fluctuation [22]. The usefulness of these symmetry restoration approaches has been recognized recently in other fields [23].

3.2. Zero-point motion and shell effect

As we have mentioned in section 3.1, the finiteness leads to the finite correlation time and the finite energy gap in the excitation spectra. In the symmetry restoration mechanism, the zero-point fluctuation associated with the ANG mode is a key element. In this subsection, we discuss effects of other zero-point motions in finite systems, which could hinder the SBS. The zero-point kinetic energy of nucleons is roughly given as $T_{\rm zpe}/A \sim 1/(mR^2) \sim 10$ MeV. This is comparable to the nuclear binding energy $B/A \sim 8$ MeV and has a non-negligible effect. In fact, since the nucleons are fermions, the Fermi energy is even larger, $t_{\rm F} \sim k_{\rm F}^2/(2m) \sim 40$ MeV. The zero-point (Fermi motion) kinetic energy generally favors the 'symmetry-preserving' state with a uniform and spherical density distribution. Since this competes with the SBS driving effect, the SBS which occurs in the thermodynamical limit may not occur in finite systems. The interplay between the zero-point motion and the interaction leads to interesting phenomena in nuclei.

The shell effect is a kind of finite-size effect in many fermion systems and is an indispensable factor in the low-energy nuclear structure. The prominent deformation hindrance effect can be found at the spherical magic numbers. The ground states of those magic nuclei favor spherical shape. Nevertheless, most of the spherical nuclei show the shape coexistence phenomena. For instance, the even-even spherical nuclei often have deformed excited 0^+ states at very low energy. It is prevalent in many semi-magic nuclei, and even true for some doubly magic nuclei. In contrast, as far as we know, when the ground state is deformed, excited 0^+ spherical states have not been clearly identified. In the Strutinsky shell correction method [22, 24], the shell effect is regarded as an origin of the nuclear deformation. It might be proper to say this in an opposite way; the heavy nuclei are 'genetically' deformed, and some special nuclei become spherical because of the finite-size (spherical shell) effect to hinder the SBS.

3.3. Shell structure and soft modes

When the symmetry breaking takes place and the nucleus is deformed, what kind of shape is realized? This depends on the underlying shell structure. Let us present a simple argument based on the one given by Bohr and Mottelson (pp 578–591 in BM2). For a spin-independent spherical potential, the single-particle energy is characterized by the radial quantum number n and the orbital angular momentum l, $\epsilon\,(n,\,l)$. When we change n and l from a certain value $(n_0,\,l_0)$

$$\epsilon\,(n,\,l) = \epsilon\,(n_0,\,l_0) + \Delta n\left(\frac{\partial\epsilon}{\partial n}\right)_0 + \Delta l\left(\frac{\partial\epsilon}{\partial l}\right)_0 + \cdots, \qquad (9)$$

where $\Delta n = n - n_0$ and $\Delta l = l - l_0$. Since n and l take only integer numbers, the ratio, $a{:}\,b \equiv (\partial\epsilon/\partial n)_0{:}\,(\partial\epsilon/\partial l)_0$ plays a very important role. If the ratio $a{:}b$ is rational, we can choose a and b as the integer numbers. Then, in the linear order (9), $\epsilon\,(n,\,l)$ and $\epsilon\,(n \pm mb,\,l \mp ma)$ are degenerate, where m is an integer number.

Now, let us define the shell frequency as

$$\omega_{\rm sh} \equiv \frac{1}{a}\left(\frac{\partial\epsilon}{\partial n}\right)_0 = \frac{1}{b}\left(\frac{\partial\epsilon}{\partial l}\right)_0. \qquad (10)$$

There are degenerate single-particle energies at intervals of $\omega_{\rm sh}$. Larger integers a and b correspond to a smaller $\omega_{\rm sh}$. Therefore, the prominent shell structure with a large shell gap $\omega_{\rm sh}$ should be associated with the small integers $(a,\,b)$. For instance, the isotropic harmonic oscillator potential has the $a{:}\,b = 2{:}1$ shell structure, with the constant $\omega_{\rm sh}$. The Coulomb potential has the strict $a{:}b = 1{:}1$, with the energy-dependent $\omega_{\rm sh}$. In general, the degeneracy is approximate and the ratio $a{:}\,b$ may change according to the location of the Fermi level.

The derivatives, $(\partial\epsilon/\partial n,\,\partial\epsilon/\partial l)$, correspond to the (angular) frequencies in the classical mechanics; $\partial\epsilon/\partial n$ is the frequency of the radial motion, while $\partial\epsilon/\partial l$ is that of the angular motion. The integer ratio $(a,\,b)$ of the frequencies means that the classical orbit is closed (periodic). Therefore, the quantum shell structure is closely related to the classical periodic orbits.

Since the nuclear potential somewhat resembles the harmonic oscillator potential, the shell structure associated with $a{:}b = 2{:}1$ is prominent. The 2:1 periodic orbit in the harmonic oscillator potential is the elliptical orbit. When there are many valence nucleons in the degenerate levels, the short-range attractive interaction favors their maximal overlap, which eventually leads to the SBS to an ellipsoidal (quadrupole) shape. In the quantum mechanical terminology, we may say that the coupling among the degenerate single-particle levels with $\Delta l = 2$ produces a soft mode. If the number of valence nucleons becomes large, this correlation may produce the quadrupole deformation.

The spin-orbit potential decreases the frequency $\partial\epsilon/\partial l$ for the single-particle levels of $j = l + 1/2$. This could lead to a new shell structure of $a{:}b = 3{:}1$ among the levels of the $j = l + 1/2$. The 3:1 frequency ratio corresponds to classical periodic orbits of the triangular shape, since the radial motion oscillates three times during the single circular motion. Thus, for heavy nuclei in which the high-j single-particle levels $(j = l + 1/2)$ are located near the Fermi level, the approximate degeneracy of the $\Delta l = 3$ levels may result in the octupole instability in open-shell configurations. For example, the neutron-deficient actinide nuclei show typical spectra of the alternating parity band, which are understood as a realization of the pear-shaped deformation of Y_{30} type [25].

The investigation of the classical periodic orbits is useful to identify a soft mode and a favorable shape. The SBS toward the quadrupole deformation in open-shell nuclei is nicely explained in this simple argument. However, it is more difficult to explain the fact that most nuclei have the prolate shape, not the oblate shape. There have been a number of works on this issue [26–29]. According to the classical periodic orbits, a recent analysis sheds new light on the prolate dominance in nuclei [30].

3.4. Fermi motion and nuclear self-consistency

In nuclei, the kinetic energy of nucleons' Fermi motion is very large. Adopting the harmonic oscillator potential model, a simple estimate of the total kinetic energy is given by

$$T_0 = \frac{1}{2}E_{\rm HO} = \frac{1}{2}\sum_{k=x,y,z}\omega_k\Sigma_k, \qquad \Sigma_k \equiv \sum_{i=1}^{A}\left(n_k + \frac{1}{2}\right)_i, \tag{11}$$

where n_k ($k = x, y, z$) are the oscillator quantum numbers of the single-particle states. For a spherical nucleus ($\omega_x = \omega_y = \omega_z = \omega_0$) filling the levels up to $n_x + n_y + n_z = N_{\rm max}$, this amounts to

$$T_0 = (1/4)\omega_0(N_{\rm max}+1)(N_{\rm max}+2)^2(N_{\rm max}+3). \tag{12}$$

Taking $Z = N = 40$ (^{80}Zr, $N_{\rm max} = 3$), this gives $T_0 = 150\omega_0 \sim 1.43$ GeV, with a standard value of $\omega_0 \approx 41\,A^{-1/3} \sim 9.5$ MeV. If we deform the harmonic oscillator to a prolate/oblate shape with $(\omega_x, \omega_y, \omega_z) = (e^{\eta}, e^{\eta}, e^{-2\eta})\omega_0$, the kinetic energy becomes

$$T(\alpha) = \frac{2e^{\eta} + e^{-2\eta}}{3}T_0, \tag{13}$$

which has the minimum value at the spherical shape $\eta = 0$. According to equation (13), a moderate prolate deformation of $e^{\eta} = 1.1$ will produce the increase in the kinetic energy by about 1%. However, since T_0 is very large, this 1% increase is significant, such as 14 MeV for $Z = N = 40$. However, the deformed ground state in ^{80}Zr is suggested by experiments observing a ground-state rotational band [31]. How does the nucleus compensate this large increase in kinetic energy?

The solution to this problem is again attributed to the nuclear self-consistency. In the harmonic oscillator model, the self-consistency condition, that the deformation of the potential is equal to that of the density distribution, can be simply expressed by equation (4-115) in BM2

$$\omega_x\Sigma_x = \omega_y\Sigma_y = \omega_z\Sigma_z. \tag{14}$$

Namely, when the nuclear potential is deformed as $(\omega_x, \omega_y, \omega_z) = (e^{\eta}, e^{\eta}, e^{-2\eta})\omega_0$, the configuration of the ground state should change accordingly, $(\Sigma_x, \Sigma_y, \Sigma_z) = (e^{-\eta}, e^{-\eta}, e^{2\eta})\Sigma_0$. Since the momentum distribution in the harmonic oscillator potential model can be calculated as $\langle p_k^2\rangle = m\omega_k\Sigma_k$ ($k = x, y, z$), the self-consistency condition (14) means the isotropic momentum (velocity) distribution (no deformation in the Fermi sphere). In other words, the shape of the nucleus is specified by the minimization of the kinetic energy which is equal to the isotropic velocity distribution.

This indicates the importance of configuration rearrangements in low-energy collective dynamics. When the nuclear deformation is changed as $(\omega_x, \omega_y, \omega_z) \to (e^{\eta}\omega_x, e^{\eta'}\omega_y, e^{-\eta-\eta'}\omega_z)$, the configuration should follow as $(e^{-\eta}\Sigma_x, e^{-\eta'}\Sigma_y, e^{\eta+\eta'}\Sigma_z)$, to keep the Fermi sphere spherical. In order to change the configuration, we need two-particle-two-hole excitations, to annihilate a time-reversal pair of nucleons in a certain single-particle orbit and create a pair in another orbit. Therefore, we expect that, during the shape evolution at low energy, the pairing interaction plays a dominant role in dynamical change of the configuration. This was supported by experimental data that the spontaneous fission life times of even-even nuclei are much shorter than those of odd and odd-odd nuclei [32].

According to the nuclear self-consistency, each configuration has its optimal shape. We may think about possibilities of realizing different shapes corresponding to different configurations in the same nucleus. This phenomenon is called 'shape coexistence'. For instance, in the harmonic oscillator model of ^{80}Zr with $N = Z = 40$, in addition to the spherical configuration ($\Sigma_x = \Sigma_y = \Sigma_z$, $\omega_x = \omega_y = \omega_z$), the self-consistency condition (14) is also satisfied with the SD configuration ($2\Sigma_x = 2\Sigma_y = \Sigma_z$, $\omega_x = \omega_y = 2\omega_z$). In fact, the shape coexistence phenomena have been observed in many areas throughout the nuclear chart [33].

3.5. Fermi sphere in the rotating frame

This idea of the isotropic velocity distribution can be extended into the one in the rotating frame (p 79 in BM2). The local velocity in the rotating frame

$$\vec{v} \equiv \vec{p}/m - (\vec{\omega}_{\rm rot} \times \vec{r}), \tag{15}$$

has an isotropic distribution $\rho_{\vec{r}}(v)$ at each $\vec{r}$. The isotropic velocity distribution means no net current relative to the rotating frame, which ends up with a rigid-body value for the moment of inertia. The deformed nucleus would have a rigid-body value of moment of inertia if the pairing correlations and the shell effects were absent.

The transformation from the laboratory frame to the rotating frame leads to the cranking Hamiltonian

$$H' = H - \vec{\omega}_{\rm rot}\cdot\vec{J}, \tag{16}$$

where $\vec{J}$ is the total angular momentum. The velocity-dependent terms (kinetic energy and the centrifugal potential) in the rotating frame can be written as $p^2/(2m) - \vec{\omega}_{\rm rot}\cdot(\vec{r}\times\vec{p}) = mv^2/2 - m(\vec{\omega}_{\rm rot}\times\vec{r})^2/2$ where $\vec{v}$ is given by equation (15). This confirms the $\vec{v}$-dependence in H' is isotropic ($\propto v^2$). This isotropic velocity distribution is still valid in rotating nuclei [34]. The cranking model (16) plays a key role in physics of high-spin nuclear structure (sections 5–7).

4. SBS and collective motions

A broken continuous symmetry leads to the emergence of two types of collective excitations. One is the massless ANG mode and the other is the massive Higgs mode [35]. Therefore, properties of the collective motions significantly change before and after the SBS takes place. In nuclei, we can observe them in the excitation spectra. We can even see how the ANG and Higgs modes appear and evolve from soft modes.

4.1. Rotational motion; ANG mode

The ANG mode is a gapless (massless) mode in the infinite system. For the case of nuclear deformation, the ANG mode

corresponds to the rotational motion of the deformed nucleus. Because of the finiteness, the spectrum is not exactly gapless, however, shows a gradual emergence of the 'quasi-degenerate' rotational spectra.

In figure 6-31 of BM2, a typical example for even-even Sm isotopes ($^{144-154}$Sm) is presented. The ^{144}Sm nucleus has the magic neutron number $N = 82$. Its ground state (0^+) is spherical and the first excited state is located at excitation energy of 1.63 MeV. Keeping the proton number the same and increasing the neutron number two by two, we clearly observe the following:

(i) The first 2^+, 4^+, $\cdots$ states lower their excitation energies. Eventually, a rotational band is formed to present the excitation spectra, $E_I \propto I(I+1)$.
(ii) The second 0^+ and the second 2^+ states lower their energies in the beginning. However, they stop decreasing at $N = 88$ (^{150}Sm).
(iii) Additional rotational bands are formed on top of the second 0^+ and 2^+ states for $N \geqslant 90$ (^{152,154}Sm).

In ^{154}Sm, the excitation energy of the first 2^+ state is only 82 keV. This is $1/20$ of that in ^{144}Sm and we may say that it is approximately degenerate with the ground state. Moreover, there appear five members ($0^+, \cdots, 8^+$) of rotational bands below 1 MeV of excitation. It should be noted that similar phenomena are observed in many regions of nuclear chart, when the neutron (proton) numbers are going away from the spherical magic number.

A regular pattern of rotational spectra allows us to distinguish the intrinsic excitations and the rotational motion. A rotational band is constructed based on each intrinsic excitation from the ground state. From these observation, we may think of the Hamiltonian subtracting the rotational energy, $H' \equiv H - \vec{J}^2/(2\mathcal{J})$. H' conserves the rotational symmetry, however, the member of the rotational bands (0^+, 2^+, ...) will be degenerate in energy. Then, a deformed wave-packet state which violates the rotational symmetry could become an eigenstate of the Hamiltonian H'.

The number of activated rotational degrees of freedom depends on the nuclear shape. For axially symmetric spheroidal shape, there is no collective rotation around the symmetry axis. In other words, the angular momentum component along the symmetry axis (called K quantum number in the following) is purely determined by the intrinsic motion. In this case, the two rotational axes perpendicular to the symmetry (z) axis are possible, but they are equivalent in the sense that they have equal moment of inertia, $\mathcal{J}_x = \mathcal{J}_y$. In contrast, if the nucleus has an equilibrium shape away from the axial symmetry (triaxial shape), the collective rotations about three axes are all activated, and they can have different moments of inertia, $\mathcal{J}_x$, $\mathcal{J}_y$, and $\mathcal{J}_z$. We may expect that the rotational spectra become richer and more complex. The wobbling motion is known to be a typical mode of excitation in the triaxial nuclei, that will be discussed in section 7.

4.2. Beta and gamma vibrations; amplitude (Higgs) mode

The quadrupole ($\lambda = 2$) vibrations produce 2^+ excitations in spherical nuclei. When the SBS takes place to produce the prolate (spheroidal) ground state, among five $\alpha_{2\mu}$ ($\mu = -2, \cdots, 2$), the two shape degrees (β and γ) remain, and rest of the degrees of freedom are absorbed in the rotational motion (Euler angle Θ). For an axially symmetric ground state, the normal modes can be classified by the vibrational angular momentum along the symmetry axis, which is often denoted by the quantum number K. The β and γ vibrations correspond to $K^\pi = 0^+$ and 2^+, respectively. Note that the $K^\pi = 1^+$ low-lying vibration does not exist, because it corresponds to the rotation of the whole nucleus.

The β vibration around the SBS minimum is associated with a collective amplitude mode of order parameter with a finite energy gap, in contrast to the 'gapless' rotational motion. This type of excitation is often referred to as the amplitude (Higgs) mode' [35]. A number of those candidates have been observed in well-known deformed regions, such as the rare-earth and actinide regions. For instance, in the rare-earth region, the excitation energies of β vibration candidates are found at $E_x \approx 1$ MeV. However, their $B(E2)$ values from the ground states to the 2^+ states in the β-vibrational bands are not large in most cases, typically a few Weisskopf units (W.u.). Instead, strong population by the pair transfer reaction has been observed in many β-vibration candidates. Therefore, their true nature is still mysterious and currently under debate [36]. We should note that an important role of the Coriolis coupling in the β vibrations has recently been pointed out [37]. See also figure 2 in section 5.1.

In contrast, the γ vibrations, whose excitation energies are also around 1 MeV, show $B(E2)$ values significantly larger than the Weisskopf units. Thus, the collective nature of the γ vibration is well established. Effects of their coupling to the rotational motion have been also studied within the generalized intensity relation (section 5.1.2).

For nuclei with the prolate shape, a naive geometric consideration may predict that the vibrational frequency along the symmetry axis ($K = 0$) is lower than that of the $K \neq 0$. This is true for high-frequency giant quadrupole resonance [38]. However, the low-lying β and γ vibrations do not follow this simple expectation (section 6-3b in BM2). They are much more sensitive to underlying shell structure.

4.3. Octupole vibrations; negative-parity modes

Octupole vibrations ($\lambda = 3$) with negative parity have been systematically observed in spherical and deformed nuclei. In spherical nuclei, it produces 3^- state. The most typical example is perhaps that in ^{208}Pb. It is split into four different normal modes with $K^\pi = 0^- \sim 3^-$ in deformed nuclei. Again, the geometric expectation for their ordering is not applicable to low-frequency octupole vibrations; namely, the $K^\pi = 0^-$ vibrational state is not necessarily the lowest among the multiplet. The rotational band is formed on top of the bandhead with the spin $I = K$ for $K = 1 \sim 3$ and $I = 1$ for $K = 0$.

4.4. A microscopic tool; QRPA

In normal degenerate Fermi systems, the most basic mode of excitation at low energy corresponds to the one-particle-one-hole (1p1h) excitations. When the pairing correlations produce the pair-condensed (BCS-like) ground state, the 1p1h excitations should be replaced by the two-quasiparticle (2qp) excitations. The quasiparticle, which is a mixture of particle and hole states, is usually defined as an eigenstate of the Hartree–Fock–Bogoliubov (HFB) equation [22, 39]. The ground state corresponds to the quasiparticle vacuum state. The 2qp excitations include not only 1p1h states, but also two-particle and two-hole states which correspond to states in neighboring nuclei with $A \pm 2$. The odd-A nuclei are expressed by one-quasiparticle states based on the quasiparticle vacuum.

The collective excitations, such as β, γ, and octupole vibrations in sections 4.2 and 4.3, are approximately given by superposition of many 2qp excitations. The most successful theory for this purpose is the QRPA [22, 39], which can describe both collective and non-collective modes of excitation. The QRPA contains backward amplitudes corresponding to 2qp annihilation on the correlated ground state, and respects the symmetry of the Hamiltonian [22, 39]. The limitation of QRPA is associated with its small-amplitude nature.

The HFB equations with the cranking Hamiltonian H' (16) is often utilized for studies of high-spin nuclear structure. The QRPA calculation with the cranking Hamiltonian H' is able to describe the rotational coupling effects, such as the alignment and stretching, on the collective and the non-collective excitations. Some examples of the QRPA calculations with H' are presented in the following sections 5–7.

5. Coriolis coupling to intrinsic motions

The SBS of the translational symmetry produces the ANG mode of the center-of-mass motion. Since it is exactly decoupled, the intrinsic motions are not affected by the speed of the nucleus in the accelerator. On the other hand, the rotational motion is not exactly decoupled, thus, the Coriolis and centrifugal effects influence intrinsic structure.

In the unified model, as is mentioned in section 4.2, the five quadrupole variables $\alpha_{2\mu}$ ($\mu = -2, \cdots, 2$) are represented by (β, γ) and three Euler angles Θ. Accordingly, the total wave function is given by a product of the intrinsic, the vibrational, and the rotational parts. If the shape fluctuation is neglected, one can write the total wave function as a product of the rotor and the intrinsic parts. When the nucleus has the axially symmetric shape, the intrinsic state has a good K-quantum number, $|K_n\rangle$. The total wave function is given by

$$|\Psi_{K_nIM}\rangle = |K_nIM\rangle \otimes |K_n\rangle, \tag{17}$$

where the rotor wave function is given by

$$\langle\Theta|KIM\rangle = \left(\frac{2I+1}{8\pi^2}\right)^{1/2} \mathcal{D}^I_{MK}(\Theta). \tag{18}$$

The additional $\mathcal{R}$ invariance requires the symmetrization of equation (17) for $K_n \neq 0$; $\{|\Psi_{K_nIM}\rangle + (-1)^{I+K}|\Psi_{\bar{K}_nIM}\rangle\}/\sqrt{2}$. The quantum nature of the angular momentum is properly treated in this rotor wave function. The Coriolis coupling, which mixes states with different K quantum numbers, can be treated in a perturbative manner. Chapter 4 of BM2 presents extensive discussion on this subject.

On the other hand, in the high-spin limit $I \to \infty$, the semiclassical approximation works well. The rotational frequency vector $\vec{\omega}_{\rm rot}$ is introduced, which leads to the cranking model (16). Especially, when the direction of $\vec{\omega}_{\rm rot}$ is parallel to a body-fixed principal axis (PA) x, we have a uniform rotation $\omega_{\rm rot}(t) = $ const., then, equation (16) reduces to

$$H' = H - \omega_{\rm rot} J_x. \tag{19}$$

This one-dimensional cranking model has been extensively applied to high-spin nuclear structure problems with a tremendous success. The nonlinear effects of rotation are automatically taken into account in the intrinsic structure, which reproduces a number of striking high-spin phenomena, such as back-bending, alignment, and band termination. A drawback is the missing quantum nature of rotation, particularly important at low spin.

5.1. Quantization of the cranking model at low spin

In the semiclassical approximation, the direction of $\vec{\omega}_{\rm rot}$ ($\vec{I}$) is assumed to be the x axis of both the intrinsic (body-fixed) and the laboratory (space-fixed) frames. The multipole operator $\tilde{Q}_{\lambda\mu}$, in which μ is defined with respect to the x axis, changes the angular momentum I to $I + \mu$. Thus, a transition matrix element between states with the angular momenta I_i and I_f is simply given by $\langle f|\tilde{Q}_{\lambda\mu}|i\rangle$, where μ should be equal to $\Delta I = I_f - I_i$. This is a good approximation at the high-spin limit (I, $\omega_{\rm rot} \to \infty$).

In contrast, at the low-spin limit ($I \sim 0$), the angular momentum is coupled to the deformation, thus, the K quantum number along the symmetry (z) axis is a good quantum number. In this limit, the multipole operator $Q_{\lambda\nu}$, defined with respect to the z axis, changes the K quantum number by $\nu = \Delta K = K_f - K_i$. In addition, the quantum mechanical nature of rotation is important at low spin. A perturbative expansion with respect to I in the unified model produces a specific I-dependence for the transition matrix element (*generalized intensity relations* in BM2). To complete the intensity relation beyond the leading order (LO), we need to determine matrix elements of intrinsic operators which take into account the Coriolis and centrifugal effects. There is no systematic method to calculate these intrinsic matrix elements in the unified model.

The cranking model (19), on the other hand, is capable of microscopic treatment of the rotational coupling to the intrinsic structure. However, the semiclassical nature of the cranking model forbids us to obtain the correct I-dependent intensity relations at low spin. This is mostly due to missing kinematics of the angular momentum algebra. We present here a feasible prescription to recover the quantum

mechanical effect, that enables us to calculate matrix elements of the intrinsic moments in the generalized intensity relations.

5.1.1. Generalized intensity relations. The main idea is as follows [40]. In the high-spin limit, the cranking treatment becomes accurate and the matrix elements of a multipole operator $Q^{(\mathrm{lab})}_{\lambda\mu}$ between the highest-weight states are given by a relation [41, 42]

$$\langle I_f I_f|Q^{(\mathrm{lab})}_{\lambda\Delta I}|I_i I_i\rangle = (I_f|\tilde{Q}_{\lambda\Delta I}|I_i), \tag{20}$$

where the state $|I)$ is a symmetry-broken state; for instance, a mean-field solution of the cranking Hamiltonian (19) with the constraint $(I|J_x|I) = I$. $\tilde{Q}_{\lambda\Delta I}$ can be expanded in terms of those defined with respect to intrinsic z axis, and the coefficients are given by the d functions

$$\tilde{Q}_{\lambda\mu} = \sum_\nu \mathcal{D}^\lambda_{\mu\nu}\left(-\frac{\pi}{2}, -\frac{\pi}{2}, 0\right)Q_{\lambda\nu} = \mathrm{i}^{-\mu}\sum_\nu d^\lambda_{\mu\nu}\left(-\frac{\pi}{2}\right)Q_{\lambda\nu}. \tag{21}$$

Now, let us propose a heuristic quantization. Although the equality in equation (20) holds only at high spin, we take the opposite low-spin limit (I, $\omega_{\mathrm{rot}} \to 0$), in which the state $|I)$ becomes a 'non-cranked' K-good intrinsic state $|K)$. Substituting equation (21) into (20), we have

$$\langle I_f I_f|Q^{(\mathrm{lab})}_{\lambda\Delta I}|I_i I_i\rangle_{\mathrm{LO}} \leftrightarrow (K_f|\tilde{Q}_{\lambda\Delta I}|K_i) = \mathrm{i}^{-\Delta I} d^\lambda_{\Delta I\Delta K}(K_f|Q_{\lambda\Delta K}|K_i). \tag{22}$$

Here, we use the symbol $\leftrightarrow$ instead of $=$, because it is obtained by applying the high-spin formula (20) to the low-spin limit. For simplicity, we omit the argument $(-\pi/2)$ of the d function. The suffix 'LO' indicates the relation in the zeroth order $O(\omega^0_{\mathrm{rot}})$, with respect to ω_{rot}.

Equation (22) is, of course, not directly applicable to low spin. However, it has a proper correspondence to the LO intensity relation in the unified model

$$\langle I_f I_f|Q^{(\mathrm{lab})}_{\lambda\Delta I}|I_i I_i\rangle_{\mathrm{LO}} = \langle K_f I_f I_f|\mathcal{D}^\lambda_{\Delta I\Delta K}|K_i I_i I_i\rangle (K_f|Q_{\lambda\Delta K}|K_i), \tag{23}$$

which is obtained using the K-good wave function (17) and the LO transformation of the multipole operator, $Q^{(\mathrm{lab})}_{\lambda\mu} = \sum_\nu \mathcal{D}^\lambda_{\mu\nu}Q_{\lambda\nu}$. Comparing equations (22) and (23), we may think of a quantization prescription

$$d^\lambda_{\Delta I\Delta K} \;\to\; \langle K_f I_f I_f|\mathcal{D}^\lambda_{\Delta I\Delta K}|K_i I_i I_i\rangle. \tag{24}$$

Then, the 'non-cranked' limit of the cranking formula reproduces the LO intensity relation in the unified model. This quantization procedure is supported by the fact that the quantities in both sides of equation (24) become identical to the Clebsch–Gordan (CG) coefficients, $\langle I_i K_i \lambda\Delta K|I_f K_f\rangle$, at the high-spin limit ($I \to \infty$). Decreasing I, the left-hand side of equation (24) is losing its validity because of its classical nature, while the right-hand side stays valid keeping its quantum nature.

The present quantization of the cranking model is applicable to higher-order Coriolis coupling terms. These terms are not easily provided in the unified model. The next leading order (NLO) is given by the first order in ω_{rot}, which produces non-zero contributions of $Q_{\lambda\nu=\Delta K\pm1}$. The NLO terms to equation (22) are given as

$$\langle I_f I_f|Q^{(\mathrm{lab})}_{\lambda\Delta I}|I_i I_i\rangle_{\mathrm{NLO}} \leftrightarrow \mathrm{i}^{-\Delta I}\omega_{\mathrm{rot}}\left(d^\lambda_{\Delta I\ \Delta K+1}\frac{\mathrm{d}(K_f|Q_{\lambda\ \Delta K+1}|K_i)}{\mathrm{d}\omega_{\mathrm{rot}}} + d^\lambda_{\Delta I\ \Delta K-1}\frac{\mathrm{d}(K_f|Q_{\lambda\ \Delta K-1}|K_i)}{\mathrm{d}\omega_{\mathrm{rot}}}\right), \tag{25}$$

where the derivatives are evaluated at $\omega_{\mathrm{rot}} = 0$. A prescription of the NLO quantization is given by

$$\omega_{\mathrm{rot}} d^\lambda_{\Delta I\ \Delta K\pm1} \quad\to\quad \langle K_f I_f I_f|\frac{1}{2\mathcal{J}}\{I_\pm, \mathcal{D}^\lambda_{\Delta I\ \Delta K\pm1}\}|K_i I_i I_i\rangle, \tag{26}$$

where $\{A, B\} = AB + BA$ and $I_\pm \equiv \mp(I_x \pm \mathrm{i}I_y)/\sqrt{2}$ in the intrinsic frame. $\mathcal{J}$ is the moment of inertia of the rotational band, which can be also calculated in the cranking model at $\omega_{\mathrm{rot}} \to 0$: $\mathcal{J} = (1/2)(\mathrm{d}(K_i|J_x|K_i)/\mathrm{d}\omega_{\mathrm{rot}} + \mathrm{d}(K_f|J_x|K_f)/\mathrm{d}\omega_{\mathrm{rot}}) \approx \mathrm{d}(K_i|J_x|K_i)/\mathrm{d}\omega_{\mathrm{rot}} \approx \mathrm{d}(K_f|J_x|K_f)/\mathrm{d}\omega_{\mathrm{rot}}$. Again, in the high-spin limit, the left and right-hand sides of equation (26) become identical, if we assume $\omega_{\mathrm{rot}} \approx I_i/\mathcal{J} \approx I_f/\mathcal{J}$.

In summary, the generalized intensity relation up to the NLO is obtained by calculating the matrix element $\langle I_f I_f|Q^{(\mathrm{lab})}_{\lambda\Delta I}|I_i I_i\rangle = \langle K_f I_f I_f|Q^{(\mathrm{LO+NLO})}_{\lambda\Delta I}|K_i I_i I_i\rangle$, using the operator

$$Q^{(\mathrm{LO+NLO})}_{\lambda\Delta I} = m^{(0)}_{\lambda\ \Delta K}\mathcal{D}^\lambda_{\Delta I\Delta K} + \frac{m^{(+1)}_{\lambda\ \Delta K+1}}{2} \times \{I_+, \mathcal{D}^\lambda_{\Delta I\ \Delta K+1}\} + \frac{m^{(-1)}_{\lambda\ \Delta K-1}}{2}\{I_-, \mathcal{D}^\lambda_{\Delta I\ \Delta K-1}\}, \tag{27}$$

where the intrinsic matrix elements are given by

$$m^{(0)}_{\lambda\ \Delta K} = (K_f|Q_{\lambda\Delta K}|K_i), \tag{28a}$$

$$m^{(\pm1)}_{\lambda\ \Delta K\pm1} = \frac{1}{\mathcal{J}}\frac{\mathrm{d}(K_f|Q_{\lambda\ \Delta K\pm1}|K_i)}{\mathrm{d}\omega_{\mathrm{rot}}}. \tag{28b}$$

The right-hand sides of these equations can be calculated with the cranking model (19) in the vicinity of $\omega_{\mathrm{rot}} \to 0$. Note that the $\mathcal{R}$-conjugate terms should be added in the right-hand side of equation (27) when the $\mathcal{R}$ invariance is present [40].

5.1.2. Applications. The cranking model (19) has been applied to calculation of the intrinsic moments in equation (28). For low-lying quadrupole vibrational excitations, we use the QRPA to calculate the intrinsic matrix elements. For even-even nuclei, the ground state is $|0) = |K = 0)$ and the vibrational state is given by the QRPA normal-mode creation operator $\hat{X}^\dagger_K$ as $|K) = \hat{X}^\dagger_K|0)$. The QRPA calculation is based on the cranked-Nilsson-BCS model with a residual multipole interaction of a separable form similar to equation (7). We reported these results for quadrupole and octupole vibrations in the even-even rare-earth nuclei in [40] in which the details of the model can be found.

In the left panel of figure 1, we present an example of the Mikhailov plot for the γ vibrations in ^{166}Er. The LO+NLO electric quadrupole operator in a form of equation (27) leads

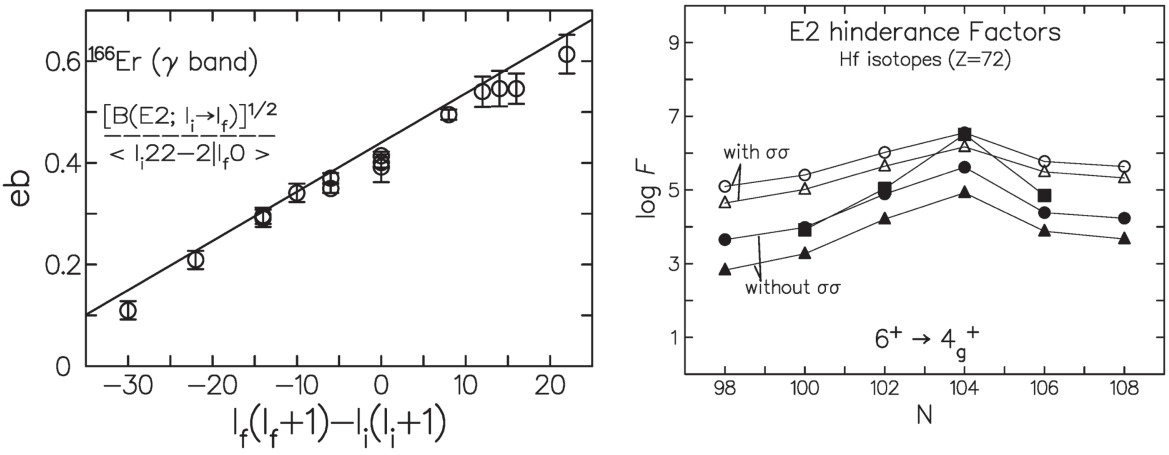

Figure 1. (Left) $E2$ transition amplitudes for the γ vibrational band in ^{166}Er. The experimental data are taken from figure 4-30 in BM2. Adapted with permission from [43]. Copyright IOP Publishing 1999. (Right) Hindrance factors of $B(E2; 6^+_{K=6} \to 4^+)$ for decay of $K^\pi = 6^+$ isomers in Hf isotopes. Calculated values are shown by circles, while the squares are the experimental data. See text for details. Adapted with permission from [43]. Copyright IOP Publishing 1999.

to the intensity relation between the $K_i = 2$ (γ) band and the $K_f = 0$ (ground) band

$$\frac{\langle I_f K_f^\pi = 0_g^+ || M(E2) || I_i K_i^\pi = 2_\gamma^+ \rangle}{\sqrt{2I_i + 1}\,\langle I_i 22 - 2 | I_f 0 \rangle} = Q_t \Big[1 + q \{ I_f(I_f + 1) - I_i(I_i + 1) \} \Big], \tag{29}$$

where Q_t and q are obtained from the intrinsic moments (28), though some modification is necessary because of the $\mathcal{R}$ invariance. See [40] for their exact formulae.

A very similar figure is shown in figure 4-30 of BM2, however, we note here that the parameters (Q_t, q) in the left panel of figure 1 is based on the microscopic calculation, while those in BM2 are determined by fitting the experimental data. The LO relation produces the same Q_t but $q = 0$. The Coriolis coupling effect in the NLO is represented by the parameter q ($m_{2\mp1}^{(\pm1)}$). For the γ vibrations, the cranking calculation always produces $q > 0$ in the rare-earth nuclei [40], which suggests the transitions $I_\gamma \to I_g$ are enhanced (hindered) for $I_g > I_\gamma$ ($I_g < I_\gamma$). This is consistent with experimental data (see [40] and references therein). We also obtain a reasonable agreement for the $M1$ transitions. However, the calculated sign of the $M1/E2$ mixing amplitudes changes from nucleus to nucleus, while the observed values are always negative [40].

The collectivity of the β vibrations measured by the strengths of the interband transitions to/from the ground band is weaker than that of the γ vibrations in most cases. However, in rare-earth nuclei in (near) the transitional region, the β vibrations produce very low excitation energies and large $B(E2; 0^+_\beta \to 2^+_g)$ values. In Gd isotopes, for example, their excitation energies are 681 and 615 keV for ^{154}Gd ($N = 90$) and ^{152}Gd ($N = 88$), respectively. The $B(E2; 0^+_\beta \to 2^+_g)$ values amount to 52 ± 8 and 178^{+53}_{-33} W.u. [44, 45]. We expect similar values of $B(E2; 0^+_g \to 2^+_\beta)$, which are predicted to be identical to $B(E2; 0^+_\beta \to 2^+_g)$ in the LO relation. Surprisingly, the observed $B(E2; 0^+_g \to 2^+_\beta)$ values are much smaller than $B(E2; 0^+_\beta \to 2^+_g)$ [36, 44, 45].

Figure 2 shows the calculated $B(E2)$ values using the the LO+NLO intensity relation identical to equation (29) with some trivial changes in the left-hand side ($K_i^\pi = 2_\gamma^+ \to K_i^\pi = 0_\beta^+$, $\langle I_i 22 - 2 | I_f 0 \rangle \to \langle I_i 020 | I_f 0 \rangle$). The LO relation cannot account at all for both large $B(E2; 0^+_\beta \to 2^+_g)$ and small $B(E2; 0^+_g \to 2^+_\beta)$ values. Owing to relatively small moments of inertia ($\mathcal{J}$) for these transitional nuclei, the inclusion of the NLO terms with large values of q nicely reproduces both of them. In BM2 (pp 168–175), the band mixing between the ground and the β bands in ^{174}Hf are presented to explain the observed intensity relations. An effect of hindrance of the shape fluctuation induced by the rotation, suggested in [49–51], may also play an important role. The Coriolis coupling effects may be a key ingredient to understand the peculiar $B(E2)$ properties of the β-vibrational bands.

Generally speaking, the Coriolis-coupling effect for the quadrupole vibrations is relatively weak, because the low-lying $K^\pi = 1^+$ collective state is missing (section 4.2). In contrast, all the members of the multiplet are present for the negative-parity octupole vibrations. Thus, we expect stronger Coriolis effects. The cranking calculation actually predicts the NLO parameters of the octupole vibrations ($|q| \sim 0.1$) larger than those of γ vibrations ($|q| \sim 0.01$) [40]. The K quantum number of the lowest mode of excitation among the octupole multiplet ($K^\pi = 0^- \sim 3^-$) changes from nucleus to nucleus. Nevertheless, the lowest mode always has $q < 0$ for transitions from the octupole band (K_i) to the ground band ($K_f = 0$), Thus, $B(E3; 3^- \to 0^+)$ is enhanced for the lowest mode. This Coriolis effect is clearly seen in Gd isotopes in figure 3.

Another application is presented here for K-forbidden transitions in decays of the high-K isomers. For K-forbidden transitions with $|\Delta K| > \lambda$, we should extend the LO+NLO relation of equation (27) because the LO term vanishes. The

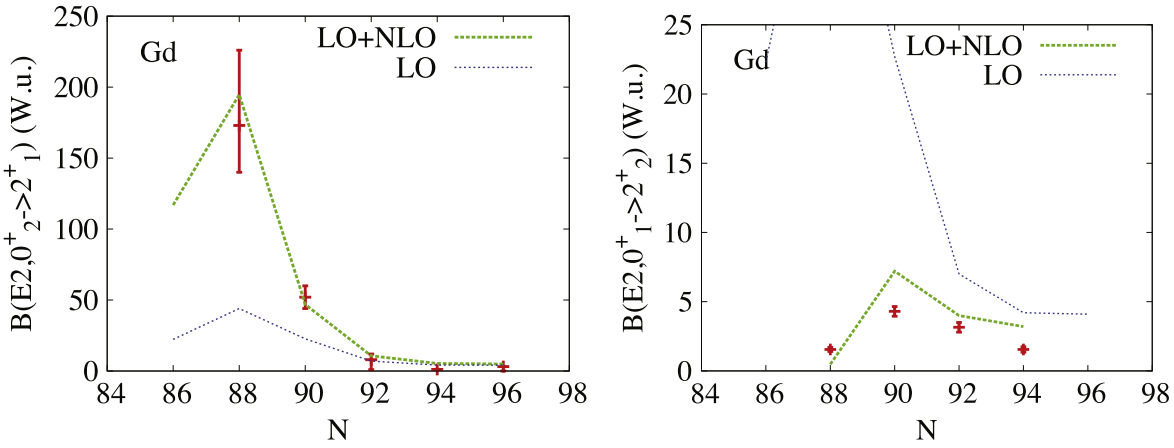

Figure 2. (Left) Calculated and experimental $B(E2; 0^+_\beta \to 2^+_g)$ values in Gd isotopes. Adapted with permission from [37]. Copyright Oxford University Press 2016. (Right) $B(E2; 0^+_g \to 2^+_\beta)$ values in Gd isotopes. Experimental data are taken from [36, 44–48]. Note that the scale of the ordinate is 1/10 of that in the left panel.

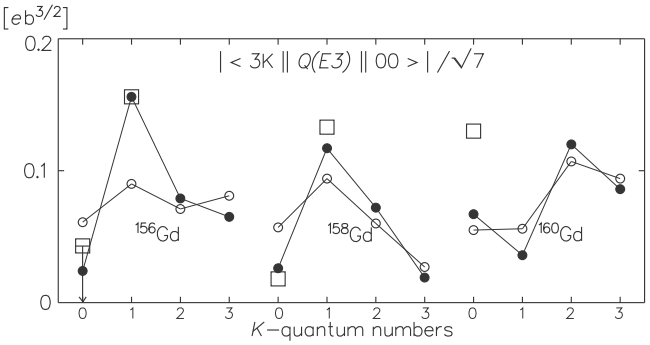

Figure 3. $E3$ transition amplitudes for the octupole vibrational states in Gd isotopes, $I^\pi_i = 3^- \to I^\pi_f = 0^+$. Open and filled circles correspond to calculated values in the LO and LO+NLO, respectively, compared with experimental data (open squares) [52]. The lowest mode of excitation among the octupole multiplet is $K = 1$ for ^{156,158}Gd and $K = 2$ for ^{160}Gd. Reproduced with permission from [53]. Copyright Elsevier 1997.

order of K forbiddenness is defined by $n = |\Delta K| - \lambda$. The N^nLO+N^{n+1}LO intensity relation for $\Delta K > 0$ is given by [40]

$$Q^{(N^n+N^{n+1}\mathrm{LO})}_{\lambda\Delta I} = m^{(-n)}_{\lambda\ \lambda}\mathcal{D}^{\lambda}_{\Delta I\lambda}(I_-)^n + \frac{m^{(-n-1)}_{\lambda\ \lambda-1}}{2} \times \{(I_-)^{n+1}, \mathcal{D}^{\lambda}_{\Delta I\ \lambda-1}\} + \mathcal{R}\text{-conj.}, \quad (30)$$

where the intrinsic moments are

$$m^{(\mp n)}_{\lambda\ \pm\lambda} = \frac{1}{n!\mathcal{J}^n}\frac{\mathrm{d}^n(K_f|Q_{\lambda\ \pm\lambda}|K_i)}{\mathrm{d}\omega^n_{\mathrm{rot}}}, \quad (31a)$$

$$m^{(\mp(n+1))}_{\lambda\ \pm(\lambda-1)} = \frac{1}{(n+1)!\mathcal{J}^{n+1}}\frac{\mathrm{d}^{n+1}(K_f|Q_{\lambda\ \pm(\lambda-1)}|K_i)}{\mathrm{d}\omega^{n+1}_{\mathrm{rot}}}. \quad (31b)$$

These formulae are applied to the 2qp $K^\pi = 6^+$ isomers in Hf isotopes. The configuration of the initial state $|K_i = 6)$ is assumed to be the proton 2qp [402 5/2] ⊗ [404 7/2]. The hindrance factors are shown in the right panel of figure 1. This is defined by

$$F \equiv \frac{B(E2; 6^+ \to 4^+)_{\mathrm{W}}}{B(E2; 6^+_{K=6} \to 4^+_g)}, \quad (32)$$

where $B(E2)_{\mathrm{W}}$ is the Weisskopf estimate of the reduced transition probability. A large hindrance factor means a long life time of the high-K isomer state.

The calculated values are shown in the right panel of figure 1 by filled symbols (circles and triangles), which are compared with experiment (filled squares). The calculation qualitatively reproduces the experimental trends. However, these values turn out to be quite sensitive to the details of the quasiparticle spectra. For instance, the triangles are obtained with slightly larger values of the proton chemical potentials (by 70 keV) than those of circles. The calculated hindrance factors differ by about one order of magnitude. The effect of the residual interaction is very significant too. The open symbols in figure 1 (right) show results including the spin-spin interaction, $V_0\vec{\sigma}\cdot\vec{\sigma}$, with $V_0 = 100$ keV, which roughly accounts for the Gallagher–Moszkowski splitting. This could change F by two orders of magnitude. Nonetheless, the neutron number dependence is rather universal, that indicates the largest hindrance at $N = 104$.

5.2. Cranking model at high spin: QRPA in the rotating frame

Rotating the nucleus very fast, the perturbative treatment in section 5.1 becomes no longer valid. Instead, the semi-classical treatment in the cranking model is better justifiable, and the direct application of the cranking model (19) has been extensively performed for a variety of high-spin phenomena. For instance, the famous back-bending phenomena have been studied and understood as the crossing between the ground band and an aligned 2qp band. This can be also interpreted as breaking a Cooper pair condensed in the ground band by the Coriolis anti-pairing effect.

In order to investigate properties of elementary modes of excitation at high spin, it is useful to use the 'routhian' $E'(\omega_{\mathrm{rot}})$ as a function of the rotational frequency ω_{rot}. The

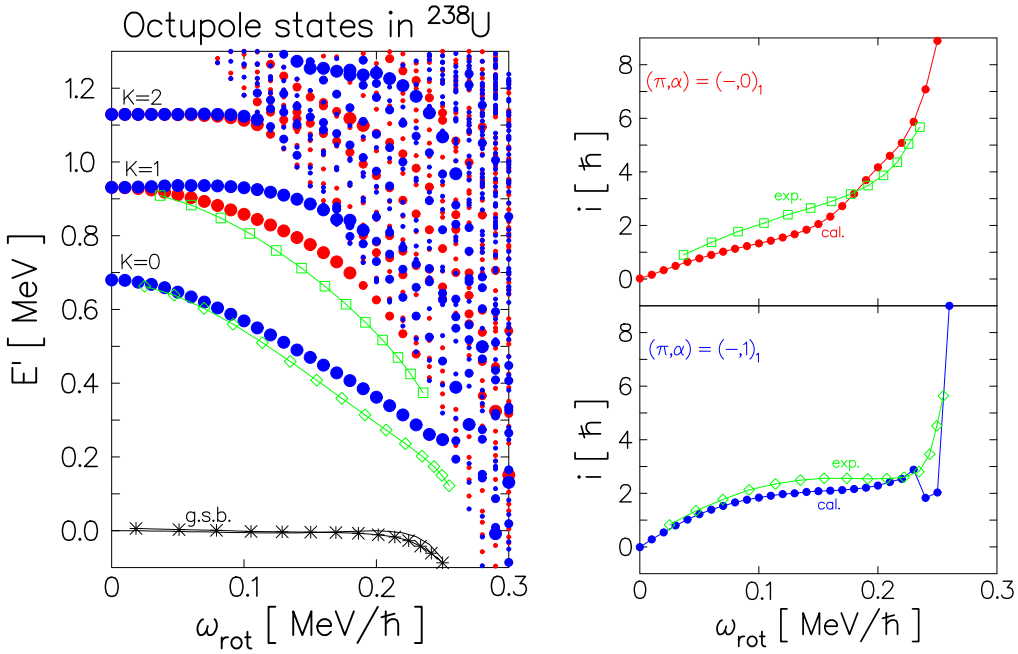

Figure 4. (Left) Excitation routhian plot as functions of rotational frequency $\omega_{\rm rot}$ for negative-parity states in ^{238}U. Large, medium, and small circles indicate the QRPA solutions with $E3$ transition amplitudes larger than $300e$ fm^3, larger than $150e$ fm^3, and less than $150e$ fm^3, respectively. The red (blue) ones correspond to the signature even (odd) states with even (odd) I. Experimental routhians are plotted by open squares. (Right) Aligned angular momentum as a function of $\omega_{\rm rot}$ for the lowest ($K^\pi = 0^-$) and the second lowest ($K^\pi = 1^-$) octupole bands in the lower and upper panels, respectively. Open squares indicate experimental data [55]. Adapted with permission from [56]. Copyright Polish Academy of Arts and Sciences 1996.

routhian here is defined as the eigenenergies of the cranking Hamiltonian (19), which can be interpreted as the energy in the rotating frame with the rotational frequency $\omega_{\rm rot}$. To make a comparison, we often convert the experimental excitation energy as a function of I, $E(I)$, into the 'routhian' $E'(\omega_{\rm rot})$. This is done as follows. First, from experimental rotational spectra $E_b(I)$, we calculate the frequency, $\omega_{\rm rot}(I) = {\rm d}E_b(I)/{\rm d}I$. Here, b is the index of the rotational band. According to the cranking Hamiltonian (19), the routhian is defined as $E'_b(\omega_{\rm rot}) = E_b(I) - \omega_{\rm rot} I_x(I)$ with $I_x(I) = \sqrt{(I+1/2)^2 - K^2}$, at discrete values of $\omega_{\rm rot}(I)$. The reference routhian $E'_{\rm ref}(\omega_{\rm rot})$ is defined, for instance, by fitting that of the ground-state band ('b' = 'g.s.'). Then, the excitation routhian relative to the reference band as a function of $\omega_{\rm rot}$ is obtained as $E'_{\rm ex}(\omega_{\rm rot}) = E'_b(\omega_{\rm rot}) - E'_{\rm ref}(\omega_{\rm rot})$ for each band 'b'. In [54], the experimental routhians in odd nuclei, which were obtained by adopting the reference band fitting the ground-state band in neighboring even-even nuclei, show nice agreement with the calculated quasiparticle routhians.

The routhian plot for the octupole vibrational bands in ^{238}U is presented in figure 4. See [10, 56] for details of the calculation. In the right panels, the alignment, defined by $i \equiv -{\rm d}E'/{\rm d}\omega_{\rm rot}$, is shown. The alignment indicates the aligned component of the angular momentum carried by the vibrational excitation. For the lowest octupole band with $K^\pi = 0^-$, the alignment quickly increases up to $i \sim 3$, which suggests that the angular momentum of the octupole phonon is almost fully aligned along the rotational axis. Then, at high spin around $\omega = 0.25$ MeV, it suddenly jumps up, which suggests the breakdown of the collective vibration by a strong Coriolis force. At $\omega_{\rm rot} \gtrsim 0.25$ MeV, it becomes an aligned 2qp state. This is seen in the left panel too. The octupole collectivity (size of the circles) suddenly decreases around $\omega_{\rm rot} = 0.25$ MeV. In contrast to the lowest band, the second lowest $K^\pi = 1^-$ band with even I shows a gradual increase in the alignment, which may suggest the gradual change of the octupole phonon into the aligned 2qp structure. The present calculation nicely agrees with the experimental data.

The argument here suggests that the vibrational excitations based on the yrast (ground-state) band tend to lose their collective character at high spin, due to the intrusion of the aligned 2qp states at low energy. In this respect, the nucleus with larger deformation may be better suited for the observation of the rapidly rotating vibrational bands. This is because the large deformation tends to hinder the alignment of the quasiparticles. Next, let us discuss such a case, the high-spin SD bands.

6. Elementary excitations in SD rotational bands

The SD state is characterized by a large prolate deformation of approximate two-to-one axis ratio. The shell structure at the SD shape is very different from that near the spherical shape. Since the low-lying modes of excitation strongly depend on the underlying shell structure, we may expect some new features in their properties.

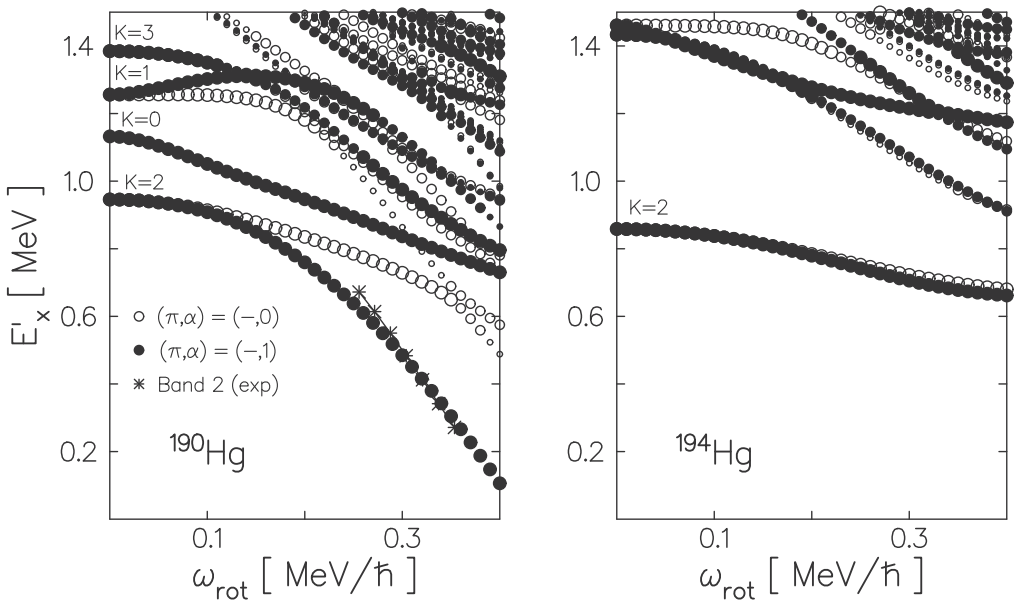

Figure 5. Excitation routhian plot for negative-parity excitations in SD ^{190}Hg (left) and ^{194}Hg (right). Open and filled circles correspond to the states with even and odd signatures, respectively. The size of circles represent the $E3$ transition amplitudes ($>200e$ fm^3, $>100e$ fm^3, and $<100e$ fm^3). Experimental excitation routhians in ^{190}Hg are shown by stars ($*$). Reproduced with permission from [56]. Copyright Polish Academy of Arts and Sciences 1996.

6.1. Octupole vibrations with $K^\pi = 0^-$ and 2^-

One of the most striking features in the SD shell structure is that the single-particle levels with opposite parity ($\pi = \pm$) coexist in a single shell. Adopting a simple harmonic oscillator potential, one can easily understand this fact: namely, for $\omega_x = \omega_y = 2\omega_z$, an orbital with the oscillator quanta (n_x, n_y, n_z) is degenerate in energy with those of $(n_x \mp 1, n_y, n_z \pm 2)$ and $(n_x, n_y \mp 1, n_z \pm 2)$. Since the parity is determined by the total quanta $N = n_x + n_y + n_z$, they have different parity. Another feature is that the observed SD bands are located around the closed shell configurations corresponding to the SD magic numbers (See figure 6-50 in BM2). In contrast, the normally deformed nucleus is a consequence of the SBS and has an open-shell configuration away from the spherical magic numbers. From these simple analysis, we may expect that the collective negative-parity modes of excitation appear at low energy.

The QRPA based on the cranked Nilsson-BCS model is applied to SD bands in the $A = 190$ region. The calculation predicts that the $K^\pi = 2^-$ octupole states are particularly low in energy, around $E'_x \lesssim 1$ MeV. Especially, in ^{194}Hg and ^{196}Pb with $N = 114$, very collective $K^\pi = 2^-$ octupole vibrations appear well below 1 MeV and their excitation routhians are roughly constant with very little signature splitting [10]. See the right panel of figure 5. Later, the interband $E1$ transitions between the octupole and ground SD bands have been measured for ^{194}Hg [57] and for ^{196}Pb [58], which confirms nice agreement with calculated routhians and the strong octupole collectivity. For $N = 110$, the calculation predicts an aligned octupole phonon, shown in the left panel of figure 5, similar to the lowest octupole band in ^{238}U in figure 4. This also nicely reproduces the experimental routhians in an excited SD band in ^{190}Hg [59]. Later, the linear polarization measurement confirms the aligned octupole vibrations [60].

In the $A = 150$ region, we theoretically predicted a possible candidate of $K^\pi = 0^-$ octupole band in SD ^{152}Dy [61]. It shows a rather constant excitation routhians in a wide range of $\omega_{\rm rot} = 0 \sim 0.7$ MeV. Later in 2002, its octupole character has been confirmed by the measurement of the interband transitions and the spin identification [62, 63]. The $\omega_{\rm rot}$-dependence of the routhian well agrees with the theoretical prediction.

6.2. Soft mode with $K^\pi = 1^-$

So far, the octupole vibrational excitations in SD rotational bands have been observed (confirmed) only for the $K^\pi = 0^-$ and 2^- modes. Theoretically, these modes are predicted to appear lower than other modes ($K^\pi = 1^-$ and 3^-), near the SD magic numbers. However, moving away from the magic closed configurations, the $K^\pi = 1^-$ modes become a soft mode.

In order to investigate the soft mode in the SD shape, we again follow the discussion in BM2 (pp 591–598), extending the argument for spherical potentials in section 3.3 to a deformed one. This is possible if the motion is separable in the three coordinates, such as the harmonic oscillator potential. In a deformed harmonic oscillator potential, the single-particle energy is specified by three numbers of the oscillator quanta, (n_x, n_y, n_z). Thus, the shell structure is characterized by the ratio of three integers, *a:b:c*, and the shell frequency given by

$$\omega_{\rm sh} \equiv \frac{1}{a}\left(\frac{\partial \epsilon}{\partial n_x}\right)_0 = \frac{1}{b}\left(\frac{\partial \epsilon}{\partial n_y}\right)_0 = \frac{1}{c}\left(\frac{\partial \epsilon}{\partial n_z}\right)_0. \qquad (33)$$

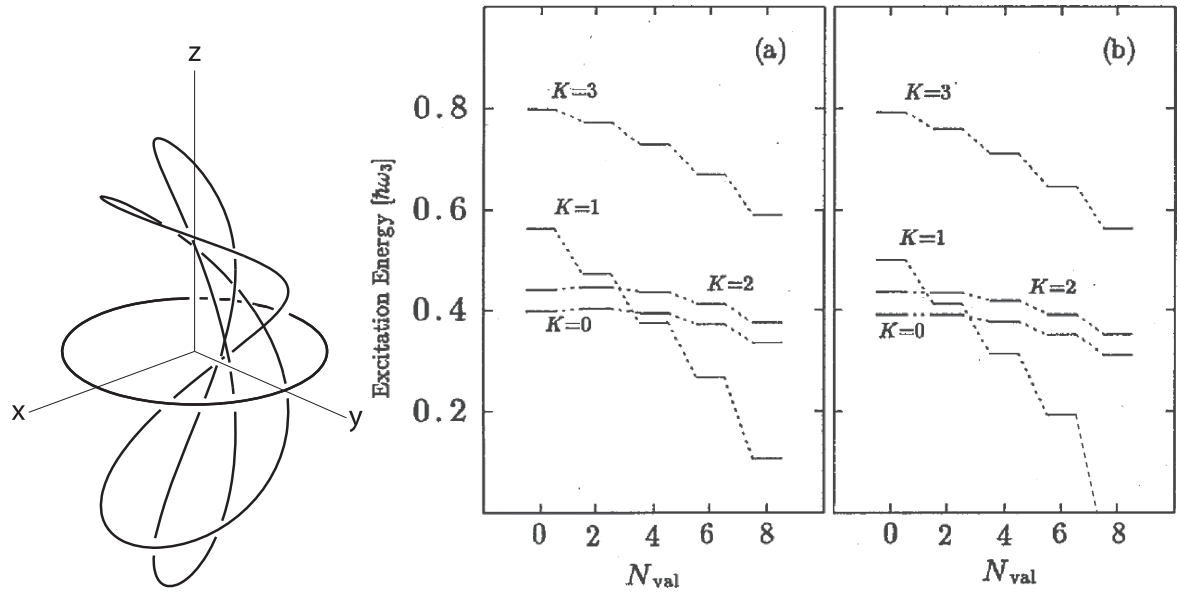

Figure 6. (Left) Typical classical periodic orbits in a potential with the a:b:c = 2:2:1 shell structure. Reproduced with permission from [64]. Copyright Elsevier 1993. (Right) Calculated excitation energies for octupole vibrations in the SD harmonic oscillator potential, with stronger pairing (a) and weak pairing interactions (b). Reproduced with permission from [65]. Copyright Oxford University Press 1991.

Since a:b:c = 1:1:1 correspond to the spherical harmonic oscillator, the simplest integer ratio next to 1:1:1 is a:b:c = 1:1:2 and 2:2:1. The SD shape we are discussing here corresponds to the latter one, which has the prolate shape.

The frequency ratio of a:b:c = 2:2:1 ($\omega_x = \omega_y = 2\omega_z = 2\omega_{\rm sh}$) creates periodic orbits shown in the left panel of figure 6. These are orbits of 'bending figure of eight'. Since the shape of the classical periodic orbits is related to the soft mode, the SD state, with many nucleons outside the closed shell, may be unstable against the banana-shaped bending mode.

In figure 6, we show the result of the QRPA calculation with the separable octupole interaction, based on the SD harmonic oscillator potential [65]. The $K^\pi = 0^-$ and 2^- modes are the lowest near the SD magic numbers. These modes are rather insensitive to the number of nucleons outside the closed shell. However, the $K^\pi = 1^-$ octupole mode dramatically decreases its energy as increasing the number of valence nucleons. With enough number of valence nucleons, the bending $K^\pi = 1^-$ mode leads to the instability.

According to the qualitative discussion on the SD shell structure, Bohr and Mottelson have already pointed out the possibility of this instability toward the bending shape, in the context of fission path (p 598 in BM2). As far as we know, this effect on the fission dynamics has not been fully studied so far.

7. Nuclear wobbling motion and precession

Most of the existing experimental data are known to be consistent with the interpretation based on the axially symmetric deformation. Even the octupole deformation (section 3.3) observed in heavy nuclei is associated with the axially symmetric one (Y_{30}). In section 6.2, we have presented a possible exotic nuclear shape in SD nuclei away from the closed shell configuration, that breaks both the axial and the parity symmetry. However, it has not been observed in experiments.

Bohr and Mottelson gave extensive discussion on the spectra of triaxial nuclei in BM2. In the beginning of section 4-5 of BM2, they said '*Although, at present (1975), there are no well-established examples of nuclear spectra corresponding to asymmetric equilibrium shapes, it appears likely that such spectra will be encountered in the exploration of nuclei under new conditions (large deformations, angular momentum, isospin, etc)'*. They were absolutely right.

The identification of the static triaxial deformation has been a longstanding issue in the nuclear structure physics. One of the difficulties is to confirm its 'static' nature clearly distinguished from the 'dynamic' one. The observation of a wobbling band was a breakthrough that provided a clear indication of the non-uniform three-dimensional rotation of a triaxial nucleus. We have really encountered this new phenomenon at *large deformation and angular momentum*.

The first observation of the wobbling band was in ^{163}Lu [66, 67]. At high spin ($I \gtrsim 20$), several regular rotational bands with large moments of inertia come down to the yrast region. The deformation of these bands have been speculated to be large ($\epsilon \sim 0.4$) and triaxial ($\gamma \sim 20^\circ$), according to calculations of the total routhian surface (TRS) with the Nilsson potential [68]. They are called the triaxial superdeformed (TSD) bands and labeled as TSD1, TSD2, etc. In addition to the stretched intraband transitions ($\Delta I = 2$), the linking transitions ($\Delta I = 1$) between TSD2 and TSD1 (yrast), between TSD3 and TSD2, and between TSD3 and TSD1, have been observed. The $E2$ character of these interband transitions is experimentally confirmed [68] and their large

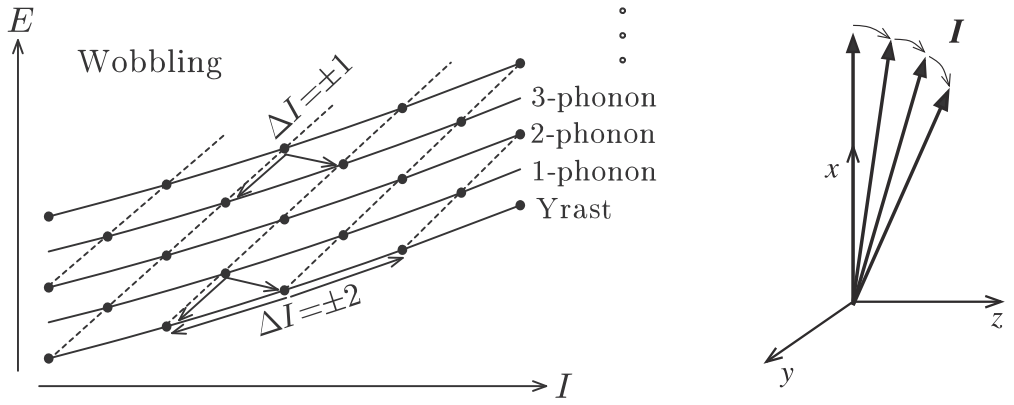

Figure 7. A schematic illustration of the wobbling motion. (Left) Excitation spectra with $\Delta I = 2$ and $\Delta I = 1$ sequences. (Right) A wobbling phonon excitation tilts the direction of the angular momentum from the x-axis. Reproduced with permission from [69]. Copyright World Scientific Publishing Co. 1992.

strengths nicely correspond to the estimate by a simple triaxial rotor model. The measured $B(E2)$ values for the interband transitions are order of 100 W.u. which is considerably larger than those of the most collective γ vibrations.

7.1. Rotor model analysis of the wobbling in the high-spin limit

The prediction based on the rotor model given by Bohr and Mottelson (section 4–5e in BM2) is recapitulated here. The rotor Hamiltonian contains three different moments of inertia, $\mathcal{J}_x > \mathcal{J}_y > \mathcal{J}_z$, with respect to the principal axes in the body-fixed frame

$$H_{\rm rot} = \frac{J_x^2}{2\mathcal{J}_x} + \frac{J_y^2}{2\mathcal{J}_y} + \frac{J_z^2}{2\mathcal{J}_z} = \frac{\vec{J}^2}{2\mathcal{J}_x} + \left(\frac{1}{2\mathcal{J}_y} - \frac{1}{2\mathcal{J}_x}\right)J_y^2 + \left(\frac{1}{2\mathcal{J}_z} - \frac{1}{2\mathcal{J}_x}\right)J_z^2. \quad (34)$$

For the lowest energy (yrast) state at a given I, the term proportional to $\vec{J}^2$ in this Hamiltonian is dominant at high spin ($I \to \infty$). This corresponds to a uniform rotation around the x axis: $E_I \approx I(I+1)/(2\mathcal{J}_x)$. In this high-spin limit, we assume $J_x \approx I$ which can be treated as a c-number. The remaining terms of the Hamiltonian (34) can be diagonalized, $[H_{\rm rot}, X^\dagger_{\rm wob}] = \omega_{\rm wob} X^\dagger_{\rm wob}$, by a linear transformation. The normal-mode (wobbling phonon) creation operator

$$X^\dagger_{\rm wob} \equiv a\frac{{\rm i}J_y}{\sqrt{2I}} - b\frac{J_z}{\sqrt{2I}}, \quad (35)$$

with the normalization $[X_{\rm wob}, X^\dagger_{\rm wob}] = 1$ leads to the following relations:

$$\frac{a}{b} = \sqrt{\left(\frac{1}{\mathcal{J}_y} - \frac{1}{\mathcal{J}_x}\right)\left(\frac{1}{\mathcal{J}_z} - \frac{1}{\mathcal{J}_x}\right)^{-1}}, \qquad ab = 1, \quad (36)$$

$$\omega_{\rm wob} = I\sqrt{\left(\frac{1}{\mathcal{J}_y} - \frac{1}{\mathcal{J}_x}\right)\left(\frac{1}{\mathcal{J}_z} - \frac{1}{\mathcal{J}_x}\right)}. \quad (37)$$

The operator for the wobbling phonon number is given by $n \equiv X^\dagger_{\rm wob} X_{\rm wob}$. In this way, the rotor Hamiltonian can be written as a sum of the rotation around the x axis and the wobbling phonon excitation: $E_{In} \approx I(I+1)/(2\mathcal{J}_x) + \omega_{\rm wob}(n + 1/2)$. A schematic figure for these spectra is shown in figure 7. In order to realize this kind of multiple band structure from one intrinsic configuration, the nucleus should be able to rotate about all three principal axes. Therefore, the nuclear shape must be triaxial. In addition, among the three moments of inertia, the one along the major rotational axis $\mathcal{J}_x$ must be the largest.

According to the LO high-spin formula (20), the intraband $B(E2; \Delta I = 2)$ strengths are proportional to the quadrupole deformation $(\tilde{Q}_{22})^2$. The $\Delta I = 1$ transitions, which are associated with the wobbling transitions, appear in the NLO with respect to $1/I$; $B(E2; \Delta I = 1)/B(E2; \Delta I = 2) \sim 1/I$. These $E2$ transition strengths were explicitly given in section 4-5e in BM2. The TRS calculation predicts the 'positive' γ shape ($\gamma \sim 20°$) for the TSD bands in ^{163}Lu. Here we use the so-called Lund convention for the triaxiality parameter γ in relation to the main rotation axis [70], where for the positive γ shape, $0 < \gamma < 60°$, the rotation (x) axis is the shortest PA, while for the negative γ shape, $-60° < \gamma < 0$, it is the intermediate PA. Then the out-of-band $E2$ transitions for the positive γ shape satisfy a relation, $B(E2; I \to I-1) > B(E2; I \to I+1)$. This is consistent with the experiments, in which only the $I \to I-1$ transitions have been observed.

The simple rotor model picture, however, disagrees with the observed data with respect to the following points:

- At $\gamma = 20°$ which is supported by the TRS calculation, the γ-dependence of the irrotational moments of inertia, which are commonly assumed in the rotor model, produces $\mathcal{J}_y > \mathcal{J}_x > \mathcal{J}_z$. This contradicts the basic assumption of $\mathcal{J}_x > \mathcal{J}_y > \mathcal{J}_z$ and the formula (37).
- According to equation (37), the wobbling frequency $\omega_{\rm wob}$ increases as a function of I. Conversely, the observed frequency decreases.

Solutions to these problems will be provided by microscopic treatments in section 7.2.

7.2. Microscopic QRPA analysis for the wobbling motion

A microscopic theory to treat the nuclear wobbling motion in the small amplitude limit is naturally provided by the QRPA

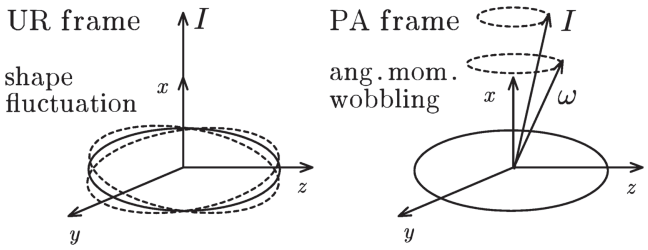

Figure 8. Two equivalent pictures of the wobbling motion: one in the uniformly rotating (UR) frame (left) and the other in the principal axis (PA) frame (right). Reproduced with permission from [69]. Copyright World Scientific Publishing Co. 1992.

in the rotating frame, or the self-consistent cranking plus QRPA [71]. Among the quadrupole tensors, $Q_{ij} \propto x_i x_j - \delta_{ij} r^2/3$ $(i, j = x, y, z)$, the negative signature operators of $Q_y \equiv -Q_{zx}$ and $Q_z = \mathrm{i}Q_{xy}$ are responsible for the wobbling motion. Adopting the separable quadrupole interaction of the form (7), the mean-field approximation simply replaces one of the operators QQ into its expectation value $\mathcal{Q}(t)$, leading to the time-dependent mean field

$$h_{\mathrm{UR}}(t) = h_{\mathrm{def}} - \omega_{\mathrm{rot}} J_x - \kappa_y \mathcal{Q}_y(t) Q_y - \kappa_z \mathcal{Q}_z(t) Q_z, \quad (38)$$

where h_{def} is a deformed single-particle Hamiltonian that contains the fields associated with diagonal tensors, $-\kappa_{ii} \mathcal{Q}_{ii} Q_{ii}$. Although, in general, h_{def} is time-dependent, we hereafter focus our discussion on the wobbling motion, and assume h_{def} is time-independent. In this treatment of equation (38), the rotational axis stays along the x axis and the wobbling motion is represented by a fluctuation in the orientation of deformed density distribution induced by $\mathcal{Q}_y(t)$ and $\mathcal{Q}_z(t)$. This picture corresponds to the uniformly rotating (UR) frame.

The small shape fluctuation induced by the off-diagonal quadrupole tensors, $\mathcal{Q}_y$ and $\mathcal{Q}_z$, is not associated with the real shape change from the equilibrium. The same effect can be realized by rotating the reference frame to the PA frame where the non-diagonal elements, $\mathcal{Q}_y$ and $\mathcal{Q}_z$, of the quadrupole tensors vanish. If we adopt this body-fixed frame, the direction of the angular momentum fluctuates. In the PA frame, since the rotation is no longer uniform, the cranking model should be extended to a time-dependent one

$$h_{\mathrm{PA}}(t) = h_{\mathrm{def}} - \vec{\omega}_{\mathrm{rot}}(t) \cdot \vec{J}. \quad (39)$$

The rotor-model analysis of Bohr and Mottelson in section 7.1 has a direct connection to the PA picture. In this picture, the frequency $\vec{\omega}_{\mathrm{rot}}$ should be treated as dynamical variables (operators). In the small amplitude limit, Marshalek proved the equivalence between the UR and the PA frames and obtained the same expression (37) for the wobbling frequency, with the moments of inertia calculated in the QRPA [71]. It is generalized to arbitrary mean-field potentials and residual interactions [11]. The two pictures are schematically illustrated in figure 8.

The microscopic QRPA calculations were first performed with the Nilsson potential and the separable quadrupole interactions [72–76]. Later, it has been done with the Woods–Saxon potential and an separable interaction which is determined by the symmetry restoration condition [11]. In general, it is difficult to perform the QRPA calculation for an odd-A nucleus, however, this is not a problem at a finite ω_{rot} because the Kramers degeneracy is lifted and the RPA vacuum is uniquely identified. The calculated QRPA moments of inertia indicate a proper ordering of moments of inertia, $\mathcal{J}_x > \mathcal{J}_y > \mathcal{J}_z$, for the wobbling mode in ^{163}Lu. Why is this ordering different from a naive expectation based on the irrotational flow?

To answer the question, it is important to distinguish the dynamic and the kinematic moments of inertia [77]. The dynamic moment of inertia is defined by the second derivative of the rotational energy, $1/\mathcal{J}^{(2)} = \mathrm{d}^2 E_I/\mathrm{d}I^2$, which is considered to be the one in the rotor model in equation (34). In contrast, the kinematic moment of inertia is defined by the first derivative, $1/\mathcal{J}^{(1)} = I^{-1}\mathrm{d}E_I/\mathrm{d}I = \omega_{\mathrm{rot}}/I$. The largest moment of inertia, $\mathcal{J}_x$, in the QRPA wobbling formalism of [71] is the kinematic one, more precisely, $\mathcal{J}_x = \mathcal{J}_x^{(1)} \equiv \langle J_x \rangle/\omega_{\mathrm{rot}}$, which is strongly influenced by the alignment of the intrinsic angular momentum along the rotational (x) axis. Generally the kinematic moment of inertia is larger than the dynamic one because of the effect of alignment. In ^{163}Lu, the odd-proton quasiparticle mainly produces the alignment. When the alignment is large enough, we could have a rigid-body-like ordering, $\mathcal{J}_x^{(1)} > \mathcal{J}_y > \mathcal{J}_z$, for the positive γ shape, even if the dynamic moments of inertia are irrotational-like, $\mathcal{J}_y > \mathcal{J}_x > \mathcal{J}_z$. The QRPA moments of inertia automatically take into account this effect. Thus, *the alignment effect is crucial for the appearance of the wobbling mode*, which was first pointed out in [74, 75].

The fact that the largest moment of inertia is the kinematic one can be justified by the simple particle-rotor model as in [78]: When the quasiparticle alignment j is present, J_x is replaced by $J_x - j$ in equation (34). Using $J_x = [\vec{J}^2 - (J_y^2 + J_z^2)]^{1/2} \approx \left(I + \frac{1}{2}\right) - (J_y^2 + J_z^2)\Big/(2I + 1)$ which is valid for in high-spin limit $I \gg 1$, we obtain

$$H_{\text{p-rot}} = \frac{(J_x - j)^2}{2\mathcal{J}_x} + \frac{J_y^2}{2\mathcal{J}_y} + \frac{J_z^2}{2\mathcal{J}_z} \approx \frac{(I - j)(I - j + 1)}{2\mathcal{J}_x} \quad (40)$$

$$+ \left(\frac{1}{2\mathcal{J}_y} - \frac{1}{2\mathcal{J}_x} + \frac{1}{2\mathcal{J}_x} \frac{j}{I + \frac{1}{2}} \right) J_y^2$$

$$+ \left(\frac{1}{2\mathcal{J}_z} - \frac{1}{2\mathcal{J}_x} + \frac{1}{2\mathcal{J}_x} \frac{j}{I + \frac{1}{2}} \right) J_z^2. \quad (41)$$

Namely the inverse of the kinematic moment of inertia

$$\frac{1}{\mathcal{J}_x^{(1)}} = \frac{\omega_{\mathrm{rot}}}{\langle J_x \rangle} \approx \frac{1}{\mathcal{J}_x} \left(1 - \frac{j}{I + \frac{1}{2}} \right), \quad (42)$$

appears in equation (41) in place of $1/\mathcal{J}_x$ in equation (34).

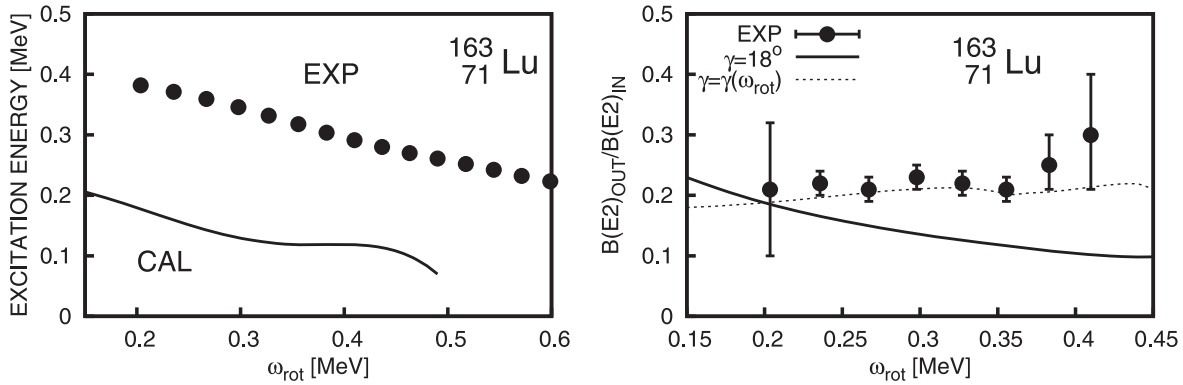

Figure 9. (Left) Calculated and experimental wobbling frequencies as functions of the rotational frequency. (Right) Calculated and experimental inter- to intraband $B(E2)$ ratio as functions of the rotational frequency. See text for details. Adapted with permission from [11]. Copyright Oxford University Press 2008.

The wobbling frequency (37) with $1/\mathcal{J}_x$ replaced by $1/\mathcal{J}_x^{(1)}$ of equation (42) first increases as spin increases and then turns to decrease. Thus the quasiparticle alignment also explains why the observed wobbling frequency decreases as a function of I. From equation (41) there is a critical angular momentum, $I_c \equiv j(1 - \mathcal{J}_x/\mathcal{J}_y)^{-1} - \frac{1}{2}$, at which the wobbling frequency vanishes, $\omega_{\rm wob} = 0$ (remember $\mathcal{J}_y > \mathcal{J}_x > \mathcal{J}_z$). Beyond I_c, the wobbling mode ceases to exist, because of the irrotational-like ordering, $\mathcal{J}_y > \mathcal{J}_x^{(1)}|_{I>I_c} > \mathcal{J}_z$. In this way, for the case where the alignment takes place along the axis of the intermediate dynamic moment of inertia, the I-dependence of the original wobbling frequency in section 7.1 drastically changes. Such a novel wobbling scheme was first pointed out in [79], although the terms proportional to j in equation (41), i.e. the effect of alignment, are interpreted as decreasing $\mathcal{J}_y$ and $\mathcal{J}_z$ instead of increasing $\mathcal{J}_x$. The observed decreasing tendency of $\omega_{\rm wob}$ in the Lu isotopes clearly suggests such a character. In [78] it is called '*transverse* wobbler' in order to distinguish it from '*longitudinal* wobbler' where the quasiparticle aligns along the axis of the largest inertia, $\mathcal{J}_x > \mathcal{J}_y > \mathcal{J}_z$. In the longitudinal wobbler, the frequency $\omega_{\rm wob}$ monotonically increases with I. In fact, the microscopic QRPA calculations also predicted the wobbling motion of increasing $\omega_{\rm wob}$ as a function of I in nuclei of negative γ shapes [72, 73], in which the irrotational-type moments of inertia satisfy the longitudinal condition, $\mathcal{J}_x > \mathcal{J}_y > \mathcal{J}_z$. A similar argument of the effect of alignment for the possible decrease of $\omega_{\rm wob}$ has been discussed also in [80].

It should be noticed that the three moments of inertia are assumed to be independent of spin I in the rotor model or the particle-rotor model. In reality, however, the microscopically calculated QRPA moments of inertia change as functions of I, although their dependencies on I are not so strong in most cases [11, 72–75]. One should take this into account in order to study precisely how the wobbling frequency changes as a function of spin. In [81], introducing a rather strong spin-dependence common to all three moments of inertia, the decreasing tendency of $\omega_{\rm wob}$ is realized in the particle-rotor coupling model with the inertia of the rigid-body-like ordering, $\mathcal{J}_x > \mathcal{J}_y > \mathcal{J}_z$.

In figure 9, we show results of the QRPA calculation based on the deformed Woods–Saxon potential [11]. Note that there are no adjustable parameters in the calculation because the minimal symmetry restoring interaction is employed, which is uniquely fixed once the deformed mean-field is given. The deformation parameters are determined by minimizing the TRS. The calculated wobbling frequency has a proper trend, though the absolute magnitude is underestimated by a few hundred keV. The large interband $B(E2)$ values are rather well reproduced in the calculation. However, the observed ratio, $B(E2; I \to I-1)_{\rm out}/B(E2; I \to I-2)_{\rm in}$, seems to increase as a function of I, while the calculated ratio decreases because of the $1/I$ dependence of the interband transition. The dotted line in the right panel of figure 9 indicates the result obtained by artificially increasing the triaxiality (γ) at higher spins. In fact, in order to explain the experimental $B(E2)$ ratios, the triaxial parameters $\gamma\,({\rm den}) \approx 20^\circ$ are necessary. The $\gamma\,({\rm den})$ is defined with respect to the intrinsic quadrupole moments calculated from the density distribution. Here, it should be noted that the triaxial parameter γ for the potential shape is significantly different from $\gamma\,({\rm den})$ [76] (see appendix for details). As far as we know, at present, none of the microscopic calculations are able to reproduce the triaxiality of $\gamma\,({\rm den}) \approx 20^\circ$. Another unsolved problem is that the observed $B(M1)$ values are significantly overestimated. In [82], the inclusion of the isovector separable orbital angular momentum interaction is suggested to improve the agreement. The nuclear wobbling motion has not been fully understood yet.

7.3. Precession: rotational band built on a high-K isomer

In section 7.2, we show that the alignment of quasiparticles is crucial for the wobbling motion to appear in the Lu isotopes with the positive γ shape. An interesting extreme case of the alignments is that the nuclear shape is axially symmetric about the alignment (x) axis; i.e. $\gamma = 60^\circ$ (oblate) or $\gamma = -120^\circ$ (prolate) in the Lund convention and the angular momentum is supplied only by the alignments of quasiparticles. It is expected that the optimal configurations of aligned quasiparticles in the states of such shapes make the high-spin isomers, or the 'yrast traps', along the yrast line, see

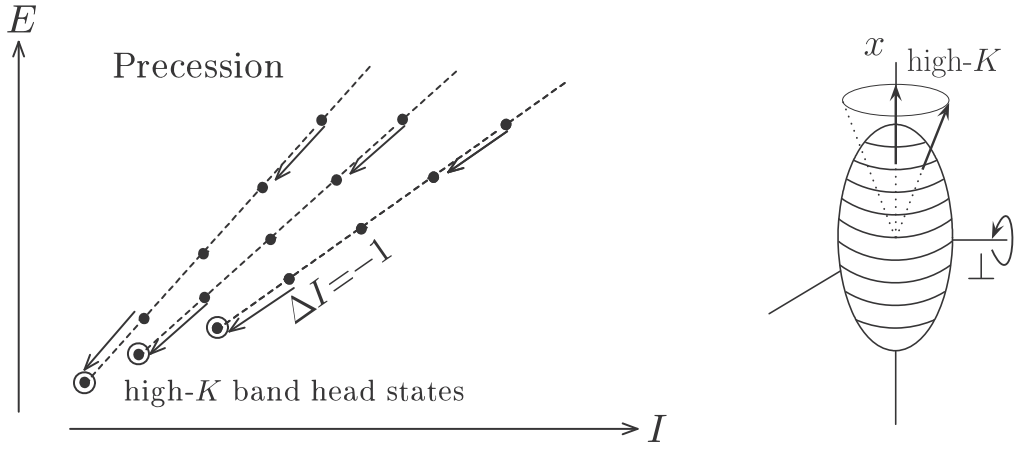

Figure 10. A schematic illustration of the precession motions. (Left) Excitation spectra from [84]. Reproduced with permission, copyright American Physical Society 2005. There are no $\Delta I = 2$ horizontal sequences leaving only one $\Delta I = 1$ vertical band for each high-K state; compare with figure 7. (Right) Superposition of the collective rotation about the perpendicular axis makes the high-K aligned angular momentum vector to precess around the symmetry axis.

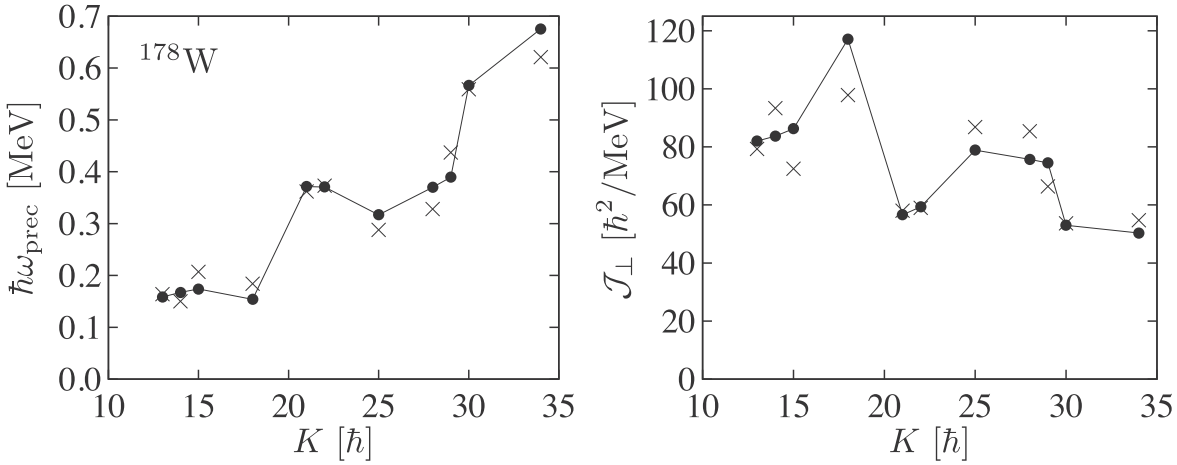

Figure 11. (Left) Calculated (filled circles) and experimental (crosses) precession frequencies $\omega_{\rm prec}$ for various high-K isomers in ^{178}W, where the experimental data is denoted by crosses. (Right) Calculated (filled circles) and experimental (crosses) moments of inertia perpendicular to the symmetry axis, estimated by $\mathcal{J}_\perp = K/\omega_{\rm prec}$. Based on the result of [91].

e.g. [83]. Although the rotational bands built on the oblate isomers are not yet observed, those on the prolate isomers have been well known [1]. They are nothing but the high-K rotational bands widely observed in the Hf and W region, where many high-j and high-Ω Nilsson orbits are concentrated near the Fermi surface. Here, Ω is the component of single-particle angular momentum along the symmetry axis.

We call this rotational motion 'precession' because the aligned angular momentum vector tilts like in the case of the wobbling motion by superimposing the collective rotation about the perpendicular axis; it is illustrated schematically in figure 10. Since the high-K isomers have been known for many years, they have been investigated by various methods; e.g., by the cranked mean-field method [85], by the RPA method based on the sloping Fermi surface [86–89], or by the tiled axis cranking method [90]. In [84] it was considered as the axially symmetric limit of the RPA wobbling formalism [71] discussed in section 7.2. In fact, the wobbling frequency in equation (37) becomes $\omega_{\rm wob} = I/\mathcal{J}_\perp - \omega_{\rm rot}$, where the perpendicular moment of inertia is denoted as $\mathcal{J}_\perp \equiv \mathcal{J}_y = \mathcal{J}_z$ in the axially symmetric limit and the rotational frequency about the main rotation axis is $\omega_{\rm rot} = I/\mathcal{J}_x^{(1)}$. Here, the dynamic moment of inertia ($\mathcal{J}_x \to 0$) is replaced by the kinematic inertia $\mathcal{J}_x^{(1)}$ with the aligned angular momentum $I_x = K$ (we here use K in place of j). On the other hand the rotor Hamiltonian (34) in this case reduces to $H_{\rm rot} = (I_y^2 + I_z^2)/(2\mathcal{J}_\perp)$ so that the energy spectrum is given simply by $E_{\text{high-}K} = [I(I+1) - K^2]/(2\mathcal{J}_\perp)$, which can be rewritten as

$$E_{\text{high-}K} = \omega_{\rm prec}\left(n + \frac{1}{2} + \frac{n(n+1)}{2K}\right), \tag{43}$$

introducing the precession phonon number $n \equiv I - K$. Here the precession frequency is given by $\omega_{\rm prec} \equiv K/\mathcal{J}_\perp = [\omega_{\rm wob} + \omega_{\rm rot}]_{I=K}$. Thus the precession motion can be described by the harmonic excitation of n-phonons as long as $n \ll K$. The difference of frequencies $\omega_{\rm prec}$ from $\omega_{\rm wob}$ is due to the fact that the wobbling motion is treated in the

body-fixed frame while the precession motion in the laboratory-frame. Remember the transformation of the energy into the routhian in the rotating frame in section 5.2, $E' = E - \omega_{\rm rot} I_x$, and that the precession mode transfers the angular momentum by one unit $\Delta I_x = 1$. Since there is no collective rotation about the x axis, the rotational frequency $\omega_{\rm rot}$ is a redundant variable and any observable quantities do not depend on it; $\omega_{\rm wob}$ does depend while $\omega_{\rm prec}$ does not. As it is discussed in [84] not only the energy but also the electromagnetic transitions, like $E2$ and $M1$, can be treated with the multi-phonon picture as long as the phonon number n is much smaller than K.

We show in figure 11 the result of precession frequencies for a number of K isomers in ^{178}W calculated by using the axially symmetric limit of the Woods–Saxon QRPA wobbling formalism [11]. Compared with the corresponding calculation of [84], in which the Nilsson mean-field potential is employed, considerable improvement can be seen and a good agreement with experimental data is obtained. In the right panel of figure 11, the estimated moments of inertia $\mathcal{J}_\perp = K/\omega_{\rm prec}$ are also shown. The agreement is much better than the simple mean-field calculation, e.g. [85], because the effect of residual interaction is taken into account in the QRPA. It can be seen that the moments of inertia take various values depending on the isomer configurations. They are considerably larger than the moment of inertia of the ground state rotational band estimated from the first 2^+ state, $\mathcal{J}_{\rm gr} \approx 28$ [$\hbar^2$/MeV]. They do not show a simple correlation with the K quantum number, and do not approach to the rigid-body value (with $\epsilon_2 = 0.240$), $\mathcal{J}_{\rm rig} \approx 88$ [$\hbar^2$/MeV], even at considerably high spin. Their properties strongly depend on what kind of quasiparticles contribute to those high-K isomers in which the numbers of quasiparticles are from four to ten. See [84] for precise configuration assignments. At an extreme high spin, we can even imagine possible existence of torus-shape isomers and their precession motions [92].

8. Summary

Bohr and Mottelson have explored a variety of fields in the nuclear structure physics. Among them, we have discussed selected topics related to the nuclear deformation and rotation. First, we presented the concept of the symmetry breaking in the unified model. The symmetry broken state is not stable in finite systems, such as nuclei. The correlation time induced by the quantum fluctuation is a key to understand the interplay between the symmetry breaking and restoration. The finite-size effect associated with the zero-point motion may hinder the symmetry breaking.

The coupling between intrinsic and rotational motions is well described by the cranking model. Since the model assumes a semiclassical treatment of the nuclear rotation (angular momentum), the model requires the quantization in the low-spin limit. We show a possible quantization of the cranking model, which is applicable to calculation of transition matrix elements at low spin. This can be regarded as a kind of hybrid model of the unified model and the cranking model. It is applied to electromagnetic decay properties of vibrational bands and high-K isomers.

In the high-spin region, the cranking model is a golden tool to study the nuclear structure under a strong Coriolis and centrifugal field. We discussed effects of the rapid rotation on the octupole vibrations, which are nicely treated with the QRPA in the UR frame (one-dimensional cranking). The calculation reproduces the experimental data, showing the phonon alignment and loss of collectivity (phonon breakdown).

The closed shell configurations of the SD states are characterized by the 2:2:1 shell structure. This shell structure has the $K^\pi = 1^-$ octupole mode as a soft mode. Away from the SD magic numbers with many valence nucleons, the prolate SD nucleus could show instability toward a bending banana shape.

The triaxial deformation produces the three-dimensional non-uniform rotation, which is called wobbling motion. The QRPA in the UR frame provides a microscopic tool to calculate the wobbling and precession modes of excitation. The experimental data are qualitatively reproduced. This microscopic study clearly indicates the importance of the quasiparticle alignment for the existence of the wobbling mode in the observed cases. The self-consistently calculated triaxial deformation seems to be smaller than what experimental data indicate, which is an important open problem.

The nucleus provides a wonderful opportunity to study a finite system going through many kinds of symmetry breaking, under a variety of extreme circumstances, such as large angular momentum, deformation, and isospin. The topics we have discussed in this paper were pioneered by Bohr and Mottelson who gave us a deep insight into nuclear structure and quantum many-body physics. There are still many open issues in these fields which are waiting for future studies.

Acknowledgments

This work was supported in part by JSPS KAKENHI Grant No. 25287065 and by Interdisciplinary Computational Science Program in CCS, University of Tsukuba.

Appendix. Remarks on the triaxial deformation

The values of the triaxiality parameter γ can be significantly different depending on their definitions. This was first pointed out in the appendix B of [34] and more recently discussed again in relation to the wobbling motion in [76]. The most basic definition is $\gamma\,({\rm den}) \equiv -\tan^{-1}(\langle Q_{22}\rangle/\langle Q_{20}\rangle)$ by using the intrinsic quadrupole moments, which is directly related to the $E2$ transition probability. In phenomenological potential models, such as the Nilsson and the Woods–Saxon potentials, the triaxial deformation $\gamma \equiv \gamma\,({\rm pot})$ is introduced to define the shape of the potential. For example, it is defined based on the stretched coordinate in the Nilsson model, $\gamma\,({\rm pot{:}Nils})$, and

on the radius parametrization $R(\theta, \phi) \propto \left(1 + \sum a_{\lambda\mu} Y_{\lambda\mu}\right)$ in the Woods–Saxon model, γ(pot:WS).

With the uniform density assumption, the triaxiality parameter γ(geo) can be calculated in the same way as γ(den) for a given γ(pot). Then, γ(den) $\approx$ γ(geo) holds in a good approximation near the self-consistent point [76], reflecting the short-range nature of the nucleon-nucleon interaction. However, it should be noted that γ(geo) is different from γ(pot), see e.g. [93]. These different definitions are sometimes confused.

Here we would like to take another well-known example for the harmonic oscillator model with the quadrupole deformed potential, $-(\omega/b^2)\beta[\cos\gamma\, Q_{20} - \sin\gamma\,(Q_{22} + Q_{2-2})/\sqrt{2}]$, where b is the oscillator length parameter for the frequency ω, and we call these β and γ as the (pot:HO)-parametrization. Then the deformed shape of potential is the ellipsoid with the anisotropic frequencies $\omega_k^2 = \omega^2\left[1 - \sqrt{\frac{5}{4\pi}}\beta\cos\left(\gamma + \frac{2\pi}{3}k\right)\right]$ $(k = 1, 2, 3 = x, y, z)$. As is discussed in section 3.4, the isotropic velocity distribution condition in equation (14) leads to $\langle x_k^2\rangle \propto \omega_k^{-2}$ and then $\gamma(\text{den}) = \gamma(\text{geo}) = \tan^{-1}[\sqrt{3}\,(\omega_y^{-2} - \omega_x^{-2})\ /(2\omega_z^{-2} - \omega_x^{-2} - \omega_y^{-2})] \approx \left(1 - 3\sqrt{\frac{5}{4\pi}}\beta\right)\gamma$ for β, $|\gamma| \ll 1$, which shows that the γ(geo) can be very different from $\gamma \equiv \gamma$(pot:HO) for larger $\beta \equiv \beta$(pot:HO) values. Similar differences are pointed out for the Nilsson and the Woods–Saxon potentials in [76]. Introducing $\epsilon = \sqrt{\frac{45}{16\pi}}\beta$ in place of β, we have

$$\gamma(\text{geo}) \approx (1 - 2\epsilon)\gamma(\text{pot:HO}) \approx \left(1 - \frac{3}{2}\epsilon\right)\gamma(\text{pot:Nils}) \approx \left(1 - \frac{8}{7}\epsilon\right)\gamma(\text{pot:WS}). \tag{A.1}$$

Strictly speaking, the ϵ is also different in each definition, but that is neglected here. The difference between γ(geo) and γ(pot) is largest for the (pot:HO)-parametrization among these three examples.

The deformed shape for the wobbling motion in the Lu isotopes is predicted to be $\epsilon \sim 0.4$ and $\gamma \sim 20°$ [68] in the (pot:Nils)-parametrization. Assuming purely ellipsoidal shape it leads to γ(geo) $\approx 11°$ [76], which is significantly smaller than the value 20°. The experimentally measured $B(E2)$ values seem to indicate γ(den) $\approx 20°$ or even larger values at higher spins [11]. In order to obtain γ(geo) $\approx$ γ(den) $\approx 20°$, γ(pot:Nils) $\approx 31°$ and γ(pot:HO) $\approx 36°$ are necessary with keeping ϵ(pot:Nils) ≈ 0.4. In the same way, assuming only the quadrupole deformation, γ(pot:WS) $\approx 28°$ is necessary with β(pot:WS) $\approx 0.4 \times \sqrt{\frac{16\pi}{45}}$. Thus the required values of the potential triaxiality parameters are considerably larger, which are not obtained in any TRS calculations. The situation is the same for the self-consistent mean-field calculation. For example, we obtain γ(den) $\approx 11°$ for ^{163}Lu by the cranked HFB calculation with the Gogny D1S force [94], which is consistent with the Nilsson TRS calculations. None of the microscopic calculations are able to reproduce the triaxiality of γ(den) $\approx 20°$, see also [82].

References

[1] Bohr A and Mottelson B R 1975 *Nuclear Structure, Vol. II* (New York: Benjamin)
[2] Anderson P W 1952 *Phys. Rev.* **86** 694–701
[3] Anderson P W 1958 *Phys. Rev.* **110** 827–35
[4] Anderson P W 1958 *Phys. Rev.* **112** 1900–16
[5] Nambu Y 1960 *Phys. Rev.* **117** 648–63
[6] Nambu Y and Jona-Lasinio G 1961 *Phys. Rev.* **122** 345–58
[7] Goldstone J 1961 *Nuovo Cimento (1955–1965)* **19** 154–64
[8] Shimizu Y R and Matsuyanagi K 1982 *Prog. Theor. Phys.* **67** 1637–40
[9] Mizutori S, Shimizu Y R and Matsuyanagi K 1990 *Prog. Theor. Phys.* **83** 666–70
[10] Nakatsukasa T, Matsuyanagi K, Mizutori S and Shimizu Y R 1996 *Phys. Rev.* C **53** 2213–26
[11] Shoji T and Shimizu Y R 2009 *Prog. Theor. Phys.* **121** 319–55
[12] Matsuzaki M, Shimizu Y R and Matsuyanagi K 1988 *Prog. Theor. Phys.* **79** 836–62
[13] Nakatsukasa T, Mizutori S and Matsuyanagi K 1993 *Prog. Theor. Phys.* **89** 847–54
[14] Matsuzaki M 2014 *Phys. Rev.* C **90** 044313
[15] Villars F M 1984 *Nucl. Phys.* A **420** 61–82
[16] Jahn H A and Teller E 1937 *Proc. R. Soc.* A **161** 220–35
[17] Berry M V 1984 *Proc. R. Soc.* A **392** 45–57
[18] Baranger M and Kumar K 1965 *Nucl. Phys.* **62** 113–32
[19] Kumar K and Baranger M 1968 *Nucl. Phys.* A **110** 529–54
[20] Bes D and Sorensen R A 1969 The pairing-plus-quadrupole model *Advances in Nuclear Physics* (*Adv. Phys. Part. Nucl.* vol 2) ed J Negele and E Vogt (New York: Plenum) p 129
[21] Brink D and Broglia R A 2005 *Nuclear Superfluidity, Pairing in Finite Systems* (Cambridge: Cambridge University Press)
[22] Ring P and Schuck P 1980 *The Nuclear Many-Body Problems* (*Texts and Monographs in Physics*) (New York: Springer)
[23] Yannouleas C and Landman U 2007 *Rep. Prog. Phys.* **70** 2067
[24] Brack M, Damgaard J, Jensen A S, Pauli H C, Strutinsky V M and Wong C Y 1972 *Rev. Mod. Phys.* **44** 320–405
[25] Butler P A and Nazarewicz W 1996 *Rev. Mod. Phys.* **68** 349–421
[26] Frisk H 1990 *Nucl. Phys.* A **511** 309–23
[27] Tajima N and Suzuki N 2001 *Phys. Rev.* C **64** 037301
[28] Hamamoto I and Mottelson B R 2009 *Phys. Rev.* C **79** 034317
[29] Takahara S, Onishi N, Shimizu Y R and Tajima N 2011 *Phys. Lett.* B **702** 429–32
[30] Arita K i 2012 *Phys. Rev.* C **86** 034317
[31] Lister C J *et al* 1987 *Phys. Rev. Lett.* **59** 1270–3
[32] Swiatecki W 1982 *Nucl. Phys.* A **376** 275–91
[33] Heyde K and Wood J L 2011 *Rev. Mod. Phys.* **83** 1467–521
[34] Shimizu Y R and Matsuyanagi K 1984 *Prog. Theor. Phys.* **71** 960–72
[35] Pekker D and Varma C 2015 *Ann. Rev. Condens. Matter Phys.* **6** 269–97
[36] Garrett P E 2001 *J. Phys. G: Nucl. Part. Phys.* **27** R1
[37] Matsuzaki M and Ueno T 2016 *Prog. Theor. Exp. Phys.* **2016** 043D03
[38] Harakeh M N and van der Woude A 2001 *Giant Resonances Oxford Studies in Nuclear Physics* (Oxford: Oxford University Press) p 24
[39] Blaizot J P and Ripka G 1986 *Quantum Theory of Finite Systems* (Cambridge, MA: MIT Press)
[40] Shimizu Y R and Nakatsukasa T 1996 *Nucl. Phys.* A **611** 22–46
[41] Marshalek E 1976 *Nucl. Phys.* A **266** 317–36
[42] Marshalek E 1977 *Nucl. Phys.* A **275** 416–44
[43] Nakatsukasa T and Shimizu Y R 1999 *J. Phys. G: Nucl. Part. Phys.* **25** 795–7
[44] Martin M J 2013 *Nucl. Data Sheets* **114** 1497–847

[45] Reich C W 2009 *Nucl. Data Sheets* **110** 2257–532
[46] Reich C W 2012 *Nucl. Data Sheets* **113** 2537–840
[47] Helmer R G 2004 *Nucl. Data Sheets* **101** 325–519
[48] Reich C W 2005 *Nucl. Data Sheets* **105** 557–774
[49] Hinohara N, Nakatsukasa T, Matsuo M and Matsuyanagi K 2009 *Phys. Rev.* C **80** 014305
[50] Hinohara N, Sato K, Nakatsukasa T, Matsuo M and Matsuyanagi K 2010 *Phys. Rev.* C **82** 064313
[51] Hinohara N, Sato K, Yoshida K, Nakatsukasa T, Matsuo M and Matsuyanagi K 2011 *Phys. Rev.* C **84** 061302
[52] McGowan F K and Milner W T 1981 *Phys. Rev.* C **23** 1926–37
[53] Nakatsukasa T and Shimizu Y R 1997 *Prog. Part. Nucl. Phys.* **38** 247–8
[54] Bengtsson R and Frauendorf S 1979 *Nucl. Phys.* A **327** 139–71
[55] Ward D *et al* 1996 *Nucl. Phys.* A **600** 88–110
[56] Nakatsukasa T 1996 *Acta Phys. Pol.* B **27** 59–70
[57] Hackman G *et al* 1997 *Phys. Rev. Lett.* **79** 4100–3
[58] Roßbach D *et al* 2001 *Phys. Lett.* B **513** 9–14
[59] Wilson A *et al* 1996 *Phys. Rev.* C **54** 559–67
[60] Korichi A *et al* 2001 *Phys. Rev. Lett.* **86** 2746–9
[61] Nakatsukasa T, Matsuyanagi K, Mizutori S and Nazarewicz W 1995 *Phys. Lett.* B **343** 19–24
[62] Lauritsen T *et al* 2002 *Phys. Rev. Lett.* **88** 042501
[63] Lauritsen T *et al* 2002 *Phys. Rev. Lett.* **89** 282501
[64] Mizutori S, Nakatsukasa T, Arita K, Shimizu Y R and Matsuyanagi K 1993 *Nucl. Phys.* A **557** 125c–144c
[65] Nakatsukasa T, Mizutori S and Matsuyanagi K 1992 *Prog. Theor. Phys.* **87** 607–26
[66] Ødegård S W *et al* 2001 *Phys. Rev. Lett.* **86** 5866–9
[67] Jensen D R *et al* 2002 *Phys. Rev. Lett.* **89** 142503
[68] Görgen A *et al* 2004 *Phys. Rev.* C **69** 031301
[69] Shoji T and Shimizu Y R 2006 *Int. J. Mod. Phys.* E **15** 1407–16
[70] Andersson G *et al* 1976 *Nucl. Phys.* A **268** 205–56
[71] Marshalek E 1979 *Nucl. Phys.* A **331** 429–63
[72] Matsuzaki M 1990 *Nucl. Phys.* A **509** 269–86
[73] Shimizu Y R and Matsuzaki M 1995 *Nucl. Phys.* A **588** 559–96
[74] Matsuzaki M, Shimizu Y R and Matsuyanagi K 2002 *Phys. Rev.* C **65** 041303
[75] Matsuzaki M, Shimizu Y R and Matsuyanagi K 2004 *Phys. Rev.* C **69** 034325
[76] Shimizu Y R, Shoji T and Matsuzaki M 2008 *Phys. Rev.* C **77** 024319
[77] Bohr A and Mottelson B R 1981 *Phys. Scr.* **24** 71
[78] Frauendorf S and Dönau F 2014 *Phys. Rev.* C **89** 014322
[79] Shimizu Y R, Matsuzaki M and Matsuyanagi K 2004 Microscopic study of wobbling motions in Hf and Lu nuclei *Proc. 5th Japan–China Joint Nuclear Physics Symp. (Fukuoka, Japan)* pp 317–26 (arXiv:nucl-th/0404063)
[80] Hamamoto I and Hagemann G B 2003 *Phys. Rev.* C **67** 014319
[81] Sugawara-Tanabe K and Tanabe K 2010 *Phys. Rev.* C **82** 051303
[82] Frauendorf S and Dönau F 2015 *Phys. Rev.* C **92** 064306
[83] de Voigt M J A, Dudek J and Szymański Z 1983 *Rev. Mod. Phys.* **55** 949–1046
[84] Shimizu Y R, Matsuzaki M and Matsuyanagi K 2005 *Phys. Rev.* C **72** 014306
[85] Faessler A and Ploszajczak M 1977 *Phys. Rev.* C **16** 2032–8
[86] Kurasawa H 1980 *Prog. Theor. Phys.* **64** 2055–75
[87] Kurasawa H 1982 *Prog. Theor. Phys.* **68** 1594–607
[88] Andersson C, Krumlinde J, Leander G and Szymaski Z 1981 *Nucl. Phys.* A **361** 147–78
[89] Skalski J 1987 *Nucl. Phys.* A **473** 40–60
[90] Frauendorf S, Neergård K, Sheikh J A and Walker P M 2000 *Phys. Rev.* C **61** 064324
[91] Shoji T 2009 *PhD Thesis* Department of Physics, Kyushu University
[92] Ichikawa T, Matsuyanagi K, Maruhn J A and Itagaki N 2014 *Phys. Rev.* C **90** 034314
[93] Hasse R W and Myers W D 1988 *Geometrical Relationships of Macroscopic Nuclear Physics* (Berlin: Springer)
[94] Shimada M 2016 *PhD Thesis* Department of Physics, Kyushu University

Time-dependent density-functional description of nuclear dynamics

Takashi Nakatsukasa

Center for Computational Sciences,University of Tsukuba,Tsukuba 305-8577,Japan
RIKEN Nishina Center,2-1 Hirosawa,Wako 351-0198,Japan

Kenichi Matsuyanagi

RIKEN Nishina Center,2-1 Hirosawa,Wako 351-0198,Japan
Yukawa Institute for Theoretical Physics,Kyoto University,Kyoto 606-8502,Japan

Masayuki Matsuo

Department of Physics,Faculty of Science,Niigata University,Niigata 950-2181,Japan

Kazuhiro Yabana

Center for Computational Sciences,University of Tsukuba,Tsukuba 305-8577,Japan

We present the basic concepts and recent developments in the time-dependent density functional theory (TDDFT) for describing nuclear dynamics at low energy. The symmetry breaking is inherent in nuclear energy density functionals (EDFs), which provides a practical description of important correlations at the ground state. Properties of elementary modes of excitation are strongly influenced by the symmetry breaking and can be studied with TDDFT. In particular, a number of recent developments in the linear response calculation have demonstrated their usefulness in description of collective modes of excitation in nuclei. Unrestricted real-time calculations have also become available in recent years, with new developments for quantitative description of nuclear collision phenomena. There are, however, limitations in the real-time approach; for instance, it cannot describe the many-body quantum tunneling. Thus, we treat the quantum fluctuations associated with slow collective motions assuming that time evolution of densities are determined by a few collective coordinates and momenta. The concept of collective submanifold is introduced in the phase space associated with the TDDFT and used to quantize the collective dynamics. Selected applications are presented to demonstrate the usefulness and quality of the new approaches. Finally, conceptual differences between nuclear and electronic TDDFT are discussed, with some recent applications to studies of electron dynamics in the linear response and under a strong laser field.

CONTENTS

I. INTRODUCTION

A. Scope of the present review

In the study of strongly correlated many-particle systems, a fundamental challenge is to find basic properties of a variety of elementary modes of excitation, and to identify the degrees of freedom that are suitable for describing the collective phenomena. The collective motion in such complex systems, with an ample supply of experimental data and theoretical study, may often lead to deeper insight into the basic concepts of quantum many-body physics.

Among a variety of many-particle systems in the universe, the nucleus provides a unique opportunity to investigate fundamental aspects of the quantum many-body problems. The nucleus is a self-bound system with finite number of fermionic particles, called nucleons, which have the isospin degrees of freedom, $(t = 1/2)$, in addition to the intrinsic spin $(s = 1/2)$. The strong interplay between the collective and single-particle degrees of freedom plays important roles in nuclei, which produces a rich variety of unique phenomena. A prominent example of the consequence of this coupling is given by the manifestation of nuclear deformation and rotational spectra. Is is also closely related with the damping and particle decay of the collective motion, the particle transfer in the heavy-ion collision, and the dissipation process in the nuclear fission. In fact, the coupling between the single-particle motion and collective motion is a key issue in nuclear structure. It is the basic idea behind the unified model of nuclei (Bohr and Mottelson, 1969, 1975), in which the collective motion is described by a shape change of the average one-body nuclear potential. It is easy to see that the basic concept of the unified model is similar to that of the mean-field theory. We therefore expect that the mean-field theory may provide a microscopic description of the phenomena described above, although it is limited to the one-body dynamics.

The self-consistent mean-field models for nuclei are currently a leading theory for describing properties of heavy nuclei (Bender *et al.*, 2003; Lunney *et al.*, 2003). They self-consistently determine the nuclear one-body mean-field potential, starting from effective energy density functionals (EDF). They are capable of describing almost all nuclei, including infinite nuclear matter, with a single universal EDF. The concept is very similar to the density functional theory (DFT) in electronic systems, utilized in atomic, molecular, and solid state physics. Major conceptual difference is that, for the isolated finite nucleus, all the currently available nuclear DFT models are designed to reproduce the *intrinsic* ground state. The self-consistent solution produces a density distribution which spontaneously violates symmetries of the system, such as translational, rotational, and gauge symmetries. This feature has advantages and disadvantages. The spontaneous breaking of symmetries (SSB) provides us with an intuitive explanation of a variety of nuclear phenomena. A typical example is the observed rotational spectra as a consequence of the intrinsic density deformation. On the other hand, when the symmetries are restored in finite nuclei, an additional correlation energy is generated. A question arises then, concerning whether all the correlation energy should be included in the EDF or not. We do not think this issue is completely set-

tled yet. (Nevertheless, there are also attempts to justify the use of symmetry-violating (wave-packet) densities in a rigorous sense, which we will present in Sec. II.) Perhaps, because of this unsettled problem, it is common to use terminologies of the mean-field theory, such as the time-dependent Hartree-Fock (TDHF) equations, instead of the time-dependent Kohn-Sham (TDKS) equations. In this article, we mainly use the DFT terminologies, since the naive mean-field theory is not applicable to nuclear systems, due to a strong two-body correlations (Sec. VI.A). Moreover, the mean-field calculation with a density-independent (state-independent) interaction cannot account for the nuclear saturation properties (Sec. I.B).

An extension of the DFT to the time-dependent DFT (TDDFT) provides a feasible description of many-body dynamics, which contains information on excited states in addition to the ground state. The TDDFT and its KS scheme are formally justified by the one-to-one correspondence between the time-dependent density and time-dependent external potential, assuming the v-representability (Runge and Gross, 1984). The TDDFT has vast applications to quantum phenomena in many-body systems. In nuclear physics applications, there exist extensive studies in simulation of the heavy-ion collision dynamics, especially of nuclear fusion and deep inelastic scattering (Negele, 1982). Ultimately, the nuclear TDDFT aims at describing nuclear excitations with different characters, such as vibration, rotation, and clustering, nuclear reactions of many kinds, such as fusion/fission, particle transfer, fragmentation, and even collective excitations in the crust and the interior of neutron stars.

One of the most extensively studied area of the nuclear TDDFT is small amplitude vibrations or linear response to external perturbations. This is a perturbative regime of the TDDFT, but it provides a powerful method to explore a variety of modes of excitation in nuclei. Many kinds of approaches to the linear response calculations have been developed and will be presented in Sec. III. In addition to the conventional matrix formalism, we present some recent developments, such as the finite amplitude method and the Green's function method for the quasiparticle formalism with finite pair densities.

It is of significant interest and challenge to go beyond the perturbative regime. Nuclei show numerous phenomena related to the large amplitude collective motion. In particular, nuclear reactions involving collective and non-collective dynamics of many nucleons are extensively studied using the real-time calculations in the past. In Sec. IV, we show some recent developments and applications. A recent review articles on the real-time approaches in normal (Simenel, 2012) and superfluid systems (Bulgac, 2013), may be supplementary to the present review. It is also of great interest to study the strong quantum nature of large amplitude collective motion, such as spontaneous fission, shape transition, shape coexistence, anharmonic vibrations, and so on. For these phenomena, the real-time simulation of the TDDFT is not directly applicable to the problems. In most cases, we need requantization of the TDDFT dynamics. The requantization of TDHF and the imaginary-time TDHF for classically forbidden dynamics were previously discussed in another review paper in great details (Negele, 1982). Unfortunately, the method has not been applied to realistic problems, due to number of difficulties, such as finding suitable periodic orbits to quantize (Baranger *et al.*, 2003). We present, in Sec. V, an alternative theory to identify an optimal collective submanifold in the TDDFT phase space. Consequently, with a small number of canonical variables, it is much more practical to quantize the collective dynamics.

Since the DFT and TDDFT are commonly adopted in many domains of quantum many-body systems, current problems and new ideas in other fields are of significant interest. Similarly to nuclear physics, there are linear response TDDFT calculations and TDDFT for large amplitude motion as an initial value problem. However, it should be noted that there are conceptual and qualitative differences of EDFs between nuclear and electronic DFT/TDDFT. These issues will be discussed in Sec. VI.

We try to make the present review somewhat pedagogical and tractable for non-practitioners, to explain essential elements of the theories. For more details, readers should be referred to literature.

B. Saturation and the mean-field picture

The saturation is a fundamental property of the nuclear system, that is analogous to the liquid. The volume and total binding energy of observed nuclei in nature are approximately proportional to the mass number A. Extrapolating the observed property to the infinite nuclear matter with neglect of the Coulomb interaction, the nuclear matter should have an equilibrium state with $\rho_0 \approx 0.17$ fm^{-3} and $B/A \approx 16$ MeV, at zero pressure and zero temperature. The empirical mass formula of Bethe and Weizsäcker (Bethe and Bacher, 1936; Weizsäcker, 1935), which is based on this liquid drop picture of nuclei, well accounts of the bulk part of the nuclear binding.

In contrast, there are many evidences pointing to the fact that the mean-free path of nucleons is larger than the size of nucleus. The great success of the nuclear shell model (Mayer and Jensen, 1955), in which nucleons are assumed to move independently inside an average one-body potential, gives one of them. The scattering experiments with incident neutrons and protons provide more quantified information on the mean-free path. In fact, the mean free path depends on the nucleon's energy, and becomes larger for lower energy (Bohr and Mottelson, 1969). Therefore, it is natural to assume that the nu-

cleus can be primarily approximated by the independent-particle model with an average one-body potential. For the symmetric nuclear matter, this approximation leads to the degenerate Fermi gas of the same number of protons and neutrons ($Z = N = A/2$). The observed saturation density of $\rho_0 \approx 0.17$ fm^{-3} gives the Fermi momentum, $k_F \approx 1.36$ fm^{-1}, which corresponds to the Fermi energy (the maximum kinetic energy), $T_F = k_F^2/2m \approx 40$ MeV.

The justification of the independent-particle motion encourage us to investigate the mean-field models of nuclei. However, the naive mean-field models cannot properly describe the nuclear saturation property. Here, the "naive" mean-field models mean those using any kind of state-independent two-body interactions. This has been known for many years (Bohr and Mottelson, 1969). Since it contains useful insights and relations to the nuclear DFT, let us explain the essential point. It is easy to consider the uniform nuclear matter with a constant attractive "mean-field" potential $V < 0$. The constancy of B/A means that it is equal to the separation energy of nucleons, S. In the Fermi-gas model, it is estimated as

$$S \approx B/A \approx -(T_F + V). \tag{1}$$

Since the binding energy is $B/A \approx 16$ MeV, the potential V is about -56 MeV. It should be noted that the relatively small separation energy is the consequence of the significant cancellation between the kinetic and the potential energies. This indicates that the nucleus has a strong quantum nature. In the mean-field theory, the total (binding) energy is given by

$$-B = \sum_{i=1}^{A} \left(T_i + \frac{V}{2} \right) = A \left(\frac{3}{5} T_F + \frac{V}{2} \right), \tag{2}$$

where we assume that the average potential results from a two-body interaction. The two kinds of expressions for B/A, Eqs. (1) and (2), lead to $T_F \approx -5V/4 \approx 70$ MeV, which is different from the previously estimated value (~ 40 MeV). Moreover, the negative separation energy ($T_F + V > 0$) contradicts the fact that the nucleus is bound! The presence of a three-body interaction may change this argument. However, solving the present contradiction would require an unrealistically strong three-body repulsive effect whose magnitude is comparable to that of the attractive two-body interaction.

To reconcile the independent-particle motion with the saturation property of the nucleus, the nuclear average potential must be state dependent. Allowing the potential V_i to depend on the state i, the potential V should be replaced by that for the highest occupied orbital V_F in Eq. (1), and by its average value $\langle V \rangle$ in the right-hand side of Eq. (2). Then, we obtain the following relation:

$$V_F \approx \langle V \rangle + T_F/5 + B/A. \tag{3}$$

The potential V_F is shallower than its average value $\langle V \rangle$. Weisskopf (1957) suggested the momentum-dependent potential V, which can be expressed in terms of an effective mass m^*:

$$V_i = U_0 + U_1 \frac{k_i^2}{k_F^2}. \tag{4}$$

In fact, the non-local mean-field potential can be expressed by the momentum dependence (Ring and Schuck, 1980). Equation (4) leads to the effective mass, $m^*/m = (1 + U_1/T_F)^{-1}$. Using Eqs. (1), (3), and (4), we obtain the effective mass given by

$$\frac{m^*}{m} = \left\{ \frac{3}{2} + \frac{5}{2} \frac{B}{A} \frac{1}{T_F} \right\}^{-1} \approx 0.4. \tag{5}$$

Quantitatively, this value disagrees with the experimental data. Although the empirical values of the effective mass vary according to the energy of nucleons, $0.7 \lesssim m^*/m \lesssim 1$, they are almost twice larger than the value of Eq. (5). Furthermore, the total energy, Eq. (2), is written as

$$-B = \frac{1}{2} \sum_{i=1}^{A} (T_i + \epsilon_i), \tag{6}$$

where ϵ_i are single-particle energies. Within the constraint of Eq. (6), it is impossible to reproduce both the total binding energy and the single-particle spectra observed in experiments. As far as we use a normal two-body interaction, these discrepancies should be present in the mean-field calculation with any interaction, because Eqs. (5) and (6) are valid in general for a saturated self-bound system. Therefore, the naive mean-field models have a fundamental difficulty to describe the nuclear saturation.

The DFT provides a practical solution to this problem, in which we start from an EDF, $E[\rho]$, instead of the interaction. The KS field is calculated as $h[\rho] = \partial E/\partial \rho$, which may contain the non-trivial density dependence different from that of the mean-field theory starting from the interaction. In nuclear physics, this additional density dependence was introduced by the density-dependent effective interaction, thus, it was called "density-dependent Hartree-Fock" (DDHF) method (Negele, 1970). In this terminology, the variation of the total energy with respect to the density contains re-arrangement potential, $\partial V_{\rm eff}[\rho]/\partial \rho$, which comes from the density dependence of the effective force $V_{\rm eff}[\rho]$. These terms are crucial to obtain the saturation and to provide a consistent independent-particle description of nuclei.

C. Symmetry breaking and restoration by the Anderson-Nambu-Goldstone (ANG) modes

One of the prominent features in the nuclear EDF approaches is the appearance of the SSB. For the system of

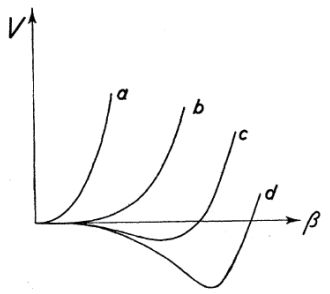

FIG. 1 Sketch of potential energy curves as functions of deformation parameter β. The curve a corresponds to spherical nuclei, b and c correspond to transitional nuclei, and d to well deformed nuclei. From Alder *et al.* (1956).

a small number of particles, such as nuclei, the SSB is hidden. The experimental measurements probe the states which preserve the symmetries of the original Hamiltonian. In nuclear physics, the state with a broken symmetry is often called "intrinsic" state. Nevertheless, we clearly observe a number of nuclear phenomena associated with effects of the SSB, both in the ground-state properties and in excitation spectra. In nuclear physics, this was realized in 1950's, soon after the experimental identification of the characteristic patterns of rotational spectra. Figure 1 is taken from a seminal review paper on the Coulomb excitation (Alder *et al.*, 1956). The nuclear potential energy function clearly indicates the nuclear deformation as the phase transition involving the SSB. The SSB in small finite-size systems has been an important concept in nuclear physics and chemistry for many years, and has become so in fields of quantum dots and ultracold atoms (Yannouleas and Landman, 2007).

The symmetry restoration is a quantum fluctuation effect. When the spontaneous breaking of the continuous symmetry occurs, there exists the Anderson-Nambu-Goldstone (ANG) modes, to restore the broken symmetry (Anderson, 1958, 1963; Goldstone, 1961; Nambu, 1960). This symmetry restoration process is extremely slow for macroscopic objects, thus, the SSB is realized in a rigorous sense. In other words, the quantum fluctuation associated with the ANG mode is negligibly small in those cases. If the deformed nucleus with extremely heavy mass ($A \to \infty$) existed, the moment of inertia $\mathcal{J}$ should be macroscopically large. Then, the excitation spectra of this heavy rotor would be nearly degenerate with the ground state, $E_I = I(I+1)/2\mathcal{J}$ for the state with the total angular momentum I, leading to a stable deformed wave packet. In reality, the restoration of the rotational symmetry even in heaviest nuclei takes place much faster than the shortest time resolution we can achieve with the present experimental technologies. In this sense, the SSB in nuclei is hidden. Nevertheless, the nucleonic motion is strongly influenced by the SSB, since the time scale of the symmetry restoration, $\tau_{\rm SSB}$, is much longer than the periodic time of single-particle motion in the nucleus of radius R, $\tau_F = R/v_F \sim 10^{-22}$ s. This is schematically illustrated in Fig. 2. We believe that it is important to distinguish these two types of correlations in nuclei, those of relatively short time scales $\tau \sim \tau_F$ (*"fast" motion*), and of long time scales $\tau \sim \tau_{\rm SSB}$ (*"slow" motion*).

The nuclear superfluidity can be understood exactly in an analogous way, as the SSB leading to the deformation in the gauge space (Brink and Broglia, 2005). The condensate of the nucleonic Cooper pairs is expressed as an intrinsic deformation in the magnitude of the pair field. The pair field creates and annihilates the pairs of nucleons giving rise to the quasiparticles that are superpositions of particles and holes, expressed by the Bogoliubov transformation. The ANG mode, called pair rotation, corresponds to the addition and removal of the nucleon pairs from the pair condensate. In this case, the "angular momentum" in the gauge space corresponds to the particle number, and the "moment of inertia" is defined by the second derivative of the ground-state energy with respect to the particle number, $\mathcal{J}_{\rm pair} = (d^2E_N/dN^2)^{-1}$. See also Sec. III.B.

Since the broken symmetry is restored by the quantum fluctuation, its time scale $\tau_{\rm SSB}$ can be estimated by the uncertainty principle. The time is proportional to the moment of inertia $\mathcal{J}$ as $\tau_{\rm SSB} \sim \mathcal{J}/\hbar$, which amounts to $10^{-20} - 10^{-19}$ s for typical deformed nuclei in the rare-earth and the actinide regions. Thus, the symmetry restoration is a slow motion, compared to the nucleonic Fermi motion. Here, it is important to distinguish this time scale of the "quantum" fluctuation from that of the "classical" rotation, $\omega_{\rm rot}^{-1} \approx \mathcal{J}/I$. The latter could be comparable to τ_F at very high spin (large I), however, the concept of the deformation (symmetry breaking) still holds. For the pair rotation, using an observed value of the moment of inertia for the pair rotation in Sn isotopes (Brink and Broglia, 2005), $\tau_{\rm SSB}$ for the symmetry breaking in the gauge space can be given by $\tau_{\rm SSB} = 10^{-21} - 10^{-20}$ s.

These concepts of SSB are invoked in the nuclear DFT and TDDFT. The symmetry restoration can be treated either by the projection method or by the (time-dependent) large-amplitude collective motion of the ANG modes (Ring and Schuck, 1980). In the present review, we mainly discuss the latter treatment with the time-dependent description.

II. BASIC FORMALISM: DFT AND TDDFT

The DFT describes a many-particle system exactly in terms of its local one-body density $\rho(\vec{r})$ alone. The DFT is based on the original theorem of Hohenberg and Kohn (HK) (Hohenberg and Kohn, 1964) which was proved for the ground-state of the many-particle system. Every ob-

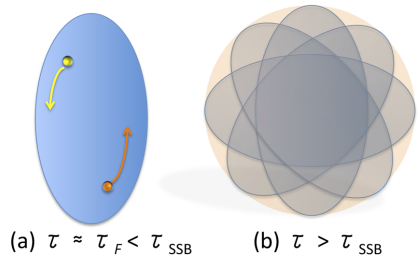

FIG. 2 (Color online) Illustration of deformed nuclei in different time scales, (a) shorter than the symmetry restoring time $\tau_{\rm SSB}$, and (b) larger than $\tau_{\rm SSB}$.

servable can be written, in principle, as a functional of density.

In nuclear physics, as is discussed in Sec. I.C, many kinds of SSB takes place without an external potential. In fact, the minimization of the nuclear EDF for finite nuclei always produces a localized density profile, which spontaneously violates the translational symmetry. Furthermore, it often violates the rotational symmetry in the real space and the gauge space. The SSB enables us to introduce an intrinsic (wave-packet) state. A possible justification of the DFT for the intrinsic state is presented in Sec. II.B.

For finite many-fermion systems, the shell effects associated with the quantum nature of the Fermi motion play a major role to determine the ground state. The KS scheme (Kohn and Sham, 1965) gives a practical treatment of the shell effects in the density functional. This is presented in Sec. II.C

The DFT is designed for calculating the ground-state properties. For excited-state properties and reactions, the TDDFT is a powerful and useful tool. The basic theorem for the TDDFT has been developed as an exact theorem (Runge and Gross, 1984), similar to the HK theorem in the static case. This is reviewed in Sec. II.D.

Both the DFT and TDDFT have been extended to the superconductors, introducing an external pair-removal and pair-addition potential (Oliveira *et al.*, 1988; Wacker *et al.*, 1994). These extensions are relevant to nuclear physics as well, to account for various properties of heavy open-shell nuclei. In this article, we call them "superconducting nuclei" or "nuclear superfluidity". Properties of the (time-dependent) Bogoliubov-de-Gennes equations will be presented in Secs. II.C and II.D.

A. Nuclear EDF models

Before presenting the theorem of DFT, we recapitulate basic equations of nuclear EDF models and their properties (Bender *et al.*, 2003; Blaizot and Ripka, 1986; Ring and Schuck, 1980).

1. Basic equations

To simplify the discussion, we assume that the EDF $F[\rho]$, which represents the total energy of the nucleus, is a functional of local density $\rho(\vec{r})$ without the spin-orbit coupling. The KS equations read with the spin index $\sigma = (\uparrow, \downarrow)$,

$$\left(-\frac{1}{2m}\nabla^2 + v_s(\vec{r})\right)\varphi_i(\vec{r}\sigma) = \epsilon_i\varphi_i(\vec{r}\sigma). \tag{7}$$

Hereafter, we use the unit $\hbar = 1$. We decompose $F[\rho]$ into two parts, $F[\rho] = T_s[\rho] + E_c[\rho]$, where $T_s[\rho] = \sum_{i=1}^{N}\langle\varphi_i|\left(-\frac{1}{2m}\nabla^2\right)|\varphi_i\rangle$ and the rest $E_c[\rho]$. The KS potential is defined by $v_s(\vec{r}) = \delta E_c/\delta\rho(\vec{r})$. The density is given by summing up the KS orbitals,

$$\rho(\vec{r}) = \sum_{\sigma}\sum_{i=1}^{N}|\varphi_i(\vec{r}\sigma)|^2. \tag{8}$$

When we take into account the nuclear superfluidity, we adopt an EDF which is a functional of ρ and (κ, κ^*), including the pair tensor $\kappa(\vec{r}, \vec{r'})$ whose definition (20) requires a symmetry-broken wave-packet state in Sec. II.B. If the EDF depends only on their diagonal parts (pair density $\kappa(\vec{r})$), $F[\rho, \kappa] = T_s[\rho, \kappa] + E_c[\rho, \kappa]$, Eq. (7) should be extended to the Bogoliubov-de-Gennes-KS (BdGKS) equations:

$$\begin{aligned}\sum_{\sigma'}\begin{pmatrix}(h_s(\vec{r})-\mu)\delta_{\sigma\sigma'} & \Delta_s(\vec{r})\gamma_{\sigma\sigma'}\\ -\Delta_s^*(\vec{r})\gamma_{\sigma\sigma'} & -(h_s(\vec{r})-\mu)^*\delta_{\sigma\sigma'}\end{pmatrix}\\ \times\begin{pmatrix}U_i(\vec{r}\sigma')\\ V_i(\vec{r}\sigma')\end{pmatrix} = E_i\begin{pmatrix}U_i(\vec{r}\sigma)\\ V_i(\vec{r}\sigma)\end{pmatrix},\end{aligned} \tag{9}$$

where $h_s(\vec{r}) \equiv -\nabla^2/(2m) + v_s(\vec{r})$, $\gamma_{\uparrow\downarrow} = -\gamma_{\downarrow\uparrow} = 1$, and $\gamma_{\uparrow\uparrow} = \gamma_{\downarrow\downarrow} = 0$. The chemical potential μ is introduced to control the total particle number. The potentials, $v_s(\vec{r})$ and $\Delta_s(\vec{r})$, are respectively defined by

$$v_s(\vec{r}) = \frac{\delta E_c}{\delta\rho(\vec{r})}, \qquad \Delta_s(\vec{r}) = \frac{\delta E_c}{\delta\kappa^*(\vec{r})}. \tag{10}$$

The normal and pair densities are given by $\rho(\vec{r}) = \sum_\sigma\sum_i|V_i(\vec{r}\sigma)|^2$ and $\kappa(\vec{r}) = \sum_i V_i^*(\vec{r}\uparrow)U_i(\vec{r}\downarrow)$, where the summation with respect to i is taken over all the states with positive quasiparticle energies, $E_i > 0$. The same convention is assumed in this article.

In nuclear physics, Eqs. (7) and (9) are often called Hartree-Fock (HF) and Hartree-Fock-Bogoliubov (HFB) equations, respectively[1]. Accordingly, the quasiparticle vacuum, $|\phi_0\rangle$, is introduced and called HFB ground state, where the Bogoliubov transformation

$$\hat{\psi}(\vec{r}\sigma) = \sum_i\left\{U_i(\vec{r}\sigma)a_i + V_i^*(\vec{r}\sigma)a_i^\dagger\right\}, \tag{11}$$

[1] The time-dependent equations are also called TDHF (TDHFB) in nuclear physics, instead of TDKS (TDBdGKS).

defines the quasiparticle annihilation and creation operators, $(a_i, a_i^\dagger)$, with the vacuum condition

$$a_i|\phi_0\rangle = 0. \tag{12}$$

These mean-field terminologies are due to practical usage of effective density-dependent interaction. The EDF is provided by the expectation value of the effective Hamiltonian at $|\phi_0\rangle$, $F[\rho,\kappa] = \langle\phi_0|\hat{H} - \mu\hat{N}|\phi_0\rangle$. The variation, $\delta(F[\rho,\kappa] - \mu\int\rho(\vec{r})d\vec{r}) = 0$, leads to Eqs. (7) and (9).

2. Properties of BdGKS equations and useful notations

Solutions of the BdGKS (HFB) equations (9) are *paired* in the following sense: For each quasiparticle eigenstate with Ψ_i^0 with a positive eigenvalue E_i, there exists a partner eigenstate, $\tilde{\Psi}_i^0$ with the negative energy $-E_i$.

$$\Psi_i^0 = \begin{pmatrix} U_i \\ V_i \end{pmatrix}, \quad \tilde{\Psi}_i^0 = \begin{pmatrix} V_i^* \\ U_i^* \end{pmatrix}.$$

Introducing the collective notation of the quasiparticles with positive [negative] energies at the ground state $\Psi^0 = (\Psi_1^0, \Psi_2^0, \cdots)$ $[\tilde{\Psi}^0 = (\tilde{\Psi}_1^0, \tilde{\Psi}_2^0, \cdots)]$, the orthonormal and completeness relations are equivalent to the unitarity condition, $\mathcal{W}\mathcal{W}^\dagger = \mathcal{W}^\dagger\mathcal{W} = 1$, of the matrix

$$\mathcal{W} \equiv \begin{pmatrix} \Psi^0 & \tilde{\Psi}^0 \end{pmatrix} = \begin{pmatrix} U_1 & U_2 \cdots & V_1^* & V_2^* & \cdots \\ V_1 & V_2 \cdots & U_1^* & U_2^* & \cdots \end{pmatrix}.$$

The generalized density matrix R^0 is defined as

$$R^0 = \begin{pmatrix} \rho & \kappa \\ -\kappa^* & 1-\rho^* \end{pmatrix} = 1 - \Psi^0\Psi^{0\dagger} = \tilde{\Psi}^0\tilde{\Psi}^{0\dagger}, \tag{13}$$

which is Hermitian and idempotent ($(R^0)^2 = R^0$). The orthonormal property immediately gives

$$R^0\Psi_i^0 = 0, \quad R^0\tilde{\Psi}_i^0 = \tilde{\Psi}_i^0. \tag{14}$$

The BdGKS equations can be rewritten in terms of R as

$$\left[H_s[R^0], R^0\right] = 0, \tag{15}$$

where $H_s[R^0]$ is the BdGKS (or HFB) Hamiltonian in the left hand side of Eq. (9).

Any unitary transformation among the quasiparticles, $a_i' = \sum U_{ij}a_j$, keeps R^0 (ρ,κ) invariant. The quasiparticles defined by Eq. (9) gives one choice of the gauge ("quasiparticle representation"). Another common choice is called "canonical representation", in which the density matrix ρ is diagonal. Note that Eqs. (13), (14), and (15) are all independent of the choice of the gauge.

In Sec. II.A.1, we used the coordinate-space representation $(\vec{r},\sigma)$, and have assumed that the density functional $E_c[\rho,\kappa]$ depends only on the diagonal densities $(\rho(\vec{r}),\kappa(\vec{r}))$ without spin dependence. It can be easily generalized to other representation $(\alpha,\beta,\cdots)$ and to functionals of density matrices in general; Hermitian $\rho_{\alpha\beta}$ and anti-symmetric $\kappa_{\alpha\beta}$. The potentials are given by

$$v_s(\alpha\beta) = \left.\frac{\delta E_c}{\delta\rho_{\beta\alpha}}\right|_{R^0}, \quad \Delta_s(\alpha\beta) = -\left.\frac{\delta E_c}{\delta\kappa^*_{\beta\alpha}}\right|_{R^0}.$$

Then, the BdGKS Hamiltonian can be written as

$$H_s[R^0](\alpha'\beta') = \left.\frac{\delta F}{\delta R_{\beta'\alpha'}}\right|_{R^0}, \tag{16}$$

where $F[R] = T_s[R] + E_c[R]$. Here, we have introduced the *primed* indices, which are double the dimension. Let the dimension of the single-particle space be d, then the *unprimed* index runs over $\alpha = 1, \cdots, d$, while the *primed* one $\alpha' = 1, \cdots, 2d$.

It is not necessary, but often useful to introduce the generalized Slater determinant (quasiparticle vacuum) $|\phi\rangle$, defined by $a_i|\phi\rangle = 0$. Then, we may denote R^0 as

$$R^0_{\alpha'\beta'} = \langle\phi|\begin{pmatrix} \hat{\psi}_\beta^\dagger\hat{\psi}_\alpha & \hat{\psi}_\beta\hat{\psi}_\alpha \\ \hat{\psi}_\beta^\dagger\hat{\psi}_\alpha^\dagger & \hat{\psi}_\beta\hat{\psi}_\alpha^\dagger \end{pmatrix}|\phi\rangle.$$

A one-body operator $\hat{O}$ can be written in a form

$$\begin{aligned}\hat{O} &= \sum_{\alpha\beta}\left[f_{\alpha\beta}\hat{\psi}_\alpha^\dagger\hat{\psi}_\beta + \frac{1}{2}\left\{g_{\alpha\beta}\hat{\psi}_\alpha^\dagger\hat{\psi}_\beta^\dagger + g'_{\alpha\beta}\hat{\psi}_\alpha\hat{\psi}_\beta\right\}\right] \\ &= \text{const.} + \frac{1}{2}\begin{pmatrix}\hat{\psi}^\dagger & \hat{\psi}\end{pmatrix}\begin{pmatrix} f & g \\ g' & -f^T\end{pmatrix}\begin{pmatrix}\hat{\psi} \\ \hat{\psi}^\dagger\end{pmatrix},\end{aligned} \tag{17}$$

where g and g' are anti-symmetric. If $\hat{O}$ is Hermitian, we have $f^T = f^*$ and $g^* = -g'$ ($g^\dagger = g'$).

The Bogoliubov transformation (11) is written with the unitary matrix $\mathcal{W}$ as

$$\begin{pmatrix} a \\ a^\dagger \end{pmatrix} = \mathcal{W}^\dagger\begin{pmatrix}\hat{\psi} \\ \hat{\psi}^\dagger\end{pmatrix}, \quad \begin{pmatrix}\hat{\psi} \\ \hat{\psi}^\dagger\end{pmatrix} = \mathcal{W}\begin{pmatrix} a \\ a^\dagger \end{pmatrix}.$$

This transforms Eq. (17) into

$$\begin{aligned}\hat{O} &= \sum_{ij}\left[O_{ij}^{(++)}a_i^\dagger a_j + \frac{1}{2}\left\{O_{ij}^{(+-)}a_i^\dagger a_j^\dagger + O_{ij}^{(-+)}a_i a_j\right\}\right] \\ &= \frac{1}{2}\begin{pmatrix} a^\dagger & a\end{pmatrix}\begin{pmatrix} O^{(++)} & O^{(+-)} \\ O^{(-+)} & O^{(--)}\end{pmatrix}\begin{pmatrix} a \\ a^\dagger\end{pmatrix},\end{aligned} \tag{18}$$

where $O^{(--)} = -O^{(++)T}$ and the constant shift is ignored. The matrices appearing in Eqs. (17) and (18) are essentially identical, but in different representation. We symbolically denote this as O. The superscript indices "+" and "−" indicate the positive- and negative-energy states; $O_{ij}^{(++)} \equiv \Psi_i^{0\dagger}O\Psi_j^0$, $O_{ij}^{(+-)} \equiv \Psi_i^{0\dagger}O\tilde{\Psi}_j^0$, $O_{ij}^{(-+)} \equiv \tilde{\Psi}_i^{0\dagger}O\Psi_j^0$, and $O_{ij}^{(--)} \equiv \tilde{\Psi}_i^{0\dagger}O\tilde{\Psi}_j^0$. The matrix elements, $O_{ij}^{(+-)}$ and $O_{ij}^{(-+)}$, correspond to the two-quasiparticle

creation and annihilation parts, respectively, which are occasionally denoted as O^{20}_{ij} and O^{02}_{ji} in literature (Avogadro and Nakatsukasa, 2011; Ring and Schuck, 1980). The block elements of the density is also written as $R = \begin{pmatrix} R^{(++)} & R^{(+-)} \\ R^{(-+)} & R^{(--)} \end{pmatrix}$. The expectation value of $\hat{O}$ is given by $\langle\phi|\hat{O}|\phi\rangle = (1/2)\mathrm{tr}[OR^0]$. These matrix notations are frequently used in Sec. III.

B. DFT theorem for a wave-packet state

The DFT is based on the HK theorem which guarantees a one-to-one mapping between a one-body density $\rho(\vec{r})$ for the ground state and an external potential $v_0(\vec{r})$. According to the recent progress (Barnea, 2007; Engel, 2007; Giraud, 2008; Messud *et al.*, 2009), the theorem is extended to functionals of the localized intrinsic density of self-bound systems. Thus, it is a functional of density $\rho(\vec{r}-\vec{R})$ where $\vec{R}$ is the center of mass. In contrast to the center-of-mass motion, a strict definition of the intrinsic state is not trivial for the rotational motion of a deformed nucleus. In this section, we show a possible justification of the functional of the wave-packet density produced by the SSB in finite systems. The arguments presented here were given by Giraud *et al.* (2008). The argument is exact for the SSB in the translational symmetry, while it is approximate for the SSB in the rotational symmetry.

1. Principles

A useful fact is that the SSB of the continuous symmetries produces ANG modes which are decoupled from the other degrees of freedom. It is exactly true in the case of translational symmetry. Consequently, there appear the collective variables associated with the ANG modes, which are symbolically denoted as (q, p). Here, p are conserved and q are cyclic variables. The decoupling allows us to define the collective subspace Σ_{ANG} in the whole Hilbert space of many-particle systems. Σ_{ANG} is the space spanned by the collective wave functions, $\{\chi(q)\}$. The subspace orthogonal to Σ_{ANG}, which is denoted as Σ_{intr}, describes the intrinsic motion.

In the ideal case of the SSB in the translational symmetry, the center-of-mass variables, $(q, p) = (\vec{R}, \vec{P})$, and the intrinsic variables, (ξ, π), are exactly decoupled. The state $|\Phi\rangle$ is rigorously given by a product wave function of $\phi(\xi)$ and $\chi(\vec{R})$.

$$|\Phi\rangle = |\phi\rangle \otimes |\chi\rangle, \quad \hat{H} = \hat{H}_{\mathrm{intr}}(\xi, \pi) + \frac{\vec{P}^2}{2M},$$

where M is the total mass. In this case, the intrinsic subspace Σ_{intr} is defined by the space spanned by $\{\phi(\xi)\}$. The intrinsic ground state is obtained by the minimization of the intrinsic energy $\langle\phi|\hat{H}_{\mathrm{intr}}|\phi\rangle$ in the subspace Σ_{intr}. The choice of the center-of-mass motion $\chi(\vec{R})$ is arbitrary for the determination of $\phi(\xi)$. Thus, we can adopt a localized form of $\chi(\vec{R})$, such as a Gaussian form $\chi(\vec{R}) \propto \exp[-(\vec{R}-\vec{R}_0)^2/2b^2]$. This leads to the wave-packet state $|\Phi\rangle$. Using the operator $\hat{P}$ which projects $\chi(q)$ onto the $\vec{P} = 0$ state, the ground-state energy can be obtained by the variation after the projection:

$$E_0 \equiv \min \left[\frac{\langle\Phi|\hat{H}\hat{P}|\Phi\rangle}{\langle\Phi|\hat{P}|\Phi\rangle} \right]_{\Sigma_{\mathrm{intr}}} \tag{19}$$

where the variation is performed only in Σ_{intr} with a fixed $\chi(\vec{R})$.

In general, the wave-packet state is constructed in an analogous way. Choosing a localized form of $\chi(q)$, e.g., $\chi(q) \propto \exp[-(q-q_0)^2/2b^2]$, the variation after projection is performed in a restricted space Σ_{intr}. The projection operator $\hat{P}$ makes the state an eigenstate of the collective momentum (symmetry operator) p; $p\hat{P}|\Phi\rangle = p_0\hat{P}|\Phi\rangle$. Then, Eq. (19) produces the ground-state energy with $p = p_0$. In nuclear physics interests, in addition to the total momentum, p may stand for either the total angular momentum J, or the neutron (proton) number N (Z). The wave-packet density profile is simply given by

$$\rho(\vec{r}) \equiv \sum_{\sigma} \langle\Phi|\hat{\psi}^\dagger(\vec{r}\sigma)\hat{\psi}(\vec{r}\sigma)|\Phi\rangle,$$

that depends on the choice of $\chi(q)$. In this article, we omit the isospin index $\tau = (n, p)$ for simplicity. Since we adopt a localized $\chi(q)$ which violates the symmetry, the density $\rho(\vec{r})$ is also localized, or "deformed".

In order to find the (wave-packet) density functional, we use the constrained search (Levy, 1979). The minimization in Eq. (19) is divided into two steps; one first considers only states that produce a given wave-packet density $\rho(\vec{r})$, and next takes the variation with respect to the density.

$$E_0 = \min_{\rho} \left\{ \min_{\Phi\to\rho} \left[\frac{\langle\Phi|\hat{H}\hat{P}|\Phi\rangle}{\langle\Phi|\hat{P}|\Phi\rangle} \right]_{\Sigma_{\mathrm{intr}}} \right\}.$$

This leads to the universal density functional

$$F[\rho] \equiv \min_{\Phi\to\rho} \left[\frac{\langle\Phi|\hat{H}\hat{P}|\Phi\rangle}{\langle\Phi|\hat{P}|\Phi\rangle} \right]_{\Sigma_{\mathrm{intr}}}.$$

Thus, the energy of the ground state with $p = p_0$ may be obtained by the minimization, $E_0 = \min F[\rho]$.

The SSB of the gauge symmetry in nuclear superfluidity is caused by the pairing correlations among nucleons. Thus, in practice, it is convenient to introduce the pair tensors for the wave-packet state as

$$\kappa(\vec{r}\sigma;\vec{r}'\sigma') \equiv \langle\Phi|\hat{\psi}(\vec{r}'\sigma')\hat{\psi}(\vec{r}\sigma)|\Phi\rangle. \tag{20}$$

In other words, it is easier to construct the density functional $F[\rho,\kappa,\kappa^*]$ than $F[\rho]$, which takes account of essential aspects of the pairing correlations. Hereafter, we denote $F[\rho,\kappa]$ omitting κ^* for simplicity. Following the above idea of the constrained search, it is easy to define the functional of ρ and κ,

$$F[\rho,\kappa] \equiv \min_{\Phi\to(\rho,\kappa)} \left[\frac{\langle\Phi|\hat{H}\hat{P}|\Phi\rangle}{\langle\Phi|\hat{P}|\Phi\rangle} \right]_{\Sigma_{\rm intr}} . \qquad (21)$$

Instead of adopting the full pair tensors of (20), one can restrict them to their "diagonal" parts, $\kappa(\vec{r}) \equiv \kappa(\vec{r}\uparrow,\vec{r}\downarrow) = -\kappa(\vec{r}\downarrow,\vec{r}\uparrow)$, in the functional. The inclusion of other form of densities, in addition to ρ and κ, can also be achieved exactly in the same manner.

Let us make a few remarks here. First, in general, $\rho(\vec{r})$ and $\kappa(\vec{r})$ are not the exact densities in the laboratory frame (Schmid and Reinhard, 1991). Thus, $F[\rho,\kappa]$ is the functional of "localized" wave-packet densities $\rho(\vec{r})$ and $\kappa(\vec{r})$. Second, when $\Sigma_{\rm ANG}$ describes the center-of-mass motion, the decoupling is exact, and in principle, $E_0 = \min F[\rho]$ gives the exact ground state energy. On the other hand, when the decoupling is approximate, such as the SSB in the rotational symmetry, $E_0 = \min F[\rho,\kappa]$ provides an approximate ground state energy with the deformed densities. In the strict sense, an "infinite" system has an exact deformed ground state with an arbitrary fixed orientation, $\chi(q) \sim \delta(q-q_0)$. This limit is not realized in finite nuclei. Nevertheless, we expect that the approximation becomes better for heavier nuclei. Third, in the approximate decoupling, the subspace $\Sigma_{\rm intr}$ should be chosen to be optimal for a certain eigenvalue of p_0. Therefore, $F[\rho,\kappa]$ may depend on p_0.

2. Practices

We have discussed the principles of the DFT for the wave-packet state. The universal density functional $F[\rho,\kappa]$ can be a functional of "local" densities, $\rho(\vec{r})$ and $\kappa(\vec{r})$, in principle. However, even if the existence is guaranteed, it is another issue in practice whether we can construct the accurate density functional in terms of $\rho(\vec{r})$ and $\kappa(\vec{r})$ only.

For a proper account of the shell effects, the inclusion of the kinetic density is the only practical solution at present (Sec. II.C). Furthermore, for the shell structure in finite nuclei with correct magic numbers, it is indispensable to take into account the spin-orbit splitting (Mayer and Jensen, 1955). Currently, we need to adopt the spin-current densities for this purpose. In the end, the currently available EDFs for realistic applications contains several kinds of densities. The Skyrme and point-coupling covariant EDFs consist of local densities, while the Gogny and covariant (relativistic) EDFs contain non-local ones. Actual forms of the EDFs can be found in Bender *et al.* (2003).

In Sec. II.B.1, we have presented an argument that the approximate decoupling for the rotational degrees of freedom justifies the use of the EDF of *deformed* densities. It is reliable for describing the correlations at $\tau \sim \tau_F$ in Fig. 2 (a). These include the shell effects and the saturation properties. Conversely, the existing EDFs have difficulties to simultaneously reproduce binding energies of spherical and deformed nuclei. This may be due to a missing correlation associated with the quantum rotation of deformed intrinsic shapes shown in Fig. 2 (b). In Sec. III.H, we show that the giant resonances (fast collective motion) are well reproduced in the linear-response calculations, while the low-energy vibrations (slow collective motion) are not as good as those. In our opinions, correlations associated with large-amplitude shape fluctuations at low energy, which are in a time scale $\tau \gg \tau_F$, are missing in the available EDF. In practice, these correlations should be treated in addition to the conventional DFT and TDDFT calculations (Bender *et al.*, 2006). We shall address this issue later, in Sec. V.

The non-universality (p_0 dependence) of $F[\rho,\kappa]$ is treated by enlarging the space $\Sigma_{\rm intr}$ to include all the p_0 states, and adding an additional condition to the constrained search of Eq. (21), for the average value of p_0 (J and N) of the wave packet. This also limits the strictness of the nuclear DFT.

C. Kohn-Sham (KS) scheme

For many-fermion systems, the Fermi motion plays an important role in various quantum phenomena, such as the shell effects. This is a main source of difficulties in the local density approximation (LDA) (Ring and Schuck, 1980). At present, a scheme given by Kohn and Sham (Kohn and Sham, 1965) only provides a practical solution for this problem. Eventually, this leads to the self-consistent equations similar to those in the mean-field approximation.

1. Normal systems

Now, we derive the KS equations (7) according to the argument by Kohn and Sham. Let us assume that the EDF is a functional of $\rho(\vec{r})$ only, $F[\rho]$. We introduce a *reference system* which is a "virtual" non-interacting system with an external potential $v_s(\vec{r})$. The ground state of the reference system is obviously given as a Slater determinant constructed by the solution of Eq. (7). Alternatively, it is obtained by the minimization of the total energy of the reference system, $E_s[\rho] = T_s[\rho] + \int v_s(\vec{r})\rho(\vec{r})d^3\vec{r}$. Since $E_s[\rho]$ is a functional of density, the minimization can be performed in terms of density variation with the particle number constraint,

$\delta(E_s[\rho] - \mu \int \rho(\vec{r})d^3\vec{r}) = 0$. This leads to

$$\mu = \frac{\delta T_s[\rho]}{\delta\rho(\vec{r})} + v_s(\vec{r}). \tag{22}$$

The state determined by Eq. (22) should be identical to that of Eq. (7).

The success of the KS scheme comes from a simple idea to decompose the kinetic energy in the physical interacting system into two parts; $T_s[\rho]$ and the rest. The former is a major origin of the shell effects, and the latter is treated as a part of "correlation energy" $E_c[\rho]$. $E_c[\rho]$ corresponds to the "exchange-correlation energy" $E_{\rm xc}[\rho]$ in electronic DFT. The EDF is given by the sum, $F[\rho] = T_s[\rho] + E_c[\rho]$. Then, the variation, $\delta(F[\rho] - \mu \int \rho(\vec{r})d\vec{r}) = 0$, leads to Eq. (22) where the potential $v_s(\vec{r})$ is defined by

$$v_s(\vec{r}) \equiv \frac{\delta E_c[\rho]}{\delta\rho(\vec{r})}.$$

Therefore, the solution of Eq. (7) provides the ground-state density of $F[\rho]$. The only practical difference between the reference system and the interacting system is that, since $v_s(\vec{r})$ is a functional of density in the latter, Eqs. (7) and (8) with v_s must be self-consistently solved. The success of the KS scheme is attributed to the goodness of the LDA for $E_c[\rho]$.

2. Superconducting systems

Next, with the density functional of Eq. (21), we introduce a non-interacting reference system under an external pair potential $\Delta_s(\vec{r})$ in addition to $v_s(\vec{r})$. The Hamiltonian with a constraint on the particle number,

$$\hat{H}_s - \mu\hat{N} = \int \left[\Delta_s^*(\vec{r})\hat{\psi}(\vec{r}\downarrow)\hat{\psi}(\vec{r}\uparrow) + \text{h.c.}\right] d^3\vec{r}$$
$$+ \sum_{\sigma=\uparrow,\downarrow} \int \hat{\psi}^\dagger(\vec{r}\sigma) \left\{-\frac{\nabla^2}{2m} + v_s(\vec{r}) - \mu\right\} \hat{\psi}(\vec{r}\sigma) d^3\vec{r}$$

can be diagonalized by the Bogoliubov transformation (11), in which (U_i, V_i) are the solutions of Eq. (9). Alternatively, Eq. (9) can be derived by minimizing

$$F_s[\rho,\kappa] - \mu N_{\rm av} = T_s[\rho,\kappa] + \int \{v_s(\vec{r}) - \mu\} \rho(\vec{r}) d^3\vec{r}$$
$$+ \int \{\Delta_s^*(\vec{r})\kappa(\vec{r}) + \Delta_s(\vec{r})\kappa^*(\vec{r})\} d^3\vec{r}.$$

where $T_s[\rho,\kappa] = \sum_\sigma \sum_i \int V_i(\vec{r}\sigma) \frac{-\nabla^2}{2m} V_i^*(\vec{r}\sigma) d^3\vec{r}$. The same minimization can be done with respect to (ρ, κ, κ^*).

$$\mu = \frac{\delta T_s}{\delta\rho(\vec{r})} + v_s(\vec{r}), \qquad 0 = \frac{\delta T_s}{\delta\kappa^*(\vec{r})} + \Delta_s(\vec{r}). \tag{23}$$

Equations (9) and (23) should provide the identical state.

According to the Kohn-Sham's idea, we express the energy density functional of the interacting system in the form $F[\rho,\kappa] \equiv T_s[\rho,\kappa] + E_c[\rho,\kappa]$. Then, the variation, $\delta(F[\rho,\kappa] - \mu \int \rho(\vec{r})d^3\vec{r}) = 0$, leads to Eq. (23) but the potentials, $v_s(\vec{r})$ and $\Delta_s(\vec{r})$, are given by Eq. (10). Equations (9) with potentials (10) constitutes the BdGKS scheme (Oliveira *et al.*, 1988).

D. Time-dependent density functional theory

1. Foundation: Runge-Gross theorem

The basic theorem of the TDDFT tells us that, starting from a common initial state $|\Phi_0\rangle$ at $t = t_0$, there is one-to-one correspondence between a pair of time-dependent densities $(\rho(\vec{r},t), \kappa(\vec{r},t))$ and a pair of time-dependent external potentials $(v(\vec{r},t), \Delta(\vec{r},t))$ (Runge and Gross, 1984; Wacker *et al.*, 1994). Here, we recapitulate the proof. The external potential is required to be expandable in a Taylor series about the initial time t_0.

$$v(\vec{r},t) = \sum_{k=0}^{\infty} \frac{1}{k!} v_k(\vec{r})(t-t_0)^k, \tag{24}$$

$$\Delta(\vec{r},t) = \sum_{k=0}^{\infty} \frac{1}{k!} \Delta_k(\vec{r})(t-t_0)^k. \tag{25}$$

If two potentials (v, v') differ merely by a time-dependent function, $c(t) = v(\vec{r},t) - v'(\vec{r},t)$, they should be regarded as *identical* potentials. For the different potentials, there should exist some non-negative integer n such that $\vec{\nabla} w_n(\vec{r}) \neq 0$ where $w_n(\vec{r}) \equiv v_n(\vec{r}) - v_n'(\vec{r})$. Similarly, the pair potentials are different if $D_n(\vec{r},t) \neq 0$ at a certain n where $D_n(\vec{r},t) \equiv \Delta_n(\vec{r},t) - \Delta_n'(\vec{r},t)$.

Let us first assume that two different external potentials, $v(\vec{r},t)$ and $v'(\vec{r},t)$, produce current densities $\vec{j}(\vec{r},t)$ and $\vec{j}'(\vec{r},t)$, respectively. The pair potential is assumed to be equal, $\Delta(\vec{r},t) = \Delta'(\vec{r},t)$. In the following, we assume the Heisenberg picture, and the quantities associated with the potentials $v'(\vec{r},t)$ are denoted with primes, while those with $v(\vec{r},t)$ are without primes. The equation of motion for the current, $\vec{j}(\vec{r},t) \equiv \langle\Phi_0|\hat{\vec{j}}(\vec{r},t)|\Phi_0\rangle$, is written as

$$i\frac{\partial}{\partial t}\vec{j}(\vec{r},t) = \langle\Phi_0|[\hat{\vec{j}}(\vec{r},t), \hat{H}(t)]|\Phi_0\rangle. \tag{26}$$

We have the same equation for $\vec{j}'(\vec{r},t)$, with $\hat{H}(t)$ replaced by $\hat{H}'(t)$. Since the field operators at $t = t_0$ are identical to each other, $\psi(\vec{r}\sigma,t_0) = \psi'(\vec{r}\sigma,t_0)$, they lead to

$$i\frac{\partial}{\partial t}\left\{\vec{j}(\vec{r},t) - \vec{j}'(\vec{r},t)\right\}\Big|_{t=t_0}$$
$$= \langle\Phi_0|[\hat{\vec{j}}(\vec{r},t_0), \hat{H}(t_0) - \hat{H}'(t_0)]|\Phi_0\rangle$$
$$= -\frac{i}{m}\rho(\vec{r},t_0)\vec{\nabla} w_0(\vec{r}).$$

If $\vec{\nabla}w_0(\vec{r}) \neq 0$, it is easy to see that $\vec{j}(\vec{r},t)$ and $\vec{j}'(\vec{r},t)$ are different at $t > t_0$. In case that $\vec{\nabla}w_0(\vec{r}) = 0$ and $\vec{\nabla}w_1(\vec{r}) \neq 0$, we need to further calculate derivative of Eq. (26) with respect to t.

$$\left(i\frac{\partial}{\partial t}\right)^2 \vec{j}(\vec{r},t)\bigg|_{t=t_0} = \langle\Phi_0|\left[\hat{\vec{j}}(\vec{r},t), i\bar{\partial}\hat{H}/\bar{\partial}t\right]_{t=t_0}|\Phi_0\rangle + \langle\Phi_0|[[\hat{\vec{j}}(\vec{r},t_0),\hat{H}(t_0)],\hat{H}(t_0)]|\Phi_0\rangle, \quad (27)$$

where $\bar{\partial}/\bar{\partial}t$ indicates the time derivative of the potentials only, not of the field operators. The second term of Eq. (27) vanishes for the difference, $\partial^2/\partial t^2\{\vec{j}(\vec{r},t) - \vec{j}'(\vec{r},t)\}|_{t=t_0}$, because $\hat{H}'(t_0) = \hat{H}(t_0) + \text{const}$. Thus,

$$\frac{\partial^2}{\partial t^2}\left\{\vec{j}(\vec{r},t_0) - \vec{j}'(\vec{r},t)\right\}\bigg|_{t=t_0} = -\frac{1}{m}\rho(\vec{r},t_0)\vec{\nabla}w_1(\vec{r}) \neq 0.$$

Again, we conclude that $\vec{j}(\vec{r},t) \neq \vec{j}'(\vec{r},t)$ at $t > t_0$. In general, if $\vec{\nabla}w_k(\vec{r}) = 0$ for $k < n$ and $\vec{\nabla}w_n(\vec{r}) \neq 0$, we repeat the same argument to reach

$$\begin{aligned}\frac{\partial^{n+1}}{\partial t^{n+1}}&\left\{\vec{j}(\vec{r},t) - \vec{j}'(\vec{r},t)\right\}_{t=t_0} \\ &= -i\langle\Phi_0|\left[\hat{\vec{j}}(\vec{r},t_0),\, \bar{\partial}^n\{\hat{H}(t) - \hat{H}'(t)\}/\bar{\partial}t^n\Big|_{t=t_0}\right]|\Phi_0\rangle \\ &= -\frac{1}{m}\rho(\vec{r},t_0)\vec{\nabla}w_n(\vec{r}) \neq 0.\end{aligned}$$

Therefore, there exists a mapping from the expandable potential $v(\vec{r},t)$ and the current density $\vec{j}(\vec{r},t)$. The continuity equation relates the current density $\vec{j}(\vec{r},t)$ with the density $\rho(\vec{r},t)$. Therefore, we can conclude that the densities $\rho(\vec{r},t)$ and $\rho'(\vec{r},t)$ are different at $t > t_0$.

Next, let us assume the different pair potentials, $\Delta(\vec{r},t)$ and $\Delta'(\vec{r},t)$. The same argument above leads to

$$\frac{\partial^{n+1}}{\partial t^{n+1}}\left\{\kappa(\vec{r},t) - \kappa'(\vec{r},t)\right\}\bigg|_{t=t_0} = f(\vec{r})D_n(\vec{r}) \neq 0,$$

where $f(\vec{r}) = i\{\rho(\vec{r},t_0) - \delta^3(0)\}$. The appearance of the delta function $\delta^3(0)$ is a consequence of the local nature of the pair potential $\Delta(\vec{r,t})$. Anyway, $f(\vec{r})$ is nonzero, and the pair densities, $\kappa(\vec{r},t)$ and $\kappa'(\vec{r},t)$, become different immediately after $t = t_0$. This completes the proof of the one-to-one correspondence between the potentials $(v(\vec{r},t), \Delta(\vec{r},t))$ and the densities $(\rho(\vec{r},t), \kappa(\vec{r},t))$. As is obvious in the proof here, the one-to-one correspondence also holds when the density $\rho(\vec{r},t)$ is replaced by the current density $\vec{j}(\vec{r},t)$.

2. TDKS scheme: van Leeuwen theorem

In practice, the KS scheme is indispensable for quantum systems. According to the basic theorem in Sec. II.D.1 there is a one-to-one correspondence between given time-dependent densities and external potentials for any system. Let us introduce a *virtual* reference system of non-interacting particles by choosing the potentials, $v_s(\vec{r},t)$ and $\Delta_s(\vec{r},t)$, in such a way that it exactly produces the densities, $\rho(\vec{r},t)$ and $\kappa(\vec{r},t)$, of a *real* interacting system. This results in the time-dependent Bogoliubov-de-Gennes-Kohn-Sham (TDBdGKS) equations:

$$i\frac{\partial}{\partial t}\begin{pmatrix}U_i(\vec{r}\sigma;t)\\ V_i(\vec{r}\sigma;t)\end{pmatrix} = \sum_{\sigma'}\begin{pmatrix}h_s(\vec{r};t)\delta_{\sigma\sigma'} & \Delta_s(\vec{r};t)\gamma_{\sigma\sigma'}\\ -\Delta_s^*(\vec{r};t)\gamma_{\sigma\sigma'} & -h_s^*(\vec{r};t)\delta_{\sigma\sigma'}\end{pmatrix}\begin{pmatrix}U_i(\vec{r}\sigma';t)\\ V_i(\vec{r}\sigma';t)\end{pmatrix}. \quad (28)$$

Here, $h_s(\vec{r},t) \equiv -\nabla^2/(2m) + v_s(\vec{r},t)$. With $\Delta_s = 0$, they reduce to the TDKS equations ($i = 1, \cdots, N$);

$$i\frac{\partial}{\partial t}\varphi_i(\vec{r},t) = h_s(\vec{r},t)\varphi_i(\vec{r},t). \quad (29)$$

The next obvious question is the following: Do such potentials in non-interacting systems exist to reproduce the densities in real systems? This question was answered affirmatively by van Leeuwen (1999) as follows. For simplicity, let us consider the TDKS equations without pairing. Hereafter, quantities associated with the reference system are denoted with a subscript "s". First, calculating the right-hand side of Eq. (26) gives $i\partial\vec{j}(\vec{r},t)/\partial t = -\rho(\vec{r},t)\vec{\nabla}v(\vec{r},t) - \vec{f}(\vec{r},t)$. Here, $\vec{f}(\vec{r},t)$ is given by the momentum-stress tensor and the interaction parts, but these details are not important in the proof. Taking the divergence of this equation and using the continuity equation, we find

$$\frac{\partial^2\rho}{\partial t^2} = \vec{\nabla}\cdot(\rho(\vec{r},t)\vec{\nabla}v(\vec{r},t)) + q(\vec{r},t), \quad (30)$$

where $q(\vec{r},t) = \vec{\nabla}\cdot\vec{f}(\vec{r},t)$. Assuming the density is identical in two systems all the times, the difference of Eq. (30) between the two leads to

$$\vec{\nabla}\cdot(\rho(\vec{r},t)\vec{\nabla}w(\vec{r},t)) = \zeta(\vec{r},t), \quad (31)$$

where $w = v - v_s$ and $\zeta = q_s - q$. This equation plays a key role in the proof. Now, the question is whether we can uniquely determine $w(\vec{r},t)$ if $\rho(\vec{r},t)$ is given.

Necessary conditions for the initial state $|\Phi_s\rangle$ of the reference system are only two: (i) The two initial states, $|\Phi_0\rangle$ and $|\Phi_s\rangle$, yield the same density, $\rho(\vec{r},t_0) = \rho_s(\vec{r},t_0)$. (ii) Their time derivatives are identical, $\dot{\rho}(\vec{r},t_0) = \dot{\rho}_s(\vec{r},t_0)$. With $|\Phi_s\rangle$ satisfying these initial conditions, we determine the solution w of Eq. (31). We should first notice that Eq. (31) does not contain time derivatives, which means that t can be regarded as a parameter. Furthermore, Eq. (31) is of the Sturm-Liouville type, thus it has a unique solution with the boundary condition, $w(\vec{r},t) = 0$ at infinity. It is now obvious that we can uniquely determine $w(\vec{r},t_0)$ at $t = t_0$ because

$\zeta(\vec{r}, t_0)$ is calculable with the initial states $|\Phi_0\rangle$ and $|\Phi_s\rangle$. This means in the Taylor-series expansion, Eq. (24), $w_0(\vec{r}) = v_0(\vec{r}) - v_{s0}(\vec{r})$ is solved. Taking the time derivative of Eq. (31) at $t = t_0$, we can determine $w_n(\vec{r})$ for higher-order terms in a recursive manner ($n = 1, 2, \cdots$). This procedure completely determines $v_s(\vec{r}, t)$.

3. TDBdGKS equation and its properties

The key quantity in TDDFT is the time-dependent potentials $(v_s(\vec{r}, t), \Delta_s(\vec{r}, t))$. So far, we simply adopt the *adiabatic approximation*: We take the BdGKS potentials in Eq. (9) from static DFT and use it in the TDBdGKS equations (28), by replacing ground-state densities with the time-dependent ones.

$$v_s(t) = v_s[\rho_0]|_{\rho_0 \to \rho(t)}\,, \quad v_s[\rho] \equiv \delta E_c/\delta\rho \tag{32}$$

and the same prescription is applied to Δ_s. This obviously lacks the memory effect.

Properties of the static BdGKS equations shown in Sec. II.A.2 also hold for the time-dependent case, except for BdGKS equation (15) which should be replaced by

$$i\frac{\partial}{\partial t}R(t) = [H_s[R](t), R(t)]\,. \tag{33}$$

Here, $H_s[R]$ is given by Eq. (16) with $R_0 \to R(t)$ in the adiabatic approximation. We use the notations same as those in Sec. II.A.2 with obvious changes introducing the time dependence, such as $\Psi^0 \to \Psi(t)$, $R^0 \to R(t)$, etc.

With respect to a time-dependent unitary transformation $\Psi(t) \to \Psi(t)U(t)$, $R(t)$ and Eq. (33) are invariant, while Eq. (28) is not. Including this gauge freedom, the TDBdGKS equations (28) should be generalized to

$$i\frac{\partial}{\partial t}\Psi(t) = H_s[R](t)\Psi(t) - \Psi(t)\Xi(t), \tag{34}$$

with a Hermitian matrix $\Xi = i(dU/dt)U^\dagger = -iUdU^\dagger/dt$. The choice of $\Xi(t)$ is arbitrary and does not affect the physical contents of the calculation. The TDBdGKS equations (28) correspond to a special gauge $\Xi(t) = 0$.

In case that the pair density and potential are absent, $\kappa(t) = \Delta(t) = 0$, Eq. (33) reduces to

$$i\frac{\partial}{\partial t}\rho(t) = [h_s[\rho](t), \rho(t)]\,. \tag{35}$$

This is equivalent to the TDKS equations,

$$i\frac{\partial}{\partial t}\varphi(t) = h_s[\rho](t)\varphi(t) - \varphi(t)\xi(t), \quad \rho(t) = \varphi(t)\varphi^\dagger(t),$$

where $\varphi(t)$ is a collective notation of the non-vanishing vectors $V_i^*(t)$, $\varphi(t) = (V_1^*(t), V_2^*(t), \cdots, V_N^*(t))$, that are upper components of $\tilde{\Psi}(t)$. The quantity $\xi(t)$ is an arbitrary $N \times N$ Hermitian matrix. A choice of $\xi(t) = 0$ leads to Eq. (29).

4. Local gauge invariance

The practical success of the TDBdGKS equations relies on the availability of a good correlation functional $E_c[\rho, \kappa]$. Many applications, so far employ the functional of the static potentials (10) with time-dependent densities (*adiabatic approximation*). Although the memory effect is missing, this simple choice guarantees exact properties of the functional, such as the harmonic potential theorem (HPT) (Dobson, 1994; Vignale, 1995). In nuclear physics applications, it is also customary to adopt a functional in the same form as the static one. Since a local density form (Skyrme-type) of the nuclear correlation energy contains the kinetic and spin-current densities, to guarantee the Galilean symmetry, it should include the time-odd densities, such as spin, current, and spin-tensor densities (Engel *et al.*, 1975). In fact, the nuclear EDFs usually respect an even stronger symmetry, the local gauge invariance, which is satisfied for systems with local interactions. The HPT and the Galilean invariance can be regarded as its special cases. The local gauge transformation modifies the one-body density matrix as $\rho(\vec{r}, \vec{r}') \to \exp[i\{\chi(\vec{r}) - \chi(\vec{r}')\}]\rho(\vec{r}, \vec{r}')$. The local density $\rho(\vec{r}) = \rho(\vec{r}, \vec{r})$ is apparently invariant, however, the kinetic and spin-current densities are not, because the transformation creates a flow with a velocity field, $\vec{v}(\vec{r}, t) = \vec{\nabla}\chi(\vec{r}, t)/m$. These densities appear with characteristic combinations with the time-odd densities to satisfy the local gauge invariance (Dobaczewski and Dudek, 1995). Note that the local gauge invariance is guaranteed if the nonlocal effect is small, but it is not required by the principles. It has been utilized to restrict the functional form of nuclear EDFs (Carlsson *et al.*, 2008).

The local $U(1)$ gauge transformation, $\hat{\psi}(\vec{r}\sigma, t) \to e^{i\chi(\vec{r},t)}\hat{\psi}(\vec{r}\sigma, t)$, with a real function $\chi(\vec{r}, t)$ changes the phase of U and V components with opposite signs (see Eq. (11)). Thus, the transformation reads

$$\bar{\Psi}(t) = \begin{pmatrix} e^{i\chi} & 0 \\ 0 & e^{-i\chi} \end{pmatrix}\Psi(t) = \exp\{i\chi(t)\mathcal{N}\}\Psi(t), \tag{36}$$

with $\mathcal{N} \equiv \begin{pmatrix} 1 & 0 \\ 0 & -1 \end{pmatrix}$. Under this transformation, the generalized density and the Hamiltonian should be transformed as

$$\begin{Bmatrix} \bar{R}(t) \\ \bar{H}_s(t) \end{Bmatrix} = e^{i\chi(t)\mathcal{N}} \begin{Bmatrix} R(t) \\ H_s(t) \end{Bmatrix} e^{-i\chi(t)\mathcal{N}}. \tag{37}$$

The transformation (37) keeps the density $\rho(\vec{r}, t)$ invariant, but multiplies $\kappa(\vec{r}, t)$ by a local phase $e^{2i\chi(\vec{r},t)}$. The transformation of the kinetic term can be obtained by shifting the momentum $\vec{p}$ to $\vec{p} - m\vec{v}(\vec{r}, t)$. The local gauge invariance of the density functionals guarantees that $H_s[R](\vec{r}, \vec{p}; t) \to \bar{H}_s[\bar{R}](\vec{r}, \vec{p}; t) = H_s[\bar{R}](\vec{r}, \vec{p} - m\vec{v}; t)$, in which the replacement of $\vec{p} \to \vec{p} - m\vec{v}$ is performed

only for the kinetic energy term, $|\vec{p}|^2/(2m) \to |\vec{p} - m\vec{v}(\vec{r},t)|^2/(2m)$. The transformed TDBdGKS equations for $\bar{R}$ and $\bar{\Psi}(t)$ are identical to Eqs. (33) and (34), but the Hamiltonian is replaced by $\bar{H}_s[\bar{R}](t) - \partial\chi/\partial t \cdot \mathcal{N}$. For instance, Eq. (33) now reads

$$i\frac{\partial}{\partial t}\bar{R}(t) = \left[\bar{H}_s[\bar{R}](t) - \frac{\partial\chi}{\partial t}\mathcal{N}, \bar{R}(t)\right]. \tag{38}$$

This is the TDBdGKS equation in a frame of a gauge function $\chi(\vec{r},t)$. Under the presence of the local gauge invariance in the EDF, the functional form of $\bar{H}_s$ is the same as H_s except that the momentum $\vec{p}$ is replaced by $\vec{p} - m\vec{v}$ in the kinetic term.

E. Equations for decoupled collective motion

In this section, we derive an equation for the decoupled collective motion. In order to elucidate the idea, let us start with the translational motion. In this case, the decoupling is exact. The boosted ground state with the center of mass at $\vec{R}_{\rm cm}(t) = \vec{v}t$ has the density, $\rho(t) = \rho(\vec{R}_{\rm cm})$, which depends on time through $\vec{R}_{\rm cm}(t) = \vec{v}t$. The total momentum $\vec{P}_{\rm cm} = Nm\vec{v}$ is a constant of motion. The TDKS equation (35) can be written as

$$i\vec{v}\cdot\frac{\partial}{\partial\vec{R}_{\rm cm}}\rho(\vec{R}_{\rm cm}) = \left[h_s[\rho(\vec{R}_{\rm cm})], \rho(\vec{R}_{\rm cm})\right].$$

Using the expression, $\rho(t) = e^{-i\vec{R}_{\rm cm}(t)\cdot\vec{p}}\bar{\rho}e^{i\vec{R}_{\rm cm}(t)\cdot\vec{p}}$ where $\bar{\rho}$ is time-independent, it leads to

$$[h_s[\rho(t)] - \vec{v}\cdot\vec{p}, \rho(t)] = 0, \tag{39}$$

which looks like a stationary equation. In fact, since $\vec{R}_{\rm cm} = \vec{v}t$ depends on time, $\rho(\vec{R}_{\rm cm})$ is moving in time. We call Eq. (39) "moving-frame" equation in the following. It should be noted that the EDFs with the Galilean symmetry is essential to reproduce the correct total mass Nm, which also influences properties of other collective motions.

1. Collective motion in general

Now, let us generalize the idea and assume that there are a pair of canonical variables $(q(t), p(t))$ corresponding to a collective motion, which determine the time dependence of the generalized density $R(q(t), p(t))$. This means that the motion described by $(q(t), p(t))$ is decoupled from the other *intrinsic* degrees of freedom. In the TDBdGKS equation (33), the time derivative is now written in terms of the collective variables as $\dot{q}\partial/\partial q + \dot{p}\partial/\partial p$. This leads to the moving-frame equation,

$$\left[H_s[R] - \dot{q}\mathring{P}(q,p) + \dot{p}\mathring{Q}(q,p), R(q,p)\right] = 0, \tag{40}$$

where $\mathring{P}(q,p)$ and $\mathring{Q}(q,p)$ are generators of the collective variables and defined by

$$i\frac{\partial}{\partial q}R(q,p) = \left[\mathring{P}(q,p), R(q,p)\right], \tag{41}$$

$$-i\frac{\partial}{\partial p}R(q,p) = \left[\mathring{Q}(q,p), R(q,p)\right]. \tag{42}$$

Note that $\dot{q}$ and $\dot{p}$ are not constant, in general. In Sec. V, we develop this idea and derive equations of motion for a collective motion decoupled from other intrinsic degrees of freedom.

Equation (40) looks like a stationary equation with constraints, $\mathring{Q}(q,p)$ and $\mathring{P}(q,p)$. However, it is important to note that the density $R(q,p)$ in Eq. (40) still varies in time because the variables (q,p) depend on time. Because of this time dependence, the "cranking terms", $-\dot{q}\mathring{P}+\dot{p}\mathring{Q}$, in Eq. (40) are not just the constraint terms in static equations, but plays a role beyond that.

To explain this point, we go back again to the translational motion. The equation (39) looks identical to the static equation with a constraint operator, $\vec{p}$. However, the cranking term induces the linear momentum, $\mathrm{Tr}[\rho\vec{p}] = Nm\vec{v}$, and the density is never static. During the time evolution $t \to t+\delta t$, the center of mass moves as $\vec{R}_{\rm cm} \to \vec{R}_{\rm cm} + \vec{v}\delta t$. Accordingly, the density also evolves, $\rho \to \rho + \delta\rho$. $\vec{R}_{\rm cm} \to \vec{R}_{\rm cm} + \delta\vec{R}$. This density variation is described by Eq. (39).

$$[h_s - \vec{v}\cdot\vec{p}, \delta\rho] + \left[\frac{\delta h_s}{\delta\rho}\delta\rho, \rho\right] = 0, \tag{43}$$

in the first order in $\delta\rho$. This is nothing but the random-phase approximation (RPA) for the translational motion. If Eq. (39) is a constrained stationary equation, obviously, it does not lead to the RPA equation.

If we define the particle (unoccupied) and hole (occupied) orbitals for $h_s[\rho] - \vec{v}\cdot\vec{p}$, the particle-particle and hole-hole components, $\vec{p}_{pp'}$ and $\vec{p}_{hh'}$, contribute to the determination of $\delta\rho$ in Eq. (43). In contrast, for the constrained mean-field equation (Ring and Schuck, 1980), the particle-particle and hole-hole matrix elements of the constrained operator are irrelevant. We think it worth emphasizing that the cranking terms in Eqs. (39) and (40) are different from constraint terms in the static equation (Hinohara *et al.*, 2007; Nakatsukasa, 2012; Nakatsukasa *et al.*, 1999). The issue will be addressed in Sec. V.

2. ANG modes and quasi-stationary solutions

The ANG modes provide examples of decoupled collective motion to which Eq. (40) is applicable. In these cases, one of the variables becomes cyclic (constant), and the generators do not depend on the variables (q,p). They are given by known one-body operators globally defined.

1. *Translational motion*

In this case, the generators $(\overset{\circ}{Q}(q,p), \overset{\circ}{P}(q,p))$ correspond to the center-of-mass coordinate and the total momentum, with $\dot{q} = \vec{v}$ and $\dot{p} = 0$. Thus, we naturally derive Eq. (39) from Eq. (40). The Galilean invariance guarantees that the translational motion with a constant velocity does not influence the *intrinsic* state. In fact, the local gauge transformation with $\chi(\vec{r}) = -m\vec{v}\cdot\vec{r}$ removes the cranking term, $-\vec{v}\cdot\vec{p}$. Then, using the ground-state solution ρ_0, which satisfies the static equation $[h_s[\rho_0], \rho_0] = 0$ ($\vec{v} = 0$), we may construct a solution of Eq. (39), $\rho(\vec{R}_{\rm cm}) = e^{im\vec{v}\cdot\vec{r}}\rho_0(\vec{R}_{\rm cm})e^{-im\vec{v}\cdot\vec{r}}$.

2. *Rotational motion*

A spatially rotating system with a constant angular velocity $\vec{\omega}$ can be described by a solution of Eq. (40) with $\dot{q} = \dot{\vec{\theta}} = \vec{\omega}$, $\dot{p} = \dot{\vec{I}} = 0$. The generator $\overset{\circ}{P}(q,p)$ corresponds to the angular momentum operator $\vec{j}$. Though we do not know the conjugate angle operator, it disappears because of the angular momentum conservation $\dot{\vec{I}} = 0$. Then, it ends up the cranking model (Inglis, 1954, 1956):

$$\left[h_s[\rho] - \vec{\omega}\cdot\vec{j}, \rho\right] = 0, \tag{44}$$

where the density $\rho(\vec{\theta})$ is a function of the angle $\vec{\theta}(t) = \vec{\omega}t$. Since there is no Galilean symmetry in the rotational motion, it is impossible to remove the cranking term by a gauge transformation. In this case, the decoupling is only approximate. In fact, the rotational motion influences the intrinsic state in non-trivial ways, such as the centrifugal stretching and the Coriolis coupling effects.

3. *Pair rotation*

In the superconducting phase with $\kappa(t) \neq 0$, in which the global gauge symmetry is broken, one may find another rotating solution in the gauge space with a constant angular velocity μ. The generator $\overset{\circ}{Q}(q,p)$ corresponds to the particle number operator[2], $q(t) = N_0$ ($\dot{q} = 0$), and $p(t) = \mu t$. Equation (40) leads to

$$[H_s[R] - \mu\mathcal{N}, R] = 0, \tag{45}$$

where $R(\theta)$ is a function of $\theta(t) = \mu t$. In terms of the time-dependent formalism, the appearance of the chemical potential μ in the stationary BdGKS equation (9) comes from the rotation in the gauge space.

When we study intrinsic excitations perpendicular to the ANG modes, we should extend the density $R(q,p)$ either by introducing the second set of variables $(q'(t), p'(t))$, or by allowing additional time dependence, $R(q,p;t)$. The former method will be adopted in Sec. V. The latter method changes the right hand side of Eq. (40) to $i\partial R/\partial t$. For the case of the pair rotation, this leads to

$$i\frac{\partial}{\partial t}R(\theta;t) = \left[H_s[R] - \mu\mathcal{N}, R(\theta;t)\right], \tag{46}$$

where μ is a function of the particle number N_0.

[2] Here, we assume that q (p) is the time-even (time-odd) variable.

F. Recent development in nuclear EDF

Finding the best density functionals is always a big challenge in the DFT, not only in nuclear systems but also in electronic systems. Since we do not know the exact interaction among nucleons, even for the uniform matter at low-density and high-density limits, the exact functional is not available. Thus, strategies in nuclear DFT is somewhat different from those in electronic systems (Sec. VI). Recent developments involve extension of the functional form and the new optimization to fit reliable calculations and experimental data. The optimization has been performed mainly for static properties, including fission isomers and barrier heights. Here, we present some efforts to improve the EDF, after those shown in Bender *et al.* (2003).

The systematic optimization of the Skyrme EDF was performed to construct the functionals of UNEDF0-2 (Kortelainen *et al.*, 2010, 2014, 2012), which produce the root-mean-square deviation from the experimental binding energies of $1.5 - 2$ MeV. These studies also show a clear deviation pattern common to all the EDFs. This indicates a necessity of novel functional forms for further improvements. The idea based on the density matrix expansion (Negele, 1982; Negele and Vautherin, 1972) is under development to create new functionals (Carlsson and Dobaczewski, 2010; Carlsson *et al.*, 2008; Stoitsov *et al.*, 2010). Other forms of EDF without the derivative terms have been also developed and produce similar accuracy (Baldo *et al.*, 2013, 2008). Although some phenomenological corrections significantly improve the reproduction of the binding energy (Goriely *et al.*, 2013), those corrections are not applicable to TDDFT calculations.

The Gogny EDF was also improved by fitting nuclear structure and neutron matter properties, leading to D1N (Chappert *et al.*, 2008) and D1M (Goriely *et al.*, 2009). A new type of the Gogny EDF has been recently proposed, which extends the density-dependent term to the one with finite range (Chappert *et al.*, 2015). Another type of EDF based on the Yukawa-type potential was also proposed (Nakada, 2013; Nakada and Inakura, 2015).

The modern covariant EDFs adopt either nonlinear meson coupling or density-dependent coupling constants. In addition, there are two types of the covariant EDF: the finite-range meson-field and the point-coupling models. Each EDF type had recent extensions of the functional form, such as inclusion of the δ meson (Roca-Maza *et al.*, 2011), the cross-coupling terms (Fattoyev *et al.*, 2010),

the exchange terms (Long *et al.*, 2007), and new version of the point-coupling models (Nikšić *et al.*, 2008; Zhao *et al.*, 2010).

The pairing EDF responsible for the pair potential Δ is another issue. The pairing energy in the Gogny EDF is calculated with the same interaction. In contrast, most of the Skyrme and covariant EDFs independently treat the pairing EDF. Different forms of the pairing EDF have been recently proposed (Margueron *et al.*, 2008; Tian *et al.*, 2009; Yamagami *et al.*, 2012, 2009; Yu and Bulgac, 2003).

Currently, it is difficult to judge which type of nuclear EDF is the best. Their accuracy for the mass prediction is rather similar to each other among the Skyrme, the Gogny, and the covariant EDFs. Since we know none of them is perfect, the error analysis on the model is important (Dobaczewski *et al.*, 2014; Erler *et al.*, 2012). Furthermore, in contrast to the optimization of EDFs with respect to stationary properties, the one with respect to dynamical properties has not been performed in a systematic manner (Bender *et al.*, 2002). To our knowledge, possibilities beyond the adiabatic approximation (Sec. VI.B) have never been examined in nuclear physics.

III. LINEAR DENSITY RESPONSE

The linear density response of interacting systems can be rigorously formulated, in principle, on the basis of the TDDFT. The formulation is basically identical to the one known as the quasiparticle-random-phase approximation (QRPA) in nuclear physics (Blaizot and Ripka, 1986; Ring and Schuck, 1980).

Since the pair rotation inevitably takes place with a finite μ, the density $R(t) = R(\theta(t))$ is not stationary even for the ground state. In order to avoid complications in deriving the QRPA linear response equations, we should start either with Eq. (46), or with Eq. (38) of a gauge function $\chi(t) = \theta(t) = \mu t$, in which the time dependence through $\theta(t)$ is hidden. The following external potential, multiplied by a parameter η, is added to $H_s[R]$.

$$\eta V(t) \equiv \eta \begin{pmatrix} v_{\rm ext}(t) & \Delta_{\rm ext}(t) \\ -\Delta^*_{\rm ext}(t) & -v^*_{\rm ext}(t) \end{pmatrix}.$$

See Sec. II.A.2 for the corresponding operator form. It is convenient to introduce a small parameter η to elucidate the linearization. The time-dependent density and the Hamiltonian are linearized with respect to η as $R(t) = R_0 + \eta\delta R(t) + O(\eta^2)$ and $H_s(t) = H_s[R_0] + \eta\delta H(t) + O(\eta^2)$. The Fourier transform of Eq. (46) leads to

$$\omega\delta R(\omega) = [H_s[R_0] - \mu\mathcal{N}, \delta R(\omega)] + [V(\omega) + \delta H(\omega), R_0], \tag{47}$$

in the linear order. This equation plays a central role in this section.

A. Linear response equations and matrix representation in the quasiparticle basis

In order to evaluate Eq. (47), it is customary to adopt the quasiparticle eigenstates at the ground state in Eq. (9). Those with positive [negative] energies, Ψ^0_i [$\tilde{\Psi}^0_i$] satisfy $(H_s - \mu\mathcal{N})\Psi^0_i = E_i\Psi^0_i$ [$(H_s - \mu\mathcal{N})\tilde{\Psi}^0_i = -E_i\tilde{\Psi}^0_i$]. We may write the time-dependent quasiparticle states as $\Psi_i(t) = e^{-iE_it}(\Psi^0_i + \eta\delta\Psi_i(t))$. Since the generalized density $R(t)$ is written in terms of the quasiparticle states $\Psi(t)$ as in Eq. (13), the fluctuating part $\delta R(t)$ in the linear order is given by

$$\begin{aligned}\delta R(t) &= -\sum_i \left\{\delta\Psi_i(t)\Psi^{0\dagger}_i + \Psi^0_i\delta\Psi^\dagger_i(t)\right\} \\ &= -\delta\Psi(t)\Psi^{0\dagger} - \Psi^0\delta\Psi^\dagger(t) \\ &= \delta\tilde{\Psi}(t)\tilde{\Psi}^{0\dagger} + \tilde{\Psi}^0\delta\tilde{\Psi}^\dagger(t),\end{aligned} \tag{48}$$

Using the notation in Sec. II.A.2, we calculate the matrix elements of Eq. (47) between these quasiparticle basis. From the orthonormal relations, it is easy to see $\delta R^{(++)} = \delta R^{(--)} = 0$. Then, only the matrix elements of $(+-)$ and $(-+)$ types are relevant for Eq. (47). Since these matrix are anti-symmetric, the $(+-)$ and $(-+)$ matrix elements of Eq. (47) read, for $i < j$,

$$\begin{aligned}(E_i + E_j - \omega)\delta R^{(+-)}_{ij}(\omega) + \delta H^{(+-)}_{ij}(\omega) &= -V^{(+-)}_{ij}(\omega), \\ (E_i + E_j + \omega)\delta R^{(-+)}_{ij}(\omega) + \delta H^{(-+)}_{ij}(\omega) &= -V^{(-+)}_{ij}(\omega).\end{aligned} \tag{49}$$

The residual fields $\delta H(\omega)$ are induced by the density fluctuation $\delta R(\omega)$, as $\delta H(\omega) = \partial H_s/\partial R|_{R=R_0} \cdot \delta R(\omega)$. Expanding their matrix elements as

$$\delta H^{(+-)}_{ij}(\omega) = \sum_{k<l} w_{ij,kl}\delta R^{(+-)}_{kl}(\omega) + \sum_{k<l} w'_{ij,kl}\delta R^{(-+)}_{kl}(\omega), \tag{50}$$

we obtain the QRPA linear response equations in the matrix form.

$$\left\{\begin{pmatrix} A & B \\ B^* & A^* \end{pmatrix} - \omega\begin{pmatrix} 1 & 0 \\ 0 & -1 \end{pmatrix}\right\}\begin{pmatrix} \delta R^{(+-)} \\ \delta R^{(-+)} \end{pmatrix} = -\begin{pmatrix} V^{(+-)} \\ V^{(-+)} \end{pmatrix}, \tag{51}$$

where $A_{ij,kl} \equiv (E_i + E_j)\delta_{ik}\delta_{jl} + w_{ij,kl}$ and $B_{ij,kl} \equiv w'_{ij,kl}$. $R^\dagger = R$ and $(H_s)^{(\pm\mp)}_{ij} = \delta E/\delta R^{(\mp\pm)}_{ji}$ provide that $w_{ij,kl}$ are Hermitian and $w'_{ij,kl}$ are symmetric.

When the external potential V is identical to a one-body operator F, the strength function is given by

$$S(\omega; F) \equiv \sum_{n>0} |\langle n|F|0\rangle|^2\,\delta(\omega - E_n) = -\frac{1}{\pi}{\rm Im}R(\omega + i\epsilon; F), \tag{52}$$

where ϵ is a positive infinitesimal and

$$\begin{aligned}R(\omega; F) &= \sum_{i<j}\left\{F^{(+-)*}_{ij}\delta R^{(+-)}_{ij}(\omega) + F^{(-+)*}_{ji}\delta R^{(-+)}_{ij}(\omega)\right\} \\ &= \frac{1}{2}{\rm Tr}\left[F\delta R(\omega)\right].\end{aligned} \tag{53}$$

B. Normal modes and eigenenergies

The QRPA normal modes are defined by the eigenvalue problem setting $V = 0$ for Eq. (51). We denote the nth eigenvalue and eigenstate by Ω_n and a column vector Z_n of the dimension $2D$, respectively; D being the number of independent two-quasiparticle pairs (ij) $(i < j)$. It is easy to show that there is a conjugate-partner eigenstate $\tilde{Z}_n$ with the eigenenergy $-\Omega_n$.

$$Z_n \equiv \begin{pmatrix} X_n \\ Y_n \end{pmatrix}, \quad \tilde{Z}_n \equiv \mathcal{I} Z_n^* = \begin{pmatrix} Y_n^* \\ X_n^* \end{pmatrix},$$

where $\mathcal{I} = \begin{pmatrix} 0 & 1 \\ 1 & 0 \end{pmatrix}$. The QRPA eigenvalue equations are

$$\mathcal{N}\mathcal{H} Z_n = \Omega_n Z_n, \quad \mathcal{N}\mathcal{H}\tilde{Z}_n = -\Omega_n \tilde{Z}_n, \tag{54}$$

with the $2D \times 2D$ Hermitian matrices,

$$\mathcal{H} \equiv \begin{pmatrix} A & B \\ B^* & A^* \end{pmatrix}, \quad \mathcal{N} \equiv \begin{pmatrix} 1 & 0 \\ 0 & -1 \end{pmatrix}. \tag{55}$$

The eigenvectors are normalized as $Z_n^\dagger \mathcal{N} Z_m = -\tilde{Z}_n^\dagger \mathcal{N} \tilde{Z}_m = \delta_{nm}$.

Let us define the following $2D \times 2D$ matrices,

$$\mathcal{Z} \equiv (Z, \tilde{Z}) = \begin{pmatrix} X & Y^* \\ Y & X^* \end{pmatrix}, \quad \Omega \equiv \begin{pmatrix} \Omega_D & 0 \\ 0 & \Omega_D \end{pmatrix}, \tag{56}$$

where Ω_D is the $D \times D$ diagonal matrix containing the eigenvalues Ω_n. Then, Eq. (54) can be written as

$$\mathcal{N}\mathcal{H}\mathcal{Z} = \mathcal{Z}\Omega\mathcal{N}. \tag{57}$$

Using the Hermicity of $\mathcal{H}$ and Eq. (57), one can prove $[\mathcal{Z}^\dagger \mathcal{N} \mathcal{Z}, \Omega\mathcal{N}] = 0$, which indicates that $\Omega\mathcal{N}$ and $\mathcal{Z}^\dagger\mathcal{N}\mathcal{Z}$ are both diagonal. Therefore, the normalization condition is written as $\mathcal{Z}^\dagger\mathcal{N}\mathcal{Z} = \mathcal{N}$, which we call "$\mathcal{N}$-orthonormalization". The matrix $\mathcal{N}$ plays a role of the norm matrix. Since this also means $\mathcal{N}\mathcal{Z}\mathcal{N} = (\mathcal{Z}^\dagger)^{-1}$, it leads to the completeness relation, $\mathcal{Z}\mathcal{N}\mathcal{Z}^\dagger = \mathcal{N}$ (Ring and Schuck, 1980). The QRPA matrix $\mathcal{H}$ can be written as

$$\mathcal{H} = \mathcal{N} \sum_n \left(Z_n \Omega_n Z_n^\dagger + \tilde{Z}_n \Omega_n \tilde{Z}_n^\dagger \right) \mathcal{N} = \mathcal{N}\mathcal{Z}\Omega\mathcal{Z}^\dagger\mathcal{N}. \tag{58}$$

From this, it is easy to find $\mathcal{Z}^\dagger\mathcal{H}\mathcal{Z} = \Omega$.

For a given one-body Hermitian operator $\hat{F}$, we define a vector F_v by their $(+-)$-type matrix elements, $F_{ij}^{(+-)}$ with $i < j$, and its RPA conjugate partner $\tilde{F}_v = \mathcal{I} F_v^*$.

$$F_v = \begin{pmatrix} F^{(+-)} \\ 0 \end{pmatrix}, \quad \tilde{F}_v = \begin{pmatrix} 0 \\ F^{(+-)*} \end{pmatrix}.$$

The transition amplitude of F between the ground and the nth excited state is given by

$$\begin{aligned} \langle n|\hat{F}|0\rangle &= \sum_{i<j} \left\{ F_{ij}^{(+-)} X_n(ij) + F_{ij}^{(+-)*} Y_n(ij) \right\} \\ &= Z_n^\dagger (F_v + \tilde{F}_v) = (F_v + \tilde{F}_v)^T Z_n^*. \end{aligned} \tag{59}$$

In most of numerical applications, the QRPA eigenvalue problem is solved by constructing the QRPA matrices in the quasiparticle- or canonical-basis representations. We may transform the non-Hermitian eigenvalue problem of Eq. (54) to a Hermitian one (Ring and Schuck, 1980). For spherical nuclei, the matrix is block-diagonal with respect to the angular momentum and the parity of two-quasiparticle states, $[ij]_M^{J\pi}$. Thus, the numerical cost is moderate in this case and many calculations were performed (See review papers by Bender *et al.* (2003) and Vretenar *et al.* (2005)). In recent years, the QRPA calculations with modern EDFs have become available for deformed nuclei (Arteaga *et al.*, 2009; Losa *et al.*, 2010; Péru and Goutte, 2008; Terasaki and Engel, 2010; Yoshida and Van Giai, 2008). The truncation of the two-quasiparticle space (ij) is usually adopted with respect to either the energy, $E_i + E_j$, or the occupation of the canonical states (ρ_i, ρ_j). The calculation of the residual kernels, $w_{ij,kl}$ and $w'_{ij,kl}$, is very demanding, because they have four quasiparticle indices.

If the residual kernel is written in a separable form with a Hermitian one-body operator $\hat{F}$,

$$w_{ij,kl} = \kappa F_{ij}^{(+-)} F_{lk}^{(-+)}, \quad w'_{ij,kl} = \kappa F_{ij}^{(+-)} F_{lk}^{(+-)},$$

the computational cost may be significantly reduced because the QRPA eigenvalue problem can be cast into a dispersion equation (Ring and Schuck, 1980). For a given set of operators $\{F^{(n)}\}$, the coupling constants $\kappa^{(mn)}$ are derived from the Skyrme EDFs (Nesterenko *et al.*, 2002). This separable RPA calculation has been performed for deformed nuclei to give a reasonable description of giant resonances (Nesterenko *et al.*, 2006).

When the continuous symmetry is broken in the ground state, there is another "ground state" degenerate in energy whose density, $R_0 + \delta R$, is infinitesimally deviated from R_0. Since both R_0 and $R_0 + \delta R$ satisfy the stationary equation (45), one can immediately derive Eq. (47) with $\omega = V = 0$. Therefore, the ANG modes appear as the zero-mode solution with $\Omega_{\rm ANG} = 0$. In this case, it is useful to rewrite Eq. (54) in the momentum-coordinate (PQ) representation (Ring and Schuck, 1980). For the ANG mode (translation/rotation/pair-rotation), the momentum ($P/J/N$) corresponds to a known operator (Sec. II.E.2). Then, it ends up the famous equation by Thouless and Valatin (1962), which determines the inertial mass and the coordinate of the ANG mode [3]. A modern technique to solve the Thouless-Valatin equation and numerical examples are presented in Hinohara (2015).

[3] We note here that there have been some other attempts to explain the finite value of moment of inertia as an analogue of the Higgs mechanism with the SSB (Fujikawa and Ui, 1986).

C. Finite amplitude method

Instead of explicitly calculating the residual kernels with four quasiparticle indices, $w_{ij,kl}$ and $w'_{ij,kl}$, it is possible to compute them in an implicit manner. A possible approach is the finite amplitude method (Nakatsukasa *et al.*, 2007). The essential idea comes from the fact that the linear response equation (49), which is identical to Eq. (51), only contains the "one-body" quantities with two quasiparticle indices. The residual fields $\delta H^{(+-)}(\omega)$ and $\delta H^{(-+)}(\omega)$ can be uniquely determined for given $\delta R_{ij}^{(\pm\mp)}$. The linear expansion in Eq. (50) is achieved by a numerical finite difference method, and δH in the left hand side is obtained without calculating $w_{ij,kl}$ and $w'_{ij,kl}$.

1. Basic idea

The Fourier component $\delta R(\omega)$ can be written in terms of their matrix elements as

$$\delta R(\omega) = \sum_{i,j} \left\{ \Psi_i^0 \delta R_{ij}^{(+-)}(\omega) \tilde{\Psi}_j^{0\dagger} + \tilde{\Psi}_i^0 \delta R_{ij}^{(-+)}(\omega) \Psi_j^{0\dagger} \right\}. \tag{60}$$

Here, the summation with respect to i and j is taken over all the positive-energy quasiparticles. Comparing Eqs. (48) and (60), we find $\delta\Psi_i(\omega) = -\sum_j \tilde{\Psi}_j^0 \delta R_{ji}^{(-+)}$ and $\delta\Psi_i^\dagger(\omega) = -\sum_j \delta R_{ij}^{(+-)} \tilde{\Psi}_j^{0\dagger}$. Using quasiparticle states slightly modified from Ψ_i^0,

$$\Psi_i(\omega) = \Psi_i^0 + \eta\delta\Psi_i(\omega) = \Psi_i^0 - \eta \sum_{j>0} \tilde{\Psi}_j^0 \delta R_{ji}^{(-+)}(\omega),$$
$$\Psi_i'^\dagger(\omega) = \Psi_i^{0\dagger} + \eta\delta\Psi_i^\dagger(\omega) = \Psi_i^{0\dagger} - \eta \sum_{j>0} \delta R_{ij}^{(+-)}(\omega) \tilde{\Psi}_j^{0\dagger},$$

the density $R_\eta(\omega) \equiv R_0 + \eta\delta R(\omega)$ can be written as

$$R_\eta(\omega) = 1 - \sum_i \Psi_i(\omega) \Psi_i'^\dagger(\omega) + O(\eta^2).$$

Note that, since the Fourier component $\delta R(\omega)$ is no longer Hermitian, $\Psi_i(\omega)$ and $\Psi_i'^\dagger(\omega)$ are not Hermitian conjugate to each other. The induced fields are now calculable in the following way.

$$\begin{aligned} \delta H_{ij}^{(+-)}(\omega) &= \Psi_i^{0\dagger} \frac{1}{\eta} \left\{ H_s[R_\eta(\omega)] - H_s[R_0] \right\} \tilde{\Psi}_j^0, \\ \delta H_{ij}^{(-+)}(\omega) &= \tilde{\Psi}_i^{0\dagger} \frac{1}{\eta} \left\{ H_s[R_\eta(\omega)] - H_s[R_0] \right\} \Psi_j^0. \end{aligned} \tag{61}$$

Rigorously speaking, the limit of $\eta \to 0$ should be taken. However, in practice, we may use a small but finite value of η. Using Eq. (61) with a small value of η, calculation of the induced residual fields $\delta H^{(\pm\mp)}$ can be achieved by calculation of matrix elements of the BdGKS Hamiltonian $H_s[R]$. This is much easier task than calculation of the residual kernels, $w_{ij,kl}$ and $w'_{ij,kl}$. It should be noted that $H_s[R_\eta]$ should be constructed self-consistently with the quasiparticles Ψ_i and $\Psi_i'^\dagger$, namely, (U, V) with a small mixture of $\delta R^{(-+)}$ and (U^*, V^*) with a small mixture of $\delta R^{(+-)}$. In order to obtain the solution $\delta R^{(\pm\mp)}$, we solve Eq. (49) iteratively, starting from initial values for $(\delta R^{(+-)}, \delta R^{(-+)})$.

2. Strength functions

For calculation of strength functions, one can solve the linear response equation with a given frequency ω by choosing the external potential V identical to the operator F. Then, according to Eqs. (52) and (53), the strength function $S(F, \omega)$ with respect to F is obtained. To obtain an energy profile of $S(F; \omega)$, we need to repeat the calculation with different values of ω.

There is another approach based on the iterative construction of the subspace in which the diagonalization is performed (Olsen *et al.*, 1988; Tretiak *et al.*, 2009). The Krylov subspace generated by a pivot vector with respect to the one-body operator F preserves the energy-weighted sum rule (EWSR) values. Therefore, it is suitable for calculating a gross energy profile of the strength function by a small number of iterations. Some more details of these iterative methods will be discussed in Sec. III.D. Applications of the finite amplitude method to calculation of the strength functions have been performed for the Skyrme EDFs (Inakura *et al.*, 2014, 2009a, 2011, 2013; Mustonen *et al.*, 2014; Nakatsukasa, 2014; Nakatsukasa *et al.*, 2011; Pei *et al.*, 2014; Stoitsov *et al.*, 2011) and the covariant EDFs (Liang *et al.*, 2013, 2014; Nikšić *et al.*, 2013). The finite amplitude method is also applied to calculation of the sum rules, which suggests approximate validity of the Thouless theorem for nuclear EDFs (Hinohara *et al.*, 2015).

3. Normal-mode eigenstates

It is often our interest to obtain the QRPA eigenmodes. These eigenmodes are, in principle, obtained if the matrix $\mathcal{H}$ in Eq. (57) is explicitly constructed. The finite amplitude method can also be used for this purpose, to facilitate the calculation of the residual kernels (Avogadro and Nakatsukasa, 2013). Suppose we set $\delta R_{kl}^{(+-)} = 1$ for a specific pair (kl) and the rest all zero. Then, the calculation of $\delta H_{ij}^{(+-)}$ using the formula (61) provides $w_{ij,kl}$. On the other hand, setting $\delta R_{kl}^{(-+)} = 1$ and the rest zero, the calculation of $\delta H_{ij}^{(+-)}$ produces $w'_{ij,kl}$. This can be easily understood from Eq. (50). In this way, the QRPA matrix can be calculated without a complicated coding process. The usefulness of the method is demonstrated for the Skyrme (Avogadro and Nakatsukasa, 2013) and

the covariant EDFs (Liang *et al.*, 2013).

When the matrix dimension becomes too large to directly handle, there are other approaches. For instance, solution of the linear response equations (51) with complex frequencies combined with the contour integral serves for this purpose (Hinohara *et al.*, 2013). This is based on the idea that the contour integral around the nth eigenenergy provides

$$(2\pi i)^{-1}\int_{C_n}\delta R_{ij}^{(+-)}(\omega)d\omega = X_n(ij)\langle n|F|0\rangle,$$
$$(2\pi i)^{-1}\int_{C_n}\delta R_{ij}^{(-+)}(\omega)d\omega = Y_n(ij)\langle n|F|0\rangle$$

for an external potential $V = F$. The contour must be chosen to enclose a single pole. This has been tested also for the charge-changing modes (Mustonen *et al.*, 2014).

The truncation of the space by an iterative procedure is another possible option. See Sec. III.D for some more details.

D. Iterative methods for solutions

In the finite amplitude method, the numerical solution of the linear response equation is obtained by using an iterative algorithm. This significantly saves computational resources, especially the necessary memory size, because all we need to calculate are one-body quantities, not two-body ones.

1. Solution for fixed energy

A possible iterative procedure for the solution of Eq. (49) is given as follows: For a given external potential $V_{ij}^{(\pm\mp)}$, we assume a certain initial value for $\delta R_{ij}^{(\pm\mp)}$ for which the residual induced fields $\delta H_{ij}^{(\pm\mp)}$ are calculated according to Eq. (61). $H_s[R_\eta]$ can be calculated with the quasiparticle states Ψ_i^0 and $\Psi_i'^{0\dagger}$ replaced by $\Psi_i(\omega)$ and $\Psi_i^\dagger(\omega)$, respectively. Then, the left hand side of Eq. (49) which is identical to that of Eq. (51), are computed. If these equations are not satisfied, we update the densities, $\delta R_{ij}^{(\pm\mp)}$, according to an adopted iterative algorithm and repeat the calculation until the convergence. When the frequency ω is complex, one should adopt an iterative algorithm which can be applied to a linear algebraic equation with a non-Hermitian matrix.

2. Diagonalization in Krylov subspace

There are recent developments based on the iterative diagonalization based on the Krylov space techniques. This is especially useful for calculations of the strength function, because it conserves the energy-weighted sum-rule (EWSR) value of odd moments. Basically, they resort to the transformation of the matrix with dimension $2D$ into the one in the Krylov subspace with dimension $2d \ll 2D$.

Using Eq. (58), we have

$$(\mathcal{NH})^L = \mathcal{Z}(\Omega\mathcal{N})^{L-1}\Omega\mathcal{Z}^\dagger\mathcal{N} = \mathcal{Z}\Omega^L\mathcal{N}^{L-1}\mathcal{Z}^\dagger\mathcal{N}. \quad (62)$$

Using the expression of transition amplitudes of Eq. (59), the EWSR value of order L is given by

$$m_L \equiv \sum_n \Omega_n^L|\langle n|F|0\rangle|^2 = \frac{1}{2}(F_v+\tilde{F}_v)^\dagger\mathcal{Z}\Omega^L\mathcal{Z}^\dagger(F_v+\tilde{F}_v).$$

For odd-L, using Eq. (62), this can be written as

$$m_L = \frac{1}{2}(F_v+\tilde{F}_v)^\dagger(\mathcal{NH})^L\mathcal{N}(F_v+\tilde{F}_v). \quad (63)$$

Therefore, starting from a pivot vector F_v and its conjugate $\tilde{F}_v$, the Krylov subspace of dimension $2d > L$,

$$\{F_v, \tilde{F}_v, (\mathcal{NH})F_v, (\mathcal{NH})\tilde{F}_v, \cdots, (\mathcal{NH})^{d-1}F_v, (\mathcal{NH})^{d-1}\tilde{F}_v\} \quad (64)$$

can span the intermediate space in Eq. (63). In Appendix A, we show that the reduction from the $2D$ into the $2d$ RPA subspace (64) conserves the sum rules m_L with odd L and $L < 2d$ (Johnson *et al.*, 1999).

To construct the subspace (64), one can adopt the Lanczos iteration algorithm. The Lanczos iteration produces an orthonormal basis set for the Krylov subspace, which makes a and b matrices tridiagonal. This works nicely for the case of a schematic separable interaction (Johnson *et al.*, 1999). However, since numerical errors are accumulated during the iterations, other algorithms, such as the non-Hermitian Arnoldi iteration, have been adopted for realistic Skyrme energy functionals (Toivanen *et al.*, 2010). Even for low-lying eigenstates, the method successfully works (Carlsson *et al.*, 2012). The conjugate gradient algorithm may be another possible solver, which was used for low-lying RPA solutions in the coordinate-space representation (Imagawa and Hashimoto, 2003; Inakura *et al.*, 2006, 2005).

E. Green's function method

It becomes increasingly important to study unbound and weakly bound nuclei in physics of rare isotopes near the drip lines. There have been a number of developments for treatment of the resonance and continuum, including the continuum shell model (Okołowicz *et al.*, 2003), the Gamow shell model (Id Betan *et al.*, 2002; Michel *et al.*, 2002), the Gamow HFB method (Michel *et al.*, 2008), the complex scaling method (Aoyama *et al.*, 2006), and the R-matrix theory (Descouvemont and Baye, 2010). In the linear response calculation based

on the TDDFT, the one-body continuum (and a part of two-body continuum) can be taken into account by the use of Green's function. In this section, we recapitulate the general formalism for superconducting cases ("continuum QRPA").

1. Response function

The QRPA linear response equation (51) can be rewritten as

$$\left(\Pi_0^{-1}(\omega) - \mathcal{W}\right) \begin{pmatrix} \delta R^{(+-)}(\omega) \\ \delta R^{(-+)}(\omega) \end{pmatrix} = \begin{pmatrix} V^{(+-)}(\omega) \\ V^{(-+)}(\omega) \end{pmatrix}, \quad (65)$$

with

$$\Pi_0^{-1}(\omega) \equiv \begin{pmatrix} \omega - A_0 & 0 \\ 0 & -\omega - A_0 \end{pmatrix}, \quad \mathcal{W} \equiv \begin{pmatrix} w & w' \\ w'^* & w^* \end{pmatrix},$$

where $(A_0)_{ij,kl} = (E_i + E_j)\delta_{ik}\delta_{jl}$ in the quasiparticle representation. Equation (65) is inverted by the QRPA response function $\Pi(\omega)$ as $\delta R(\omega) = \Pi(\omega)V(\omega)$, where

$$\Pi(\omega) = (\Pi_0^{-1}(\omega) - \mathcal{W})^{-1} = (1 - \Pi_0(\omega)\mathcal{W})^{-1}\Pi_0(\omega). \quad (66)$$

Here, $\Pi_0(\omega)$ can be schematically written as

$$\Pi_0(\omega) = \sum_i \left\{ \mathcal{G}_0(\omega - E_i)\tilde{\Phi}_i\tilde{\Phi}_i^\dagger + \tilde{\Phi}_i\tilde{\Phi}_i^\dagger\mathcal{G}_0(-\omega - E_i) \right\}, \quad (67)$$

using the Green's function $\mathcal{G}_0(E)$. Its derivation is given in Appendix B. The precise forms of Eq. (67) are given by Eqs. (B4) and (B5).

The strength function with respect to the operator F is obtained according to Eqs. (52) and (53). For $\omega \geq 0$,

$$S(\omega; F) = -\frac{1}{2\pi}\mathrm{Im}\left[F^\dagger \Pi(\omega + i\eta)F\right].$$

From Eq. (B1), one can see that, without the residual interaction $\mathcal{W} = 0$, this leads to the unperturbed strength function, $(1/2)\sum_{ij}|V_{ij}^{(+-)}|^2\delta(\omega - E_i - E_j)$.

Since the response function has four indices, in general, their calculation and inverse operation in Eq. (66) are very difficult tasks. It becomes practical when we need only their diagonal elements. The functional of local densities, such as Skyrme functionals with local potentials, provides an example in which the coordinate-space representation $\{\vec{r}\}$ allows us the diagonal representation. The presence of the spin-orbit and finite-range exchange terms makes its application more difficult.

2. Boundary condition

One of the motivation of the Green's function formalism is the exact treatment of the continuum. This can be done by imposing the proper boundary condition in the Green's functions in Eq. (67). The density response in the time domain can be given by

$$\delta R(t) = \int \Pi(t - t')V(t')dt'.$$

Here, $\Pi(t - t')$ should be zero for $t < t'$; $\Pi(t) = \theta(t)\Pi(t)$. This causality condition is achieved by adding a positive infinitesimal to ω in its the Fourier component $\Pi(\omega)$. Thus, the replacement of $\omega \to \omega + i\eta$ leads to the retarded (outgoing) boundary condition for $\mathcal{G}_0(\omega - E_i)$ and the advanced (incoming) boundary condition for $\mathcal{G}_0(-\omega - E_i)$ in the expression of Π_0. For $\omega > E_i$, the outgoing asymptotic behavior is important for the former Green's function, which describes escaping of a particle or a Cooper pair. This provides an exact treatment of the continuum in the linear density response.

For superconducting systems with the ground-state BdGKS solution with $\kappa \neq 0$, the Green's function with the outgoing (incoming) boundary condition can be constructed for a spherical system using the partial-wave expansion (Belyaev *et al.*, 1987). The quasiparticle states Ψ_i^0 whose energy is smaller than the absolute value of the chemical potential, $E_i < |\mu|$, are bound and discrete, while those with $E_i > |\mu|$ are unbound with continuum spectra. The summation over the quasiparticle states in Eq. (67) must be performed with respect to all the negative-energy states $\tilde{\Psi}_i^0$. This is not trivial because the index i are not discrete but continuous. To overcome this difficulty, the contour integral in the complex energy plane is useful (Matsuo, 2001). The spectral representation of the Green's function (B3) leads to

$$\sum_i f(-E_i)\tilde{\Phi}_i\tilde{\Phi}_i^\dagger = (2\pi i)^{-1}\int_C f(E)\mathcal{G}_0(E), \quad (68)$$

for arbitrary function $f(E)$. Here, the contour C is chosen to enclose the negative part of the real axis. Replacing the summation in Eq. (67) by the contour integral of Eq. (68), the response function is able to describe escaping of one-particle and two-particle decays from excited states. Therefore, the QRPA linear response theory with the Green's function can describe correlations among two escaping particles.

the negative-energy quasiparticles $\tilde{\Psi}_i^0$ are nothing but hole states and the summation over i runs over only the hole states. This method is known as the continuum RPA, and much easier than the continuum QRPA. The numerical applications were first achieved for spherical systems (Shlomo and Bertsch, 1975; Zangwill and Soven, 1980). The continuum RPA calculations with the Gogny EDFs have been recently achieved for spherical systems, by transforming the RPA eigenvalue equation (54) into those for the channel functions (De Donno *et al.*, 2011).

For deformed systems, decomposing the BdGKS Hamiltonian into its spherical and deformed parts, $H_s =$

$H_{\rm sph} + V_{\rm def}$, we can use the identity

$$\mathcal{G}_0^{(\pm)}(E) = \mathcal{G}_{\rm sph}^{(\pm)}(E) + \mathcal{G}_{\rm sph}^{(\pm)}(E) V_{\rm def} \mathcal{G}_0^{(\pm)}(E),$$

where $\mathcal{G}_{\rm sph}^{(\pm)}(E)$ is the Green's function for the spherical Hamiltonian $H_{\rm sph}$. This method with the three-dimensional coordinate-space representation has been applied to normal systems, such as photoabsorption in molecules (Nakatsukasa and Yabana, 2001, 2003; Yabana *et al.*, 2006) and light nuclei (Nakatsukasa and Yabana, 2005), however, not to superconducting systems. For deformed superconducting nuclei, although the full continuum linear response calculation has not been achieved yet, the construction of the Green's function has been carried out by using the coupled-channel scheme (Oba and Matsuo, 2009). The similar method was developed earlier for normal systems, and applied to linear density response in axial symmetric molecules (Levine, 1984; Levine and Soven, 1983, 1984).

F. Real-time method

Another approach to the linear response is to solve the TDBdGKS equation (28) directly in real time, with a weak perturbative external field. In the calculation, we do not linearize the equation. Thus, the same numerical code could serve for studies of the non-linear dynamics (Sec. IV). This is particularly convenient for calculation of the strength function $S(F;E)$ for a wide range of energy, associated with a one-body operator F which does not excite the ANG modes. On the contrary, the method is not suitable for obtaining information on a few excited normal modes. This is due to the uncertainty principle; The achieved energy resolution ΔE is inversely proportional to the duration of time evolution T.

A bulk property of the linear response is determined by time evolution of a short period of time. For instance, the EWSR value associated with a one-body operator F is obtained instantly as

$$m_1 = \sum_n \Omega_n |\langle n|F|0\rangle|^2 = \frac{1}{2\eta}\,\frac{d}{dt}{\rm Tr}\left[FR(t)\right]\Big|_{t=0},$$

where the initial state is boosted by the operator F as $\Psi_i(t=0) = \begin{pmatrix} e^{i\eta F}U_i \\ e^{-i\eta F}V_i \end{pmatrix}$, where the parameter η is a small number. This is generally true for all odd-L moments, $m_L \propto d^L {\rm Tr}[FR(t)]/dt^L|_{t=0}$.

1. Strength functions

The real-time calculation of the strength function is performed in the following way. The initial state is the ground state, and an external potential $V(t) = f(t)F$, which is proportional to the operator F, is activated at time $t = 0$. In the linear regime, the function $f(t)$ should be small to validate the linear response. The strength function (52) can be obtained as

$$S(\omega;F) = \frac{-1}{2f(\omega)}{\rm Im}\int_{-\infty}^{\infty} {\rm Tr}[FR(t)]g(t)e^{i\omega t}dt, \qquad (69)$$

where $f(\omega)$ is a Fourier transform of $f(t)$. If we choose $f(t) = f_0\delta(t)$, we have $f(\omega) = f_0$ which excites all the normal modes with equal strength. In the linear regime, $\int {\rm Tr}[FR(t)]e^{i\omega t}dt$ is proportional to $f(\omega)$. Thus, Eq. (69) gives a unique result.

In order to get a smooth energy profile $S(\omega;F)$, the time dependence in the integrand in Eq. (69) must vanish at $t = T$. In practice, it is customary to include the damping factor $g(t)$ in the integrand in Eq. (69), e.g., the exponential damping associated with a smearing width γ; $g(t) = \theta(t)\theta(T-t)e^{-\gamma t/2}$. The idea of the real-time method was proposed in Błocki and Flocard (1979) to calculate the energies of the giant resonances. The strength functions are calculated with modern Skyrme EDFs (Fracasso *et al.*, 2012; Maruhn *et al.*, 2005; Nakatsukasa and Yabana, 2005; Umar and Oberacker, 2005), and including pairing effects (Ebata *et al.*, 2014, 2010; Hashimoto, 2012; Hashimoto and Nodeki, 2007; Scamps and Lacroix, 2014; Stetcu *et al.*, 2011; Tohyama and Umar, 2002).

2. Absorbing boundary condition

In general, an external potential $V(t)$ excites the system into a superposition of many different elementary modes of excitation. Therefore, the particle decays simultaneously occur at different energies. In contrast to the linear response equation with fixed frequency ω, we do not know the asymptotic form in the real-time method. Nevertheless, in the linear regime, there is a useful method to realize an approximate outgoing boundary condition for normal systems.

A key is that the ground-state KS orbitals $\varphi_i(\vec{r})$ and the transition density in the linear response $\delta\rho(\vec{r},t) = \sum_i \varphi_i(\vec{r})\delta\varphi_i^*(\vec{r},t) + {\rm c.c.}$ are both localized in space. During the time evolution, we may simply *absorb* the outgoing waves from $\varphi_i(\vec{r},t)$ in an outer region ($r > r_0$) where $\varphi_i(\vec{r})|_{r>r_0} = 0$. This can be approximately done by choosing a proper absorbing imaginary potential in the outer region. Note that, in the linear regime, the particle number is still conserved, because $\int_{\rm out}\delta\rho(\vec{r},t)d\vec{r} = 0$. This absorbing boundary condition has been adopted in nuclear TDDFT calculations (Nakatsukasa and Yabana, 2002, 2004, 2005; Reinhard *et al.*, 2006) and treated in a rigorous manner (Pardi and Stevenson, 2013). It is also used in other fields of physical problems (Muga *et al.*, 2004; Yabana *et al.*, 2011). For the superconducting case, even at the ground state of finite localized systems, most of $U_i(\vec{r},\sigma)$ are not localized in space. Thus, the applica-

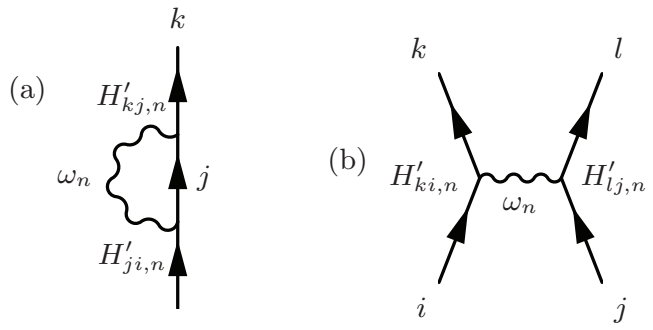

FIG. 3 Second-order diagrams for particle-vibration coupling, contributing to (a) self-energy part $\Sigma_{ki}(E)$, and (b) effective two-particle interactions.

tion of the absorbing boundary condition is not trivial in this case.

G. Extension: Particle-vibration coupling

The QRPA calculation is successful to reproduce a variety of properties of nuclear excitations, especially of high-lying giant resonances. However, it has known limitations too. For instance, the widths of giant resonances in heavy nuclei are not well accounted for, although the peak energy and summed strength are well reproduced. The continuum QRPA is capable of calculating the escaping width of neutrons, however, it does not describe the spreading associated with coupling to complex configurations, such as many-particle-many-hole states. A possible improvement is explicit inclusion of higher-order terms and two-body correlations, which will be presented in Sec. V.D.5. Another approach, which is discussed here, is the particle-vibration coupling (PVC) scheme. The PVC is also supposed to be responsible for the fact that the experimental single-particle level density near the Fermi level is higher than that in modern EDFs whose effective masses are smaller than unity.

The idea of the PVC is very old, and connected to the essential concept of the Bohr-Mottelson's unified model. That is to say, the single-particle motion and the vibrational (collective) motion in nuclei are coupled and influence each other. In earlier times, a phenomenological potential with a schematic separable interaction, $(\kappa/2)\hat{F}\hat{F}$, was used in many applications, which is essentially inspired by the field coupling, $H' = \kappa\alpha\hat{F}$, of Bohr and Mottelson (1975). The PVC produces dressed (renormalized) single-particle states. This affects many kinds of single-particle properties, including self-energies, single-particle moments, transfer matrix elements, and fragmentation of single-particle strengths (See Fig. 3 (a)). It is also expected to contribute to effective two-particle interactions, as Fig. 3 (b), which may be partially responsible for the attractive pairing interaction.

The causal single-particle Green's function obeys the Dyson's equation

$$G(E) = G_0(E) + G_0(E)\Sigma(E)G(E),$$

where $G_0(E)$ is the unperturbed Green's function similar to Eq. (B3) with the causal boundary condition, and $\Sigma(E)$ is the proper self-energy part. The self-energy is alternatively denoted as $M(E)$ and called "mass operator" (Mahaux *et al.*, 1985). In the PVC, $\Sigma(E)$ takes account of coupling to collective vibrations. Normally, low-lying collective vibrational states are selectively included in $\Sigma(E)$. The lowest-order contribution to $\Sigma(E)$ is in the second order coupling in H', as seen in Fig. 3 (a). The diagonal approximation is often adopted for the Dyson's equation, namely, only the diagonal matrix elements of $\Sigma(E)$ in the quasiparticle basis are taken into account.

Recently, the PVC calculation has been carried out with modern EDFs (Brenna *et al.*, 2012; Cao *et al.*, 2014; Colò *et al.*, 2010; Litvinova and Ring, 2006; Litvinova and Afanasjev, 2011; Niu *et al.*, 2014). It is extended to the quasiparticle-vibration coupling (Litvinova, 2012; Litvinova *et al.*, 2008; Yoshida, 2009). They have shown successful description of various kinds of nuclear phenomena, though there exist some ambiguities due to selection of vibrational modes to be taken into account. For weakly bound systems, vibrational states as well as the single-particle states may be in the continuum. As we discussed in Sec. III.E.2, this can be handled by the proper boundary condition for the Green's function. The Dyson's equation in the coordinate-space representation provides a scheme to treat the continuum boundary condition, using a causal response function Π also with the continuum (Mizuyama *et al.*, 2012). This was done for spherical normal systems, so far.

It is not so straightforward to formulate the PVC consistent with the principle of the DFT. A subtraction prescription is proposed (Tselyaev, 2007, 2013) and applied to the PVC (Litvinova *et al.*, 2010) and the second RPA (Gambacurta *et al.*, 2015). For the Skyrme EDF (zero-range effective interactions), some attempts have been recently made to renormalize the divergent second-order diagrams and to produce new EDFs for PVC calculations (Brenna *et al.*, 2014; Moghrabi *et al.*, 2012). To our knowledge, full respect of the Pauli principle and construction of the *DFT-based* particle-vibration coupling theory remain as challenging subjects.

H. Illustrative examples

Recent trends in the linear response studies for nuclei are calculations with all the residual fields (interactions), continuum, pairing, and deformed ground states. Let us show some examples.

1. Giant resonances and ground-state deformation

One of the successful applications of the nuclear EDF to linear response is the study of giant resonances. The giant resonances are high-frequency collective modes of excitation in nuclei, which exhausts a major part of the energy-weighted sum-rule of the transition strengths. They are usually classified according to the spin S, isospin T, and multipolarity L. Their properties are supposed to reflect some basic quantities of the nuclear matter, such as the incompressibility, the symmetry energy, and the effective mass (Harakeh and van der Woude, 2001; Ring and Schuck, 1980). Among them, the isovector giant dipole resonance ($S = 0$, $T = 1$, $L = 1$), which is excited by the photoabsorption, is best known for a long time. The giant dipole resonance is simply characterized by the out-of-phase oscillation of neutrons and protons. The symmetry energy plays a major role in determination of its peak position. Figure 4 shows the photoabsorption cross section for Nd and Sm isotopes. These isotopes are classical examples in the rare-earth region exhibiting the spontaneous shape transition in the ground state from spherical to prolate-deformed shapes, with increasing the neutron number from $N = 82$ (^{142}Nd and ^{144}Sm) to $N = 92$ (^{152}Nd and ^{144}Sm) (Bohr and Mottelson, 1975). The experimental intrinsic quadrupole moment Q_0 is estimated from $B(E2; 2_1^+ \to 0_{\rm gs}^+)$ values, assuming the strong-coupling rotor (Bohr and Mottelson, 1975; Ring and Schuck, 1980). The self-consistent calculation with SkM* and the pairing energy functional (Yamagami *et al.*, 2009) nicely reproduces these values for $N \geq 86$. The development of nuclear deformation leads to a broadening and peak splitting in the photoabsorption cross section. It is the well-known deformation splitting associated with two oscillation modes parallel to the symmetry axis ($K^\pi = 0^-$) and perpendicular to that ($K^\pi = 1^-$).

The calculation involves solving the eigenvalue problem of Eq. (57) within the space truncated with the two-quasiparticle energies $E_i + E_j \leq 60$ MeV. The photoabsorption cross section is obtained from the $E1$ transition strengths, according to Eq. (59), smeared with the Lorentzian width of 2 MeV. This smearing width is the only free parameter in the calculation, which accounts for the spreading effect beyond the present QRPA treatment (See Sec. III.G). It should be noted that, for light systems ($A \lesssim 40$), the agreement is not as good as in heavy nuclei (Erler *et al.*, 2010). This may suggest an insufficient surface symmetry energy in current EDFs.

The isoscalar and isovector giant monopole resonances ($L = 0$) also show the deformation splitting for $N \geq 86$, which is consistent with the experimental data. The excitation energies of the split peaks are shown in Fig. 5 for Sm. This splitting is due to the coupling to the $K^\pi = 0^+$ component of the giant quadrupole resonance ($L = 2$). The monopole and quadrupole are decoupled for spherical nuclei. However, they are coupled in deformed nuclei, the lower peak in Fig. 5 appears at the $K^\pi = 0^+$ peak of the corresponding giant quadrupole resonance.

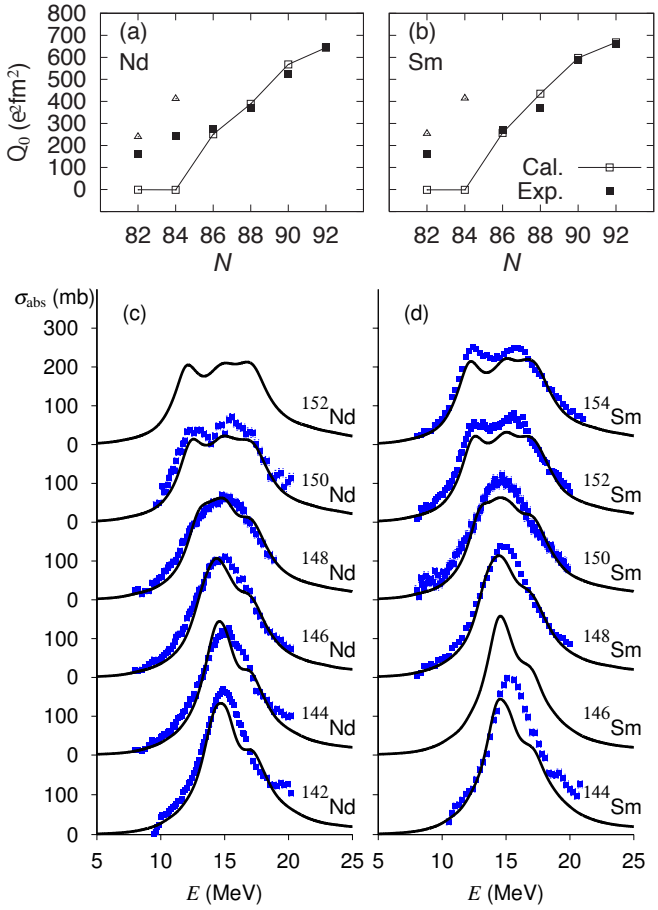

FIG. 4 (Color online) Deformation and photoabsorption in Nd and Sm isotopes, calculated with the Skyrme energy functional of SkM*. Calculated and experimental intrinsic quadrupole moments are denoted by open and closed symbols, respectively, for (a) Nd and (b) Sm isotopes. For spherical nuclei with $N = 82$ and 84, we also plot the values (triangles) extracted from the QRPA calculation for $B(E2; 2^+ \to 0^+)$. Photoabsorption cross sections for (c) Nd and (d) Sm isotopes. for Nd and Sm isotopes. The solid lines show the calculation and blue symbols are experimental data (Carlos *et al.*, 1974, 1971). Adapted from Yoshida and Nakatsukasa (2011).

The deformation of the momentum distribution (Fermi sphere) plays an essential role in the restoring force for the isoscalar giant resonances (Ring and Schuck, 1980). A typical well-studied example is the giant quadrupole resonance whose energy is approximately fit by $64A^{-1/3}$ MeV. The nuclear EDFs in the KS scheme nicely account for this effect of the quantum Fermi liquid, producing the correct mass number dependence. For deformed systems, in addition to this, the deformation splitting among $K^\pi = 0^+$, 1^+, and 2^+ peaks is well reproduced. The simple pairing-plus-quadrupole interaction produces the K

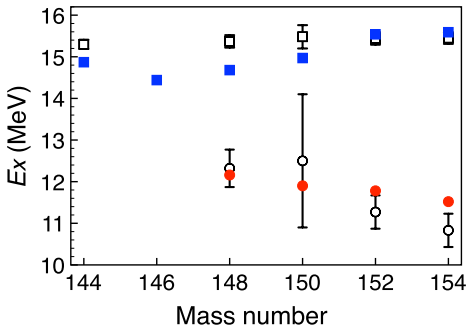

FIG. 5 (Color online) The excitation energies of the isoscalar giant monopole resonances in the Sm isotopes; calculated values (closed symbols) and experimental data (open symbols) (Itoh *et al.*, 2003). From Yoshida and Nakatsukasa (2013).

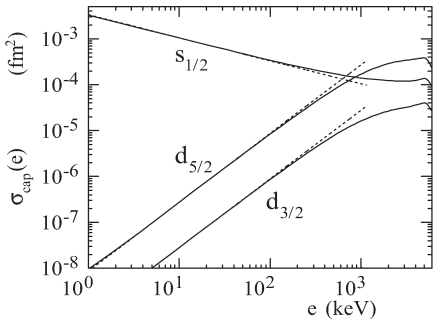

FIG. 6 Neutron capture cross sections n+^{141}Sn as functions of neutron energy e, for incident neutrons in $s_{1/2}$, $d_{3/2}$, and $d_{5/2}$ states. The Skyrme SLy4 EDF and the density-dependent pairing EDF is used. The dotted lines indicate the power law scaling $\propto e^{l-1/2}$. From Matsuo (2015).

splitting, $E_{K=2}-E_{K=0}$, of about 7 MeV for ^{154}Sm. This is too large and inconsistent with experiments (Kishimoto *et al.*, 1975). It is due to the violation of the nuclear self-consistency between the shapes of the potential and the density distribution. The calculation of the SkM* functional predicts the K splitting of 2.8 MeV (Yoshida and Nakatsukasa, 2013).

Systematic calculations with Skyrme EDFs for spherical nuclei have been performed using the canonical-basis QRPA (Paar *et al.*, 2003; Terasaki and Engel, 2006). The QRPA computer codes for deformed nuclei based on the matrix diagonalization have been developed for the Skyrme EDF (Losa *et al.*, 2010; Terasaki and Engel, 2010; Yoshida and Nakatsukasa, 2011; Yoshida and Van Giai, 2008), the Gogny EDF (Péru *et al.*, 2011; Péru and Goutte, 2008), and the covariant EDF (Arteaga *et al.*, 2009). The calculations for deformed systems require large computational resources for construction and storage of matrix $\mathcal{H}$ in Eq. (55). Systematic calculations for a wide range of nuclei have been performed by avoiding explicit calculations of $\mathcal{H}$, with the finite amplitude method (Inakura *et al.*, 2009b, 2011; Nakatsukasa *et al.*, 2011), and with the real-time method in Sec. IV.A (Ebata *et al.*, 2014; Scamps and Lacroix, 2013b).

2. Low-lying quadrupole states

Low-lying states associated with the quadrupole vibrations have been one of the major interests in nuclear structure problems. Systematic analysis of the QRPA calculations for the first excited $J^\pi = 2^+$ states in spherical nuclei, and for the gamma vibrations ($K^\pi = 2^+$) in deformed rare-earth nuclei have been performed by Terasaki and Engel (2011) and Terasaki *et al.* (2008) using the Skyrme EDFs. They qualitatively agree with the trend of experimental data for spherical nuclei. Overall agreement of the QRPA results with experiments are better than that of other approaches based on the generator coordinate method (Sabbey *et al.*, 2007). However, the agreement is not quite as good for deformed nuclei. The five-dimensional collective Hamiltonian for the large amplitude quadrupole motion may give a better description (Bertsch *et al.*, 2007; Delaroche *et al.*, 2010). The problems in the description of low-frequency quadrupole modes of excitation will be discussed in Sec. V.

3. Charge-exchange modes

The isovector excitations have charge-changing ($\tau_\pm$) modes. For spherical nuclei, the calculations have been performed mostly with the Skyrme EDFs, (Bender *et al.*, 2002; Engel *et al.*, 1999; Fracasso and Colò, 2005; Paar *et al.*, 2007), but also with the covariant EDFs (Liang *et al.*, 2008; Niu *et al.*, 2013; Paar *et al.*, 2004). The deformed QRPA calculations for the charge-exchange modes have been performed with the separable approximation (Sarriguren, 2012; Sarriguren *et al.*, 2001). Very recently, the full QRPA calculations have become available too (Martini *et al.*, 2014; Mustonen and Engel, 2013; Yoshida, 2013). The neutrino-nucleus reaction was also studied including inelastic neutral-current scattering (Dapo and Paar, 2012). The Gamow-Teller strength distribution ($S = 1$, $T = 1$) significantly affects the β-decay half-lives and the waiting point of the rapid neutron capture process (r-process). To determine the r-process path far away from the stability line, the reliable theoretical estimates are highly desired.

4. Nuclear response in the continuum

For nuclei near the neutron drip line, weakly bound neutrons may produce large transition strength just above the threshold. The examples were observed in low-energy electric dipole ($E1$) strength in light halo nuclei,

such as ^{11}Be (Nakamura *et al.*, 1994) and ^{11}Li (Ieki *et al.*, 1993; Nakamura *et al.*, 2006; Shimoura *et al.*, 1995; Zinser *et al.*, 1997). The enhancement is not associated with the collectivity, but due to the quantum mechanical "threshold effect". Whether the *collective* low-energy dipole resonances exist in heavier neutron-rich nuclei is still an open question (Hansen and Jonson, 1987; Ikeda, 1992). In order to properly address these issues in which the continuum plays an important role, the Green's function method in Sec. III.E is a powerful tool. For doubly-closed spherical nuclei, we may neglect the pairing, and the continuum RPA calculations have been extensively performed to study a variety of strength functions (See Paar *et al.* (2007) and Sagawa (2001) and references therein). However, for open-shell and heavier systems, we need to simultaneously treat the deformation and the paring correlations. This has not been achieved yet, however, partially done with modern EDFs; the Green's function method for deformed systems (Nakatsukasa and Yabana, 2005) and that for superconducting systems (Daoutidis and Ring, 2011; Matsuo, 2015; Mizuyama *et al.*, 2009; Serizawa and Matsuo, 2009).

The photo-absorption of neutron-rich nuclei leads to neutron decays if the excitation energy exceeds the neutron separation energy, which is very low in nuclei near the neutron-drip line. It has been known that one can decompose the strength function (the photo-absorption cross section) in the continuum RPA into partial strength functions for individual channels of particle escape (Nakatsukasa and Yabana, 2001; Zangwill and Soven, 1980). Matsuo (2015) has recently extended the idea to the continuum QRPA. The decomposition allows, using the reciprocity theorem for the inverse processes, to compute the cross section of the direct neutron capture cross sections for different entrance channels separately. Figure 6 shows those for n+^{141}Sn, calculated from the E1 strength functions in the continuum QRPA. In this example, the cross section follows the power-law scaling rule. This would not be the case if there was a low-energy resonance.

IV. REAL-TIME CALCULATIONS BEYOND THE LINEAR REGIME

In nuclear physics, the real-time real-space calculations of the TDDFT have been explored since 1970's, starting with simplified energy functionals (Bonche *et al.*, 1976). It became the primary approach for studying low-energy heavy-ion collisions. Since the Pauli blocking hinders the two-body collisions, the method was thought to work well at low energy, typically lower than the Fermi energy of about 40 MeV. There is an excellent review paper on these developments in early years, before 1982 (Negele, 1982). In recent years, we have observed important progresses in the real-time calculations with respect to several aspects.

1. *Realistic EDF*

In earlier works, it was common to adopt simplified EDFs such that the spin-orbit term is neglected. Recent calculations remove these restrictions and incorporate the full EDF self-consistently. The adopted EDFs for time-dependent calculations have become as realistic as those for static calculations. Most time-dependent calculations beyond the linear regime have been performed with Skyrme energy functionals (Kim *et al.*, 1997; Maruhn *et al.*, 2014; Simenel, 2012; Umar and Oberacker, 2006c). These changes produce even qualitative differences in nuclear dynamics. For instance, the famous fusion window anomaly was significantly hindered by the inclusion of the spin-orbit term in EDFs (Reinhard *et al.*, 1988; Umar *et al.*, 1986). Extensive studies have been performed recently for studies of nuclear dynamics, such as quasi-fission (Oberacker *et al.*, 2014; Scamps *et al.*, 2015; Umar *et al.*, 2015), charge equilibration (Iwata *et al.*, 2010a,b), and high-spin rotation (Ichikawa *et al.*, 2014).

2. *TDBdGKS (TDHFB) scheme*

Until very recently, the dynamical pairing correlations were always neglected in the real-time calculations. In the TDBdGKS scheme, the number of quasiparticle orbitals is identical to the dimension of the single-particle model space we adopt. Therefore, the real-time solution of the TDBdGKS (TDHFB) equations requires extremely heavy computational tasks.

Applications of the full TDBdGKS scheme for realistic nuclear EDF were performed with the spherical symmetry restriction (Avez *et al.*, 2008). Later, it has been achieved with no assumption on the spatial symmetry with the Skyrme (Bulgac, 2013; Stetcu *et al.*, 2015, 2011) and Gogny EDFs (Hashimoto, 2012). However, the applications are very limited at present, because of its high computational demands and some problems inherent in the TDBdGKS including the preparation of the initial state and treatment of the non-vanishing wave functions at the boundary. An approximate feasible approach is shown in Sec. IV.A.

3. *Nucleus-nucleus potential and friction parameters*

To get insight into nuclear dynamics with energy dissipation, several ideas have been proposed in late 1970's and 1980's to extract "macroscopic" quantities, such as the nucleus-nucleus potential and the friction parameter associated with the one-body dissipation (Brink and Stancu, 1981; Cusson *et al.*, 1985; Koonin *et al.*, 1977). These ideas, which have been combined with realistic EDFs and recent computational advances, lead to further developments producing a number of new results in recent years. Two different approaches will be presented in Sec. IV.B.

4. *Transfer reaction and fluctuations*

The particle-number projection method in a restricted coordinate space has been proposed to study the mass

(charge) distribution in transfer reactions (Simenel, 2010). It is identical to the method based on the decomposition of the Slater determinant proposed in Koonin *et al.* (1977), however, the former has a significant computational advantage for heavier systems. The recent calculations with realistic EDFs show qualitative agreements with experiments. See Sec. IV.C.

The TDDFT simulations for heavy-ion collision in early days showed that, although the average values of one-body observables were well reproduced, their fluctuations were underestimated. Accordingly, for the transfer reaction, the calculated production rates are well reproduced in major channels, however, not good in rare channels. In order to overcome the difficulties, the fluctuation around the TDDFT path is taken into account (Sec. IV.C.2).

A. Approximate schemes for TDBdGKS equations

Although the real-time calculation based on the full TDBdGKS equations in the three-dimensional space becomes available for a few cases (Hashimoto, 2012; Stetcu *et al.*, 2015, 2011), it is still a very demanding task. Thus, its approximate schemes are useful at present.

The easiest and old one is introduction of the fixed fractional occupation numbers for KS orbitals. For the stationary BCS (ground) state, each orbital ϕ_i has a time-reversal-conjugate partner, $\phi_{\bar{i}}$, and the occupation probability $\rho_i = |v_i|^2$. Then, for the time evolution, we simply neglect the pair potential, $\Delta_{ij}(t) = 0$. The TDKS equations for N_c orbitals ($N_c > N$) are solved in real time. Thus, the pairing effect is taken into account only in the fractional occupation which is completely determined at the preparation of the initial state. In this scheme, the pair potentials play no role in the time evolution.

To include the dynamical pairing in a minimum way, we may keep the diagonal form of the Hamiltonian, but with the pair potential $\Delta_{i\bar{j}}(t) = -\Delta_i(t)\delta_{ij}$. The quasiparticles are given by the canonical pair of orbitals ϕ_i and $\phi_{\bar{i}}$ multiplied by complex factors ($|u_i|^2 + |v_i|^2 = 1$).

$$\Phi_i = \begin{pmatrix} u_i\phi_i \\ -v_i^*\phi_{\bar{i}}^* \end{pmatrix}, \quad \Phi_{\bar{i}} = \begin{pmatrix} u_i\phi_{\bar{i}} \\ v_i^*\phi_i^* \end{pmatrix}.$$

Then, the TDBdGKS equations (28) are factorized into 2×2 form. Using the relation $\Delta_{i\bar{i}}\phi_{\bar{i}}^* = -\Delta_i\phi_i$, the TDBdGKS equations are split into

$$\begin{aligned} i\frac{\partial}{\partial t}\phi_i(t) &= \{h_s[\rho(t)] - \mu - \eta_i(t)\}\,\phi_i(t), \quad i \leftrightarrow \bar{i}, \\ i\frac{d}{dt}\rho_i(t) &= \kappa_i(t)\Delta_i^*(t) - \kappa_i^*(t)\Delta_i(t), \\ i\frac{d}{dt}\kappa_i(t) &= \{\eta_i(t) + \eta_{\bar{i}}(t)\}\,\kappa_i(t) + \Delta_i(t)\,\{2\rho_i(t) - 1\}, \end{aligned} \tag{70}$$

where $\rho_i(t) \equiv |v_i(t)|^2$, $\kappa_i(t) \equiv u_i(t)v_i(t)$, and $\eta_i(t)$ are parameters to control the phase of the canonical orbitals $\phi_i(t)$. The $\eta_i(t)$ are arbitrary, if the diagonal form of the pair potential is consistent with the gauge invariant EDFs. When it is violated in practice, a choice of the minimal phase change was proposed (Ebata *et al.*, 2010).

When the pair potential is calculated from the anti-symmetrized two-body interaction $\bar{v}$, $\Delta_i(t) = -\sum_{j>0}\kappa_j(t)\bar{v}_{i\bar{i},j\bar{j}}$. The densities are constructed as

$$\begin{aligned} \rho(\alpha\beta,t) &= \sum_i \rho_i(t)\phi_i(\alpha;t)\phi_i^*(\beta;t), \\ \kappa(\alpha\beta,t) &= \sum_{i>0}\kappa_i(t)\left\{\phi_i(\alpha;t)\phi_{\bar{i}}(\beta;t) - \phi_{\bar{i}}(\alpha;t)\phi_i(\beta;t)\right\}. \end{aligned}$$

Equations similar to Eq. (70) were derived using the time-dependent variational principle some time ago (Błocki and Flocard, 1976) and revisited in terms of the TDBdGKS equations (Ebata *et al.*, 2010). The conservation of the average particle number is guaranteed for arbitrary choice of μ, however, the energy conservation depends on the choice of the parameter $\eta_i(t)$ (Ebata *et al.*, 2010), and the current conservation is violated in this approximation (Scamps *et al.*, 2012). The equations may describe dynamical pairing effects, coupled to motion of the canonical orbitals. The method has been applied to real-time calculations for linear response (Ebata *et al.*, 2014, 2010; Scamps and Lacroix, 2013b), neutron transfer reactions (Scamps and Lacroix, 2013a), and fusion/fission reactions (Ebata and Nakatsukasa, 2014, 2015; Scamps *et al.*, 2015).

B. Heavy-ion collision: Nucleus-nucleus potential and one-body dissipation

In real-time calculation of heavy-ion collision, so far, the TDKS equations with $\kappa = \Delta = 0$ are solved in most applications. The initial state is prepared as two nuclei in their ground states, placed well separated in space. First, we locate the two nuclei, (N_L, Z_L) in the left and (N_R, Z_R) in the right, with respect to the z coordinate. In this initial state, each KS orbital $|\phi_i\rangle$ belongs to either "left" or "right", and those in the left nucleus are boosted toward right by $|\phi_i(t=0)\rangle = e^{ik_L z}|\phi_i\rangle$, while those in the right by $|\phi_i(t=0)\rangle = e^{-ik_R z}|\phi_i\rangle$. Then, the time evolution of KS orbitals is computed to obtain the density $\rho(\alpha\beta;t) = \sum_i \rho_i(t)\phi_i(\alpha;t)\phi_i^*(\beta;t)$.

Recently, there are a number of works to extract the nucleus-nucleus potential and the friction from non-empirical TDDFT calculations. To achieve this, we should divide the total system into two parts, one associated with a small number of collective degrees of freedom, and the rest of the Hilbert space called "intrinsic" space. To our understanding, so far, this division is guided by "a priori" assumptions, not by the TDDFT dynamics itself.

1. Density-constraint calculation

Among many kinds of densities, for the colliding nuclei under consideration, the normal density distribution $\rho(\vec{r};t)$ and the current density, $\vec{j}(\vec{r};t) = 1/(2i)(\vec{\nabla} - \vec{\nabla}')\rho(\vec{r},\vec{r'};t)|_{\vec{r}=\vec{r'}}$, are regarded as quantities associated with collective motion. Then, the collective energy associated with the collisional motion is assumed to be a functional of $\rho(\vec{r})$ and $\vec{j}(\vec{r})$, which is defined as the minimization with constraints on the density and the current.

$$E_{\rm coll}\left[\rho(\vec{r},t),\vec{j}(\vec{r},t)\right] = \min_{\rho\to(\rho(\vec{r}),\vec{j}(\vec{r}))} F[\rho] - E_L - E_R, \quad (71)$$

where E_L and E_R are the ground-state energies of two nuclei. For the initial state with two nuclei far apart ($t = 0$), this approximately corresponds to the sum of the kinetic energy of center of mass of each nucleus, $P_L^2/(2A_Lm) + P_R^2/(2A_Rm)$, and the Coulomb energy between the two, $Z_LZ_Re^2/|\vec{R}_L - \vec{R}_R|$. Since the total energy is conserved during the time evolution, we have $E_{\rm total} \approx E_L + E_R + E_{\rm coll}(t = 0)$.

The TDDFT simulation of the heavy-ion collision produces the time-dependent density $\rho(\vec{r},t)$ and current $\vec{j}(\vec{r},t)$. From these, the intrinsic excitation energy during the collision is given by

$$E^*(t) = E_{\rm total} - E_{\rm coll}\left[\rho(\vec{r};t),\vec{j}(\vec{r};t)\right] - E_L - E_R. \quad (72)$$

Furthermore, the collective energy is divided into two; $E_{\rm coll}[\rho(\vec{r}),\vec{j}(\vec{r})] = E_{\rm kin}[\rho(\vec{r}),\vec{j}(\vec{r})] + V_{\rm pot}[\rho(\vec{r})]$ and the nucleus-nucleus potential is defined by the latter, obtained by minimization with a constraint on $\rho(\vec{r})$.

$$V_{\rm pot}\left[\rho(\vec{r})\right] = \min_{\rho\to\rho(\vec{r})} F[\rho] - E_L - E_R. \quad (73)$$

This minimization automatically produces $\vec{j}(\vec{r}) = 0$ for even-even nuclei. In practice, since the density and current constraint calculation of Eq. (71) is computationally demanding, the density constraint calculation of Eq. (73) is performed. Then, the collective kinetic energy is assumed to be

$$E_{\rm kin}\left[\rho(\vec{r}),\vec{j}(\vec{r})\right] = \frac{1}{2m}\int \frac{|\vec{j}(\vec{r})|^2}{\rho(\vec{r})}d\vec{r}. \quad (74)$$

So far, all the quantities are calculated as functions of time t. A possible mapping from t to a collective coordinate $R(t)$ is given in Sec. IV.B.2.

The idea and computational algorithm of this method are proposed in Cusson *et al.* (1985). Extensive studies have been performed in recent years by Oberacker, Umar, and coworkers (Oberacker and Umar, 2013; Oberacker *et al.*, 2010; Simenel *et al.*, 2013; Umar *et al.*, 2010; Umar and Oberacker, 2006a,b, 2007, 2008; Umar *et al.*, 2012a, 2009, 2012b). The TDDFT naturally provides dynamical change of the nuclear structure during collisions. Therefore, the potential $V_{\rm pot}$ in Eq. (73) contains such polarization effects. However, the separation between the collective energy (71) and the dissipation energy (72) is less reliable when two nuclei are significantly overlapped. Even without any dissipation, the current density $\vec{j}(\vec{r})$ is reduced in the overlapping region because two nuclei are moving to opposite directions. This leads to the reduction of $E_{\rm coll}$ ($E_{\rm kin}$) and to overestimation of E^*.

2. Mapping to one-dimensional Hamilton equations of motion

Another even simpler method is based on the explicit introduction of the one-dimensional (1D) collective coordinate and momentum. We recapitulate here the method presented in Washiyama and Lacroix (2008) to extract the nucleus-nucleus potential $V_{\rm pot}(R)$ and friction parameter $\gamma(R)$. Similar methods are proposed earlier (Brink and Stancu, 1981; Koonin *et al.*, 1977). We introduce the relative distance between two nuclei, $R(t)$, calculated as the distance between two centers of mass in the left and the right. Assuming the head-on collision on the z-axis, $R(t) = (1/A_R)\int_R z\rho(\vec{r},t)d\vec{r} - (1/A_L)\int_L z\rho(\vec{r},t)d\vec{r}$. The momentum $P(t)$ is calculated as $P(t) = (A_L\int_R j_z(\vec{r},t)d\vec{r} - A_R\int_L j_z(\vec{r},t)d\vec{r})/(A_L + A_R)$. Here, the integration $\int_{R(L)} d\vec{r}$ are defined by $\int_{R(L)} d\vec{r}f(\vec{r}) = \int d\vec{r}f(\vec{r})\theta(\pm(z - z_0))$. The $z = z_0$ plane can be chosen, for instance, as the plane of the lowest density (neck position). The TDDFT calculation produces $R(t)$ and $P(t)$ as functions of time, which are assumed to obey the 1D classical Hamilton equation of motion:

$$\frac{dR}{dt} = \frac{P}{\mu(R)}, \quad \frac{dP}{dt} = -\frac{dV_{\rm pot}}{dR} - \gamma(R)\frac{dR}{dt}, \quad (75)$$

where the first equation provides the definition of the reduced mass $\mu(R)$. There are two unknown quantities remaining, the force $dV_{\rm pot}/dR$ and the friction parameter $\gamma(R)$. Assuming weak energy dependence of these quantities, we can estimate these by performing the TDDFT simulation with two slightly different initial energies. Note that, because of the head-on assumption, the parameter $\gamma(R)$ may represent only the radial friction, not the tangential one.

Since the density-constraint calculation at different $R(t)$ is not necessary in this approach, it is computationally easier than the previous one. Similarly to the density constrained calculation, the calculated relative momentum decreases after two nuclei touch, even if no dissipation takes place. In addition, the assumption, that R and P are canonical conjugate variables, becomes questionable as well.

C. Heavy-ion collision: Transfer reaction

1. Number projection

The mass number distribution after the collision was estimated for a schematic EDF (Koonin *et al.*, 1977). It is based on the decomposition of the single Slater determinant in a restricted space, and has been used for electron transfer processes in atomic collisions (Ludde and Dreizler, 1983; Nagano *et al.*, 2000). Recently, an alternative expression has been given using the particle number projection (Simenel, 2010). They are identical in principle, however, the latter has a computational advantage over the previous expression.

Let us divide the space V into two regions; one is V_f and the rest $V_{\bar{f}} = V - V_f$. The particle number in the space V_f, N_f, is defined by $\hat{N}_f = \int_f \hat{\psi}^\dagger(\vec{r}\sigma)\hat{\psi}(\vec{r}\sigma)d\vec{r}$. The particle number projection in the right space, $\hat{P}_f(N)$, is given by

$$\hat{P}_f(N) = \frac{1}{2\pi}\int_0^{2\pi} d\theta e^{i\theta(N-\hat{N}_f)}$$

Let us define the matrix $B_{ij}(\theta)$ as $B_{ij}(\theta) \equiv \langle\phi_i|\phi_j\rangle_{\bar{f}} + e^{-i\theta}\langle\phi_i|\phi_j\rangle_f$, with the overlap in the spaces V_f and $V_{\bar{f}}$ given by

$$\langle\phi_i|\phi_j\rangle_{f(\bar{f})} \equiv \sum_\sigma \int_{f(\bar{f})} \phi_i^*(\vec{r}\sigma)\phi_j(\vec{r}\sigma)d\vec{r}.$$

The probability that the N particles are present in V_f is given by

$$P_N = \frac{1}{2\pi}\int_0^{2\pi} d\theta e^{i\theta N}\det B(\theta) \tag{76}$$

In the real-time simulation, after the two nuclei collide and separate again, we specify the region V_f where one of the nucleus is located. Then, the mass number distribution is calculated according to Eq. (76). The production cross section of the nucleus with N particles is estimated by repeating the same calculation with different impact parameter b.

$$\sigma(N) = 2\pi\int dbbP_N(b). \tag{77}$$

This is most useful for the calculations of transfer reaction cross section $\sigma_{\pm N,\pm Z}$. When the pair potential is present, the number projection is required for the initial state too.

The expectation value of the operator in each reaction product can also be evaluated with the present technique (Sekizawa and Yabana, 2014, 2015; Sonika *et al.*, 2015). For instance, the one-body operator local in the coordinate, $\hat{O} = \sum_\sigma \int O(\vec{r})\hat{\psi}^\dagger(\vec{r}\sigma)\hat{\psi}(\vec{r}\sigma)d\vec{r}$, is given by

$$O_N = \frac{1}{2\pi P_N}\int_0^{2\pi} d\theta e^{i\theta N}\det B(\theta) \sum_i \left(\langle\phi_i|O|\phi_i\rangle_L + e^{-i\theta}\langle\phi_i|O|\phi_i\rangle_R\right)$$

2. Fluctuations

The TDDFT provides feasible approaches to nuclear collective dynamics in a large-amplitude nature, and has been successful to describe mean values of one-body observables. However, it has been known for some time that it underestimates fluctuations (Koonin *et al.*, 1977; Negele, 1982). As far as we calculate the one-body observables according to the KS orbitals, a severe limitation comes from mainly two sources: One is missing effect of two-body collisions. The inclusion of the nucleon-nucleon collision is treated by a stochastic approaches (Aichelin, 1991) or by explicit inclusion of two-body correlations (Shun-jin and Cassing, 1985). Although the two-body collision becomes less important at lower energy, there is another well-known limitation, which we address here. The TDDFT is described by a single time-dependent mean-field (KS) potential. The collision of nuclei, in general, leads to superposition of different final states, $|\Phi^{(1)}\rangle$, $|\Phi^{(2)}\rangle$, $\cdots$, for which different mean fields should exist, $v_s^{(1)}(\vec{r})$, $v_s^{(2)}(\vec{r})$, $\cdots$. Since these dynamics in multi-channels are described by a single average mean field $v_s^{(\mathrm{av})}$, the TDDFT naturally hinders the fluctuation. This may be crucial at low energies, in which one-body dynamics are supposed to play a dominant role (Ikeda *et al.*, 1986).

A practical way to improve the situation is given by replacing the quantum fluctuation by classical statistical ensemble in the initial state. Each state is evolved in time with its own mean field. This is often called "stochastic mean field theory" (Ayik, 2008; Lacroix and Ayik, 2014).

The quantum fluctuation at the initial state is estimated by the fluctuation of one-body operator $\hat{A}$ in a Slater determinant

$$\sigma_A^2 \equiv \langle\hat{A}^2\rangle - \langle\hat{A}\rangle^2 = \sum_{ij}\left|\langle\phi_i|\hat{A}|\phi_j\rangle\right|^2\rho_i(1-\rho_j).$$

For normal systems at zero temperature, the occupation is integer number, $\rho_i = 0$ or 1. In order to describe this quantum fluctuation by the classical statistical average as $\langle\hat{A}\rangle = \mathrm{tr}[\overline{\rho^{(n)}}A]$ and $\sigma_A^2 = \overline{(\mathrm{tr}[\delta\rho^{(n)}A])^2}$, we use random Gaussian numbers for one-body density, $\rho^{(n)} = \overline{\rho^{(n)}} + \delta\rho^{(n)}$, which satisfies the ensemble average values

$$\overline{\rho_{ij}^{(n)}} = \rho_i\delta_{ij}, \tag{78}$$

$$\overline{\delta\rho_{ij}^{(n)}\delta\rho_{kl}^{(n)}} = \frac{1}{2}\delta_{il}\delta_{jk}\left\{\rho_i(1-\rho_j) + \rho_j(1-\rho_i)\right\}. \tag{79}$$

Starting from each initial configuration $\rho^{(n)}$, $\rho^{(n)}(t)$ evolves in time following the TDKS equation, Eq. (35), with the density given by

$$\rho^{(n)}(t) = \sum_{ij} |\phi_i^{(n)}(t)\rangle \rho_{ij}^{(n)} \langle \phi_j^{(n)}(t)|.$$

Since the off-diagonal elements of $\rho_{ij}^{(n)}$ are non-zero, we need to solve the time evolution of not only the hole states, but also the particle states.

For calculations of small fluctuations around the TDKS trajectory in the observable $\hat{A}$ at $t = t_f$, instead of performing the forward time evolution of $\delta\rho(t)$ with the initial fluctuation of Eqs. (78) and (79), we may utilize a backward time evolution. The time evolution of $\delta\rho(t)$ is described by a unitary operator $U(t)$ as $\rho(t) = U(t)\rho(t=0)U^\dagger(t)$ in general. Note that the linear approximation with respect to $\delta\rho^{(n)}$ leads to the operator $U(t)$ independent of the event label (n), Thus, the fluctuating part of the observable $\hat{A}$ can be written as

$$\delta A^{(n)}(t_f) = \mathrm{tr}\left[\hat{A}\delta\rho^{(n)}(t_f)\right] = \mathrm{tr}\left[\hat{B}\delta\rho^{(n)}(0)\right],$$

where t_f represents the final time when the observation is made and $t = 0$ is the initial time. Here, the one-body Hermitian operator $\hat{B}$ is given by $B_{ij} = \left\{U^\dagger(t_f)\hat{A}U(t_f)\right\}_{ij}$. The fluctuation of $\hat{A}$ at $t = t_f$ is now given by the ensemble average at $t = 0$.

$$\sigma_A^2 = \overline{\left\{\delta A^{(n)}(t_f)\right\}^2} = \sum_{ijkl} B_{ij}B_{kl}\overline{\delta\rho_{ji}^{(n)}\delta\rho_{lk}^{(n)}} \quad (80)$$

$$= \sum_{ij} |B_{ij}|^2 \rho_i(1-\rho_j) \quad (81)$$

In fact, Eq. (81) is the same as the one previously derived with the variational approach by Balian-Vénéroni (Balian and Vénéroni, 1985). It is easy to see that Eq. (81) can be alternatively written as $-\mathrm{tr}[[B,\rho(0)]^2]/2$ with $\rho_{ij}(0) = \rho_i\delta_{ij}$. Thus, modifying the TDDFT density $\rho(t)$ at $t = t_f$ as $\eta_\epsilon(t_f) \equiv e^{i\epsilon\hat{A}}\rho(t_f)e^{-i\epsilon\hat{A}}$, the backward evolution of $\eta_\epsilon(t)$ up to $t = 0$ gives the following expression

$$\sigma_A^2 = \lim_{\epsilon\to 0}\frac{1}{2\epsilon^2}\mathrm{tr}\left[\left\{U^\dagger(t_f)\eta_\epsilon(t_f)U(t_f) - \rho(0)\right\}^2\right]. \quad (82)$$

This is useful for practical calculations (Simenel, 2011, 2012). The KS wave functions $|\phi_i(t_f)\rangle$ are modified to $e^{i\epsilon\hat{A}}\phi_i(t_f)$ with small ϵ, then, calculate the backward time evolution to $t = 0$. This will provide $U^\dagger(t_f)\eta_\epsilon(t_f)U(t_f)$. Several different values of ϵ may be enough to identify its quadratic dependence. More details and derivation can be found in Simenel (2012).

D. Illustrative examples

In this section, we present some examples of recent calculations in studies of nuclear collision dynamics. The full TDBdGKS calculation of collision dynamics has not been achieved, but is under progress (Stetcu *et al.*, 2015). Most of recent calculations beyond the linear regime have been performed based on the TDKS equations with the Skyrme EDFs.

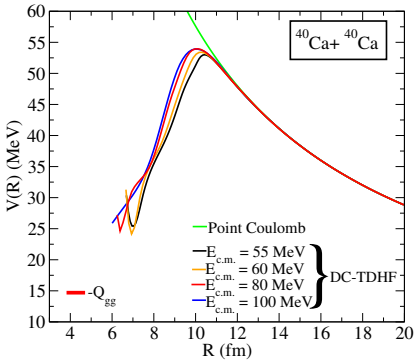

FIG. 7 (Color online) Internucleus potential for ^{40}Ca+^{40}Ca for different energies. The horizontal axis is the distance between two ^{40}Ca nuclei. The green line indicates the Coulomb potential assuming the point charge $20e$ at the center of each nucleus. "DC-TDHF" is an abbreviation of the density-constrained TDHF. From Umar *et al.* (2009).

1. Internucleus potential and precompound excitation

Extensive studies using the real-time simulation have been performed for microscopic derivation of the nucleus-nucleus potential and dissipation energy at initial stages of the nuclear fusion. This can be done with the density-constraint calculation shown in Sec. IV.B. The real-time simulation for the fusion reaction produces the time evolution of the density $\rho(\vec{r},t)$, the current $\vec{j}(\vec{r},t)$, etc. At the beginning, the total energy is given by $E_{\mathrm{total}} = E_{\mathrm{coll}}(t = 0) + E_L + E_R$. After the two nuclei touch, E_{total} is also shared by the intrinsic excitation energy E^*.

According to Eq. (73), (72) and (74), Umar *et al.* (2009) estimated the nucleus-nucleus potential $V(R)$ and the intrinsic excitation $E^*(R)$ for ^{40}Ca+^{40}Ca. These are illustrated in Figs. 7 and 8. The amount of the dissipative energy E^* is roughly proportional to the bombarding energy $E_{\mathrm{cm}} = E_{\mathrm{coll}}(t = 0)$, while the potential V_{pot} is approximately independent of the choice of E_{cm}. The excitation energy for the fused system ^{80}Zr is expected to be $E_{\mathrm{total}} - E_{\mathrm{g.s.}}(^{80}\mathrm{Zr})$ at the end. The calculated E^* at the capture point near $R = 6$ is still lower than this value by about 20 MeV. It is confirmed that this 20 MeV is due to the difference in the density distribution between at the ground state of ^{80}Zr and at the capture point.

The internucleus potential obtained from the mapping to the one-dimensional (1D) classical equation of motion (75) seems to be similar to the one of the density-constrained calculation for some light systems (Washiyama and Lacroix, 2008). However, in heavier sys-

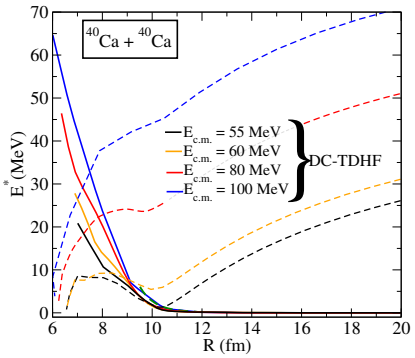

FIG. 8 (Color online) Excitation energy E^* (solid lines) in Eq. (72) for ^{40}Ca+^{40}Ca collision at different energies. The dashed lines indicate the collective kinetic energy $E_{\rm kin}$ in Eq. (74). From Umar *et al.* (2009).

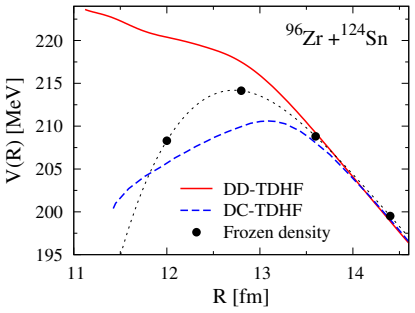

FIG. 9 (Color online) Internucleus potential for ^{96}Zr+^{124}Sn calculated at $E_{\rm cm} = 230$ MeV. The red solid curve is based on Eq. (75), while the blue dashed line is the one of the density-constrained calculation of Eq. (73). The frozen density potential is plotted by the filled circles. "DD-TDHF" is an abbreviation of the dissipative-dynamics TDHF. From Washiyama (2015).

tems where the dissipation becomes more relevant, they may produce different potentials. In fact, for the heavy systems with $Z_L Z_R \gtrsim 1600$, it is known that the fusion probability is significantly hindered. An example is given by the fact that the fusion cross section of ^{96}Zr+^{124}Sn ($Z_L Z_R = 2000$) is much smaller than that of ^{40}Ar+^{180}Hf ($Z_L Z_R = 1296$), both leading to the same fused system, ^{220}Th (Sahm *et al.*, 1985). This was supposed to be due to the strong energy dissipation inside the Coulomb barrier (Swiatecki, 1982). The quasi-fission before the formation of a compound nucleus may play a primary role in the fusion hindrance. Although the TDDFT cannot fully take into account the collisional damping, it reproduces some features of the quasi-fission process (Oberacker *et al.*, 2014; Simenel, 2012).

Figure 9 shows the calculated potential for ^{96}Zr+^{124}Sn. The potential of the density-constrained calculation shows a maximum around $R = 13.1$ fm and decreases at $R < 13$ fm. This is very different from the one obtained by mapping to the 1D classical equations, which keeps rising even at $R < 13$ fm. This must be attributed to the difference in the decomposition of the total energy into $V(R)$, $E_{\rm kin}(R)$, and $E^*(R)$. Since we can expect the $E_{\rm kin}$ in these two methods are rather similar, the intrinsic excitation $E^*(R)$ should compensate the difference in $V(R)$. The relation between the two methods in IV.B.1 and IV.B.2 is not clear at present. The further studies are desired to clarify the microscopic origin of the fusion hindrance (Guo and Nakatsukasa, 2012; Simenel, 2012). It is also related to a conceptual question: *What are the collective variables, the potential, and the inertial mass for proper description of many kinds of nuclear reaction?* This is the main subject of Sec. V.

2. Multi-nucleon transfer reaction

Another example of low-energy nuclear reaction is the multi-nucleon transfer reaction for heavy-ion collisions. At energies near the Coulomb barrier, this reaction involves many kinds of quantum non-equilibrium many-body dynamics, such as shell effects, neck formation, and tunneling. The GRAZING model (Winther, 1994) is frequently used to describe the multi-nucleon transfer reaction. This model is based on statistical treatment of the single-particle transfer processes and a semi-classical formulation of coupled-channel method. The TDKS (TDHF) simulation may provide an alternative microscopic approach to the low-energy transfer reaction and help our fundamental understanding of the quantum dynamics.

After the real-time simulation at the impact parameter b, the transfer probability $P_{N,Z}(b)$ for each channel of (N, Z) can be calculated according to Eq. (76). Repeating the calculation with different values of b, the cross section $\sigma_{N,Z}$ is calculated as Eq. (77). An example for the ^{48}Ca+^{124}Sn reaction is presented in Fig. 10, showing the production cross sections of Ar ($-2p$), K ($-1p$), Ca ($0p$), Sc ($+1p$), Ti ($+2p$) isotopes. The horizontal axis corresponds to the neutron number of fragments. In the major channels of $0p$ and $\pm 1p$, the experimental data are well reproduced. The calculated mass distribution is rather symmetric with respect to the neutron number around $N = 28$. The experimental data seem to suggest that this symmetry is broken for the $\pm 2p$ channels. In general, the discrepancy becomes more prominent for rarer channels with large number of exchanged nucleons (Sekizawa and Yabana, 2013). Nevertheless, the quality of the agreement is the same as the GRAZING calculation. It should be noted that the simulation was carried out using the Skyrme SLy5 EDF and there were no free parameters.

As we have seen in Fig. 10, in the $\pm 2p$ channels, the neutrons tend to move together with the protons, which is not reproduced in the calculation. This is due to the fact that the TDDFT calculation does not have correla-

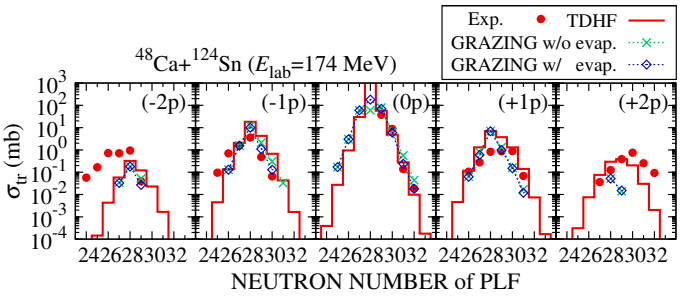

FIG. 10 (Color online) Transfer cross sections for ^{48}Ca+^{124}Sn reaction at $E_{\rm lab} = 174$ MeV. The red solid lines show the TDDFT results with the particle-number projection. The experimental data and the GRAZING results are taken from Corradi *et al.* (1997). See text for details. From Sekizawa and Yabana (2013).

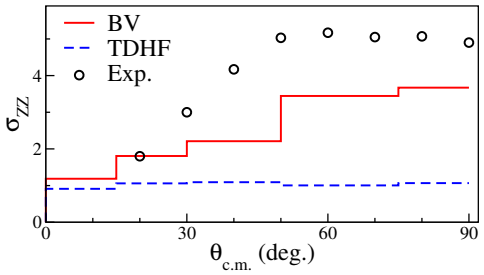

FIG. 11 (Color online) The fluctuation in the proton number distribution, $\sigma_{ZZ} \equiv (\langle Z^2\rangle - \langle Z\rangle^2)^{1/2}$, for final fragments in the ^{40}Ca+^{40}Ca reaction. The horizontal axis corresponds to the scattering angle that is determined by the impact parameter in the TDDFT calculation. The circles show experimental data (Roynette *et al.*, 1977). From Simenel (2011).

tions between neutron and proton distributions, namely, $P_{N,Z} = P_N P_Z$. This missing correlation and fluctuation has been studied by Simenel (2011) for ^{40}Ca+^{40}Ca at $E_{\rm cm} = 128$ MeV, using the Balian-Vénéroni formula analogous to Eq. (82). For small impact parameter b, he has found strong correlation between proton and neutron distributions. In addition, the fluctuation of the proton distribution is compared with the available experiment in Fig. 11. The conventional TDDFT simulation significantly underestimates the fluctuation. It is enhanced by the formula (82) getting closer to the experimental data, though it is not enough for the perfect reproduction.

V. COLLECTIVE SUBMANIFOLD AND REQUANTIZATION OF TDDFT

In this section, we introduce an assumption that the time-evolution of the densities are determined by a few collective coordinates and momenta, $R(q,p)$, as we have done in Sec. II.E. This leads to a microscopic derivation of the collective Hamiltonian describing large amplitude collective phenomena. We then quantize the collective variables and obtain the collective Schrödinger equation. Numerical examples are given for low-frequency quadrupole collective excitations which are dominating in low-lying states in almost all nuclei. We focus on recent advances and basic ideas of the approaches based on the TDDFT but relations to other time-independent approaches are also briefly discussed.

A. Problems in large-amplitude collective motion

First, let us discuss conceptual problems in TDDFT studies beyond the linear regime in nuclear physics. We have presented in Sec. III that excitation energies and transition amplitudes can be obtained in the linear response. For instance, the Fourier analysis on the time evolution of the density, such as Eq. (69), allows us to extract those quantities. In this case, when we scale the external field by a parameter f as $V \to fV$, the density fluctuation $\delta R(\omega)$ is invariant except for the same linear scaling, $\delta R(\omega) \to f\delta R(\omega)$. This allows us to uniquely define the transition densities.

In principle, the TDDFT can describe exact dynamics of many-body systems (see Sec. II.D). However, in nuclear EDFs, at least, we do not know in practice how to extract information on excited states and genuine quantum phenomena which involve large-amplitude many-body dynamics. Perhaps, most typical example is given by spontaneous fission phenomena. Even if the nucleus is energetically favored by dividing it into two fragments, the non-linearity of the TDDFT forbids the tunneling.

Beyond the linear regime, as the oscillating amplitudes become larger, the nonlinear effects play more important roles. In fact, there are some attempts to quantify the nonlinear coupling strengths between different modes of excitation using real-time TDDFT calculations (Simenel and Chomaz, 2003; Simenel *et al.*, 2001, 2007). In addition to the linear response, the quadratic dependence is identified to extract the coupling between dipole and quadrupole modes (Simenel and Chomaz, 2009). Nevertheless, the practical real-time method to quantify energy spectra of anharmonic vibrations has not been established.

Our strategy to these difficulties is to adopt the "requantization" procedure. Perhaps, this is not perfectly consistent with the original principle of TDDFT which should be "exact" and does not require additional quantum fluctuation in the theory. However, as we have noted in Secs. I.C and II.B.2, since the present nuclear EDF is reliable within a certain time scale (typically the SSB time scale), the quantum fluctuations associated with longer time scales should be addressed additionally. The TDDFT dynamics of Eq. (33) can be parameterized with classical canonical variables (ξ^α, π_α) which obey the classical Hamilton equations (Blaizot and Ripka, 1986). The space spanned by these variables are called "TDHFB phase space", whose dimension is twice the number

of two-quasiparticle pairs. Therefore, in nuclear physics, the issue has been often discussed in terms of the requantization of the TDDFT dynamics. Further arguments on the requantization are given by the stationary phase approximation to the functional integral formulation of the many-body quantum theory (Negele, 1982).

To describe long time-scale slow motion in nuclei, we introduce small number of collective variables. In low-energy spectra in nuclei, we observe a number of states which possess properties very difficult to quantify with the real-time TDDFT simulations; for instance, states with fluctuating shapes, those with mixture of different shapes, anharmonic nature of many phonon states, quasi-rotational spectra which show features between phonon-like and rotational-like excitations. Nuclear fission also provides another typical example of nuclear large amplitude collective motion. These low-energy dynamics in nuclei requires us to develop practical theories applicable to nuclear large-amplitude collective motion (LACM).

B. Fundamental concepts for low-energy nuclear dynamics and historical remarks

In Sec. III, we present the QRPA method, as a small-amplitude approximation of the TDDFT, for microscopically describing various kinds of collective excitations around the equilibrium points, given by $[H_{\rm eff}[R_0] - \mu\mathcal{N}, R_0] = 0$. In this Sec. V, we review the recent advances of the approaches aiming at microscopic description of LACM by extending the basic ideas of the QRPA to non-equilibrium states far from the local minima of the EDF. Construction of microscopic theory of LACM has been a difficult long-standing subject in nuclear structure theory. The issues in 1980's were discussed in a proceedings (Abe and Suzuki, 1983), including the one by Villars (1983) which summarized problems and questions for theories of nuclear collective motion. Since then, we have achieved a significant progress in theoretical formulation and applications to real nuclear phenomena in recent years.

1. Basic ideas

The basic idea for constructing, on the basis of the time-dependent density functional method, a microscopic theory of large-amplitude collective phenomena (at zero temperature) is to introduce an assumption that time evolution of the density is determined by a few collective coordinates $q(t) = \{q_1(t), q_2(t), \cdots, q_f(t)\}$ and collective momenta $p(t) = \{p_1(t), p_2(t), \cdots, p_f(t)\}$. We assume that the time-dependent density can be written as $R(t) = R(q(t), p(t))$. At this stage, p and q are introduced as parameters in place of the time t. We shall see, however, that it is possible to formulate a theory such that they are canonical variables obeying the Hamilton equations of motion, i.e, they are classical dynamical variables. Accordingly, we call them "collective variables". The great merit of this approach is, obviously, that they are readily quantized, according to the standard canonical quantization. In this way, we can derive, microscopically and self-consistently, the quantum collective Hamiltonian describing LACM. Because of developments in the nuclear-theory history, we call this canonical quantization procedure "collective quantization of time-dependent self-consistent mean field". In the TDDFT terminology, this can be regarded as the inclusion of missing correlations in long time scales. In Sec. V.C, we develop this idea in a more concrete form.

Notes on terminology and notation

Because of these practical and historical reasons, it is customary to use the terminology and the notation of mean-field theories, such as TDHF and TDHFB instead of TDDFT (TDKS, TDBdGKS). We follow this tradition in this section. The theory presented here takes account of correlations and fluctuations beyond the mean field, which correspond to those missing in current nuclear EDFs.

In order to help comprehensibility, we introduce the TDHF(B) state $|\phi(t)\rangle$ in Sec. V.C, which is defined by the quasiparticle vacuum $a_i(t)|\phi(t)\rangle = 0$ at every time t (time-dependent version of Eq. (12)). Accordingly, we also use the Hamiltonian $\hat{H}$ which is related to the EDF as $E[\rho] = \langle\phi(t)|\hat{H}|\phi(t)\rangle$.

2. ANG modes associated with broken symmetries and quantum fluctuations in finite systems

We discussed in Sec. II.E.2 how to treat the collective motions restoring the symmetries spontaneously broken in the mean fields for three typical examples (center-of-mass motion, pair rotation in gauge space, and three-dimensional rotation in coordinate space). Let us recall, in particular:

1. The ANG modes restoring the gauge invariance broken in the BCS theory of superconductivity have been experimentally observed in nuclei as the pairing rotational modes (Brink and Broglia, 2005).
2. The rotational spectra widely seen in nuclei can be regarded as ANG modes restoring the spherical symmetry spontaneously broken in the mean field (Alder *et al.*, 1956; Bohr and Mottelson, 1975; Frauendorf, 2001).
3. We know generators of the collective variables for the ANG modes, at least for one of $\overset{\circ}{Q}$ and $\overset{\circ}{P}$ in Sec. II.E. Those are given by global one-body operators, such as $\hat{\vec{R}}_{\rm cm}$ and $\hat{\vec{P}}_{\rm cm}$ for the translation, $\hat{\vec{J}}$ for the rotation, and $\hat{N}$ for the pair rotation. However, the generators conjugate to $\hat{\vec{J}}$ and $\hat{N}$ are not trivial.

On the other hand, we should keep in mind that the

mean fields of finite quantum systems always accompany quantum fluctuations. One of the most important characteristics of low-energy excitation spectra of nuclei is that the amplitudes of the quantum shape fluctuation often become very large. Among large-amplitude shape fluctuation phenomena, we should be, of course, referred to the well-known spontaneous fission, which can be regarded as macroscopic quantum tunnelings through the potential barrier generated by the self-consistent mean field. To construct a microscopic theory capable of describing such large-amplitude shape fluctuations/evolutions has been a challenge in nuclear structure theory. Historically, such attempts started in 1950's to formulate a microscopic theory of collective model of Bohr and Mottelson. The major approach at that time is to introduce collective coordinates explicitly as functions of coordinates of individual nucleons and separate collective shape degrees of freedom from the rest (see, *e.g.*, Tomonaga (1955)). This turned out to fail in description of low-energy modes of shape fluctuations. One of the important lessons we learned from these early attempts is that, in contrast to the ANG modes, it is not trivial at all to define microscopic structure of collective coordinates appropriate for low-energy shape vibrations. The low-energy collective vibrations are associated with fluctuations of order parameters characterizing the mean field (Stringari, 1979). In this sense, it may be categorized as a kind of Higgs amplitude modes (Pekker and Varma, 2015), but we need to go beyond the small-amplitude approximation for fluctuations about the equilibrium points in order to describe them.

After the initial success of the BCS+QRPA approach for small amplitude oscillations in 1960's, attempts to construct a microscopic theory of LACM started in mid 1970's. At that time, real-time TDHF (TDDFT) calculations for heavy-ion collisions also started, using semi-realistic EDFs. These attempts introduced collective coordinates as parameters specifying the time-evolution of the self-consistent mean field, instead of explicitly defining them as functions of coordinates of individual nucleons. This was a historical turning point in basic concept of collective coordinate theory: In these new approaches, it is unnecessary to define *global* collective operators, as functions of coordinates of individual nucleons. As we shall see in Sec. V.C, it is sufficient to determine infinitesimal generators for time-evolution of the self-consistent mean field, *locally* at every point of the the collective variables (q, p). Note that we use, in this section, the term *local* to indicate the neighbor of a point (q, p) in the collective space, instead of the conventional coordinate $\vec{r}$ in the three-dimensional coordinate space. In general, the microscopic structures of the infinitesimal generators for shape evolution may change as functions of (q, p). From this point of view, it is not only unnecessary but also inappropriate to introduce the global operators in order to describe low-energy shape fluctuations. This is in sharp contrast with the high-frequency giant quadrupole resonances for which the small-amplitude approximation works well and the mass-quadrupole operator can be regarded as an approximate collective coordinate operator.

3. Characteristics of quadrupole excitation spectra in low-lying states

Low-frequency quadrupole vibrations of the nucleus may be regarded as collective surface excitations of a finite superfluid system. Accordingly, pairing correlations and varying shell structure of the self-consistent mean field play essential roles in their emergence (Åberg *et al.*, 1990; Bender *et al.*, 2003; Bohr and Mottelson, 1975; Matsuyanagi *et al.*, 2013; Rowe and Wood, 2010). For nuclei in the transitional region from spherical to deformed, amplitudes of quantum shape fluctuation remarkably increase. This corresponds to soft modes of the quantum phase transition towards symmetry-violating equilibrium deformations of the mean filed. The gain in binding energies due to the symmetry breaking is comparable in magnitude to the vibrational zero-point energies. The transitional region is prevalent in nuclear chart, and those nuclei exhibit a rich variety of excitation spectra in systematics.

In finite quantum systems like nuclei, the rotational ANG modes may couple rather strongly with quantum shape fluctuation modes. For instance, even when the self-consistent mean field acquires a deep local minimum at a finite value of β, the nucleus may exhibit a large-amplitude shape fluctuation in the γ degree of freedom, if the deformation potential is flat in this direction. Here, as usual, β and γ represent the magnitudes of axially symmetric and asymmetric quadrupole deformations, respectively. Such a situation is widely observed in experiments and called γ-soft nuclei. The rotational degrees of freedoms about three principal axes are all activated once the axial symmetry is dynamically broken due to the quantum shape fluctuation. Consequently, rotational spectra in such γ-soft nuclei do not exhibit a simple $I(I+1)$ pattern. Such an interplay of the shape fluctuation and rotational modes may be regarded as a characteristic feature of finite quantum systems and provides an invaluable opportunity to investigate the process of the quantum phase transition through analysis of quantum spectra.

Thus, we need to treat the two kinds of collective variables, *i.e.*, those associated with the symmetry-restoring ANG modes and those for quantum shape fluctuations, in a unified manner to describe low-energy excitation spectra of nuclei.

C. Microscopic derivation of collective Hamiltonian

1. Extraction of collective submanifold

As we have mentioned in Sec. V.A, the TDHFB dynamics is represented as the classical Hamilton equations for canonical variables in the TDHFB phase space, (ξ^α, π_α) (Kuriyama *et al.*, 2001; Negele, 1982; Yamamura and Kuriyama, 1987). The dimension of this phase space is huge, $\alpha = 1, \cdots, D$ where D is the number of all the two-quasiparticle pairs. The TDHFB state vector $|\phi(t)\rangle = |\phi(\xi(t), \pi(t))\rangle$ is regarded as a generalized coherent state moving on a trajectory in the TDHFB phase space. For low-energy fluctuations in collective motion, however, we assume that the time evolution is governed by a few collective variables.

During the attempts to construct microscopic theory of LACM since the latter half of the 1970s, significant progress has been achieved in the fundamental concepts of collective motion. Especially important is the recognition that microscopic derivation of the collective Hamiltonian is equivalent to extraction of a collective submanifold embedded in the TDHFB phase space, which is approximately decoupled from other "non-collective" degrees of freedom. From this point of view we can say that collective variables are nothing but local canonical variables which can be flexibly chosen on this submanifold. Here, we recapitulate recent developments achieved on the basis of such concepts.

Attempts to formulate a LACM theory without assuming adiabaticity of large-amplitude collective motion were initiated by and led to the formulation of the self-consistent collective coordinate (SCC) method (Marumori *et al.*, 1980). In these approaches, collective coordinates and collective momenta are treated on the same footing. In the SCC method, basic equations determining the collective submanifold are derived by requiring maximal decoupling of the collective motion of interest from other non-collective degrees of freedom. The collective submanifold is invariant with respect to the choice of the coordinate system, whereas the collective coordinates depend on it. The idea of coordinate-independent theory of collective motion was developed also by Rowe (1982), and Yamamura and Kuriyama (1987). This idea gave a significant impact on the fundamental question, "what are the collective variables?". The SCC method was first formulated for the canonical form of the TDHF without pairing. Later, it is extended to that of TDHFB for describing nuclei with superfluidity (Matsuo, 1986).

In the SCC method, the TDHFB state $|\phi(t)\rangle$ is written as $|\phi(q,p)\rangle$ under the assumption that the time evolution is governed by a few collective coordinates $q = (q^1, q^2, \cdots, q^f)$ and collective momenta $p = (p_1, p_2, \cdots, p_f)$. Note that the parameterizing the TDHFB state with the $2f$-degrees of freedom (q,p) is nothing but defining a submanifold inside the TDHFB phase space (ξ^α, π_α), which we call "collective submanifold". The time-dependent densities are readily obtained from the TDHFB state $|\phi(q,p)\rangle$ by

$$\rho(\vec{r}; q, p) = \sum_\sigma \langle \phi(q,p)|\hat{\psi}^\dagger(\vec{r}\sigma)\hat{\psi}(\vec{r}\sigma)|\phi(q,p)\rangle,$$
$$\kappa(\vec{r}; q, p) = \langle \phi(q,p)|\hat{\psi}(\vec{r}\downarrow)\hat{\psi}(\vec{r}\uparrow)|\phi(q,p)\rangle.$$

The following basic equations determine the TDHFB state $|\phi(q,p)\rangle$ parameterized by (q,p) and its time evolution, which gives the definition of the submanifold.

1. *Invariance principle of the TDHFB equation*

We require that the TDHFB equation of motion is invariant in the collective submanifold. This requirement can be written in a variational form as

$$\delta\langle\phi(q,p)|\left\{i\frac{\partial}{\partial t} - \hat{H}\right\}|\phi(q,p)\rangle = 0. \tag{83}$$

Here, the variation δ is given by $\delta|\phi(q,p)\rangle = a_i^\dagger a_j^\dagger|\phi(q,p)\rangle$ in terms of the quasiparticle operators $\{a_i^\dagger, a_j\}$, which satisfy the vacuum condition $a_i|\phi(q,p)\rangle = 0$. Under the basic assumption, the time derivative is replaced by

$$\frac{\partial}{\partial t} = \sum_{i=1}^f \left(\dot{q}^i\frac{\partial}{\partial q^i} + \dot{p}_i\frac{\partial}{\partial p_i}\right) = \dot{q}^i\frac{\partial}{\partial q^i} + \dot{p}_i\frac{\partial}{\partial p_i}.$$

Hereafter, to simplify the notation, we adopt the Einstein summation convention to remove $\sum_{i=1}^f$. Accordingly, Eq. (83) is rewritten as

$$\delta\langle\phi(q,p)|\left\{\dot{q}^i\overset{\circ}{P}_i(q,p) - \dot{p}_i\overset{\circ}{Q}^i(q,p) - \hat{H}\right\}|\phi(q,p)\rangle = 0 \tag{84}$$

in terms of the local infinitesimal generators defined by

$$\overset{\circ}{P}_i(q,p)|\phi(q,p)\rangle = i\frac{\partial}{\partial q^i}|\phi(q,p)\rangle, \tag{85}$$

$$\overset{\circ}{Q}^i(q,p)|\phi(q,p)\rangle = -i\frac{\partial}{\partial p_i}|\phi(q,p)\rangle. \tag{86}$$

These are one-body operators which can be written as linear combinations of bilinear products $\{a_i^\dagger a_j^\dagger, a_i^\dagger a_j, a_j a_i\}$ of the quasiparticle operators defined with respect to $|\phi(q,p)\rangle$. Equations (84), (85) and (86) correspond to Eqs. (40), (41), and (42) in Sec. II.E, respectively.

2. *Canonicity conditions*

We require q and p to be canonical variables. According to the theorem of Frobenius and Darboux (Arnold, 1989), pairs of canonical variables (q,p) exist for the TDHFB states $|\phi(q,p)\rangle$ satisfying the following *canonicity conditions*,

$$\langle\phi(q,p)|\overset{\circ}{P}_i(q,p)|\phi(q,p)\rangle = p_i + \frac{\partial S}{\partial q^i}, \tag{87}$$

$$\langle\phi(q,p)|\overset{\circ}{Q}^i(q,p)|\phi(q,p)\rangle = -\frac{\partial S}{\partial p_i}, \tag{88}$$

where S is an arbitrary differentiable function of q and p (Marumori *et al.*, 1980; Yamamura and Kuriyama, 1987).

By specifying S we can fix the type of allowed canonical transformations among the collective variables (q,p). We shall discuss typical examples in subsequent subsections and call the canonicity conditions with a specified function S "*canonical-variable conditions*." Taking derivatives of Eqs. (87) and (88) with respect to p_i and q^i, respectively, we can readily confirm that the local infinitesimal generators satisfy the 'weakly' canonical commutation relations,

$$\langle\phi(q,p)|\left[\overset{\circ}{Q}{}^i(q,p),\overset{\circ}{P}_j(q,p)\right]|\phi(q,p)\rangle = i\delta_{ij}.$$

Taking variations of Eq. (84) in the direction of the collective variables, q and p, generated by $\overset{\circ}{P}_i$ and $\overset{\circ}{Q}{}^i$, we obtain the Hamilton equations of motion,

$$\frac{dq^i}{dt} = \frac{\partial\mathcal{H}}{\partial p_i}, \quad \frac{dp_i}{dt} = -\frac{\partial\mathcal{H}}{\partial q^i}. \tag{89}$$

Here, the total energy $\mathcal{H}(q,p) \equiv \langle\phi(q,p)|\hat{H}|\phi(q,p)\rangle$ plays the role of the classical collective Hamiltonian.

3. *Equation of collective submanifold*

The invariance principle (84) and Eq. (89) lead to the equation of collective submanifold:

$$\delta\langle\phi(q,p)|\left\{\hat{H} - \frac{\partial\mathcal{H}}{\partial p_i}\overset{\circ}{P}_i(q,p) - \frac{\partial\mathcal{H}}{\partial q^i}\overset{\circ}{Q}{}^i(q,p)\right\}|\phi(q,p)\rangle = 0. \tag{90}$$

Taking variations $\delta_\perp$ in the directions orthogonal to q and p, we can immediately find $\delta_\perp\langle\phi(q,p)|\hat{H}|\phi(q,p)\rangle = 0$. This implies that the energy expectation value is stationary with respect to all variations except for those along directions tangent to the collective submanifold. In other words, the large-amplitude collective motion is decoupled from other modes of excitation.

2. Solution with (η,η^*) expansion

In the original paper of the SCC method (Marumori *et al.*, 1980), the TDHFB state $|\phi(q,p)\rangle$ is written as

$$|\phi(q,p)\rangle = U(q,p)|\phi_0\rangle = e^{i\hat{G}(q,p)}|\phi_0\rangle.$$

Here, $U(q,p)$ represents a time-dependent unitary transformation from the HFB ground state $|\phi_0\rangle$ taken as an initial state; $U(q,p) = 1$ at $q = p = 0$. It is written in terms of an Hermitian one-body operator $\hat{G}(q,p)$.

With use of complex variables $\eta = (\eta_1,\eta_2,\cdots,\eta_f)$ defined by

$$\eta_i = \frac{1}{\sqrt{2}}(q^i + ip_i), \quad \eta_i^* = \frac{1}{\sqrt{2}}(q^i - ip_i),$$

we can rewrite the TDHFB state as

$$|\phi(\eta,\eta^*)\rangle = U(\eta,\eta^*)|\phi_0\rangle = e^{i\hat{G}(\eta,\eta^*)}|\phi_0\rangle,$$

Correspondingly, we define local infinitesimal generators, $\overset{\circ}{O}{}_i^\dagger(\eta,\eta^*)$ and $\overset{\circ}{O}_i(\eta,\eta^*)$, by

$$\overset{\circ}{O}{}_i^\dagger(\eta,\eta^*)|\phi(\eta,\eta^*)\rangle = \frac{\partial}{\partial\eta_i}|\phi(\eta,\eta^*)\rangle,$$
$$\overset{\circ}{O}_i(\eta,\eta^*)|\phi(\eta,\eta^*)\rangle = -\frac{\partial}{\partial\eta_i^*}|\phi(\eta,\eta^*)\rangle.$$

Replacing (q,p) by (η,η^*), the equation of collective submanifold (90) is rewritten as

$$\delta\langle\phi_0|U^\dagger(\eta,\eta^*)\left\{\hat{H} - \frac{\partial\mathcal{H}}{\partial\eta_i^*}\overset{\circ}{O}{}_i^\dagger(\eta,\eta^*) - \frac{\partial\mathcal{H}}{\partial\eta_i}\overset{\circ}{O}_i(\eta,\eta^*)\right\} \times U(\eta,\eta^*)|\phi_0\rangle = 0. \tag{91}$$

Here, the variation is to be performed only for the HFB ground state $|\phi_0\rangle$.

We assume the following canonical-variable conditions,

$$\langle\phi(\eta,\eta^*)|\overset{\circ}{O}{}_i^\dagger(\eta,\eta^*)|\phi(\eta,\eta^*)\rangle = \frac{1}{2}\eta_i^*, \tag{92}$$

$$\langle\phi(\eta,\eta^*)|\overset{\circ}{O}_i(\eta,\eta^*)|\phi(\eta,\eta^*)\rangle = \frac{1}{2}\eta_i, \tag{93}$$

which are obtained by a specific choice of $S = -\frac{1}{2}\sum_i q^i p_i$ in the canonicity conditions, (87) and (88). From Eqs. (92) and (93), we can easily obtain the "weak" boson commutation relations,

$$\langle\phi(\eta,\eta^*)|\left[\overset{\circ}{O}_i(\eta,\eta^*),\overset{\circ}{O}{}_j^\dagger(\eta,\eta^*)\right]|\phi(\eta,\eta^*)\rangle = \delta_{ij}.$$

Because only linear canonical transformations among η and η^* keep Eqs. (92) and (93) invariant, these canonical-variable conditions are suitable to a solution of the variational equation (91) with a power series expansion of $\hat{G}$ with respect to (η,η^*),

$$\hat{G}(\eta,\eta^*) = \hat{G}_i^{(10)}\eta_i^* + \hat{G}_i^{(01)}\eta_i + \hat{G}_{ij}^{(20)}\eta_i^*\eta_j^* + \hat{G}_{ij}^{(11)}\eta_i^*\eta_j + \hat{G}_{ij}^{(02)}\eta_i\eta_j + \cdots$$

Requiring that the variational principle (91) holds for every power of (η,η^*), we can successively determine the one-body operator $\hat{G}^{(m,n)}$ with $m+n = 1,2,3,\cdots$. This method of solution is called the "(η,η^*)-expansion method." Because (η,η^*) are complex canonical variables, they are replaced by boson operators after the canonical quantization. The lowest linear order corresponds to the QRPA. Accordingly, the collective variables (η_i,η_i^*) correspond to a specific QRPA mode in the small-amplitude limit. However, in the higher orders, the microscopic structure of $\hat{G}$ changes as a function of (η,η^*) due to the mode-mode coupling effects among different QRPA modes. In this sense, the (η,η^*)-expansion method may be regarded as a dynamical extension of the boson expansion method (Matsuo and Matsuyanagi, 1985a). Thus, the SCC method with the (η,η^*) expansion is a powerful method of treating anharmonic

effects to the QRPA vibrations originating from mode-mode couplings. This is shown in its application to the two-phonon states of anharmonic γ vibration (Matsuo and Matsuyanagi, 1985b; Matsuo *et al.*, 1985). The SCC method was also used for derivation of the 5D collective Hamiltonian and analysis of the quantum phase transition from spherical to deformed shapes (Yamada, 1993) and for constructing diabatic representation in the rotating shell model (Shimizu and Matsuyanagi, 2001). The validity of the canonical quantization procedure, including a treatment of the ordering ambiguity problem, was examined in (Matsuo and Matsuyanagi, 1985a).

3. Solution with adiabatic expansion

The (η, η^*) expansion about a single HFB equilibrium point is not suitable for treating situations where a few local minima energetically compete in the HFB potential energy surface. It is also difficult to apply the expansion method to a collective motion which goes far away from the equilibrium, such as nuclear fission. These low-energy LACM's in nuclei are often characterized by "slow" motion. For describing adiabatic LACM extending over very far from the HFB equilibrium, a new method of solution has been proposed (Matsuo *et al.*, 2000). In this method, the basic equations of the SCC method are solved by an expansion with respect to the collective momenta, keeping full orders in the collective coordinates. It is called "adiabatic SCC (ASCC) method." Similar methods have been developed also by Klein *et al.* (1991) and Almehed and Walet (2004).

A microscopic theory for adiabatic LACM is constructed by the ASCC method in the following way. We assume that the TDHFB state $|\phi(q,p)\rangle$ can be written in a form

$$|\phi(q,p)\rangle = \exp\left\{ip_i\hat{Q}^i(q)\right\}|\phi(q)\rangle, \tag{94}$$

where $\hat{Q}^i(q)$ are one-body operators corresponding to infinitesimal generators of p_i locally defined at the state $|\phi(q)\rangle$ which represents a TDHFB state $|\phi(q,p)\rangle$ at $p \to 0$. This state $|\phi(q)\rangle$ is called a "moving-frame HFB state." See Fig. 12 for illustrations. We use the canonical-variable conditions different from (92) and (93),

$$\langle\phi(q,p)|\mathring{P}_i(q,p)|\phi(q,p)\rangle = p_i, \tag{95}$$

$$\langle\phi(q,p)|\mathring{Q}^i(q,p)|\phi(q,p)\rangle = 0, \tag{96}$$

which are obtained by putting S =const. in the canonicity conditions (87) and (88). Because (95) and (96) are invariant only against point transformations, $q \to q'(q)$ (more generally, similarity transformations) which do not mix p and q, these canonical-variable conditions are suitable for the adiabatic expansion with respect to the collective momenta p.

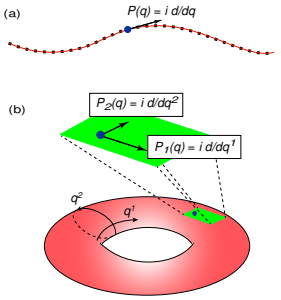

FIG. 12 (Color online) Schematic illustrations of collective submanifold in the TDHFB space. (a) 1D collective path specified by a series of the states $|\phi(q)\rangle$ with a local generator $P(q) = id/dq$. (b) A section of a 2D collective hypersurface and local generators of the collective coordinate, $(\hat{P}_1(q), \hat{P}_2(q))$.

We insert the above form of the TDHFB state (94) into the equation of collective submanifold (91) and the canonical variable conditions, (95) and (96), and make a power-series expansion in p. We can determine the microscopic structures of $\hat{Q}^i(q)$ and $|\phi(q)\rangle$ by requiring that these equations hold for every power of p. We take into account up to the second order. The canonical variable conditions, (95) and (96), then yield the 'weakly' canonical commutation relations,

$$\langle\phi(q)|\left[\hat{Q}^i(q), \hat{P}_j(q)\right]|\phi(q)\rangle = i\delta_{ij}.$$

We also obtain $\langle\phi(q)|\hat{Q}^i(q)|\phi(q)\rangle = 0$ and $\langle\phi(q)|\hat{P}_i(q)|\phi(q)\rangle = 0$, which are trivially satisfied. Here, the displacement operators $\hat{P}_i(q)$ are defined by

$$\hat{P}_i(q)|\phi(q)\rangle = i\frac{\partial}{\partial q^i}|\phi(q)\rangle.$$

Note that $\hat{Q}^i(q)$ and $\hat{P}_i(q)$ operate on $|\phi(q)\rangle$, while $\mathring{Q}^i(q,p)$ and $\mathring{P}_i(q,p)$ on $|\phi(q,p)\rangle$. The time derivatives $\dot{q}^i$ and $\dot{p}_i$ are determined by the Hamilton equations of motion (89) with the classical collective Hamiltonian $\mathcal{H}(q,p)$ expanded with respect to p up to the second order,

$$\mathcal{H}(q,p) = V(q) + \frac{1}{2}B^{ij}(q)p_ip_j,$$

$$V(q) = \mathcal{H}(q,p=0), \quad B^{ij}(q) = \left.\frac{\partial^2\mathcal{H}}{\partial p_i\partial p_j}\right|_{p=0}.$$

The collective inertia tensors $B_{ij}(q)$ are defined as the inverse matrix of $B^{ij}(q)$, $B^{ij}B_{jk} = \delta^i_k$. Under these preparation, the following equations, which constitute the core of the ASCC method, can be derived (Matsuo *et al.*, 2000). Here, to further simplify the expression, we show the case for normal systems with TDHF.

1. *Moving-frame HF(B) equation*

$$\delta\langle\phi(q)|\hat{H}_M(q)|\phi(q)\rangle = 0, \tag{97}$$

where $\hat{H}_M(q)$ represents the Hamiltonian in the frame attached to the moving mean field,

$$\hat{H}_M(q) = \hat{H} - \frac{\partial V}{\partial q^i}\hat{Q}^i(q).$$

2. *Moving-frame (Q)RPA equations*

$$\delta\langle\phi(q)|\left[\hat{H}_M(q), \hat{Q}^i(q)\right] - \frac{1}{i}B^{ij}(q)\hat{P}_j(q) + \frac{1}{2}\left[\frac{\partial V}{\partial q^j}\hat{Q}^j(q), \hat{Q}^i(q)\right]|\phi(q)\rangle = 0, \quad (98)$$

$$\delta\langle\phi(q)|[\hat{H}_M(q), \frac{1}{i}\hat{P}_i(q)] - C_{ij}(q)\hat{Q}^j(q) - \frac{1}{2}\left[\left[\hat{H}_M(q), \frac{\partial V}{\partial q^k}\hat{Q}^k(q)\right], B_{ij}(q)\hat{Q}^j(q)\right]|\phi(q)\rangle = 0, \quad (99)$$

where

$$C_{ij}(q) = \frac{\partial^2 V}{\partial q^i \partial q^j} - \Gamma^k_{ij}\frac{\partial V}{\partial q^k},$$
$$\Gamma^k_{ij}(q) = \frac{1}{2}B^{kl}\left(\frac{\partial B_{li}}{\partial q^j} + \frac{\partial B_{lj}}{\partial q^i} - \frac{\partial B_{ij}}{\partial q^l}\right).$$

The double-commutator term in Eq. (99) arises from the q-derivative of the infinitesimal generators $\hat{Q}^i(q)$ and represents the curvatures of the collective submanifold. Diagonalizing the matrix, $B^{ik}C_{kj}$, at each point of q, we may identify the local normal modes and eigenfrequencies $\omega_i(q)$ of the moving-frame QRPA equations.

Extension from TDHF to TDHFB for superfluid nuclei can be achieved by introducing the particle number $n \equiv N - N_0$ and their conjugate angle θ as additional collective variables. See Sec. V.C.4 and Matsuo *et al.* (2000) for more details.

Solving Eqs. (97), (98), and (99) self-consistently, we can determine the state $|\phi(q)\rangle$ and the microscopic expressions of the infinitesimal generators, $\hat{Q}^i(q)$ and $\hat{P}_i(q)$, in bilinear forms of the quasiparticle creation and annihilation operators defined locally with respect to $|\phi(q)\rangle$. See Fig. 12. Note that these equations reduce to the HF(B) and (Q)RPA equations at the equilibrium point where $\partial V/\partial q^i = 0$. Therefore, they are natural extensions of the HFB-QRPA equations to non-equilibrium states. Here, we remark on some key points of the ASCC method.

1. *Difference from the constrained HFB equations*

The moving-frame HFB equation (97) resembles the constrained HFB equation. An essential difference is that the infinitesimal generators $\hat{Q}^i(q)$ are here self-consistently determined together with $\hat{P}_i(q)$ as solutions of the moving-frame QRPA equations, (98) and (99), at every point of the collective coordinate q. Thus, contrary to constrained operators in the constrained HFB theory, their microscopic structure changes as functions of q. The optimal "constraining" operators are locally determined at each q. The collective submanifold embedded in the TDHFB phase space is extracted in this way.

2. *Meaning of the term "adiabatic"*

The word of "adiabatic approximation" is frequently used with different meanings. In the present context, we use this term for the approximate solution of the variational equation (84) by taking into account up to the second order in an expansion with respect to the collective momenta p. It is important to note that the effects of finite frequency of the LACM are taken into account through the moving-frame QRPA equation. No assumption is made, such as that the kinetic energy of LACM is much smaller than the lowest two-quasiparticle excitation energy at every point of q.

3. *Collective inertial mass*

Although the collective submanifold is invariant against coordinate transformations, $q \to q'(q)$, the collective inertial tensors $B_{ij}(q)$ depends on the adopted coordinate system. The scale of the coordinates can be arbitrary chosen as far as the canonical-variable conditions are satisfied. Note, however, that it is convenient to adopt a conventional coordinate system, such as the quadrupole (β, γ) variables, to obtain physical insights and to find the effects of time-odd components in the mean field (see Sec. V.D.1).

4. *Canonical quantization*

The collective inertia tensors $B_{ij}(q)$ take a diagonal form when the classical collective Hamiltonian is represented in terms of the local normal modes of the moving-frame QRPA equations. We can then make a scale transformation of the collective coordinates q such that they become unity. The kinetic energy term in the resulting collective Hamiltonian depends only on p. Thus, there is no ordering ambiguity between q and p in the canonical quantization procedure.

4. Inclusion of the pair rotation and gauge invariance

In the QRPA at the HFB equilibrium, the ANG modes like the number fluctuation (pairing rotational) modes are decoupled from other normal modes. Thereby, the QRPA restores the gauge invariance (number conservation) broken in the HFB mean field (Brink and Broglia, 2005). It is desirable to keep this nice property beyond the small-amplitude approximation. Otherwise, spurious number-fluctuation modes would heavily mix in the LACM of interest. This can be achieved in the SCC method (Matsuo, 1986).

Introducing the number-fluctuation $n = N - N_0$ and their conjugate angle θ as additional collective variables, we generalize the TDHFB state (94) to

$$|\phi(q, p, \theta, n)\rangle = e^{-i\theta\hat{N}}|\phi(q, p, n)\rangle,$$
$$|\phi(q, p, n)\rangle = e^{i\left[p_i\hat{Q}^i(q) + n\hat{\Theta}(q)\right]}|\phi(q)\rangle,$$

where $\hat{\Theta}(q)$ denotes the infinitesimal generator for the pair-rotation degree of freedom. The state vector $|\phi(q,p,n)\rangle$ may be regarded as an intrinsic state for the pair rotation. In practice, $(\hat{N},\hat{\Theta}(q))$ should be doubled to treat both neutrons and protons. The extension of the equation for the collective submanifold (84) is straightforward;

$$\delta\langle\phi(q,p,\theta,n)|\left\{i\dot{q}^i\frac{\partial}{\partial q^i}+i\dot{p}_i\frac{\partial}{\partial p_i}+i\dot{\theta}\frac{\partial}{\partial\theta}-\hat{H}\right\}|\phi(q,p,\theta,n)\rangle=0.$$

Note that $\dot{n}=0$, because the Hamilton equations for the canonical conjugate pair (n,θ) are

$$\dot{\theta}=\frac{\partial\mathcal{H}}{\partial n},\quad \dot{n}=-\frac{\partial\mathcal{H}}{\partial\theta},$$

and the classical collective Hamiltonian $\mathcal{H}(q,p,\theta,n)\equiv\langle\phi(q,p,\theta,n)|\hat{H}|\phi(q,p,\theta,n)\rangle$ does not depend on θ.

Expanding in n as well as p up to the second order, we can determine $\hat{\Theta}(q)$ simultaneously with $\hat{Q}^i(q)$ and $\hat{P}_i(q)$ such that the moving-frame equations become invariant against the rotation of the gauge angle θ.

Hinohara *et al.* (2007) investigated the gauge-invariance properties of the ASCC equations and extended the infinitesimal generators $\hat{Q}^i(q)$ to include quasiparticle creation-annihilation parts in addition to two-quasiparticle creation and annihilation parts. This is the reason why Eqs. (98) and (99) are written in a more general form than those originally given by Matsuo *et al.* (2000). The gauge invariance implies that we need to fix the gauge in numerical applications. A convenient procedure of the gauge fixing is discussed in Hinohara *et al.* (2007). A more general consideration on the gauge symmetry is given from a viewpoint of constrained dynamical systems (Sato, 2015).

D. Relations to other approaches

In Sec. V.C, we reviewed the basics of a microscopic theory of LACM focusing on new developments in the ASCC method, achieved after 2000. In this section, we discuss the relations of the above formulation to other approaches to LACM. Typical approaches developed up to 1980 are described in detail in the textbook of Ring and Schuck (1980), and achievements during 1980-2000 are well summarized in the review by Dang *et al.* (2000).

1. Constrained HFB + adiabatic perturbation

This method is convenient and widely used in the microscopic description of LACM. The theory is based on the *adiabatic* assumption that the collective motion is much slower than the single-particle motion (see remarks in Sec. V.C.3). We first postulate a few one-body operators, $\hat{F}_i$, corresponding to collective coordinates α^i. The collective potential energy is given by the constrained HFB (or constrained HF + BCS) equations

$$\delta\langle\phi_0(\alpha)|\hat{H}-\mu^i(\alpha)\hat{F}_i|\phi_0(\alpha)\rangle=0,$$
$$\alpha^i=\langle\phi_0(\alpha)|\hat{F}_i|\phi_0(\alpha)\rangle,$$

where $\mu^i(\alpha)$ are the Lagrange multipliers. Then, assuming that the frequency of the collective motion is much smaller than the two-quasiparticle energies, we calculate the collective kinetic energy $T_{\rm coll}$ using the adiabatic perturbation theory; $T_{\rm coll}=(1/2)D_{ij}(\alpha)\dot{\alpha}^{i*}\dot{\alpha}^j$, where

$$D_{ij}(\alpha)=2\sum_n\frac{\langle\phi_0(\alpha)|\frac{\partial}{\partial\alpha^{i*}}|\phi_n(\alpha)\rangle\langle\phi_n(\alpha)|\frac{\partial}{\partial\alpha^j}|\phi_0(\alpha)\rangle}{E_n(\alpha)-E_0(\alpha)}$$

are called Inglis-Belyaev cranking masses (Ring and Schuck, 1980). Here $|\phi_0(\alpha)\rangle$ and $|\phi_n(\alpha)\rangle$ represent the ground and two-quasiparticle excited states for a given set of values $\alpha=\{\alpha^i\}$. In most of applications, it is simplified furthermore, by an assumption that the derivatives of the constrained HFB Hamiltonian with respect to α^i is proportional to $\hat{F}_i$, which leads to

$$D_{ij}(\alpha)=\frac{1}{2}\left[\mathcal{M}_1^{-1}(\alpha)\mathcal{M}_3(\alpha)\mathcal{M}_1^{-1}(\alpha)\right]_{ij}$$
$$\mathcal{M}_n(\alpha)_{ij}=\sum_n\frac{\langle\phi_0(\alpha)|\hat{F}_i^{\dagger}|\phi_n(\alpha)\rangle\langle\phi_n(\alpha)|\hat{F}_j|\phi_0(\alpha)\rangle}{(E_n(\alpha)-E_0(\alpha))^n},$$

These cranking masses were used in conjunction with phenomenological mean-field models in the study of fission dynamics (Brack *et al.*, 1972). In recent years, it has become possible to carry out such studies using self-consistent mean fields obtained by solving the constrained HFB equations (Baran *et al.*, 2011). The Inglis-Belyaev cranking masses have also been used for low-frequency quadrupole collective dynamics (Delaroche *et al.*, 2010; Libert *et al.*, 1999; Próchniak *et al.*, 2004; Yuldashbaeva *et al.*, 1999). At present, a systematic investigation on low-lying quadrupole spectra is underway in terms of the five dimensional (5D) collective Hamiltonian (see Sec. V.E.1), which is derived from the relativistic (covariant) density functionals and by using the Inglis-Belyaev cranking formula (Fu *et al.*, 2013; Li *et al.*, 2010a, 2009, 2010b, 2011; Nikšić *et al.*, 2009, 2011).

A problem of the Inglis-Belyaev cranking formula is that time-odd mean-field effects are ignored, thus, it underestimates the collective masses (inertial functions) (Dobaczewski and Dudek, 1995). Moving mean fields induce time-odd components that change sign under time reversal. However, the Inglis-Belyaev cranking formula ignores their effects on the collective masses. By taking into account such time-odd corrections to the cranking masses, one can better reproduce low-lying spectra (Hinohara *et al.*, 2012). For rotational moments of inertia, we may estimate the time-odd corrections taking

the limit of $\omega_{\rm rot} \to 0$ for the quasi-stationary solution of Eq. (44). Since this provides about $20-40$ % enhancement from the Inglis-Belyaev formula, the similar enhancement factors of $1.2-1.4$ have been often utilized for vibrational inertial masses without solid justification. A better treatment of the time-odd mean-field effects is required for describing the masses of collective motion and the effective mass of single-particle motion in a self-consistent manner. For this purpose, it is highly desirable to apply the microscopic theory of LACM in Sec. V.C.3 to the TDDFT with realistic EDFs. At present, however, it remains as a challenge for future.

2. Adiabatic TDHF theory

Attempts to derive collective Hamiltonian using adiabatic approximation to time evolution of mean fields started in 1960's (Baranger and Kumar, 1965; Belyaev, 1965). In these pioneer works, the collective quadrupole coordinates (β, γ) were defined in terms of expectation values of the quadrupole operators and the 5D collective Hamiltonian was derived using the pairing plus quadrupole (P+Q) force model (Bes and Sorensen, 1969). During 1970's this approach was generalized to a theory applicable to any effective interaction. This advanced approach is called *adiabatic TDHF* (ATDHF) theory (Baranger and Vénéroni, 1978; Brink *et al.*, 1976; Goeke and Reinhard, 1978).

In the ATDHF theory, the density matrix $\rho(t)$ is written in the following form and expanded as a power series with respect to the collective momentum $\chi(t)$.

$$\begin{aligned}\rho(t) &= e^{i\chi(t)}\rho_0(t)e^{-i\chi(t)} \\ &= \rho_0(t) + [i\chi, \rho_0] + \frac{1}{2}[i\chi, [i\chi, \rho_0]] + \cdots \\ &= \rho_0(t) + \rho_1(t) + \rho_2(t) + \cdots\end{aligned}$$

Correspondingly, the time-dependent mean-field Hamiltonian $h(t)$ is also expanded with respect to a power of $\chi(t)$.

$$h[\rho(t)] = W_0(t) + W_1(t) + W_2(t) + \cdots$$

Inserting these into the TDHF (TDKS) equation (35), we obtain for the time-odd part

$$i\dot{\rho}_0 = [W_0, \rho_1] + [W_1, \rho_0],$$

and the time-even part

$$i\dot{\rho}_1 = [W_0, \rho_0] + [W_0, \rho_2] + [W_1, \rho_1] + [W_2, \rho_0].$$

These are the basic equations of the ATDHF.

Let us introduce collective coordinates $\alpha = (\alpha^1, \cdots, \alpha^f)$ as parameters describing the time evolution of the density matrix $\rho_0(t)$ as

$$\rho_0(t) = \rho_0(\alpha(t)), \quad \dot{\rho}_0(t) = \sum_i \frac{\partial \rho_0}{\partial \alpha^i}\dot{\alpha^i}.$$

Baranger and Vénéroni (1978) proposed iterative procedures to solve the ATDHF equations for the density matrix parameterized in this way, but this idea has not been realized until now. The ATDHF does not reduce to the RPA in the small amplitude limit if a few collective coordinates are introduced by hand. In fact it gives a collective mass different from that of RPA (Giannoni and Quentin, 1980a,b).

The ATDHF theory developed by Villars (1977) aims at self-consistently determining optimum collective coordinates on the basis of the time-dependent variational principle. This approach, however, encountered a difficulty that we cannot get a unique solution of its basic equations determining the collective path. This non-uniqueness problem was later solved by treating the second-order terms of the momentum expansion in a self-consistent manner (Klein *et al.*, 1991; Mukherjee and Pal, 1982). It was shown that, when the number of collective coordinate is only one, a collective path maximally decoupled from non-collective degrees of freedom runs along a valley in the multi-dimensional potential-energy surface associated with the TDHF states.

In order to describe low-frequency collective motions, it is necessary to take into account the pairing correlations. Thus, we need to develop the adiabatic TDHFB (ATDHFB) theory. This is one of the reasons why applications of the ATDHF theory have been restricted to collective phenomena where the pairing correlations play minor roles, such as low-energy collisions between spherical closed-shell nuclei (Goeke *et al.*, 1983a). When large-amplitude shape fluctuations take place, single-particle level crossings often occur. To follow the adiabatic configuration across the level crossing points, the pairing correlation plays an essential role. Thus, an extension to ATDHFB is indispensable for the description of low-frequency collective excitations.

In the past, Dobaczewski and Skalski (1981) tried to develop the ATDHFB theory assuming the axially symmetric quadrupole deformation parameter β as the collective coordinate. Quite recently, Li *et al.* (2012) tried to derive the 5D quadrupole collective Hamiltonian on the basis of the ATDHFB. However, the extension of ATDHF to ATDHFB is not as straightforward as we naively expect. This is because, as we discussed in Sec. V.C.4, we need to decouple the pair-rotational degrees of freedom (number fluctuation) from the LACM of interest.

3. Boson expansion method

Boson expansion method is an efficient microscopic method of describing anharmonic (non-linear) vibrations going beyond the harmonic approximation of QRPA. In this approach, we first construct a collective subspace spanned by many-phonon states of vibrational quanta (determined by the QRPA) in the huge-dimensional shell-

model space. These many-phonon states are mapped onto many-boson states in an ideal boson space. Anharmonic effects neglected in the QRPA are treated as higher order terms in the power series expansion with respect to the boson creation and annihilation operators. Starting from the QRPA about a spherical shape, one can thus derive the 5D quadrupole collective Hamiltonian in a fully quantum mechanical manner. The boson expansion method has been successfully applied to low-energy quadrupole excitation spectra in a wide range of nuclei including those lying in transitional regions of quantum phase transitions from spherical to deformed shapes (Klein and Marshalek, 1991; Sakamoto and Kishimoto, 1988).

In the time-dependent mean-field picture, state vectors in the boson expansion method are written in terms of the creation and annihilation operators $(\Gamma_i^\dagger, \Gamma_i)$ of the QRPA eigen-modes, or, equivalently, in terms of the collective coordinate and momentum operators $(\hat{Q}^i, \hat{P}_i)$,

$$|\phi(t)\rangle = e^{i\hat{G}(t)}|\phi_0\rangle,$$
$$i\hat{G}(t) = \eta_i(t)\Gamma_i^\dagger - \eta_i^*(t)\Gamma_i = ip_i(t)\hat{Q}^i - iq^i(t)\hat{P}_i.$$

With increasing amplitudes of the quadrupole shape vibration $|\eta_i(t)|$ ($|q_i(t)|$), anharmonic (non-linear) effects become stronger. Strong non-linear effects may eventually change even the microscopic structure of the collective operators $(\hat{Q}_i, \hat{P}_i)$ determined by the QRPA. In such situations, it is desirable to construct a theory that allows variations of microscopic structure of collective operators as functions of $q_i(t)$. The SCC method has accomplished this task (See Sec. V.C).

4. Generator coordinate method

In the generator coordinate method (GCM), quantum eigenstates of collective motion are described as superpositions of states $|\phi(\alpha)\rangle$ labeled by the parameters, $\alpha = (\alpha^1, \cdots, \alpha^f)$, which are called *generator coordinates*.

$$|\Psi\rangle = \int d\alpha f(\alpha)|\phi(\alpha)\rangle.$$

$|\phi(\alpha)\rangle$ are *generating functions*, normally chosen as mean field states (Slater determinants), which provide non-orthogonal basis for a collective subspace. The Ritz variational principle then leads to the Hill-Wheeler equation

$$\int d\alpha f^*(\alpha)\langle\phi(\alpha)|\hat{H} - E|\phi(\alpha')\rangle = 0$$

determining the weight function $f(\alpha)$. Here $\int d\alpha$ denotes multiple integration with respect to the f-dimensional generator coordinates, and volume elements of integration are absorbed in the weight function $f(\alpha)$.

The GCM has been used for a wide variety of nuclear collective phenomena (Bender, 2008; Egido and Robledo, 2004; Reinhard and Goeke, 1987; Robledo and Bertsch, 2011; Shimada *et al.*, 2015). For low-frequency quadrupole collective motion in superfluid nuclei, although the proper generator coordinates are not obvious, a possible choice may be the axial and triaxial deformation parameters (β, γ), and the pairing gaps for neutrons and protons (Δ_n, Δ_p). In addition, to treat the rotational motions associated with spatial and gauge deformations, the analytic solution of the angular-momentum eigenstates and the number eigenstates are constructed by integration over the Euler angles of rotation $\Omega = (\vartheta_1, \vartheta_2, \vartheta_3)$, and the gauge angles (φ_n, φ_p), respectively. In the major applications at the present time, however, the pairing gaps (Δ_n, Δ_p) are not treated as generator coordinates to reduce the dimensionality of integration. This leads to the following superpositions

$$|\Psi^i_{NZIM}\rangle = \int d\beta d\gamma \sum_K f^i_{NZIK}(\beta,\gamma)\hat{P}_N\hat{P}_Z\hat{P}_{IMK}|\phi(\beta,\gamma)\rangle,$$

where $\hat{P}_{IMK}$ and $\hat{P}_N$ ($\hat{P}_Z$) denote projection operators for angular momentum in three-dimensional space and the neutron (proton) number, respectively. It has been a great challenge in nuclear structure physics to carry out high-dimensional numerical integrations for solving the GCM equation using the constrained HFB states. In recent years, remarkable progress has been taking place, which makes it possible to carry out large-scale numerical computations (Bender and Heenen, 2008; Rodríguez, 2014; Rodríguez and Egido, 2010, 2011; Yao *et al.*, 2014, 2011, 2010) A recent example is shown in Fig. 13. As we have seen in Sec. II, the HFB calculations using the density-dependent effective interactions are better founded by DFT. Correspondingly, the modern GCM calculation is often referred to as *multi-reference DFT* (Bender and Heenen, 2008).

The GCM is a useful fully quantum approach but the following problems remain to be solved.

1. *Numerical stability*

In numerical calculation, one needs to find an optimum discretization (selection of basis) for the generator coordinates α, because the continuum limit of integration is not stable in general (Bonche *et al.*, 1990). It is usually determined semi-empirically but a deeper understanding of its physical basis is desirable. Another problem is a singular behavior that may occur during the symmetry projections in calculations with use of effective interactions that depend on non-integer power of density. Currently, efforts are underway to overcome this problem (Anguiano *et al.*, 2001; Dobaczewski *et al.*, 2007; Duguet *et al.*, 2009).

2. *Necessity of complex coordinates*

It is well known that one can derive a collective Schrödinger equation by making Gaussian overlap approximation (GOA) to the GCM equation (Griffin and Wheeler, 1957; Onishi and Une, 1975; Reinhard and

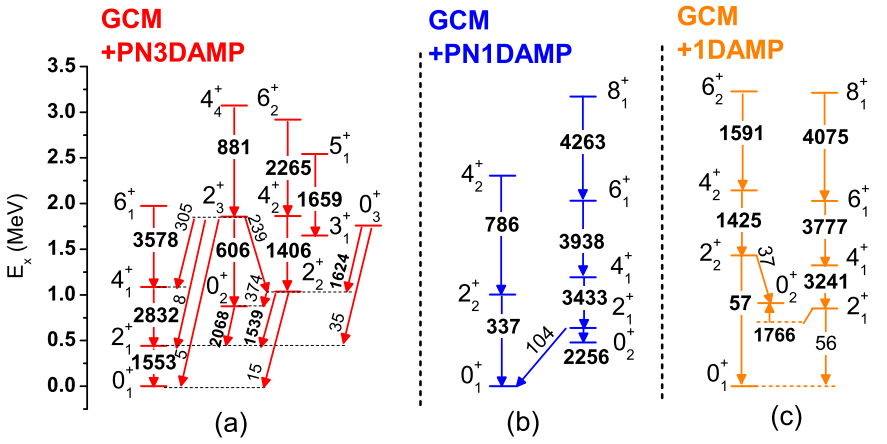

FIG. 13 (Color online) Low-lying spectra and $B(E2)$ values in $e^2\mathrm{fm}^4$ for ^{76}Kr; (a) experimental data from Clément *et al.* (2007), (b) the relativistic GCM calculations in the (β,γ) plane with the particle number and the angular momentum projections, (c) the calculation of the 5D collective Hamiltonian using the cranking inertial masses (Sec. V.D.1). From Yao *et al.* (2014).

Goeke, 1987; Rohoziński, 2012). There is no guarantee, however, that dynamical effects associated with time-odd components of moving mean field are sufficiently taken into account in the collective masses (inertia functions) obtained through this procedure. In the case of center of mass motion, we need to use complex generator coordinates to obtain the correct mass, implying that collective momenta conjugate to collective coordinates should also be treated as generator coordinates (Peierls and Thouless, 1962; Ring and Schuck, 1980). The GOA with respect to the momenta leads to a theory very similar to ATDHF (Goeke *et al.*, 1983b). Realistic applications with complex generator coordinates are so far very few.

3. *Choice of generator coordinates*

The most fundamental question is how to choose the optimum generator coordinates. It is desirable to variationally determine the generating functions $|\phi(\alpha)\rangle$ themselves. Let S denotes the space spanned by $|\phi(\alpha)\rangle$. The equation determining the space S is then given by

$$\int_S d\alpha f^*(\alpha)\langle\phi(\alpha)|\hat{H}-E|\delta\phi(\alpha')\rangle_\perp = 0, \qquad (100)$$

where $|\delta\phi(\alpha')\rangle_\perp$ denotes a variation perpendicular to the space S. Let us add an adjective "optimum" to the generator coordinate determined by solving the above variational equation. It was shown that the mean-field states parameterized by a single optimum generator coordinate run along a valley of the collective potential energy surface (Holzwarth and Yukawa, 1974). This line of investigation was further developed (Reinhard and Goeke, 1979) and greatly stimulated the challenge toward constructing microscopic theory of LACM. However, direct applications of Eq. (100) to realistic EDFs may have a problem. As we discussed in Sec. V.A, the missing correlations in nuclear EDFs are those in long ranges and long time scales. The variation in Eq. (100) may take account for additional short-range correlations, which could lead to unphysical solutions (Fukuoka *et al.*, 2013; Shinohara *et al.*, 2006).

Finally, we note that conventional GCM calculations parameterized by a few real generator coordinates do not reduce to the (Q)RPA in the small-amplitude limit. It is equivalent to RPA only when all the particle-hole degrees of freedom are treated as complex generator coordinates (Jancovici and Schiff, 1964). An extension to the QRPA is not straightforward either. Thus, systematic comparison of collective inertia masses evaluated by different approximations including the ASCC, the ATDHFB, the GCM+GOA, and the adiabatic cranking methods is desirable for a better understanding of their physical implications.

5. Time-dependent density matrix theory and higher QRPA

The TDHF theory describes time-evolution of one-body density matrix $\rho_{ij} = \langle\phi|c_j^\dagger c_i|\phi\rangle$ on the basis of the time-dependent variational principle. To generalize this approach, one may consider, in addition to ρ_{ij}, time-evolution of two-body correlation matrix $C_{ijkl} = \langle\phi|c_k^\dagger c_l^\dagger c_j c_i|\phi\rangle - \rho_{ik}\rho_{jl} + \rho_{il}\rho_{jk}$. This approach is called time-dependent density matrix (TDDM) theory (Shunjin and Cassing, 1985). The extended RPA (Tohyama and Schuck, 2007) and the second RPA (Drozdz *et al.*, 1990; Gambacurta *et al.*, 2011, 2012; Tohyama and Nakatsukasa, 2012) can be derived as approximations to the small-amplitude limit of the TDDM theory (Tohyama and Gong, 1989), and have been used to the analysis of damping mechanisms of giant resonances and anharmonicities of low-frequency vibrations.

In the TDDM theory, the pairing correlations are taken into account by the two-body correlations C_{ijkl}.

This requires a large computational cost, however. The TDDM theory using the HFB quasiparticle representations is not available. On the other hand, the higher QRPA may provide another practical approach to its small-amplitude approximation. In the higher QRPA, in addition to the two-quasiparticle creation and annihilation operators in the conventional QRPA, $\Gamma_n^{(2)\dagger} = \sum_{i,j}\left(\psi_{ij}^{n(2)}a_i^\dagger a_j^\dagger + \varphi_{ij}^{n(2)}a_j a_i\right)$, equations of motion for four quasiparticle creation and annihilation operators,

$$\Gamma_n^{(4)\dagger} = \sum_{i,j,k,l}\left(\psi_{ijkl}^{n(4)}a_i^\dagger a_j^\dagger a_k^\dagger a_l^\dagger + \phi_{ijkl}^{n(4)}a_i^\dagger a_j^\dagger a_l a_k + \varphi_{ijkl}^{n(4)}a_l a_k a_j a_i\right),$$

are derived. This approach may be suitable for describing various mode-mode coupling effects and anharmonicities arising from Pauli-principle effects in two-phonon states where two QRPA vibrational quanta are excited. We note that the $a_i^\dagger a_j^\dagger a_l a_k$ terms in $\Gamma_n^{(4)\dagger}$ are often ignored ($\phi_{ijkl}^{n(4)} = 0$). It is known, however, that collectivities of two-phonon states cannot be well described without these terms, because they are responsible for making the ratio $B(E2; 2\text{ phonon} \to 1\text{ phonon})/B(E2; 1\text{ phonon} \to \text{g.s.}) = 2$ in the harmonic limit (Tamura and Udagawa, 1964). This problem may be overcome by using the quasiparticle New Tamm-Dancoff method (Kanesaki *et al.*, 1973a,b; Sakata *et al.*, 1981). In the limit of vanishing pairing correlations, the quasiparticle-pair scattering terms, $a_i^\dagger a_j^\dagger a_l a_k$, reduce to the particle-hole-pair scattering terms. Their effects are taken into account in the extended RPA, while they are ignored in the second RPA (Tohyama, 2001).

To our knowledge, no attempt has been made to introduce collective variables and derive collective Hamiltonian on the basis of the TDDM theory.

E. Application to shape coexistence/fluctuation phenomena

1. Five-dimensional quadrupole collective Hamiltonian

Vibrational and rotational motions of the nucleus can be described as time evolution of a self-consistent mean field. This is the basic idea underlying the unified model of Bohr and Mottelson (Bohr, 1976; Mottelson, 1976). In this approach, the five-dimensional (5D) collective Hamiltonian describing the quadrupole vibrational and rotational motions is given by (Bohr and Mottelson, 1975; Próchniak and Rohoziǹski, 2009)

$$H = T_{\rm rot} + T_{\rm vib} + V(\beta,\gamma), \tag{101}$$

with $T_{\rm rot} = \frac{1}{2}\sum_k \mathcal{J}_k\omega_k^2$ and $T_{\rm vib} = \frac{1}{2}D_{\beta\beta}\dot\beta^2 + D_{\beta\gamma}\dot\beta\dot\gamma + \frac{1}{2}D_{\gamma\gamma}\dot\gamma^2$, where ω_k and $\mathcal{J}_k$ in the rotational energy $T_{\rm rot}$ are the three components of the angular velocities and the corresponding moments of inertia, respectively, while $(D_{\beta\beta}, D_{\beta\gamma}, D_{\gamma\gamma})$ in $T_{\rm vib}$ represent the inertial masses of the vibrational motion. Note that $\mathcal{J}_{k=1,2,3}$ and $(D_{\beta\beta}, D_{\beta\gamma}, D_{\gamma\gamma})$ are functions of β and γ. The "deformation parameters" β and γ are here treated as dynamical variables, and $\dot\beta$ and $\dot\gamma$ represent their time-derivatives. They are related to expectation values of the quadruple operators (with respect to the time-dependent mean-field states) and their variations in time. Note also that they are defined with respect to the principal axes of the body-fixed (intrinsic) frame that is attached to the instantaneous shape of the time-dependent mean-field.

In the case that the potential energy $V(\beta,\gamma)$ has a deep minimum at finite value of β and $\gamma = 0^\circ$ (or $\gamma = 60^\circ$), a regular rotational spectrum with the $I(I+1)$ pattern may appear. In addition to the ground band, we expect the β- and γ-bands to appear, where vibrational quanta with respect to the β and γ degrees of freedom are excited. Detailed investigations on the γ-vibrational bands over many nuclei have revealed, however, that they usually exhibit significant anharmonicities (nonlinearities). The β vibrational bands are even more mysterious, that they couple, sometimes very strongly, with the pairing-vibrational modes (associated with fluctuations of the pairing gap). Recent experimental data indicate the strong need for a radical review on their characters (Heyde and Wood, 2011).

2. Microscopic derivation of the 5D collective Hamiltonian

For collective submanifolds of two dimensions (2D) or higher dimensions, an enormous amount of numerical computation is necessary to find fully self-consistent solutions of the ASCC equations. To handle this problem, a practical approximation scheme, called "local QRPA" (LQRPA) method, has been developed (Hinohara *et al.*, 2010; Sato and Hinohara, 2011; Sato *et al.*, 2012). This scheme may be regarded as a non-iterative solution of Eqs. (97)-(99) without the consistency in the generator $\hat{Q}^i(q)$ between the moving-frame HFB equation and the moving-frame QRPA equations. It may also be regarded as a first-step of the iterative procedure for solving the self-consistent equations. Further approximation is that, instead of treating the 5D collective coordinates simultaneously, we first derive the 2D collective Hamiltonian for vibrational motions corresponding to the (β,γ) deformations, and subsequently take into account the three-dimensional (3D) rotational motions associated with Euler angles at each point of (β,γ). With this procedure, we can easily derive the 5D collective Hamiltonian.

First, we solve the moving-frame HFB equations.

$$\delta\langle\phi(q)|\hat{H}_{\rm M}(q)|\phi(q)\rangle = 0,$$
$$\hat{H}_{\rm M}(q) = \hat{H} - \sum_\tau \lambda^{(\tau)}(q)\tilde{N}^{(\tau)} - \sum_{m=0,2}\mu_m(q)\hat{D}_{2m}^{(+)}.$$

This equation corresponds to Eq. (97) for the 2D case with $q = (q^1, q^2)$ and with $\hat{Q}^i(q)$ replaced by the mass

quadrupole operators $\hat{D}^{(+)}_{2m}$. The variables (β,γ) are defined by

$$\beta\cos\gamma = \eta D^{(+)}_{20}(q) = \eta\langle\phi(q)|\hat{D}^{(+)}_{20}|\phi(q)\rangle, \quad (102)$$

$$\frac{1}{\sqrt{2}}\beta\sin\gamma = \eta D^{(+)}_{22}(q) = \eta\langle\phi(q)|\hat{D}^{(+)}_{22}|\phi(q)\rangle, \quad (103)$$

where η is a scaling factor with the dimension of L^{-2}. These equations determine the relation between $q = (q^1, q^2)$ and (β,γ).

Next, we solve the following equations for $i = 1$ and 2:

$$\delta\langle\phi(q)|[\hat{H}_{\rm M}(q), \hat{Q}^i(q)] - \frac{1}{i}B^i(q)\hat{P}_i(q)|\phi(q)\rangle = 0,$$
$$\delta\langle\phi(q)|[\hat{H}_{\rm M}(q), \frac{1}{i}\hat{P}_i(q)] - C_i(q)\hat{Q}^i(q)|\phi(q)\rangle = 0.$$

These are the moving-frame QRPA equations without the curvature terms and called local QRPA (LQRPA) equations.

Displacement of the quadrupole deformation are related to that of (q_1, q_2) by

$$dD^{(+)}_{2m} = \sum_{i=1,2}\frac{\partial D^{(+)}_{2m}}{\partial q^i}dq^i, \qquad m = 0, 2.$$

Making a scale transformation such that the inertial masses with respect to the collective coordinates (q_1, q_2) become unity and using the above relation, we can write the kinetic energy of vibrational motions in terms of time-derivatives of the quadrupole deformation:

$$T_{\rm vib} = \frac{1}{2}\sum_{i=1,2}(\dot{q^i})^2 = \frac{1}{2}\sum_{m,m'=0,2}M_{mm'}\dot{D}^{(+)}_{2m}\dot{D}^{(+)}_{2m'},$$
$$M_{mm'}(\beta,\gamma) = \sum_{i=1,2}\frac{\partial q^i}{\partial D^{(+)}_{2m}}\frac{\partial q^i}{\partial D^{(+)}_{2m'}}.$$

With Eqs. (102) and (103), it is straightforward to rewrite the above expression using the time-derivatives of (β,γ).

Subsequently, we solve the LQRPA equations for 3D rotational motions at every point of q. This is given by replacement of $Q^i(q) \to \hat{\Psi}^k(q)$ and $B^i(q)\hat{P}_i(q) \to \hat{I}_k/\mathcal{J}_k(q)$, where $\hat{\Psi}^k(q)$ represents the local angle operator conjugate to the angular momentum $\hat{I}_k$. The solution provides the moments of inertia $\mathcal{J}_k(\beta,\gamma) = 4\beta^2 D_k(\beta,\gamma)\sin^2(\gamma - 2\pi k/3)$ which determine the rotational masses $D_k(\beta,\gamma)$ and the rotational energy $T_{\rm rot}$.

We can quantize the collective Hamiltonian (101) using the quantization scheme for curvilinear coordinates (so-called the Pauli prescription). The quantized rotational and vibrational Hamiltonians are given, respectively, by $\hat{T}_{\rm rot} = \frac{1}{2}\sum_k \hat{I}^2_k/\mathcal{J}_k$ and

$$\hat{T}_{\rm vib} = \frac{-1}{2\sqrt{WR}}\left\{\frac{1}{\beta^4}\left[\frac{\partial}{\partial\beta}\left(\beta^4\sqrt{\frac{R}{W}}D_{\gamma\gamma}\frac{\partial}{\partial\beta}\right)\right]\right.$$
$$- \frac{\partial}{\partial\beta}\left(\beta^2\sqrt{\frac{R}{W}}D_{\beta\gamma}\frac{\partial}{\partial\gamma}\right)\Big]$$
$$+ \frac{1}{\beta^2\sin 3\gamma}\left[-\frac{\partial}{\partial\gamma}\left(\sqrt{\frac{R}{W}}\sin 3\gamma D_{\beta\gamma}\frac{\partial}{\partial\beta}\right)\right.$$
$$\left.\left. + \frac{\partial}{\partial\gamma}\left(\sqrt{\frac{R}{W}}\sin 3\gamma D_{\beta\beta}\frac{\partial}{\partial\gamma}\right)\right]\right\}. \quad (104)$$

with $\beta^2 W = D_{\beta\beta}D_{\gamma\gamma} - D^2_{\beta\gamma}$ and $R = D_1 D_2 D_3$.

The collective wave functions are written as

$$\Psi_{IMk}(\beta,\gamma,\Omega) = \sum_{K=0}^{I}\Phi_{IKk}(\beta,\gamma)\langle\Omega|IMK\rangle,$$

where $\Phi_{IKk}(\beta,\gamma)$ and $\langle\Omega|IMK\rangle$ represent the vibrational and rotational wave functions, respectively. Solving the collective Schrödinger equations

$$\left(\hat{T}_{\rm rot} + \hat{T}_{\rm vib} + V(\beta,\gamma)\right)\Psi_{IMk}(\beta,\gamma,\Omega) = E_{IMk}\Psi_{IMk}(\beta,\gamma,\Omega),$$

we obtain quantum spectra of quadrupole collective motion. Details of the above derivation are given in Hinohara *et al.* (2010) and Matsuyanagi *et al.* (2016).

F. Illustrative examples

The spherical shell structure gradually changes following the deformation of the mean field. If we plot single-particle level diagrams as functions of deformation parameters, significant gaps, called 'deformed magic numbers,' appear at the Fermi surface for certain deformations. Such deformed shell effects stabilize some deformed shapes of the mean field. Accordingly, in the HFB calculations, we may encounter multiple local minima with different shapes in similar energies. The LACM connecting multiple local minima via tunneling through potential barriers may take place to generate the shape fluctuation. These phenomena may be regarded as a kind of macroscopic quantum tunneling. Note that the barriers are not external fields but self-consistently generated as a consequence of quantum dynamics of the many-body system under consideration. Quantum spectra of low-energy excitation that involve dynamics associated with different shapes have been observed in almost all regions of the nuclear chart (Heyde and Wood, 2011). When different kinds of quantum eigenstates associated with different shapes coexist in the same energy region, we may call it "shape coexistence phenomenon". This is the case when shape mixing due to tunneling motion is weak and collective wave functions retain their localization about

different equilibrium shapes. On the other hand, if the shape mixing is strong, large-amplitude shape fluctuations extending to different local minima may occur. Below, we illustrate these concepts with numerical applications of the LQRPA method to the oblate-prolate shape coexistence/fluctuation phenomena.

Figures 14 and 15 show some results of application of the ASCC and QRPA methods to the oblate-prolate shape coexistence phenomenon in ^{68}Se. It is clearly seen in Fig. 14 that the collective potential exhibits two local minima corresponding to the oblate and prolate shapes. They are associated with the deformed magic numbers at $N = Z = 34$ appearing for both shapes (Hamamoto, 2012). The valley runs in the triaxially deformed region and the barrier connecting the oblate and prolate minima is low. This is an intermediate situation between the oblate-prolate shape coexistence and the γ-unstable model of Wilets and Jean (1956). In the former, the barrier is high and the mixing of the oblate and prolate shapes is suppressed, while the collective potential is flat with respect to the γ degree of freedom in the latter. The theoretical calculation indicates that large-scale quantum shape fluctuation occurs along the triaxial valley.

In Fig. 14, the collective path (one-dimensional collective submanifold) self-consistently determined by solving the ASCC equations, (97), (98), and (99), is indicated. The self-consistent collective path runs along the valley to connect the prolate and oblate minima. The inertial mass $B(q)$ is also determined by Eqs. (98) and (99). For one dimensional case, properly choosing the scale of the collective coordinate q, one can make $B(q) = B$ constant. The moments of inertia $J_k(q)$ are calculated by solving the Thouless-Valatin equations at every point on the collective path.

The collective wave functions displayed in Fig. 14(b) are obtained by solving the collective Schrödinger equation for the 4D collective Hamiltonian (the 1D collective path plus 3D rotational degrees of freedom) microscopically derived with the ASCC method (Hinohara *et al.*, 2009). The ground state shows a γ-unstable feature, and accordingly the second 0^+ state also shows strong mixing between the prolate and oblate shapes. However, increasing the angular momentum, the yrast (yrare) band becomes more and more oblate (prolate) dominant. The nuclear shape is localized (stabilized) by the rotation.

In order to confirm that the one-dimensional collective coordinate is enough for the low-energy dynamics of ^{68}Se, it is desirable to find the two-dimensional collective submanifold. This is approximately done according to the LQRPA (Sec. V.E.2), in which the self-consistency between the moving-frame HFB and QRPA equations is ignored, and no iteration is performed. Figure 15 shows a result of the application of the LQRPA method for deriving the 5D collective Hamiltonian (the 2D vibrational and 3D rotational coordinates). The potential $V(\beta, \gamma)$ is shown in Fig. 15 (a). The vibrational

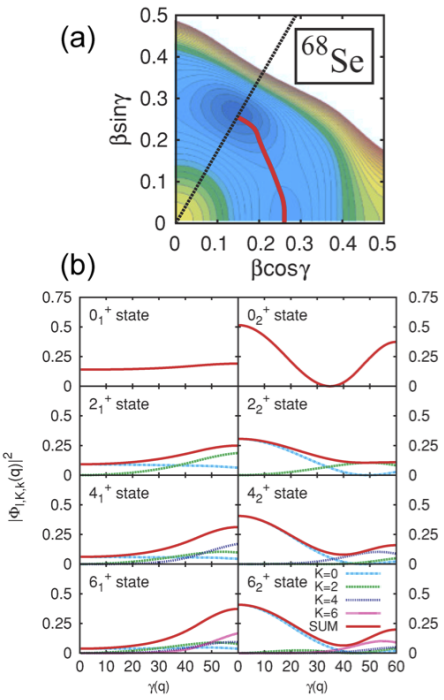

FIG. 14 (Color online) Application of the ASCC method to the oblate-prolate shape coexistence phenomenon in ^{68}Se. (a) The collective path for ^{68}Se obtained by the ASCC method. The solid (red) line shows the collective path running along the valley of the potential energy surface projected on the (β, γ) deformation plane. (b) Vibrational wave functions squared of the lowest (left) and the second-lowest states (right) for each angular momentum. In each panel, different K-components of the vibrational wave functions and the sum of them are plotted as functions of $\gamma(q)$. For excitation spectra, see Fig. 15. Adapted from Hinohara *et al.* (2009).

masses $D_{\beta\beta}(\beta, \gamma)$ and $D_{\gamma\gamma}(\beta, \gamma)$ significantly change as functions of (β, γ). In addition, considerable variation in the (β, γ)-plane is also observed in the paring gaps (monopole and quadrupole) and the rotational moments of inertia. Due to the time-odd contributions of the moving HFB self-consistent field, the collective inertial masses (the vibrational masses and the rotational moments of inertia) calculated with the LQRPA method are larger than those evaluated with the Inglis-Belyaev cranking formula. Their ratios also change as functions of (β, γ) (Hinohara *et al.*, 2010).

A remarkable agreement with experiment is seen in Fig. 15(b). An improvement over the 4D calculation is mostly due to the angular momentum dependence of the optimal 1D collective path. The calculated collective wave functions in Fig. 15(c) clearly indicate the importance of the fluctuation with respect to the γ-degree of freedom, which is consistent with the 1D collective path shown in Fig. 14. However, this path should gradually shifts to larger β with increasing angular momentum. This stretching effect is missing in the 4D calculation.

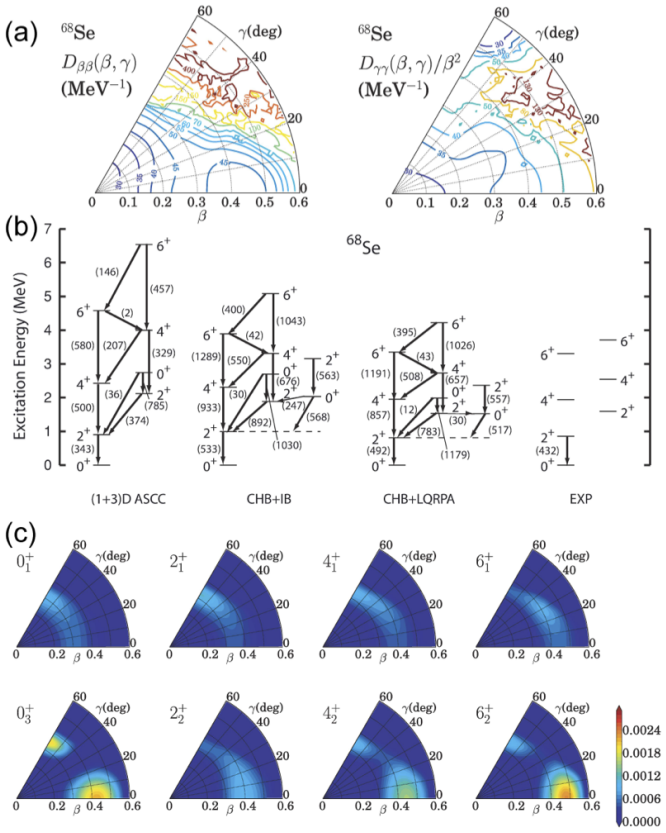

FIG. 15 (Color online) Application of the LQRPA method to the oblate-prolate shape coexistence/fluctuation phenomenon in ^{68}Se. (a) Collective inertial masses, $D_{\beta\beta}(\beta,\gamma)$ and $D_{\gamma\gamma}(\beta,\gamma)$, (b) Excitation spectrum, (c) Vibrational wave functions $\beta^4 \sum_K |\Phi_{IKk}(\beta,\gamma)|^2$. Adapted from Hinohara *et al.* (2010).

VI. RELATION TO TDDFT IN ELECTRONIC SYSTEMS

DFT and TDDFT have been extensively applied to electronic systems, matters composed of electrons and nuclei such as atoms, molecules, nano-materials, and solids (Dreizler and Gross, 1990; Gross and Maitra, 2012; Koch and Holthausen, 2001; Martin, 2004; Parr and Yang, 1989; Sholl and Steckel, 2009; Ullrich, 2012). Electrons in matters always need treatment by quantum mechanics, and nuclear motions can be in most cases treated by classical mechanics. In this chapter, we discuss DFT and TDDFT for electrons in matters, stressing similarities with and differences from nuclear DFT.

An apparent difference between electronic and nuclear systems is the interaction. The Hamiltonian of electronic systems is composed of the attractive one-body Coulomb potential between electrons and nuclei, and the repulsive Coulomb interaction among electrons. Besides the difference in the interaction, the researchers in the two fields have different concepts on the DFT and TDDFT. We first discuss these conceptual differences in Sec. VI.A, and describe the electronic EDFs in practical use in Sec. VI.B. We then describe applications of TDDFT in electronic systems. As in nuclear physics, there are two distinct applications: linear response TDDFT and TDDFT for large amplitude motion as an initial value problem. Former applications include electronic excitations and optical responses in molecules and solids, while the latter applications include electron dynamics in matters induced by strong laser pulses.

A. Conceptual difference between electronic and nuclear (TD)DFT

In electronic systems, DFT and TDDFT are considered as "self-contained" theories that can in principle be exact if accurate functionals are obtained. Improvements of the quality of the calculations should be achieved through improvement of the EDFs. There are other theoretical frameworks that can also in principle exactly describe properties of electron many-body systems, many-body perturbation theory (MBPT) in condensed matter physics and wave function based methods in the field of quantum chemistry. These three approaches, (TD)DFT, MBPT, and wave function based methods are recognized as completely different theories and to constitute independent, self-contained theoretical frameworks. In practical applications, DFT and MBPT are sometimes used simultaneously: for example, Green's functions that appear in the MBPT are approximately constructed from solutions of the KS equation. However, in such cases, the mixed use of different theories are clearly recognized, with some reasons such as computational conveniences.

The (TD)DFT in nuclear physics is rather different from this: for example, DFT and MBPT are often used in a mixed way. One of the reasons for this difference is probably due to different roles of the genuine Hartree-Fock (HF) approximation. In electronic systems, the HF approximation provides a reasonable starting point for the MBPT. The solutions of the HF and the KS equations are clearly different. In nuclear systems, on the other hand, the HF calculation using a bare nuclear force does not provide any useful result. The KS solution is the only appropriate starting point for the MBPT.

There are also qualitative differences in applications and interpretations of DFT and TDDFT between two kinds of systems. One example is the size of the system that the DFT and TDDFT are applied to: In nuclear applications, the DFT and TDDFT are usually adopted for studies of nuclei with a few tens of nucleons or more. In contrast, for electronic systems, the DFT and TDDFT are applied to as small as a few electron systems, even one electron system! For one electron system, of course, no potential originating from the EDF should appear. However, due to an approximate nature of the EDF in practical use, this property is often violated. The condition of vanishing potential for one electron system is used

to improve the EDF to remove the self-interaction error, which is known as the self-interaction correction (Perdew and Zunger, 1981).

Another important difference appears in interpretation of linear response TDDFT calculations. In nuclear TDDFT, we understand that the linear response TDDFT is accurate only for processes characterized by small amplitude oscillation around the ground state. Low-lying excited states are characterized by large amplitude motion and are considered to need requantization, as described in Sec. V. In electronic TDDFT, on the other hand, the linear response TDDFT has been applied to any electronic excitations no matter how the properties of the states are. The necessity of requantization has not been recognized in electronic TDDFT. The linear response TDDFT for electronic excitations and optical responses is simply called "TDDFT". The *linear response* is regarded merely as a computational method, not as an approximation to the TDDFT.

We also find differences in the treatment of collision effects. In nuclear physics, theories of the two-body nucleon-nucleon collisions have been developed, so as to treat these effects in addition to the TDDFT. In contrast, efforts been made to incorporate electron-electron collision effects within the TDKS formalism in electronic TDDFT, introducing correlation potentials with retardation. One example is an attempt to describe double ionization of atoms by strong laser pulse, which we will discuss in Sec. VI.C. There are also attempts to treat electron-electron collisions as an extension of quantum chemistry methods such as multi-configuration TDHF and time-dependent configuration interaction theories (Caillat *et al.*, 2005).

In electronic systems, DFT and TDDFT have been widely applied to extended systems. In describing electronic motions in infinitely periodic systems (crystalline solids), the KS equation is solved in a unit cell of the solid, which is called "first-principles band calculations". Extended systems are classified into metallic and insulating systems, depending on presence or absence of the band gap. Applying an external field to insulators, there appears a dielectric polarization and a surface charge. The surface charge has an influence on electrons inside the solid. Since it is the long-range effect, it cannot be incorporated in the LDA. To include the polarization effect in the DFT, density polarization functional theory (Gonze and Lee, 1997) has been developed in which the polarization is treated as an independent degree of freedom. A similar argument is applicable to electron dynamics in the TDDFT. Consider a current flowing in an extended system, or in a finite system, for example, a circular current flowing a nano material of ring shape. It is difficult to incorporate effects of the current on electron dynamics by local approximation. For such cases, time-dependent current density functional theory (TDCDFT) treating current and vector potential as basic variables has been developed (Ullrich, 2012). The TDCDFT also attracts interests to incorporate retardation effects. It has been realized that the retardation effects cannot be introduced consistently in TDDFT, if one assumes the LDA (Dobson, 1994). In the TDCDFT, it is possible to include the retardation effect in the local approximation scheme (Vignale and Kohn, 1996).

B. Energy density functionals

In this section, we describe properties of EDFs of electronic systems in practical use, with some emphasis on differences from those in nuclear systems. As in nuclear TDDFT, the adiabatic approximation of Eq. (32) is usually adopted for most applications of electronic TDDFT; one employs the same EDF as that in the static calculation, replacing a static density with a time-dependent density without retardation. Therefore, here, we mainly describe EDF for the static (ground state) calculations. At the end of this section, we briefly mention progresses beyond the adiabatic approximation.

In nuclear DFT, a general form of the EDF as a functional of density, density gradient, kinetic energy density, current density, spin density, pair density, and so on has been considered since early stage of its progress (Engel *et al.*, 1975). In contrast, electronic DFT started with an EDF of density only in the LDA and gradually developed to include more complex elements.

Energy density of a uniform system as a function of density is the most fundamental information for the EDF. Accurate energy density of an electron gas system in the ground state has been obtained around 1980 (Ceperley and Alder, 1980). It has been obtained by the MBPT at high density and by numerical calculations using quantum Monte Carlo method at medium and low density, connecting to the energy density of the Wigner crystal at very low density. Since then, a number of LDA calculations have been carried out for various systems, utilizing analytic forms of functional which are obtained by fitting the numerical energy density. When treating systems with spin polarization such as isolated atoms and ferromagnetic materials, local spin density approximation treating densities of spin up and spin down as basic variables has been developed.

As a step toward higher accuracy from the LDA, EDFs including a gradient of electron density have been developed. A group of EDFs with density gradient that are widely used today is called the generalized gradient approximation (GGA). They are constructed around 1990 and succeeded to increase the accuracy substantially from the LDA (Sousa *et al.*, 2007). To further improve the accuracy, EDFs including a kinetic energy density have been developed. They are called the meta-GGA (Tao *et al.*, 2003). In developing these new EDFs, exact analytical properties, that should be satisfied by EDF, are

respected. These attempts to increase the accuracy of the EDFs employing more and more elements are named the Jacob's ladder of the DFT by Perdew *et al.* (2005).

At present, most successful EDFs in the sense of accurate description of measured properties are those called "hybrid functional" (Koch and Holthausen, 2001). They use a mixture of semi-local and nonlocal forms for the exchange energy. The ratio of the mixture, which is determined empirically, is chosen to be about 3:1. In molecules, the functional named B3LYP (Stephens *et al.*, 1994) is known to give good results for many systems and has been quite often used (Laurent and Jacquemin, 2013). In infinitely periodic systems, hybrid functionals have also been proposed (Heyd *et al.*, 2003). However, the use is somewhat limited because calculation of the nonlocal exchange terms is computationally expensive in plane wave basis method that is popular in the solid-state calculations.

In electronic systems, computational methods to solve the KS equation is classified into two. One is the local basis expansion method in which the basis functions are given with respect to atomic positions. This is adopted in most quantum chemistry codes for molecules. The other is the grid representation either in the coordinate or in the momentum spaces. The grid representation in momentum, which is often called the plane wave basis method, has been widely adopted in computational codes of crystalline solids. Recently, the real-space grid representation becomes more and more popular, since it is superior for calculations with massively parallel computers (Andrade *et al.*, 2012; Enkovaara *et al.*, 2010). In the grid approach, it is difficult to describe inner orbitals that are strongly bound to nuclei. The pseudo-potential methods have been developed to avoid the difficulty. In the local basis expansion methods, nonlocal exchange terms can be managed with a reasonable computational cost. However, in the grid representation methods, the computational cost becomes extremely high. This situation is similar to the nuclear DFT calculations. In Skyrme HF calculations in which no nonlocal term appears, the real-space grid representation is a popular computational method, while in the HF calculations with Gogny interaction, the basis expansion method such as the harmonic oscillator basis is used to handle the nonlocal Fock terms.

Even with hybrid functionals, it is not possible to incorporate long-range electron correlations that are responsible for the van der Waals forces which are important between two neutral molecules. For this problem, one practical and successful approach is to add a long-range potential energy, $-C/R^6$, to every pair of atoms, on top of the DFT (Grimme, 2006). Microscopic approaches to construct EDFs incorporating the long-range electron correlations have also been actively pursued (Berland *et al.*, 2015).

While accurate calculation of the ground-state energy is the principal goal of the DFT calculations, orbital energies, in particular the energy gap between occupied and unoccupied orbitals, are important to describe electronic excitations and dynamics in TDDFT. Comparing energy gaps of insulators obtained from eigenvalues of the KS equation with measured energy gaps, the KS energy gaps are systematically too small. For a better description of energy gaps, potentials as functionals of the density gradient and of the kinetic energy density have been developed. For atoms and molecules, a potential named LB94 (van Leeuwen and Baerends, 1994), which includes the density gradient, has been successfully used for optical response calculations. The potential is so constructed that it has the correct asymptotic form, $-e^2/r$, which should be satisfied in electrically neutral systems. For extended systems, the meta-GGA potential that includes kinetic energy density was proposed by Tran and Blaha (2009), which attracts recent interests. These potentials are directly given as a functional of density, gradient of the density, and kinetic energy density. The EDFs that provide these potentials are not constructed. We do not know even whether such EDFs exist or not.

Beyond the adiabatic approximation is certainly an important issue. In the linear response TDDFT, the number of excited states is equal to the number of $1p-1h$ configurations. If one would hope to describe many-particle-many-hole-like configurations within the linear response TDDFT, frequency dependence of the exchange correlation kernel, the second derivative of the energy density functional with respect to densities, should be crucial. Inclusion of electron-electron collision effects through energy density functional will also require the frequency dependencies. Although extensive efforts have been made to construct nonadiabatic functionals, the functionals which are useful for wide purposes have not yet been obtained. A nonadiabatic energy functional in TDCDFT proposed by Vignale and Kohn (1996) has been tested for several problems. In that functional, the nonadiabaticity has been discussed making relations to the viscoelastic stresses of electronic quantum liquid.

C. Applications

1. Linear Response

Among applications of electronic TDDFT, the linear response TDDFT in the adiabatic approximation has been widely used and highly successful to describe electronic excitations and optical responses of molecules. As in nuclear TDDFT, the basic idea is to extract excitation energies and response functions from the density change induced by a weak external field applied to molecules.

Historically, optical responses of spherical systems have been investigated first. Using a similar approach to that in nuclear theory employing the continuum Green's function, optical responses of rare gas atoms have been

investigated by Zangwill and Soven (1980) and of metallic clusters by Ekardt (1984), respectively (Sec. III.E).

In middle 1990's and later, efficient computational methods have been developed for linear response TDDFT calculations of molecules without any spatial symmetries. A matrix diagonalization method preparing occupied and unoccupied orbitals has been developed by Casida *et al.* (1998) and has been named "Casida method" (Sec. III.B). A method solving linear Schrödinger-like equation for a given external field with a fixed frequency is known as the Sternheimer method (Nakatsukasa and Yabana, 2001). Real-time method has also been developed (Yabana and Bertsch, 1996; Yabana *et al.*, 2006), solving the TDKS equation in real time after an impulsive external field applied to the system (Sec. III.F). The matrix diagonalization method is the most widely used in practical purposes. The real time method is superior to calculate collective excitations to which a large number of electron-hole pairs contribute. After middle 1990's, linear response TDDFT has been implemented in many quantum chemistry codes as a tool to calculate electronically excited states of molecules with reasonable accuracy and cost. Using these codes, researchers who do not have much knowledge and experience on TDDFT, including experimentalists, can easily perform the linear response TDDFT calculations of molecules. After 2011, the number of papers that include TDDFT as keywords exceeds 1,000 per year.

As the method has been applied to a wide variety of molecules, it has been realized that linear response TDDFT with local or semilocal approximation fails systematically (Ullrich, 2012). For example, electronic excitation energies of long-chain molecules are systematically underestimated. Excitation energies of charge-transfer excitations, in which the electron and the hole are spatially remote, are also underestimated. These failures are attributed to the incomplete cancellation of the electron self-energy.

Linear responses of extended systems are characterized by dielectric functions, $\epsilon(\vec{q},\omega)$. The dielectric functions of metallic systems that are dominated by plasmon are reasonably described by the adiabatic TDDFT. In contrast, it does not give satisfactory results for semiconductors and insulators. In these solids, optical responses around the band gap energy are characterized by excitons, bound excited states of electrons and holes. It has been realized that the excitons cannot be described in the adiabatic TDDFT with local approximations (Onida *et al.*, 2002). For optical responses in semiconductors and insulators, the GW-plus-Bethe-Salpeter approach, solving the Bethe-Salpeter equation with the Green functions containing self-energy given by GW approximation, has been quite successful (Rohlfing and Louie, 2000).

2. Electron dynamics under strong field

In nuclear physics, TDDFT calculations as initial value problems have been developed in the studies of heavy ion collisions. In electronic systems, similar initial-value approaches have been widely applied to interactions of a strong laser pulse with matters.

One of active frontiers of laser science is to produce strong and ultra-short light pulses and to explore their interaction with matters. At extremely intense limit, high energy phenomena such as vacuum breakdown and nuclear reactions induced by strong laser pulses are actively investigated (Di Piazza *et al.*, 2012). In material sciences, interactions of light pulses whose scales are approaching to atomic units have been attracting significant interests. When the magnitude of the laser electric field approaches to those of binding electrons to ions, the electron dynamics induced by the laser pulse will become extremely nonlinear (Brabec and Krausz, 2000). The shortest light pulse available today is comparable to the period of hydrogen atom. Using such a ultra-short laser pulse as a flash light, there have been intense attempts to take snapshots of electron dynamics in atoms, molecules, and solids (Krausz and Ivanov, 2009). To theoretically investigate extremely nonlinear and ultrafast electron dynamics in matters, computational approaches solving time-dependent Schrödinger equation for one-electron systems and TDKS equation for many-electron systems have been extensively developed.

In strong laser pulse irradiations on atoms and molecules, various phenomena like tunnel and multiphoton ionizations, above threshold ionization, high harmonic generation, and Coulomb explosion have been described by the real-time TDDFT (Chu and Telnov, 2004; Marques and Gross, 2004; Ullrich, 2012). In the interaction of strong laser pulses with metallic clusters, nonlinear interactions between strong laser pulse and the plasmon, collective electronic excitation, play an important role (Calvayrac *et al.*, 2000; Wopperer *et al.*, 2015). In the multiple ionizations of atoms at relatively low laser intensities, it is known that the secondary ionizations proceed mainly through the rescattering process: an ionized electron is accelerated by the applied laser pulse and collides with the atom from which the electron was first emitted. This collision process has been regarded as a test case to develop EDFs that could describe collision effects. However, it turned out that finding such functional is, as anticipated, not an easy task (Ullrich, 2012).

Recently, interactions of strong laser pulses with solids have been attracting interests, aiming at exploring new phenomena that could bring innovative optical devices. The TDDFT calculations have been carried out to analyze nonlinear electron dynamics in solids, including ultrafast current generation in transparent material (Wachter *et al.*, 2014), and coupled dynamics of electrons and macroscopic electromagnetic fields (Yabana *et al.*,

2012)

Real-time TDDFT calculations have been applied to fields other than laser sciences. One example is electron transfer dynamics in ion collisions. Electronic TDHF calculations have been also applied to nuclear fusion reactions in astrophysical environments to investigate electronic screening effects (Shoppa *et al.*, 1993). Collision of energetic ions impinging on graphene sheet has been explored (Bubin *et al.*, 2012; Zhang *et al.*, 2012). Collisions between multiply ionized and neutral atoms have been investigated (Nagano *et al.*, 2000).

3. Coupled dynamics of electrons and atoms

Before ending this section, we present a simultaneous description of electronic and atomic motions. In nuclear physics, there is no degrees of freedom corresponding to atomic motion. However, coupling of a slow collective motion with fast internal motions as in nuclear fusion and fission dynamics may have some similarities.

If the material has an energy gap and electrons always stay in their ground state, we may assume the adiabatic, Born-Oppenheimer approximation. In such cases, we may separate the problem into two steps: For a given atomic configuration, we first solve the static KS equation to obtain the electronic ground state. Then the forces acting on atoms are calculated using the Feynman-Hellman theorem. Finally the atomic motions are calculated solving the Newton's equation. This is the so-called ab-initio molecular dynamics calculation, initiated with a slightly different implementation by Car and Parrinello (1985).

Simultaneous descriptions of electronic excitation and atomic motion, which are often termed nonadiabatic molecular dynamics, are much more involved. We first consider a simple molecule where one or at most a few electronic states are important. When the electronic levels are well separated, we may assume the Newtonian motion for atoms on the adiabatic potential energy surface. When the two electronic states come close in energy at a certain atomic configuration, quantum transitions between different potential energy surfaces need to be treated. The potential energy surfaces may be efficiently calculated by the linear response TDDFT. Such simulations have been widely applied to photo-molecule interactions (Persico and Granucci, 2014). We note that, in such simulations, the TDKS equation needs not to be solved in real time.

How can we treat cases in which a number of electronic levels are close in energy and transitions frequently take place? The electronic excitation spectra can even form the continuum in solids. There is an alternative method called the Ehrenfest dynamics. In this method, the TDKS equations for electrons and Newtonian equations for atoms are solved simultaneously in real time, as coupled equations. At each time, the force acting on each atom is calculated from the electron density (Shinohara *et al.*, 2010; Tavernelli, 2015).

These two methods are conceptually very different. The former method utilizes the linear response TDDFT to prepare potential energy surfaces, while the latter utilizes solution of real time TDKS equation as an initial value problem. At present, it is empirically decided which method to use for a given problem. Accumulation of results will eventually make it possible to assess the quality of approximation of the two approaches.

VII. SUMMARY AND FUTURE OUTLOOK

The TDDFT using modern nuclear EDFs provides a unified, systematic, and quantitative description of nuclear structure and reaction. Thanks to its non-trivial density dependence, these EDFs are capable of simultaneously reproducing the bulk properties of nuclei (saturation, EOS, etc.) and properties of individual nucleus (shell effects, deformation, etc.). The nuclear EDF also shows various kinds of spontaneous breaking of the symmetry (SSB). Especially, the translational symmetry is always violated for finite nuclei. The SSB can be incorporated in a stringent manner by the DFT theorems for the wave-packet states. Nevertheless, there remain several open questions for rigorous justification of the DFT in nuclear physics (Giraud, 2010). Because of significant increase in computational resources and development in parallelized computer programs, the TDDFT serves as modern approaches to a variety of nuclear phenomena which were addressed only with phenomenological models. Since all the parameters in nuclear EDFs are basically fixed, it can provide non-empirical predictions. In the present review, we summarize recent developments in the three categories: Linear density response, real-time method, and requantization of TDDFT collective submanifold.

The linear density response around the ground state is known as (Q)RPA in nuclear physics. Recent calculations treat all the residual fields induced by the density variations in the EDF. This is particularly important for the separation of ANG modes associated with the SSB. The program coding and numerical computation have been facilitated by the finite amplitude method and other iterative methods to the linear response. These developments significantly reduce the computational costs and necessary memory capacity for heavy deformed nuclei.

The treatment of the continuum is another issue which has been extensively studied in recent years to explore unique properties of weakly bound nuclei near the drip lines. The most complete formalism is the continuum QRPA simultaneously treating the continuum in the particle-hole and particle-particle (hole-hole) channels with the Green's function method. However, so far, the

numerical calculation has been achieved only for spherical systems.

The real-time TDDFT calculation provides useful insights into nuclear many-body dynamics, such as microscopic understanding of nuclear reaction and energy dissipation. One of the recent major achievements is the large-scale 3D calculation in the TDBdGKS (TDHFB) scheme (Sec IV). Although the full calculations for nuclear dynamics in this scheme are so far limited to the linear response, one can expect further applications to large amplitude dynamics in near future. Meantime, the approximate treatment of the BCS-like pairing may provide a useful guidance for that (Sec. IV.A).

A microscopic derivation of the internucleus potential and the dissipation has been developed by several authors recently, and applied to many systems (Sec. IV.B). This provides a connection between the microscopic TDDFT simulation and the phenomenological potential approaches to nuclear fusion. The method even quantitatively describes the sub-barrier fusion reaction for some cases, by extracting the potential from the TDDFT calculation (Umar and Oberacker, 2007, 2008). These methods may be justifiable before two nuclei overlaps substantially in the fusion process. However, it requires further developments and studies in clarifying the entire dynamics in the fusion process. The real-time TDDFT studies of quasifission are in progress too (Sec. IV).

Recent studies on the multi-nucleon transfer reaction show a reasonable agreement with experimental mass distribution (Sec. IV.C). The fluctuations in major channels seem to be taken into account by the TDDFT simulation with the particle-number projection. However, some discrepancies were also identified, especially in minor channels. For the improvement, the stochastic mean-field and Baranger-Véneroni variational approaches may provide a tool to correct these missing fluctuations and correlations (IV.C.2). It has been partially successful but further studies are desired.

At present, all the available nuclear EDFs seem not to be able to express,in the KS scheme, correlations associated with low-energy modes of (slow) collective motion. They have been addressed by additional correlations beyond the KS scheme, which includes the particle-vibration coupling, the higher random-phase approximation, the time-dependent density-matrix (TDDM) method, the generator coordinate method (GCM), and so on. In this review, we put some emphasis on the requantization of the TDDFT collective submanifold to take into account the missing correlations (Sec V). The self-consistent derivation of a collective Hamiltonian (submanifold) suitable for description of low-energy large amplitude motion can be achieved by solving the adiabatic self-consistent collective coordinate (ASCC) equations. The inertial masses include time-odd effects and are guaranteed to produce the correct total mass for the translation. The method also overcomes known difficulties in the adiabatic TDHF method. It has been applied to studies of nuclear quadrupole dynamics in the pairing-plus-quadrupole model. For the aim of deriving collective Hamiltonian for various kinds of large amplitude collective motion (LACM) on the basis of the modern EDFs, the finite-amplitude method and new iterative solvers in Sec. III.D may be utilized to numerically solve the moving-frame QRPA equations in an efficient way.

The collective inertial masses should be studied furthermore. The collective inertial mass, which is locally defined, represents the inertia of the many-body system against an infinitesimal change of the collective coordinate. As the single-particle-energy spectrum in the mean field changes during the LACM, the level crossing at the Fermi energy successively occurs. We expect that the configuration rearrangement at the level crossing is essential to keep the system at low energy. Thus, for low-energy nuclear dynamics, the pairing correlation plays an essential role in determination of the collective mass parameters (Barranco *et al.*, 1990). It remains as an interesting subject to investigate how the self-consistent determination of the optimal directions of collective motion and the finite frequency $\omega(q)$ of the moving-frame QRPA modes affect the level crossing dynamics of the superfluid nuclear systems.

In addition to the quadrupole collective motions, large-amplitude collective phenomena associated with instability toward octupole deformations of the mean field as well as interplay of the quadrupole and octupole modes of excitations have been widely observed in low-lying states of nuclei (Butler and Nazarewicz, 1996). In the high-spin yrast region where the nucleus is highly excited but cold (zero-temperature), new types of rotations and vibrations may emerge (Satuła and Wyss, 2005), such as wobbling motions (Frauendorf and Dönau, 2014; Hamamoto and Hagemann, 2003; Shoji and Shimizu, 2009) and superdeformed shape vibrations (Nakatsukasa *et al.*, 1996). It is quite interesting to apply the microscopic theory of LACM to these new collective phenomena (Matsuyanagi *et al.*, 2010). Macroscopic quantum tunnelings through self-consistently generated barriers, like spontaneous fissions and deep sub-barrier fusions, are, needless to say, great challenges of nuclear structure physics.

In electronic TDDFT, the linear response is considered to be exact, and the anharmonic large amplitude nature should not matter (Sec. VI.A). The failures in describing a certain class of excited states are due to incomplete EDFs, not to the limited applicability of the linear response. This makes a striking contrast to the concept of nuclear DFT/TDDFT. Because of these conceptual differences, major efforts in the electronic DFT/TDDFT are devoted to improvement in quality of EDFs. Construction of a practical and accurate EDF including the retardation effects beyond the adiabatic local density approximation is currently under investigation. This is a challenging subject in the electronic TDDFT. Neverthe-

less, using the adiabatic EDFs, there have been numerous successful applications both in the linear response and the initial-value TDDFT for molecules and solids (Sec. VI.C).

The nuclear many-body dynamics in the large-amplitude collective motion is still a big challenge for nuclear physics. This review has described theoretical and computational progress in the nuclear TDDFT studies, which we think significant in last decades. We hope it provides stimulus to researchers in the field.

ACKNOWLEDGMENTS

We are grateful to many collaborators and colleagues, including P. Avogadro, S. Ebata, N. Hinohara, T. Inakura, H. Z. Liang, K. Mizuyama, K. Sato, K. Sekizawa, K. Washiyama. and K. Yoshida. This work was supported in part by JSPS KAKENHI Grants No. 24105006, No. 25287065, No. 26400268, and No. 15H03674.

Appendix A: Krylov reduction of the RPA space

It is easy to see that the $2d$ Krylov subspace (64) contains the RPA-conjugate partners. In fact, $(\mathcal{NH})^m F_v$ and $(\mathcal{NH})^m \tilde{F}_v$ are RPA conjugate to each other ($(\mathcal{NH})^m \tilde{F}_v = (-1)^m \mathcal{I}\{(\mathcal{NH})^m F_v\}^*$). We can show this using $\mathcal{HI} = \mathcal{IH}^*$ and $\{\mathcal{N}, \mathcal{I}\} = 0$.

Next, let us map the RPA equation in the $2D$ space to that in the $2d$ space. Suppose that we construct the $\mathcal{N}$-orthonormalized basis, $\{Q_1, \cdots, Q_d; \tilde{Q}_1, \cdots, \tilde{Q}_d\}$ from Eq. (64). Let us define the $2D \times 2d$ rectangular matrix, $\mathcal{Q} \equiv (Q, \tilde{Q})$, which is a projection from the $2D$ full space into the $2d$ subspace. For instance, the Hamiltonian and the norm matrix in Eq. (55) are transformed into $2d \times 2d$ Hermitian matrices, as

$$h \equiv \mathcal{Q}^\dagger \mathcal{H} \mathcal{Q} = \begin{pmatrix} a & b \\ b^* & a^* \end{pmatrix}, \quad n \equiv \mathcal{Q}^\dagger \mathcal{N} \mathcal{Q} = \begin{pmatrix} 1 & 0 \\ 0 & -1 \end{pmatrix}.$$

Here, a and b are $d \times d$ matrices, given by $a_{ij} \equiv Q_i^\dagger \mathcal{NH} Q_j = -(\tilde{Q}_i^\dagger \mathcal{NH} \tilde{Q}_j)^*$ and $b_{ij} \equiv Q_i^\dagger \mathcal{NH} \tilde{Q}_j = -(\tilde{Q}_i^\dagger \mathcal{NH} Q_j)^*$. The eigenvectors

$$z_n \equiv \begin{pmatrix} x_n \\ y_n \end{pmatrix}, \quad \tilde{z}_n \equiv \begin{pmatrix} y_n^* \\ x_n^* \end{pmatrix}$$

are obtained by the diagonalizing the $2d \times 2d$ matrix, nh. In analogy to Eq. (56), we define the matrix notation

$$z \equiv (z, \tilde{z}) = \begin{pmatrix} x & y^* \\ y & x^* \end{pmatrix}, \quad \omega \equiv \begin{pmatrix} \omega_d & 0 \\ 0 & \omega_d \end{pmatrix}.$$

The eigenvalue equation (57) is mapped to

$$nhz = z\omega n. \tag{A1}$$

It is easy to show that the reduction (A1) preserves the sum rules m_L with odd L. Since the subspace (64) is complete for intermediate states ($L < 2d$) in Eq. (63), we can replace the norm matrix $\mathcal{N}$ by $\mathcal{Q}n\mathcal{Q}^\dagger$. Then, Eq. (63) can be rewritten as

$$\begin{aligned} m_L &= \frac{1}{2}(F_v + \tilde{F}_v)^\dagger \mathcal{Q}(nh)^L n \mathcal{Q}^\dagger (F_v + \tilde{F}_v) \\ &= \frac{1}{2}(F_v + \tilde{F}_v)^\dagger \mathcal{Q} z \omega^L z^\dagger \mathcal{Q}^\dagger (F_v + \tilde{F}_v) = \sum_{n=1}^{d} \omega_n^L |\langle n|F|0\rangle|^2, \end{aligned}$$

where we used the relation $z^\dagger h z = \omega$ which is derived from Eq. (A1). Here, $z^\dagger \mathcal{Q}^\dagger (F_v + \tilde{F}_v)$ is nothing but the transition strength $\langle n|F|0\rangle$ calculated with the approximate eigenvectors, $Z' = \mathcal{Q}z = \begin{pmatrix} X' & Y'^* \\ Y' & X'^* \end{pmatrix}$.

Appendix B: Response function with the Green's function

In this appendix, we show the derivation of Eq. (67). The unperturbed (independent-particle) density response $\delta R^0(\omega)$ is defined by the limit of the vanishing residual kernels, $w = w' = 0$. Since the response function $\Pi_0(\omega)$ is diagonal in the quasiparticle basis, it can be easily obtained from Eq. (65) as

$$\begin{aligned} \delta R^0(\omega) &= \sum_{i,j} \left\{ \frac{\Psi_i^0 V_{ij}^{(+-)} \tilde{\Psi}_j^{0\dagger}}{\omega - E_i - E_j} + \frac{\tilde{\Psi}_i^0 V_{ij}^{(-+)} \Psi_j^{0\dagger}}{-\omega - E_i - E_j} \right\} \\ &= \sum_{i,j} \left\{ \frac{\Psi_i^0 \Psi_i^{0\dagger} V \tilde{\Psi}_j^0 \tilde{\Psi}_j^{0\dagger}}{\omega - E_i - E_j} + \frac{\tilde{\Psi}_i^0 \tilde{\Psi}_i^{0\dagger} V \Psi_j^0 \Psi_j^{0\dagger}}{-\omega - E_i - E_j} \right\}, \end{aligned} \tag{B1}$$

which has poles at the two-quasiparticle energies, $\omega = \pm(E_i + E_j)$. Note that we have converted the quasiparticle representation to a general form (cf. the transition densities of Eq. (60)). Adding the following zero in the right hand side,

$$\sum_{i,j} \left\{ \frac{\tilde{\Psi}_i^0 \tilde{\Psi}_i^{0\dagger} V(\omega) \tilde{\Psi}_j^0 \tilde{\Psi}_j^{0\dagger}}{\omega + E_i - E_j} + \frac{\tilde{\Psi}_i^0 \tilde{\Psi}_i^{0\dagger} V(\omega) \tilde{\Psi}_j^0 \tilde{\Psi}_j^{0\dagger}}{-\omega - E_i + E_j} \right\} = 0,$$

leads to an expression

$$\begin{aligned} \delta R^0(\omega) = \sum_i \Big\{ &\mathcal{G}_0(\omega - E_i) V(\omega) \tilde{\Psi}_i^0 \tilde{\Psi}_i^{0\dagger} \\ &+ \tilde{\Psi}_i^0 \tilde{\Psi}_i^{0\dagger} V(\omega) \mathcal{G}_0(-\omega - E_i) \Big\}. \end{aligned} \tag{B2}$$

Here, the Green's function $\mathcal{G}_0(E)$ is given by

$$\mathcal{G}_0(E) = (E - H_s[R_0])^{-1} = \sum_i \left\{ \frac{\Psi_i^0 \Psi_i^{0\dagger}}{E - E_i} + \frac{\tilde{\Psi}_i^0 \tilde{\Psi}_i^{0\dagger}}{E + E_i} \right\}. \tag{B3}$$

This Green's function contains both normal and abnormal Green's function, $G_0(E)$ and $F_0(E)$, in the 2×2

matrix form. Equation (B2) can also be derived by the Fourier transform of Eq. (48)

$$\delta R^0(\omega) = \sum_i \left\{ \delta\tilde{\Psi}_i(\omega)\tilde{\Psi}_i^{0\dagger} + \tilde{\Psi}_i^0 \delta\tilde{\Psi}_i^\dagger(-\omega) \right\}$$

and $\delta\tilde{\Psi}_i(\omega) = \mathcal{G}_0(\omega - E_i)V(\omega)\tilde{\Psi}_i^0$.

Now, let us adopt a single-particle representation, $\{\alpha\}$. It should be noted that, since the quasiparticle state has upper and lower components, $U(\alpha)$ and $V(\alpha)$, the quantities with two single-particle indices, such as $V(\omega)$, $\delta R^0(\omega)$, and $\mathcal{G}_0(E)$, are expressed in 2×2 matrix form. The response function, $\Pi_0(\omega)$ and $\Pi(\omega)$, with four indices should be expressed in the $(2\times 2)\otimes(2\times 2)$ form. In order to avoid these complications, we adopt the primed indices, $\alpha', \beta', \cdots$, which are given after Eq. (16).

Equation (B2) is represented as

$$\begin{aligned} \delta R^0(\alpha'\beta';\omega) &= \textstyle\sum_{\mu'\nu'} \Pi_0(\alpha'\beta',\mu'\nu';\omega)V(\mu'\nu';\omega), \\ \Pi_0(\alpha'\beta',\mu'\nu';\omega) &= \textstyle\sum_i \Big\{ \mathcal{G}_0(\alpha'\mu';\omega - E_i)\tilde{\Phi}_i(\nu')\tilde{\Phi}_i^\dagger(\beta') \\ &\quad + \tilde{\Phi}_i(\alpha')\tilde{\Phi}_i^\dagger(\mu')\mathcal{G}_0(\nu'\beta';-\omega - E_i) \Big\}. \end{aligned} \tag{B4}$$

Similarly, the residual kernel $\mathcal{W}$ is represented by four indices. In principle, according to Eq. (66), we may obtain the QRPA response function $\Pi(\omega)$ and the density response $\delta R(\omega)$.

Here, we distinguish the upper $\Psi_i^{0(1)} = U_i$ and lower components $\Psi_i^{0(2)} = V_i$ of the quasiparticle Ψ_i^0, and introduce the 2×2 matrix form for the density $\delta R^{(mn)}$ and the external potential $V^{(mn)}$, and the $(2\times 2)\otimes(2\times 2)$ form for the response function $\Pi^{(mn,pq)}$ and the residual kernels $\mathcal{W}^{(mn,pq)}$, with the indices $m, n, p, q = 1$ and 2. If the potential and residual kernels have the diagonal character, $V^{(mn)}(\alpha\beta) = V^{(mn)}(\alpha)\delta_{\alpha\beta}$, $\mathcal{W}^{(mn,pq)}(\alpha\beta,\mu\nu) = \mathcal{W}^{(mn,pq)}(\alpha,\mu)\delta_{\alpha\beta}\delta_{\mu\nu}$, we may simplify Eq. (B4) to its diagonal representation

$$\begin{aligned} &\Pi_0^{(mn,pq)}(\alpha,\beta;\omega) = \\ &\quad \sum_i \Big\{ \mathcal{G}_0^{(mp)}(\alpha\beta;\omega - E_i)\tilde{\Phi}_i^{(q)}(\beta)\tilde{\Phi}_i^{(n)\dagger}(\alpha) \\ &\quad + \tilde{\Phi}_i^{(m)}(\alpha)\tilde{\Phi}_i^{(p)\dagger}(\beta)\mathcal{G}_0^{(qn)}(\beta\alpha;-\omega - E_i) \Big\}. \end{aligned} \tag{B5}$$

and the unperturbed density response is given by

$$\delta R_0^{(mn)}(\alpha\alpha) = \sum_{p,q=1,2} \sum_\beta \Pi_0^{(mn,pq)}(\alpha,\beta)V^{(pq)}(\beta).$$

REFERENCES

Abe, Y., and T. Suzuki, Eds. (1983), *Microscopic theories of nuclear collective motions*, Progress of Theoretical Physics Supplement, Vol. 74-75.

Åberg, S., H. Flocard, and W. Nazarewicz (1990), Annual Review of Nuclear and Particle Science **40**, 439.

Aichelin, J. (1991), Physics Reports **202**, 233 .

Alder, K., A. Bohr, T. Huus, B. Mottelson, and A. Winther (1956), Rev. Mod. Phys. **28**, 432.

Almehed, D., and N. R. Walet (2004), Phys. Rev. C **69**, 024302.

Anderson, P. W. (1958), Phys. Rev. **110**, 827.

Anderson, P. W. (1963), Phys. Rev. **130**, 439.

Andrade, X., J. Alberdi-Rodriguez, D. A. Strubbe, M. J. T. Oliveira, F. Nogueira, A. Castro, J. Muguerza, A. Arruabarrena, S. G. Louie, A. Aspuru-Guzik, A. Rubio, and M. A. L. Marques (2012), Journal of Physics: Condensed Matter **24**, 233202.

Anguiano, M., J. Egido, and L. Robledo (2001), Nuclear Physics A **696**, 467 .

Aoyama, S., T. Myo, K. Katō, and K. Ikeda (2006), Progress of Theoretical Physics **116**, 1.

Arnold, V. I. (1989), *Mathematical methods of classical mechanics* (Springer-Verlag, New York).

Arteaga, D. P., E. Khan, and P. Ring (2009), Phys. Rev. C **79**, 034311.

Avez, B., C. Simenel, and P. Chomaz (2008), Phys. Rev. C **78**, 044318.

Avogadro, P., and T. Nakatsukasa (2011), Phys. Rev. C **84**, 014314.

Avogadro, P., and T. Nakatsukasa (2013), Phys. Rev. C **87**, 014331.

Ayik, S. (2008), Physics Letters B **658**, 174 .

Baldo, M., L. M. Robledo, P. Schuck, and X. Viñas (2013), Phys. Rev. C **87**, 064305.

Baldo, M., P. Schuck, and X. Viñas (2008), Physics Letters B **663**, 390 .

Balian, R., and M. Vénéroni (1985), Annals of Physics **164**, 334.

Baran, A., J. A. Sheikh, J. Dobaczewski, W. Nazarewicz, and A. Staszczak (2011), Phys. Rev. C **84**, 054321.

Baranger, M., and K. Kumar (1965), Nuclear Physics **62**, 113 .

Baranger, M., M. Strayer, and J.-S. Wu (2003), Phys. Rev. C **67**, 014318.

Baranger, M., and M. Vénéroni (1978), Annals of Physics **114**, 123 .

Barnea, N. (2007), Phys. Rev. C **76**, 067302.

Barranco, F., G. F. Bertsch, R. A. Broglia, and E. Vigezzi (1990), Nuclear Physics A **512**, 253 .

Belyaev, S. T. (1965), Nuclear Physics **64**, 17 .

Belyaev, S. T., A. V. Smirnov, S. V. Tolokonnikov, and S. A. Fayans (1987), Soviet Journal of Nuclear Physics **45**, 783.

Bender, M. (2008), The European Physical Journal Special Topics **156**, 217.

Bender, M., G. F. Bertsch, and P.-H. Heenen (2006), Phys. Rev. C **73**, 034322.

Bender, M., J. Dobaczewski, J. Engel, and W. Nazarewicz (2002), Phys. Rev. C **65**, 054322.

Bender, M., and P.-H. Heenen (2008), Phys. Rev. C **78**, 024309.

Bender, M., P. H. Heenen, and P.-G. Reinhard (2003), Rev. Mod. Phys. **75**, 121.

Berland, K., V. R. Cooper, K. Lee, E. Schröder, T. Thonhauser, P. Hyldgaard, and B. I. Lundqvist (2015), Reports on Progress in Physics **78**, 066501.

Bertsch, G. F., M. Girod, S. Hilaire, J.-P. Delaroche, H. Goutte, and S. Péru (2007), Phys. Rev. Lett. **99**, 032502.

Bes, D., and R. A. Sorensen (1969), in *Advances in Nuclear*

Physics, Advances in the Physics of Particles and Nuclei, Vol. 2, edited by J. Negele and E. Vogt (Plenum Press) p. 129.

Bethe, H. A., and R. F. Bacher (1936), Rev. Mod. Phys. **8**, 82.

Blaizot, J.-P., and G. Ripka (1986), *Quantum Theory of Finite Systems* (MIT Press, Cambridge).

Błocki, J., and H. Flocard (1976), Nucl. Phys. A **273**, 45.

Błocki, J., and H. Flocard (1979), Physics Letters B **85**, 163 .

Bohr, A. (1976), Rev. Mod. Phys. **48**, 365.

Bohr, A., and B. R. Mottelson (1969), *Nuclear Structure, Vol. I* (W. A. Benjamin, New York).

Bohr, A., and B. R. Mottelson (1975), *Nuclear Structure, Vol. II* (W. A. Benjamin, New York).

Bonche, P., J. Dobaczewski, H. Flocard, P.-H. Heenen, and J. Meyer (1990), Nuclear Physics A **510**, 466 .

Bonche, P., S. Koonin, and J. W. Negele (1976), Phys. Rev. C **13**, 1226.

Brabec, T., and F. Krausz (2000), Rev. Mod. Phys. **72**, 545.

Brack, M., J. Damgaard, A. S. Jensen, H. C. Pauli, V. M. Strutinsky, and C. Y. Wong (1972), Rev. Mod. Phys. **44**, 320.

Brenna, M., G. Colò, and P. F. Bortignon (2012), Phys. Rev. C **85**, 014305.

Brenna, M., G. Colò, and X. Roca-Maza (2014), Phys. Rev. C **90**, 044316.

Brink, D., and R. A. Broglia (2005), *Nuclear Superfluidity, Pairing in Finite Systems* (Cambridge University Press, Cambridge).

Brink, D. M., M. J. Giannoni, and M. Veneroni (1976), Nuclear Physics A **258**, 237 .

Brink, D. M., and F. Stancu (1981), Phys. Rev. C **24**, 144.

Bubin, S., B. Wang, S. Pantelides, and K. Varga (2012), Phys. Rev. B **85**, 235435.

Bulgac, A. (2013), Annual Review of Nuclear and Particle Science **63**, 97.

Butler, P. A., and W. Nazarewicz (1996), Rev. Mod. Phys. **68**, 349.

Caillat, J., J. Zanghellini, M. Kitzler, O. Koch, W. Kreuzer, and A. Scrinzi (2005), Phys. Rev. A **71**, 012712.

Calvayrac, F., P.-G. Reinhard, E. Suraud, and C. Ullrich (2000), Physics Reports **337**, 493 .

Cao, L.-G., G. Colò, H. Sagawa, and P. F. Bortignon (2014), Phys. Rev. C **89**, 044314.

Car, R., and M. Parrinello (1985), Phys. Rev. Lett. **55**, 2471.

Carlos, P., H. Beil, R. Bergère, A. Leprêtre, A. D. Miniac, and A. Veyssière (1974), Nuclear Physics A **225**, 171 .

Carlos, P., H. Beil, R. Bergere, A. Lepretre, and A. Veyssiere (1971), Nuclear Physics A **172**, 437 .

Carlsson, B. G., and J. Dobaczewski (2010), Phys. Rev. Lett. **105**, 122501.

Carlsson, B. G., J. Dobaczewski, and M. Kortelainen (2008), Phys. Rev. C **78**, 044326.

Carlsson, B. G., J. Toivanen, and A. Pastore (2012), Phys. Rev. C **86**, 014307.

Casida, M. E., C. Jamorski, K. C. Casida, and D. R. Salahub (1998), The Journal of Chemical Physics **108**, 4439.

Ceperley, D. M., and B. J. Alder (1980), Phys. Rev. Lett. **45**, 566.

Chappert, F., M. Girod, and S. Hilaire (2008), Physics Letters B **668**, 420 .

Chappert, F., N. Pillet, M. Girod, and J.-F. Berger (2015), Phys. Rev. C **91**, 034312.

Chu, S. I., and D. A. Telnov (2004), Phys. Rep. **390**, 1, invited review article.

Clément, E., A. Görgen, W. Korten, E. Bouchez, A. Chatillon, J.-P. Delaroche, M. Girod, H. Goutte, A. Hürstel, Y. L. Coz, A. Obertelli, S. Péru, C. Theisen, J. N. Wilson, M. Zielińska, C. Andreoiu, F. Becker, P. A. Butler, J. M. Casandjian, W. N. Catford, T. Czosnyka, G. d. France, J. Gerl, R.-D. Herzberg, J. Iwanicki, D. G. Jenkins, G. D. Jones, P. J. Napiorkowski, G. Sletten, and C. N. Timis (2007), Phys. Rev. C **75**, 054313.

Colò, G., H. Sagawa, and P. F. Bortignon (2010), Phys. Rev. C **82**, 064307.

Corradi, L., A. M. Stefanini, J. H. He, S. Beghini, G. Montagnoli, F. Scarlassara, G. F. Segato, G. Pollarolo, and C. H. Dasso (1997), Phys. Rev. C **56**, 938.

Cusson, R., P.-G. Reinhard, M. Strayer, J. Maruhn, and W. Greiner (1985), Zeitschrift für Physik A Atoms and Nuclei **320**, 475.

Dang, G. D., A. Klein, and N. R. Walet (2000), Physics Reports **335**, 93 .

Daoutidis, I., and P. Ring (2011), Phys. Rev. C **83**, 044303.

Dapo, H., and N. Paar (2012), Phys. Rev. C **86**, 035804.

De Donno, V., G. Co', M. Anguiano, and A. M. Lallena (2011), Phys. Rev. C **83**, 044324.

Delaroche, J. P., M. Girod, J. Libert, H. Goutte, S. Hilaire, S. Péru, N. Pillet, and G. F. Bertsch (2010), Phys. Rev. C **81**, 014303.

Descouvemont, P., and D. Baye (2010), Reports on Progress in Physics **73**, 036301.

Di Piazza, A., C. Müller, K. Z. Hatsagortsyan, and C. H. Keitel (2012), Rev. Mod. Phys. **84**, 1177.

Dobaczewski, J., and J. Dudek (1995), Phys. Rev. C **52**, 1827.

Dobaczewski, J., W. Nazarewicz, and P.-G. Reinhard (2014), Journal of Physics G: Nuclear and Particle Physics **41**, 074001.

Dobaczewski, J., and J. Skalski (1981), Nuclear Physics A **369**, 123 .

Dobaczewski, J., M. V. Stoitsov, W. Nazarewicz, and P.-G. Reinhard (2007), Phys. Rev. C **76**, 054315.

Dobson, J. F. (1994), Phys. Rev. Lett. **73**, 2244.

Dreizler, R. M., and E. K. U. Gross (1990), *Density Functional Theory: An Approach to the Quantum Many-Body Problem* (Springer, Berlin).

Drozdz, S., S. Nishizaki, J. Speth, and J. Wambach (1990), Physics Reports **197**, 1 .

Duguet, T., M. Bender, K. Bennaceur, D. Lacroix, and T. Lesinski (2009), Phys. Rev. C **79**, 044320.

Ebata, S., and T. Nakatsukasa (2014), JPS Conference Proceedings **1**, 013038.

Ebata, S., and T. Nakatsukasa (2015), JPS Conference Proceedings **6**, 020056.

Ebata, S., T. Nakatsukasa, and T. Inakura (2014), Phys. Rev. C **90**, 024303.

Ebata, S., T. Nakatsukasa, T. Inakura, K. Yoshida, Y. Hashimoto, and K. Yabana (2010), Phys. Rev. C **82**, 034306.

Egido, J., and L. Robledo (2004), in *Extended Density Functionals in Nuclear Structure Physics*, Lecture Notes in Physics, Vol. 641, edited by G. Lalazissis, P. Ring, and D. Vretenar (Springer Berlin Heidelberg) pp. 269–302.

Ekardt, W. (1984), Phys. Rev. Lett. **52**, 1925.

Engel, J. (2007), Phys. Rev. C **75**, 014306.

Engel, J., M. Bender, J. Dobaczewski, W. Nazarewicz, and

R. Surman (1999), Phys. Rev. C **60**, 014302.
Engel, Y. M., D. M. Brink, K. Goeke, S. J. Krieger, and D. Vautherin (1975), Nucl. Phys. A **249**, 215.
Enkovaara, J., C. Rostgaard, J. J. Mortensen, J. Chen, M. Dułak, L. Ferrighi, J. Gavnholt, C. Glinsvad, V. Haikola, H. A. Hansen, H. H. Kristoffersen, M. Kuisma, A. H. Larsen, L. Lehtovaara, M. Ljungberg, O. Lopez-Acevedo, P. G. Moses, J. Ojanen, T. Olsen, V. Petzold, N. A. Romero, J. Stausholm-Møller, M. Strange, G. A. Tritsaris, M. Vanin, M. Walter, B. Hammer, H. Häkkinen, G. K. H. Madsen, R. M. Nieminen, J. K. Nørskov, M. Puska, T. T. Rantala, J. Schiøtz, K. S. Thygesen, and K. W. Jacobsen (2010), Journal of Physics: Condensed Matter **22**, 253202.
Erler, J., N. Birge, M. Kortelainen, W. Nazarewicz, E. Olsen, A. M. Perhac, and M. Stoitsov (2012), Nature **486**, 509 .
Erler, J., P. Klüpfel, and P.-G. Reinhard (2010), Journal of Physics G: Nuclear and Particle Physics **37**, 064001.
Fattoyev, F. J., C. J. Horowitz, J. Piekarewicz, and G. Shen (2010), Phys. Rev. C **82**, 055803.
Fracasso, S., and G. Colò (2005), Phys. Rev. C **72**, 064310.
Fracasso, S., E. B. Suckling, and P. D. Stevenson (2012), Phys. Rev. C **86**, 044303.
Frauendorf, S. (2001), Rev. Mod. Phys. **73**, 463.
Frauendorf, S., and F. Dönau (2014), Phys. Rev. C **89**, 014322.
Fu, Y., H. Mei, J. Xiang, Z. P. Li, J. M. Yao, and J. Meng (2013), Phys. Rev. C **87**, 054305.
Fujikawa, K., and H. Ui (1986), Progress of Theoretical Physics **75**, 997.
Fukuoka, Y., S. Shinohara, Y. Funaki, T. Nakatsukasa, and K. Yabana (2013), Phys. Rev. C **88**, 014321.
Gambacurta, D., M. Grasso, and F. Catara (2011), Phys. Rev. C **84**, 034301.
Gambacurta, D., M. Grasso, V. De Donno, G. Co', and F. Catara (2012), Phys. Rev. C **86**, 021304.
Gambacurta, D., M. Grasso, and J. Engel (2015), Phys. Rev. C **92**, 034303.
Giannoni, M. J., and P. Quentin (1980a), Phys. Rev. C **21**, 2060.
Giannoni, M. J., and P. Quentin (1980b), Phys. Rev. C **21**, 2076.
Giraud, B. G. (2008), Phys. Rev. C **77**, 014311.
Giraud, B. G. (2010), Journal of Physics G: Nuclear and Particle Physics **37**, 064002.
Giraud, B. G., B. K. Jennings, and B. R. Barrett (2008), Phys. Rev. A **78**, 032507.
Goeke, K., R. Y. Cusson, F. Grümmer, P.-G. Reinhard, and H. Reinhardt (1983a), Progress of Theoretical Physics Supplement **74-75**, 33.
Goeke, K., F. Grümmer, and P.-G. Reinhard (1983b), Annals of Physics **150**, 504 .
Goeke, K., and P.-G. Reinhard (1978), Annals of Physics **112**, 328 .
Goldstone, J. (1961), Il Nuovo Cimento **19**, 154.
Gonze, X., and C. Lee (1997), Phys. Rev. B **55**, 10355.
Goriely, S., N. Chamel, and J. M. Pearson (2013), Phys. Rev. C **88**, 061302.
Goriely, S., S. Hilaire, M. Girod, and S. Péru (2009), Phys. Rev. Lett. **102**, 242501.
Griffin, J. J., and J. A. Wheeler (1957), Phys. Rev. **108**, 311.
Grimme, S. (2006), Journal of Computational Chemistry **27**, 1787.
Gross, E. K. U., and N. T. Maitra (2012), "Fundamentals of time-dependent density functional theory," Chap. Introduction to TDDFT (Springer Berlin Heidelberg, Berlin, Heidelberg) pp. 53–99.
Guo, L., and T. Nakatsukasa (2012), EPJ Web of Conferences **38**, 09003.
Hamamoto, I. (2012), Phys. Rev. C **85**, 064329.
Hamamoto, I., and G. B. Hagemann (2003), Phys. Rev. C **67**, 014319.
Hansen, P. G., and B. Jonson (1987), Europhys. Lett. **4**, 409.
Harakeh, M. N., and A. van der Woude (2001), *Giant resonances*, Oxford Studies in Nuclear Physics 24 (Oxford University Press, Oxford).
Hashimoto, Y. (2012), The European Physical Journal A **48**, 1.
Hashimoto, Y., and K. Nodeki (2007), "A numerical method of solving time-dependent hartree-fock-bogoliubov equation with gogny interaction," Preprint: arXiv:0707.3083.
Heyd, J., G. E. Scuseria, and M. Ernzerhof (2003), The Journal of Chemical Physics **118**, 8207.
Heyde, K., and J. L. Wood (2011), Rev. Mod. Phys. **83**, 1467.
Hinohara, N. (2015), Phys. Rev. C **92**, 034321.
Hinohara, N., M. Kortelainen, and W. Nazarewicz (2013), Phys. Rev. C **87**, 064309.
Hinohara, N., M. Kortelainen, W. Nazarewicz, and E. Olsen (2015), Phys. Rev. C **91**, 044323.
Hinohara, N., Z. P. Li, T. Nakatsukasa, T. Nikšić, and D. Vretenar (2012), Phys. Rev. C **85**, 024323.
Hinohara, N., T. Nakatsukasa, M. Matsuo, and K. Matsuyanagi (2007), Prog. Theor. Phys. **117**, 451.
Hinohara, N., T. Nakatsukasa, M. Matsuo, and K. Matsuyanagi (2009), Phys. Rev. C **80**, 014305.
Hinohara, N., K. Sato, T. Nakatsukasa, M. Matsuo, and K. Matsuyanagi (2010), Phys. Rev. C **82**, 064313.
Hohenberg, P., and W. Kohn (1964), Phys. Rev. **136**, B864.
Holzwarth, G., and T. Yukawa (1974), Nuclear Physics A **219**, 125 .
Ichikawa, T., K. Matsuyanagi, J. A. Maruhn, and N. Itagaki (2014), Phys. Rev. C **90**, 034314.
Id Betan, R., R. J. Liotta, N. Sandulescu, and T. Vertse (2002), Phys. Rev. Lett. **89**, 042501.
Ieki, K., D. Sackett, A. Galonsky, C. A. Bertulani, J. J. Kruse, W. G. Lynch, D. J. Morrissey, N. A. Orr, H. Schulz, B. M. Sherrill, A. Sustich, J. A. Winger, F. Deák, A. Horváth, A. Kiss, Z. Seres, J. J. Kolata, R. E. Warner, and D. L. Humphrey (1993), Phys. Rev. Lett. **70**, 730.
Ikeda, K. (1992), Nucl. Phys. A **538**, 355c.
Ikeda, K., S. Yoshida, and S. Yamaji (1986), Zeitschrift für Physik A Atomic Nuclei **323**, 285.
Imagawa, H., and Y. Hashimoto (2003), Phys. Rev. C **67**, 037302.
Inakura, T., W. Horiuchi, Y. Suzuki, and T. Nakatsukasa (2014), Phys. Rev. C **89**, 064316.
Inakura, T., H. Imagawa, Y. Hashimoto, S. Mizutori, M. Yamagami, and K. Matsuyanagi (2006), Nuclear Physics A **768**, 61 .
Inakura, T., H. Imagawa, Y. Hashimoto, M. Yamagami, S. Mizutori, and K. Matsuyanagi (2005), The European Physical Journal A - Hadrons and Nuclei **25**, 545.
Inakura, T., T. Nakatsukasa, and K. Yabana (2009a), Phys. Rev. C **80**, 044301.
Inakura, T., T. Nakatsukasa, and K. Yabana (2009b), Eur. Phys. J. A **42**, 591.
Inakura, T., T. Nakatsukasa, and K. Yabana (2011), Phys. Rev. C **84**, 021302.

Inakura, T., T. Nakatsukasa, and K. Yabana (2013), Phys. Rev. C **88**, 051305.
Inglis, D. R. (1954), Phys. Rev. **96**, 1059.
Inglis, D. R. (1956), Phys. Rev. **103**, 1786.
Itoh, M., H. Sakaguchi, M. Uchida, T. Ishikawa, T. Kawabata, T. Murakami, H. Takeda, T. Taki, S. Terashima, N. Tsukahara, Y. Yasuda, M. Yosoi, U. Garg, M. Hedden, B. Kharraja, M. Koss, B. K. Nayak, S. Zhu, H. Fujimura, M. Fujiwara, K. Hara, H. P. Yoshida, H. Akimune, M. N. Harakeh, and M. Volkerts (2003), Phys. Rev. C **68**, 064602.
Iwata, Y., T. Otsuka, J. A. Maruhn, and N. Itagaki (2010a), Nuclear Physics A **836**, 108 .
Iwata, Y., T. Otsuka, J. A. Maruhn, and N. Itagaki (2010b), Phys. Rev. Lett. **104**, 252501.
Jancovici, B., and D. Schiff (1964), Nuclear Physics **58**, 678 .
Johnson, C. W., G. F. Bertsch, and W. D. Hazelton (1999), Computer Physics Communications **120**, 155 .
Kanesaki, N., T. Marumori, F. Sakata, and K. Takada (1973a), Progress of Theoretical Physics **49**, 181.
Kanesaki, N., T. Marumori, F. Sakata, and K. Takada (1973b), Progress of Theoretical Physics **50**, 867.
Kim, K.-H., T. Otsuka, and P. Bonche (1997), Journal of Physics G: Nuclear and Particle Physics **23**, 1267.
Kishimoto, T., J. M. Moss, D. H. Youngblood, J. D. Bronson, C. M. Rozsa, D. R. Brown, and A. D. Bacher (1975), Phys. Rev. Lett. **35**, 552.
Klein, A., and E. R. Marshalek (1991), Rev. Mod. Phys. **63**, 375.
Klein, A., N. R. Walet, and G. D. Dang (1991), Annals of Physics **208**, 90 .
Koch, W., and M. C. Holthausen (2001), *A Chemist's Guide to Density Functional Theory* (Wiley-VCH, Weinheim).
Kohn, W., and L. J. Sham (1965), Phys. Rev. **140**, A1133.
Koonin, S. E., K. T. R. Davies, V. Maruhn-Rezwani, H. Feldmeier, S. J. Krieger, and J. W. Negele (1977), Phys. Rev. C **15**, 1359.
Kortelainen, M., T. Lesinski, J. Moré, W. Nazarewicz, J. Sarich, N. Schunck, M. V. Stoitsov, and S. Wild (2010), Phys. Rev. C **82**, 024313.
Kortelainen, M., J. McDonnell, W. Nazarewicz, E. Olsen, P.-G. Reinhard, J. Sarich, N. Schunck, S. M. Wild, D. Davesne, J. Erler, and A. Pastore (2014), Phys. Rev. C **89**, 054314.
Kortelainen, M., J. McDonnell, W. Nazarewicz, P.-G. Reinhard, J. Sarich, N. Schunck, M. V. Stoitsov, and S. M. Wild (2012), Phys. Rev. C **85**, 024304.
Krausz, F., and M. Ivanov (2009), Rev. Mod. Phys. **81**, 163.
Kuriyama, A., K. Matsuyanagi, F. Sakata, K. Takada, and M. Yamamura (2001), Progress of Theoretical Physics Supplement **141**, 1.
Lacroix, D., and S. Ayik (2014), The European Physical Journal A **50**, 95, 10.1140/epja/i2014-14095-8.
Laurent, A. D., and D. Jacquemin (2013), International Journal of Quantum Chemistry **113**, 2019.
van Leeuwen, R. (1999), Phys. Rev. Lett. **82**, 3863.
van Leeuwen, R., and E. J. Baerends (1994), Phys. Rev. A **49**, 2421.
Levine, Z. H. (1984), Phys. Rev. A **30**, 1120.
Levine, Z. H., and P. Soven (1983), Phys. Rev. Lett. **50**, 2074.
Levine, Z. H., and P. Soven (1984), Phys. Rev. A **29**, 625.
Levy, M. (1979), Proceedings of the National Academy of Sciences **76**, 6062.
Li, Z. P., T. Nikšić, P. Ring, D. Vretenar, J. M. Yao, and J. Meng (2012), Phys. Rev. C **86**, 034334.
Li, Z. P., T. Nikšić, D. Vretenar, and J. Meng (2010a), Phys. Rev. C **81**, 034316.
Li, Z. P., T. Nikšić, D. Vretenar, J. Meng, G. A. Lalazissis, and P. Ring (2009), Phys. Rev. C **79**, 054301.
Li, Z. P., T. Nikšić, D. Vretenar, P. Ring, and J. Meng (2010b), Phys. Rev. C **81**, 064321.
Li, Z. P., J. M. Yao, D. Vretenar, T. Nikšić, H. Chen, and J. Meng (2011), Phys. Rev. C **84**, 054304.
Liang, H., T. Nakatsukasa, Z. Niu, and J. Meng (2013), Phys. Rev. C **87**, 054310.
Liang, H., T. Nakatsukasa, Z. Niu, and J. Meng (2014), Physica Scripta **89**, 054018.
Liang, H., N. Van Giai, and J. Meng (2008), Phys. Rev. Lett. **101**, 122502.
Libert, J., M. Girod, and J.-P. Delaroche (1999), Phys. Rev. C **60**, 054301.
Litvinova, E. (2012), Phys. Rev. C **85**, 021303.
Litvinova, E., and P. Ring (2006), Phys. Rev. C **73**, 044328.
Litvinova, E., P. Ring, and V. Tselyaev (2008), Phys. Rev. C **78**, 014312.
Litvinova, E., P. Ring, and V. Tselyaev (2010), Phys. Rev. Lett. **105**, 022502.
Litvinova, E. V., and A. V. Afanasjev (2011), Phys. Rev. C **84**, 014305.
Long, W., H. Sagawa, N. V. Giai, and J. Meng (2007), Phys. Rev. C **76**, 034314.
Losa, C., A. Pastore, T. Døssing, E. Vigezzi, and R. A. Broglia (2010), Phys. Rev. C **81**, 064307.
Ludde, H. J., and R. M. Dreizler (1983), Journal of Physics B: Atomic and Molecular Physics **16**, 3973.
Lunney, D., J. M. Pearson, and C. Thibault (2003), Rev. Mod. Phys. **75**, 1021.
Mahaux, C., P. F. Bortignon, R. A. Broglia, and C. H. Dasso (1985), Physics Reports **120**, 1.
Margueron, J., H. Sagawa, and K. Hagino (2008), Phys. Rev. C **77**, 054309.
Marques, M., and E. Gross (2004), Annual Review of Physical Chemistry **55**, 427, pMID: 15117259.
Martin, R. M. (2004), *Electronic Structure: Basic Theory and Practical Methods* (Cambridge University Press, Cambridge).
Martini, M., S. Péru, and S. Goriely (2014), Phys. Rev. C **89**, 044306.
Maruhn, J. A., P.-G. Reinhard, P. D. Stevenson, J. R. Stone, and M. R. Strayer (2005), Phys. Rev. C **71**, 064328.
Maruhn, J. A., P.-G. Reinhard, P. D. Stevenson, and A. S. Umar (2014), Computer Physics Communications **185**, 2195 .
Marumori, T., T. Maskawa, F. Sakata, and A. Kuriyama (1980), Progress of Theoretical Physics **64**, 1294.
Matsuo, M. (1986), Progress of Theoretical Physics **76**, 372.
Matsuo, M. (2001), Nucl. Phys. A **696**, 371.
Matsuo, M. (2015), Phys. Rev. C **91**, 034604.
Matsuo, M., and K. Matsuyanagi (1985a), Progress of Theoretical Physics **74**, 288.
Matsuo, M., and K. Matsuyanagi (1985b), Progress of Theoretical Physics **74**, 1227.
Matsuo, M., T. Nakatsukasa, and K. Matsuyanagi (2000), Prog. Theor. Phys. **103**, 959.
Matsuo, M., Y. R. Shimizu, and K. Matsuyanagai (1985), in *Proceedings of The Niels Bohr Centennial Conference on Nuclear Structure*, edited by R. Broglia, G. Hagemann, and B. Herskind (North Holland) p. 161.

Matsuyanagi, K., N. Hinohara, and K. Sato (2013), "Bcs-pairing and nuclear vibrations," in *Fifty Years of Nuclear BCS*, Chap. 9 (World Scientific, Singapore) pp. 111–124.
Matsuyanagi, K., M. Matsuo, T. Nakatsukasa, N. Hinohara, and K. Sato (2010), J. Phys. G **37**, 064018.
Matsuyanagi, K., M. Matsuo, T. Nakatsukasa, K. Yoshida, N. Hinohara, and K. Sato (2016), Journal of Physics G: Nuclear and Particle Physics **43**, 024006.
Mayer, M. G., and J. H. D. Jensen (1955), *Elementary theory of nuclear shell structure* (John Wiley & Sons, New York).
Messud, J., M. Bender, and E. Suraud (2009), Phys. Rev. C **80**, 054314.
Michel, N., K. Matsuyanagi, and M. Stoitsov (2008), Phys. Rev. C **78**, 044319.
Michel, N., W. Nazarewicz, M. Płoszajczak, and K. Bennaceur (2002), Phys. Rev. Lett. **89**, 042502.
Mizuyama, K., G. Colò, and E. Vigezzi (2012), Phys. Rev. C **86**, 034318.
Mizuyama, K., M. Matsuo, and Y. Serizawa (2009), Phys. Rev. C **79**, 024313.
Moghrabi, K., M. Grasso, X. Roca-Maza, and G. Colò (2012), Phys. Rev. C **85**, 044323.
Mottelson, B. (1976), Rev. Mod. Phys. **48**, 375.
Muga, J. G., J. P. Palao, B. Navarro, and I. L. Egusquiza (2004), Phys. Rep. **395**, 357.
Mukherjee, A., and M. Pal (1982), Nuclear Physics A **373**, 289 .
Mustonen, M. T., and J. Engel (2013), Phys. Rev. C **87**, 064302.
Mustonen, M. T., T. Shafer, Z. Zenginerler, and J. Engel (2014), Phys. Rev. C **90**, 024308.
Nagano, R., K. Yabana, T. Tazawa, and Y. Abe (2000), Phys. Rev. A **62**, 062721.
Nakada, H. (2013), Phys. Rev. C **87**, 014336.
Nakada, H., and T. Inakura (2015), Phys. Rev. C **91**, 021302.
Nakamura, T., A. M. Vinodkumar, T. Sugimoto, N. Aoi, H. Baba, D. Bazin, N. Fukuda, T. Gomi, H. Hasegawa, N. Imai, M. Ishihara, T. Kobayashi, Y. Kondo, T. Kubo, M. Miura, T. Motobayashi, H. Otsu, A. Saito, H. Sakurai, S. Shimoura, K. Watanabe, Y. X. Watanabe, T. Yakushiji, Y. Yanagisawa, and K. Yoneda (2006), Phys. Rev. Lett. **96**, 252502.
Nakamura, T., *et al.* (1994), Phys. Lett. B **331**, 296.
Nakatsukasa, T. (2012), Progress of Theoretical and Experimental Physics **2012**, 01A207.
Nakatsukasa, T. (2014), Journal of Physics: Conference Series **533**, 012054.
Nakatsukasa, T., P. Avogadro, S. Ebata, T. Inakura, and K. Yoshida (2011), Act. Phys. Pol. B **42**, 609.
Nakatsukasa, T., T. Inakura, and K. Yabana (2007), Phys. Rev. C **76**, 024318.
Nakatsukasa, T., K. Matsuyanagi, S. Mizutori, and Y. R. Shimizu (1996), Phys. Rev. C **53**, 2213.
Nakatsukasa, T., N. Walet, and G. D. Dang (1999), Phys. Rev. C **61**, 014302.
Nakatsukasa, T., and K. Yabana (2001), J. Chem. Phys. **114**, 2550.
Nakatsukasa, T., and K. Yabana (2002), Prog. Theor. Phys. Suppl. **146**, 447.
Nakatsukasa, T., and K. Yabana (2003), Chem. Phys. Lett. **374**, 613.
Nakatsukasa, T., and K. Yabana (2004), Eur. Phys. J. A **20**, 163.
Nakatsukasa, T., and K. Yabana (2005), Phys. Rev. C **71**, 024301.
Nambu, Y. (1960), Phys. Rev. **117**, 648.
Negele, J. W. (1970), Phys. Rev. C **1**, 1260.
Negele, J. W. (1982), Rev. Mod. Phys. **54**, 913.
Negele, J. W., and D. Vautherin (1972), Phys. Rev. C **5**, 1472.
Nesterenko, V. O., W. Kleinig, J. Kvasil, P. Vesely, P.-G. Reinhard, and D. S. Dolci (2006), Phys. Rev. C **74**, 064306.
Nesterenko, V. O., J. Kvasil, and P.-G. Reinhard (2002), Phys. Rev. C **66**, 044307.
Nikšić, T., N. Kralj, T. Tutiš, D. Vretenar, and P. Ring (2013), Phys. Rev. C **88**, 044327.
Nikšić, T., Z. P. Li, D. Vretenar, L. Próchniak, J. Meng, and P. Ring (2009), Phys. Rev. C **79**, 034303.
Nikšić, T., D. Vretenar, and P. Ring (2008), Phys. Rev. C **78**, 034318.
Nikšić, T., D. Vretenar, and P. Ring (2011), Progress in Particle and Nuclear Physics **66**, 519 .
Niu, Y. F., G. Colò, and E. Vigezzi (2014), Phys. Rev. C **90**, 054328.
Niu, Z. M., Y. F. Niu, H. Z. Liang, W. H. Long, T. Nikšić, D. Vretenar, and J. Meng (2013), Physics Letters B **723**, 172 .
Oba, H., and M. Matsuo (2009), Phys. Rev. C **80**, 024301.
Oberacker, V. E., and A. S. Umar (2013), Phys. Rev. C **87**, 034611.
Oberacker, V. E., A. S. Umar, J. A. Maruhn, and P.-G. Reinhard (2010), Phys. Rev. C **82**, 034603.
Oberacker, V. E., A. S. Umar, and C. Simenel (2014), Phys. Rev. C **90**, 054605.
Okołowicz, J., M. Płoszajczak, and I. Rotter (2003), Physics Reports **374**, 271 .
Oliveira, L. N., E. K. U. Gross, and W. Kohn (1988), Phys. Rev. Lett. **60**, 2430.
Olsen, J., H. J. A. Jensen, and P. Jørgensen (1988), Journal of Computational Physics **74**, 265 .
Onida, G., L. Reining, and A. Rubio (2002), Rev. Mod. Phys. **74**, 601.
Onishi, N., and T. Une (1975), Progress of Theoretical Physics **53**, 504.
Paar, N., T. Nikšić, D. Vretenar, and P. Ring (2004), Phys. Rev. C **69**, 054303.
Paar, N., P. Ring, T. Nikšić, and D. Vretenar (2003), Phys. Rev. C **67**, 034312.
Paar, N., D. Vretenar, E. Khan, and G. Colò (2007), Reports on Progress in Physics **70**, 691.
Pardi, C. I., and P. D. Stevenson (2013), Phys. Rev. C **87**, 014330.
Parr, R. G., and W. Yang (1989), *Density-Functional Theory of Atoms and Molecules* (Oxford University Press, New York).
Pei, J. C., M. Kortelainen, Y. N. Zhang, and F. R. Xu (2014), Phys. Rev. C **90**, 051304.
Peierls, R. E., and D. J. Thouless (1962), Nuclear Physics **38**, 154 .
Pekker, D., and C. Varma (2015), Annual Review of Condensed Matter Physics **6**, 269.
Perdew, J. P., A. Ruzsinszky, J. Tao, V. N. Staroverov, G. E. Scuseria, and G. I. Csonka (2005), The Journal of Chemical Physics **123**, 062201, http://dx.doi.org/10.1063/1.1904565.
Perdew, J. P., and A. Zunger (1981), Phys. Rev. B **23**, 5048.
Persico, M., and G. Granucci (2014), Theoretical Chemistry Accounts **133**, 1526, 10.1007/s00214-014-1526-1.

Péru, S., G. Gosselin, M. Martini, M. Dupuis, S. Hilaire, and J.-C. Devaux (2011), Phys. Rev. C **83**, 014314.

Péru, S., and H. Goutte (2008), Phys. Rev. C **77**, 044313.

Próchniak, L., P. Quentin, D. Samsoen, and J. Libert (2004), Nuclear Physics A **730**, 59 .

Próchniak, L., and S. G. Rohoziǹski (2009), Journal of Physics G: Nuclear and Particle Physics **36**, 123101.

Reinhard, P.-G., and K. Goeke (1979), Phys. Rev. C **20**, 1546.

Reinhard, P.-G., and K. Goeke (1987), Reports on Progress in Physics **50**, 1.

Reinhard, P.-G., P. D. Stevenson, D. Almehed, J. A. Maruhn, and M. R. Strayer (2006), Phys. Rev. E **73**, 036709.

Reinhard, P.-G., A. S. Umar, K. T. R. Davies, M. R. Strayer, and S.-J. Lee (1988), Phys. Rev. C **37**, 1026.

Ring, P., and P. Schuck (1980), *The nuclear many-body problems*, Texts and monographs in physics (Springer-Verlag, New York).

Robledo, L. M., and G. F. Bertsch (2011), Phys. Rev. C **84**, 054302.

Roca-Maza, X., X. Viñas, M. Centelles, P. Ring, and P. Schuck (2011), Phys. Rev. C **84**, 054309.

Rodríguez, T. R. (2014), Phys. Rev. C **90**, 034306.

Rodríguez, T. R., and J. L. Egido (2010), Phys. Rev. C **81**, 064323.

Rodríguez, T. R., and J. L. Egido (2011), Physics Letters B **705**, 255 .

Rohlfing, M., and S. G. Louie (2000), Phys. Rev. B **62**, 4927.

Rohoziǹski, S. G. (2012), Journal of Physics G: Nuclear and Particle Physics **39**, 095104.

Rowe, D. J. (1982), Nuclear Physics A **391**, 307 .

Rowe, D. J., and J. Wood (2010), *Fundamentals of Nuclear Models, Foundational Models* (World Scientific, Singapore).

Roynette, J. C., H. Doubre, N. Frascaria, J. C. Jacmart, N. Poffe, and M. Riou (1977), Physics Letters B **67**, 395 .

Runge, E., and E. K. U. Gross (1984), Phys. Rev. Lett. **52**, 997.

Sabbey, B., M. Bender, G. F. Bertsch, and P.-H. Heenen (2007), Phys. Rev. C **75**, 044305.

Sagawa, H. (2001), Prog. Theor. Phys. Suppl. **142**, 1.

Sahm, C. C., H. G. Clerc, K.-H. Schmidt, W. Reisdorf, P. Armbruster, F. P. Hessberger, J. G. Keller, G. Münzenberg, and D. Vermeulen (1985), Nuclear Physics A **441**, 316 .

Sakamoto, H., and T. Kishimoto (1988), Nuclear Physics A **486**, 1 .

Sakata, F., T. Marumori, and K. Takada (1981), Progress of Theoretical Physics Supplement **71**, 48.

Sarriguren, P. (2012), Phys. Rev. C **86**, 034335.

Sarriguren, P., E. M. de Guerra, and A. Escuderos (2001), Nuclear Physics A **691**, 631 .

Sato, K. (2015), Progress of Theoretical and Experimental Physics **2015**, 123D01.

Sato, K., and N. Hinohara (2011), Nuclear Physics A **849**, 53 .

Sato, K., N. Hinohara, K. Yoshida, T. Nakatsukasa, M. Matsuo, and K. Matsuyanagi (2012), Phys. Rev. C **86**, 024316.

Satuła, W., and R. A. Wyss (2005), Reports on Progress in Physics **68**, 131.

Scamps, G., and D. Lacroix (2013a), Phys. Rev. C **87**, 014605.

Scamps, G., and D. Lacroix (2013b), Phys. Rev. C **88**, 044310.

Scamps, G., and D. Lacroix (2014), Phys. Rev. C **89**, 034314.

Scamps, G., D. Lacroix, G. F. Bertsch, and K. Washiyama (2012), Phys. Rev. C **85**, 034328.

Scamps, G., C. Simenel, and D. Lacroix (2015), Phys. Rev. C **92**, 011602.

Schmid, K., and P.-G. Reinhard (1991), Nuclear Physics A **530**, 283 .

Sekizawa, K., and K. Yabana (2013), Phys. Rev. C **88**, 014614.

Sekizawa, K., and K. Yabana (2014), Phys. Rev. C **90**, 064614.

Sekizawa, K., and K. Yabana (2015), EPJ Web of Conferences **86**, 00043.

Serizawa, Y., and M. Matsuo (2009), Progress of Theoretical Physics **121**, 97.

Shimada, M., S. Tagami, and Y. R. Shimizu (2015), Progress of Theoretical and Experimental Physics **2015**, 10.1093/ptep/ptv073.

Shimizu, Y. R., and K. Matsuyanagi (2001), Progress of Theoretical Physics Supplement **141**, 285.

Shimoura, S., T. Nakamura, M. Ishihara, N. Inabe, T. Kobayashi, T. Kubo, R. H. Siemssen, I. Tanihata, and Y. Watanabe (1995), Phys. Lett. B **348**, 29.

Shinohara, S., H. Ohta, T. Nakatsukasa, and K. Yabana (2006), Phys. Rev. C **74**, 054315.

Shinohara, Y., K. Yabana, Y. Kawashita, J.-I. Iwata, T. Otobe, and G. F. Bertsch (2010), Phys. Rev. B **82**, 155110.

Shlomo, S., and G. Bertsch (1975), Nucl. Phys. A **243**, 507.

Shoji, T., and Y. R. Shimizu (2009), Progress of Theoretical Physics **121**, 319.

Sholl, D., and J. A. Steckel (2009), *Density Functional Theory: A Practical Introduction* (Wiley-Interscience, Hoboken).

Shoppa, T. D., S. E. Koonin, K. Langanke, and R. Seki (1993), Phys. Rev. C **48**, 837.

Shun-jin, W., and W. Cassing (1985), Annals of Physics **159**, 328 .

Simenel, C. (2010), Phys. Rev. Lett. **105**, 192701.

Simenel, C. (2011), Phys. Rev. Lett. **106**, 112502.

Simenel, C. (2012), The European Physical Journal A **48**, 1.

Simenel, C., and P. Chomaz (2003), Phys. Rev. C **68**, 024302.

Simenel, C., and P. Chomaz (2009), Phys. Rev. C **80**, 064309.

Simenel, C., P. Chomaz, and G. de France (2001), Phys. Rev. Lett. **86**, 2971.

Simenel, C., P. Chomaz, and G. d. France (2007), Phys. Rev. C **76**, 024609.

Simenel, C., R. Keser, A. S. Umar, and V. E. Oberacker (2013), Phys. Rev. C **88**, 024617.

Sonika,, B. J. Roy, A. Parmar, U. K. Pal, H. Kumawat, V. Jha, S. K. Pandit, V. V. Parkar, K. Ramachandran, K. Mahata, A. Pal, S. Santra, A. K. Mohanty, and K. Sekizawa (2015), Phys. Rev. C **92**, 024603.

Sousa, S. F., P. A. Fernandes, , and M. J. Ramos (2007), The Journal of Physical Chemistry A **111**, 10439.

Stephens, P. J., F. J. Devlin, C. F. Chabalowski, and M. J. Frisch (1994), The Journal of Physical Chemistry **98**, 11623.

Stetcu, I., C. A. Bertulani, A. Bulgac, P. Magierski, and K. J. Roche (2015), Phys. Rev. Lett. **114**, 012701.

Stetcu, I., A. Bulgac, P. Magierski, and K. J. Roche (2011), Phys. Rev. C **84**, 051309.

Stoitsov, M., M. Kortelainen, S. K. Bogner, T. Duguet, R. J. Furnstahl, B. Gebremariam, and N. Schunck (2010), Phys. Rev. C **82**, 054307.

Stoitsov, M., M. Kortelainen, T. Nakatsukasa, C. Losa, and W. Nazarewicz (2011), Phys. Rev. C **84**, 041305.
Stringari, S. (1979), Nuclear Physics A **325**, 199 .
Swiatecki, W. J. (1982), Nuclear Physics A **376**, 275 .
Tamura, T., and T. Udagawa (1964), Nuclear Physics **53**, 33 .
Tao, J., J. P. Perdew, V. N. Staroverov, and G. E. Scuseria (2003), Phys. Rev. Lett. **91**, 146401.
Tavernelli, I. (2015), Accounts of Chemical Research **48**, 792, pMID: 25647401.
Terasaki, J., and J. Engel (2006), Phys. Rev. C **74**, 044301.
Terasaki, J., and J. Engel (2010), Phys. Rev. C **82**, 034326.
Terasaki, J., and J. Engel (2011), Phys. Rev. C **84**, 014332.
Terasaki, J., J. Engel, and G. F. Bertsch (2008), Phys. Rev. C **78**, 044311.
Thouless, D. J., and J. G. Valatin (1962), Nucl. Phys. **31**, 211.
Tian, Y., Z. Y. Ma, and P. Ring (2009), Physics Letters B **676**, 44 .
Tohyama, M. (2001), Phys. Rev. C **64**, 067304.
Tohyama, M., and M. Gong (1989), Zeitschrift für Physik A Atoms and Nuclei **332**, 269.
Tohyama, M., and T. Nakatsukasa (2012), Phys. Rev. C **85**, 031302.
Tohyama, M., and P. Schuck (2007), The European Physical Journal A **32**, 139.
Tohyama, M., and A. Umar (2002), Physics Letters B **549**, 72 .
Toivanen, J., B. G. Carlsson, J. Dobaczewski, K. Mizuyama, R. R. Rodríguez-Guzmán, P. Toivanen, and P. Veselý (2010), Phys. Rev. C **81**, 034312.
Tomonaga, S.-I. (1955), Progress of Theoretical Physics **13**, 467.
Tran, F., and P. Blaha (2009), Phys. Rev. Lett. **102**, 226401.
Tretiak, S., C. M. Isborn, A. M. N. Niklasson, and M. Challacombe (2009), The Journal of Chemical Physics **130**, 054111.
Tselyaev, V. I. (2007), Phys. Rev. C **75**, 024306.
Tselyaev, V. I. (2013), Phys. Rev. C **88**, 054301.
Ullrich, C. A. (2012), *Time-Dependent Density Functional Theory: Concepts and Applications* (Oxford University Press, New York).
Umar, A. S., J. A. Maruhn, N. Itagaki, and V. E. Oberacker (2010), Phys. Rev. Lett. **104**, 212503.
Umar, A. S., and V. E. Oberacker (2005), Phys. Rev. C **71**, 034314.
Umar, A. S., and V. E. Oberacker (2006a), Phys. Rev. C **74**, 061601.
Umar, A. S., and V. E. Oberacker (2006b), Phys. Rev. C **74**, 021601.
Umar, A. S., and V. E. Oberacker (2006c), Phys. Rev. C **73**, 054607.
Umar, A. S., and V. E. Oberacker (2007), Phys. Rev. C **76**, 014614.
Umar, A. S., and V. E. Oberacker (2008), Phys. Rev. C **77**, 064605.
Umar, A. S., V. E. Oberacker, and C. J. Horowitz (2012a), Phys. Rev. C **85**, 055801.
Umar, A. S., V. E. Oberacker, J. A. Maruhn, and P.-G. Reinhard (2009), Phys. Rev. C **80**, 041601.
Umar, A. S., V. E. Oberacker, J. A. Maruhn, and P.-G. Reinhard (2012b), Phys. Rev. C **85**, 017602.
Umar, A. S., V. E. Oberacker, and C. Simenel (2015), Phys. Rev. C **92**, 024621.
Umar, A. S., M. R. Strayer, and P.-G. Reinhard (1986), Phys. Rev. Lett. **56**, 2793.
Vignale, G. (1995), Phys. Rev. Lett. **74**, 3233.
Vignale, G., and W. Kohn (1996), Phys. Rev. Lett. **77**, 2037.
Villars, F. (1977), Nuclear Physics A **285**, 269 .
Villars, F. M. H. (1983), Progress of Theoretical Physics Supplement **74-75**, 184.
Vretenar, D., A. V. Afanasjev, G. A. Lalazissis, and P. Ring (2005), Physics Reports **409**, 101 .
Wachter, G., C. Lemell, J. Burgdörfer, S. A. Sato, X.-M. Tong, and K. Yabana (2014), Phys. Rev. Lett. **113**, 087401.
Wacker, O. J., R. Kümmel, and E. K. U. Gross (1994), Phys. Rev. Lett. **73**, 2915.
Washiyama, K. (2015), Phys. Rev. C **91**, 064607.
Washiyama, K., and D. Lacroix (2008), Phys. Rev. C **78**, 024610.
Weisskopf, V. F. (1957), Nuclear Physics **3**, 423 .
Weizsäcker, C. (1935), Zeitschrift für Physik **96**, 431.
Wilets, L., and M. Jean (1956), Phys. Rev. **102**, 788.
Winther, A. (1994), Nuclear Physics A **572**, 191 .
Wopperer, P., P. Dinh, P.-G. Reinhard, and E. Suraud (2015), Physics Reports **562**, 1 , electrons as probes of dynamics in molecules and clusters: A contribution from Time Dependent Density Functional Theory.
Yabana, K., and G. F. Bertsch (1996), Phys. Rev. B **54**, 4484.
Yabana, K., Y. Kawashita, T. Nakatsukasa, and J.-I. Iwata (2011), in *Charged Particle and Photon Interactions with Matter: Recent Advances, Applications, and Interfaces* (CRC Press Taylor & Francis) pp. 65–86.
Yabana, K., T. Nakatsukasa, J.-I. Iwata, and G. F. Bertsch (2006), Physica Status Solidi (b) **243**, 1121.
Yabana, K., T. Sugiyama, Y. Shinohara, T. Otobe, and G. F. Bertsch (2012), Phys. Rev. B **85**, 045134.
Yamada, K. (1993), Progress of Theoretical Physics **89**, 995.
Yamagami, M., J. Margueron, H. Sagawa, and K. Hagino (2012), Phys. Rev. C **86**, 034333.
Yamagami, M., Y. R. Shimizu, and T. Nakatsukasa (2009), Phys. Rev. C **80**, 064301.
Yamamura, M., and A. Kuriyama (1987), Progress of Theoretical Physics Supplement **93**, 1.
Yannouleas, C., and U. Landman (2007), Reports on Progress in Physics **70**, 2067.
Yao, J. M., K. Hagino, Z. P. Li, J. Meng, and P. Ring (2014), Phys. Rev. C **89**, 054306.
Yao, J. M., H. Mei, H. Chen, J. Meng, P. Ring, and D. Vretenar (2011), Phys. Rev. C **83**, 014308.
Yao, J. M., J. Meng, P. Ring, and D. Vretenar (2010), Phys. Rev. C **81**, 044311.
Yoshida, K. (2009), Phys. Rev. C **79**, 054303.
Yoshida, K. (2013), Progress of Theoretical and Experimental Physics **2013**, 113D02.
Yoshida, K., and T. Nakatsukasa (2011), Phys. Rev. C **83**, 021304.
Yoshida, K., and T. Nakatsukasa (2013), Phys. Rev. C **88**, 034309.
Yoshida, K., and N. Van Giai (2008), Phys. Rev. C **78**, 014305.
Yu, Y., and A. Bulgac (2003), Phys. Rev. Lett. **90**, 222501.
Yuldashbaeva, E. K., J. Libert, P. Quentin, and M. Girod (1999), Physics Letters B **461**, 1 .
Zangwill, A., and P. Soven (1980), Phys. Rev. A **21**, 1561.
Zhang, H., Y. Miyamoto, and A. Rubio (2012), Phys. Rev.

Lett. **109**, 265505.
Zhao, P. W., Z. P. Li, J. M. Yao, and J. Meng (2010), Phys. Rev. C **82**, 054319.
Zinser, M., F. Humbert, T. Nilsson, W. Schwab, H. Simon, T. Aumann, M. J. G. Borge, L. V. Chulkov, J. Cub, and T. W. E. et al. (1997), Nucl. Phys. A **619**, 151.